METAL ORGANIC FRAMEWORKS: FROM ANTICANCER MULTIFUNCTIONAL DRUG DELIVERY SYSTEMS TO NOVEL VACCINE ADJUVANTS

Katarzyna Anna Morley

A Thesis Submitted for the Degree of PhD
at the
University of St Andrews

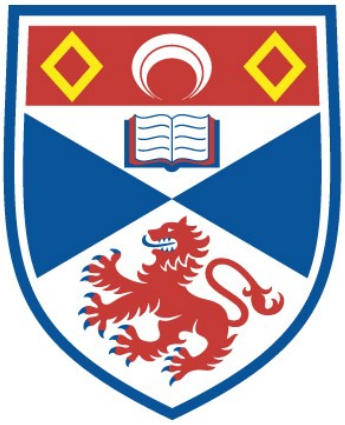

2016

METAL ORGANIC FRAMEWORKS: FROM ANTICANCER MULTIFUNCTIONAL DRUG DELIVERY SYSTEMS TO NOVEL VACCINE ADJUVANTS

Katarzyna Anna Morley

A Thesis Submitted in application for the Degree of PhD in the School of Chemistry at the University of St Andrews

August 2016

Declaration

I, Katarzyna Morley, hereby certify that this thesis, which is approximately 35 000 words in length, has been written by me, and that it is the record of work carried out by me, or principally by myself in collaboration with others as acknowledged, and that it has not been submitted in any previous application for a higher degree.

I was admitted as a research student in September, 2012 and as a candidate for the degree of PhD in September, 2013; the higher study for which this is a record was carried out in the University of St Andrews between 2012 and 2015.

Date signature of candidate

I hereby certify that the candidate has fulfilled the conditions of the Resolution and Regulations appropriate for the degree of PhD in the University of St Andrews and that the candidate is qualified to submit this thesis in application for that degree.

Date signature of supervisor

In submitting this thesis to the University of St Andrews I understand that I am giving permission for it to be made available for use in accordance with the regulations of the University Library for the time being in force, subject to any copyright vested in the work not being affected thereby. I also understand that the title and the abstract will be published, and that a copy of the work may be made and supplied to any bona fide library or research worker, that my thesis will be electronically accessible for personal or research use unless exempt by award of an embargo as requested below, and that the library has the right to migrate my thesis into new electronic forms as required to ensure continued access to the thesis. I have obtained any third-party copyright permissions that may be required in order to allow such access and migration, or have requested the appropriate embargo below.

The following is an agreed request by candidate and supervisor regarding the publication of this thesis:

PRINTED COPY & ELECTRONIC COPY

Embargo on all print copy and electronic copy for a period of 2 years on the following ground:

- Publication would be commercially damaging to the supervisor, or the University

Supporting statement for printed embargo request:

Chapter 6 – MOFs as an example for potential adjuvant applications, fully performed at School of Pharmacy, UCL, with Dr Gareth Williams needs to be protected as there is a plan for commercialisation of this idea and also some publishing will follow.

Date signature of candidate signature of supervisor

Courses Attended

Homogenous Catalysis	Prof. Paul Kramer
Chemistry of phosphorus and related elements	Dr A. Aitken
Functional materials	Dr F. D. Morrison
Advanced polymer science	Prof P. Wormald
Fortran	Dr T. van Mourik

Acknowledgements

I would like to thank my supervisor, Prof. Russell Morris for his help and guidance throughout this complex project.

Also, I am grateful to Dr Gareth Williams for his advice, patience in explaining the complexity of vaccine mechanism and contributing a lot in finding the ways of solving the impossible and the possibility to extend my research and enriching my thesis in the biological testing done for drug delivery systems as well as opening a new avenue of applications for MOFs as vaccine adjuvants. Many thanks to Dr Ilona Kubajewska for her patience and help with setting up the biological assays and broad discussions on immune-response signals and cell work.

Thanks to my colleagues for their good advice and creating a good atmosphere in the office: Sam Morris, Laura McCormick, Paul Wheatley, Yuyang Tien, Daniel Firth. Thanks also to the other Morris group members who have helped with my research. A special thanks goes to Mrs Sylvia Williamson for her patient and helping me out with BET measurements.

Of course, I must thank my parents, Izabela and Jerzy, for their support and encouragement throughout my PhD.

Lastly, I would like to thank my now husband Alexander Morley whom I met in St Andrews and who supported me immensely through my PhD project, cheering me up which gave me the motivation to finish the research that is illustrated in this thesis.

Finally, thank you to the EPSRC for providing the funding that has allowed me to carry out this research.

Publication

Incorporation of cisplatin into the metal-organic frameworks UiO66-NH_2 and UiO66 – encapsulation vs. Conjugation.

Katarzyna A. Mocniak, Ilona Kubajewska, Dominic E.M. Spillane, Gareth R. Williams and Russell E. Morris *RSC Advances*, **2015**, 5, 83648 - 83656

Abstract

The research presented in this thesis aims to assess the capacity of metal organic frameworks for potential applications as drug delivery systems and novel vaccine adjuvants.

The opening chapter (Chapter 1) provides a reader with a background to the field, metal organic frameworks synthesis routes and their potential applications in medicine and insight into the basics of immunology and biological assays as well as the anti-cancer drugs mechanisms and how it can be used to target the tumour cells.

Chapter 3 describes the experimental techniques used in this research combining biological with chemical testing.

Investigation of Zr-MOFs (UiO66 and UiO66-NH_2) and CPO – 27 (CPO Mg and CPO Ni) for their potential application as drug delivery systems for cisplatin is presented and compared in Chapter 4, as well as two different drug incorporation techniques (conjugation and physical encapsulation) in the case of UiO66-NH_2. The route proved to be more efficient when compared with encapsulation for the same MOF, and overall the most promising candidate for a drug delivery system for cisplatin, due to its large pores, was UiO66.

Chapter 5 focuses on the potential application of Zr-MOFs and CPO-27 (Mg and Ni) as a drug delivery system for 5-Fluorouracil, a drug which because of its sparse solubility in water is challenging when it comes to its administration in the human body. Chapter 7 investigates the possibility to design multiple drug delivery systems utilising MOFs that contain cisplatin and fluorouracil in their framework, loading them with nitric oxide to increase the anti-cancer action and also to prevent thrombosis that may pose a danger to patients who undergo anti-cancer therapies. Chapter 6 describes the new concept of investigating MOFs (Zr-MOFs and Al-MOFs) as potential candidates as vaccine adjuvants. The research concluded that the performance of Al-MOFs, was better when compared to commercially available adjuvants.

Table of Contents

Chapter 1. Introduction

1.1. Metal-organic frameworks for biological applications

The development of new materials is crucial for industry as well as for everyday life. Metal–organic frameworks (MOFs) are a relatively new class of materials that offers great potential in many applications[1-3] e.g. in gas storage[4-11], gas purification and separation[12], heterogeneous catalysis[13-15], imaging[16-18], luminescence[19] and biomedicine[20-24]. For more than 20 years, MOFs have been a hot topic in terms of their superb properties: large surface areas with pore sizes that can be adjusted depending on the usage and adsorption capacities as well as the fact that their density is low[25, 26]. These properties play a great role in the applications in catalysis, gas storage and gas separation. Their exceptional properties (e.g. swelling of the crystallographic network in the presence of different guest molecules[26]), are very interesting for some applications in which zeolites cannot be used and offer easy and non-complicated synthesis. In comparison with the zeolite materials, an inorganic or organic template must be used and its removal may cause the structure to collapse[1]. In contrast to zeolites, MOFs are easier to synthesise and do not require the generation of a template, as they have an organic linker and a metal in their structure. It is important to mention that a lot of names have been given to these porous materials (e.g. porous coordination networks, porous coordination polymers, metal-organic frameworks etc.). These materials are highly attractive to research as well as the industrial world and the number of publications is remarkable[1, 2]. Especially important applications are in gas storage, drug storage and delivery[27]. There is a question left to answer, how many MOFs structures are there. This depends on how the MOF is defined. Well, if we take the provisional recommendations on MOF terminology from IUPAC that says a MOF is a coordination polymer with an open framework containing potential voids[28] then our search will be based on a transition metal that is bonded to a nitrogen or an oxygen via a polymeric bond. It does not require a 3D framework only that it will be repeated. According to CCDC data base, there are 38 062 structures up to the 1st of Dec 2012[29].

Number of publications regarding MOFs sky-rocketed over the years as depicted in Figure 1-1 below.

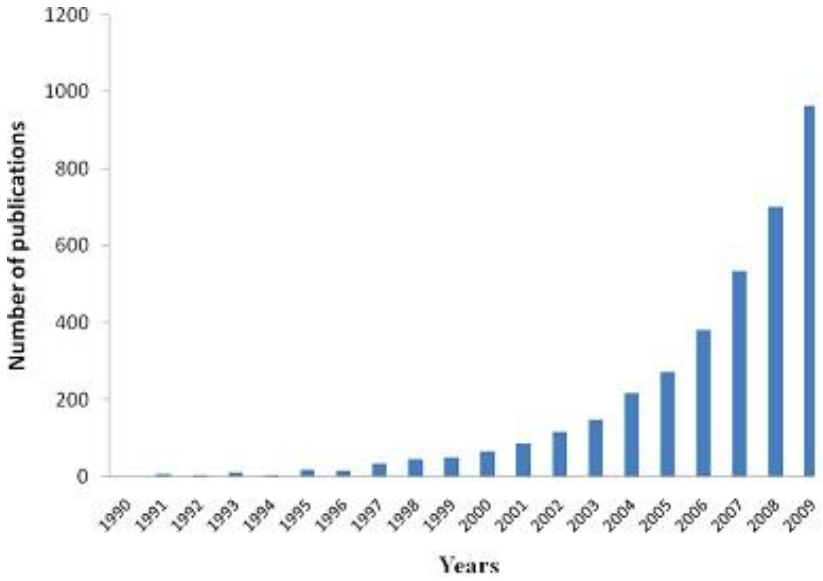

Figure 1-1 Number of publications on MOFs[30]. Source: Web Science.

Discovered by Robson in 1989[31], metal-organic frameworks are a relatively young group of advanced porous materials that consists of a metal ion, the inorganic part and the organic linker. The number of possible combinations is infinite. The most commonly used linkers are depicted in the Figure 1-2 below.

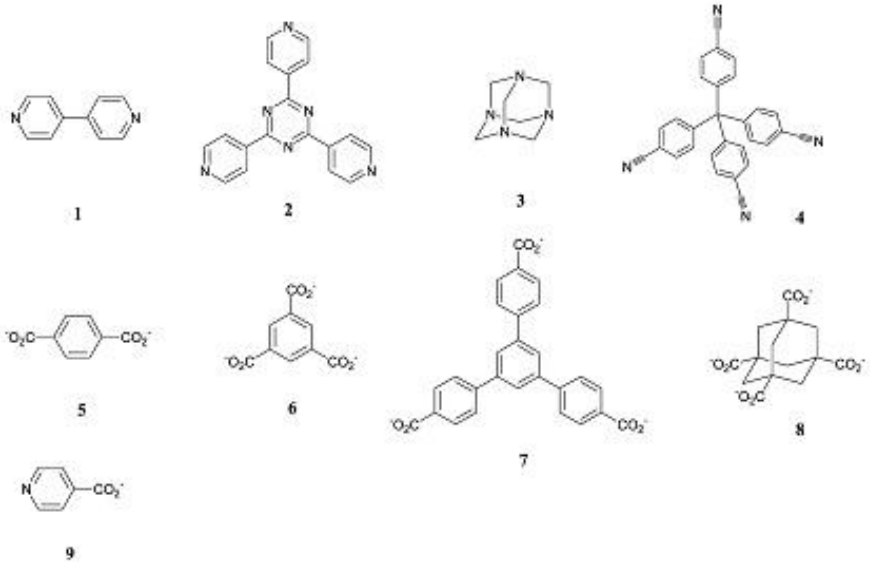

Figure 1-2 Some example of linkers that are used to synthesise MOFs. 4,4-bipyridine (1),1,3,5-Tris(4-pyridyl)-2,4,6-triazine (2), hexamethylenetetramine (3), tetra(4-cyanophenyl)methane (4). Terephthalic acid BDC 1,4- benzene dicarboxylate (5), benzene-1,3,5-tricarboxylic acid (6), 1,3,5-Tris(4-carboxyphenyl)benzene (7), Hexamethylenetetracarboxylic acid (8), 4-Pyridinecarboxylic acid (9)[2].

One of the key properties of MOFs is the tuneable size of the pores that can sometimes adjust their porosity upon the loading with gases or molecules; or also as easily by exchanging the metal atom or the linker forming new structures[20]. A quite interesting property for MOFs as recently reported, is the so-called reversible breathing or swelling effect, which gives rise to flexible pore size depending on the guest molecules hosted by the porous structure[26, 32]. To give an example, the cell volume of the dry structures increases by 50-230% in case of the MIL-53 (Cr) and (Fe) isoreticular family[33]. The term isoreticular was introduced by Yaghi[34] to describe the structure formed with "the same preferred topology" with the only difference in the metal ion and the size of the links. In the same framework it is possible to exchange the metal ions and keep the topology of the material the same. This is not the case with the rigid bonds found in zeolites. The cages and tunnels of MOFs are larger and thus, so are the specific surface areas of 500 – 6000 m^2/g BET[35] or even 6240 reported for MIL-200[36], with low densities, generally 0.2-1 g/cm^3 (density of Li metal 0.56 g/cm^3)[37] and with the exceptionally low density of 0.126 g/cm^3 and big pores 8–43.2 Å[21, 22, 30, 33, 34] recently reported for MOF-399[34]. Just recently, the reported surface areas of MOFs are about 10000 m^2/g which makes them the materials for special missions and in this matter superior to zeolites and carbons[38]. These features give MOFs an edge in a variety of applications such as gas storage, catalysis, separation and recently drug and bioactive gases loading with a controllable release[39, 40]. Also, thanks to the open metal sites of the inorganic part of the MOF, bioactive gases such as NO, CO and H_2S can be successfully loaded inside the molecule as a result of their chemical nature[41].

For bio-applications, the following criteria must be fulfilled – the MOFs should be non-toxic, which requires both the linker and the metal to be inert; the release of the drug or the bioactive gas must be controllable; and also the excretion of the MOF after the drug administration should be possible[24]. That is why the endogeneous linker is the most preferable candidate, as it could have bioactive functionality in the human body. What is meant by "endogeneous" is the fact of being the part of or produced by the human body. An example of such a linker is Niacin (vitamin B_3) that together with non-toxic iron molecules (50% of lethal

dose LD_{50}=30g/kg) builds BioMIL-1 (Figure 1-5). Nicotinic acid that controls the blood pressure and can control cholesterol and has antilipemic properties[42].

Figure 1-3 gives an overview how we cluster MOFs, and Figure 1-4 shows the variety of MOF structures comprising of endogeneous linker, that may make them more biocompatible. Coordination polymer is the most general term and MOFs are best described as 3-dimentional coordination networks, IUPAC set the recommendations for nomenclature of coordination polymers and MOFs[43].

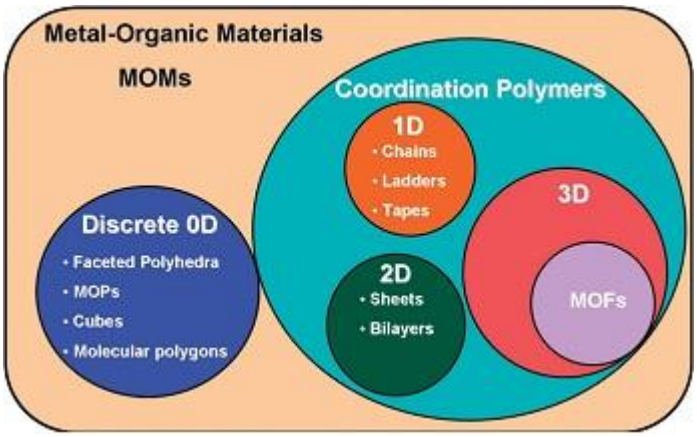

Figure 1-3 Variety of the coordination polymer, the 3D ones are referred as MOFs[44]

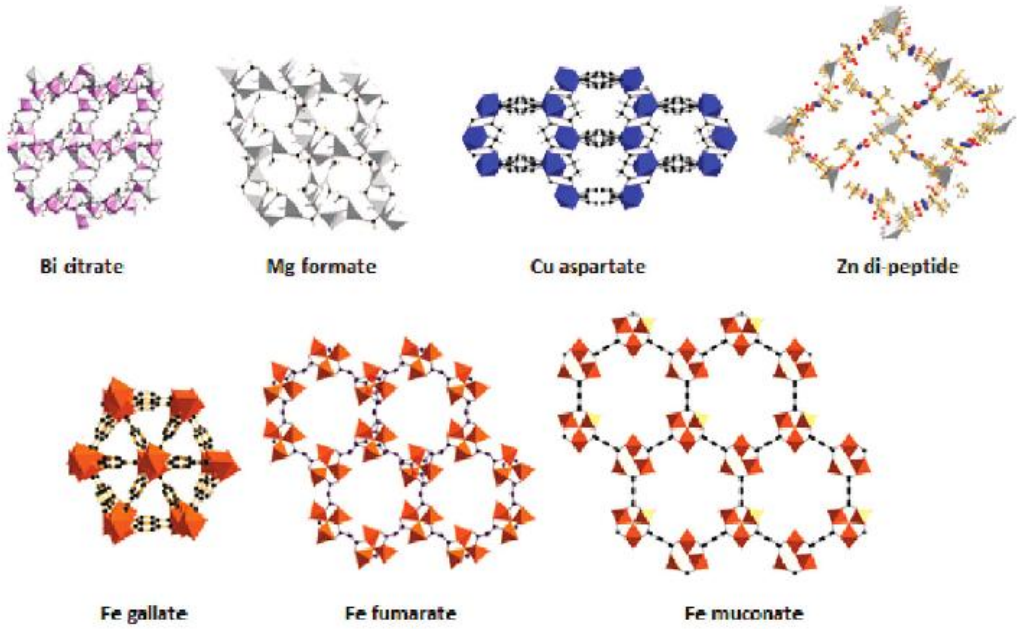

Figure 1-4 View of some of the MOFs structures based on the endogenous linkers. The colourful polyhedra are metal ions and carbon is in black[20].

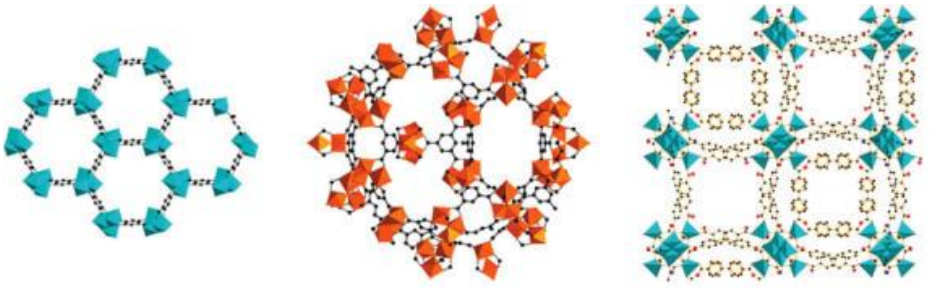

Figure 1-5 A view of some MOFs with endogenous linkers. Here from the left: CPO-27 (Zn, Mg), MIL-100 (Fe), Bio-MOF-1[20].

1.2. Nitric oxide – a friend or a foe?

Nitric oxide is a very interesting molecule thanks to its antithrombotic and antibacterial properties, the discovery of which brought a Nobel Prize in 1998 for Robert F Furchgott, Louis J Ignarro and Ferid Murad. It became the "molecule of the year" six years earlier after the discovery of a wide spectrum of its bio-properties like relaxation of the smooth muscle, prevention of platelet clotting and neurotransmission[45]. The nitric oxide molecule has got 11 valance electrons, in which 5 electrons of Nitrogen [$2s^2 2p^3$] and 6 of oxygen [$2s^2 p^4$] are responsible for bonding that emerges from sp-orbitals mixing leading to π-bonding. Figure 1-6 illustrates a schematic diagram of the molecular orbital in nitric oxide. The bond order defined as the difference between bonding electrons and anti-bonding electrons divided by two, for nitric oxide is 2.5.

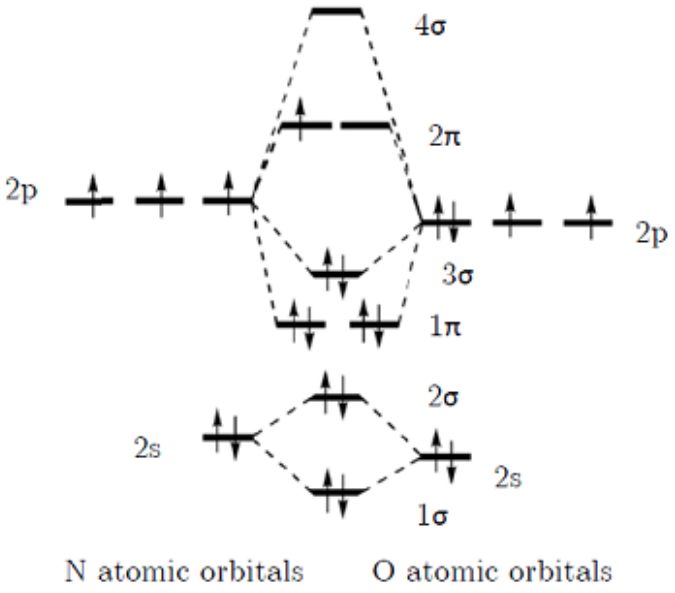

Figure 1-6 Molecular orbital diagram of nitric oxide[46].

This free radical molecule (it has an unpaired electron in the 2π orbital) can interact with transition metals and an unpaired electron could accept an electron and thus acting as an anti-oxidant[47]. NO is an important gas-transmitter in a human body and has a positive impact on blood platelet adhesion and cell division and is responsible for vasodilation (relaxation of the blood vessels) and control of blood pressure[48, 49]. It has been stipulated that biologically active amount of nitric oxide for certain applications may vary and for example to offer anti-thrombosis action, only a small dose is necessary (4 ppm), however, for anti-bacterial protection - a 10 times higher dose of nitric oxide is required[50]. Antibacterial, wound healing and anti-blood-clotting properties of NO have already been tested *in vitro* and *in vivo* to assess its efficacy[51]. Several studies shown that NO assists with wound healing and prevents forming of the blood clots[35, 50, 51]. NO – donor therapy is based on the generation of the accurate amount of NO in the right spot in the human body[52]. Not only have MOFs recently been used for NO delivery but also zeolites[53] and functionalised nanoparticle silica[54] and polymers[55, 56]. MOFs can deliver pure gas without any other oxides and the release of the gas can be controlled and triggered by exposure of the MOF-powder to water. For example CPO-27: Ni showed the exceptional uptake of NO up to 7 mmol/g, prolonged release under H_2O over time up to 3 weeks and after 2 years the loaded material showed no loss in NO storage[24, 41], which compared to HKUST-1 of 2 μmol/g at 298 K, gives the value 2500 times higher. This level of loading (HKUST-1) is still sufficient for biological applications, but for antibacterial would not be enough[57]. The mechanism of action is still unknown and the NO dose that would suppress the tumour growth must be yet identified, it is stipulated that above certain threshold NO is carcinogenic[58].

Not only anti-thrombotic and anti-bacterial properties of nitric oxide are of interest but also its potential application as anti-cancer agent that may show higher efficacy when compared to conventional therapies involving anti-cancer drugs[59]. In the human body, nitric oxide is produced by nitric oxide synthases (NOSs), a family of enzymes with catalytic properties, in the process of L-Arginine oxidation. This biological reaction needs to be supported by NADPH enzyme

complex (nicotinamide adenine dinucleotide phosphate-oxidase) and oxygen and as products, generates L-citrulline and NO[60].

There are three forms of nitric oxide synthase enzyme: NOS-II, whose the main function is cytotoxicity and defence of the host, and its primary site of action is either in macrophages or tumour cells, NOS-I responsible for neurotransmission/relaxation of smooth muscle and finally NOS-III, in charge of smooth muscle proliferation control and minimising clotting of blood platelets. NOS-II action can be regulated when stimulated by variety of cytokines and ligands: TNF-α, interferon, IL-1 and endotoxins[61] and is induced in different cell types for example macrophages and dendritic cells[62].

Some research conducted, showed that NO can cause apoptotic death of cancer cell at elevated concentrations[63] or can lead to suppression of tumour early development[64] and also of its growth and metastasis[65 66], which could potentially open another avenue for therapies other than radio – and chemotherapies[45].

1.3. Anticancer drugs and drug delivery systems.

The interest in pharmaceuticals and therapies is seeing a substantial growth every year with a lot of new drugs being approved by FDA (Food and Drug Administration). Despite the fact that research is aided with computational chemistry and biology helping in drug discovery immensely, drug development that leads to successful commercialization is still a very time-consuming and expensive process, taking between 10-15 years of development, clinical trials and ca. $1.8 bn of cost per drug before it lands on the shelves of a drug store[67, 68]. Figure 1-7 depicts the total market sales in billion of $ and its growth over years. The trend shows that starting from 2012 there is a growth potential over the last 2 years. Table 1-1 depicts the top 5 drugs that had quite an influence on the sales revenues of the companies who made discoveries, however, the expiration dates of patents is alarming, which is pushing the companies to maximize their revenues within the time frame of an existing patent. As it is really tricky and time-consuming to successfully come up with new drugs every time, there is a paradigm that by preparing the formulations of these drugs and working on drug delivery systems instead, would result in therapeutics of much higher efficacy.

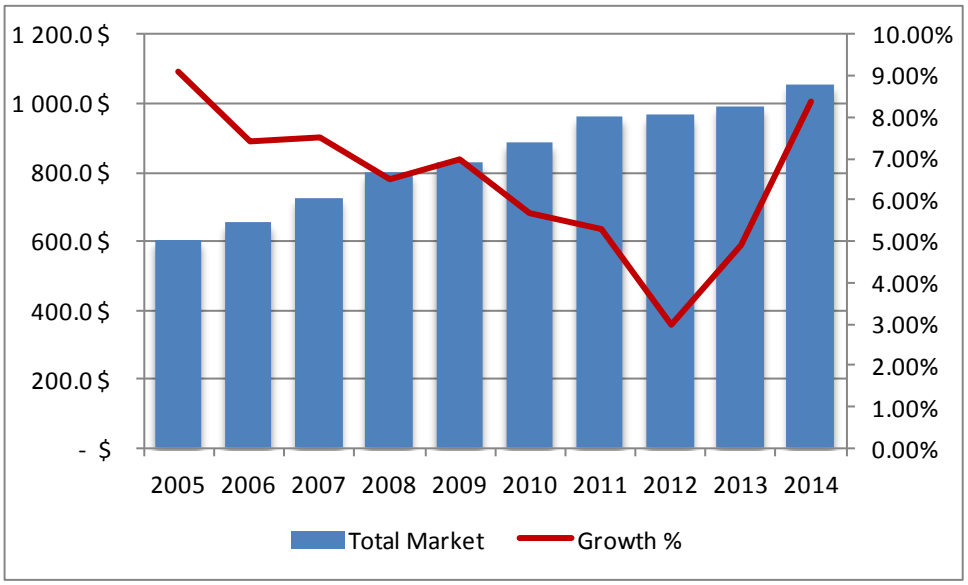

Figure 1-7 Total market sales in pharmaceuticals/drugs sector according to IMS Health (American company providing information services and technology for the healthcare industry).

Product	Manufacturer	Sales (USD million)	% of company sales	Patent expire date
Lipitor	Pfizer	12657	22.8	2011
Plavix	Sanofi-Aventis/BMS	8817	17.3	2012
Seretide	GSK	8469	25.2	2013
Nexium	Astra Zeneca	8362	23.5	2014
Seroquel	Astra Zeneca	6816	19.2	2012*

Table 1-1 Top 5 Medicines worldwide and the percentage of company sales as of 2010 that it generated[68]. *)the patent expired in 2010 in the US and in Europe in 2012.

The application of biocompatible and non-toxic polymers has contributed a lot to modern medicine as it impacts on a vast field of biosciences including the areas such as: tissue engineering, diagnostics and therapeutic strategies. Different naturally-occurring and synthetic polymers are used to develop state-of-the-art drug delivery systems, just to mention a few: chitosan, alginate, gelatin, dextran, albumin. These polymers may help chemotherapy be more selective as it offers a secure platform for controlled release that does not lead to overdose in some human body regions[67]. Metal organic frameworks have found wide applications in many fields, but there is still one which needs to be more developed and further research should be carried out in order to give satisfying results – it is the bio-application of MOFs[27]. There is a challenge to navigate the cargo in the region invaded by cancer by using different targets in the cancer tissue[69]. These could be

the changed mitochondria[70], leaky cellular walls and lower pH values in the tumour tissue. Normal physiological conditions have a pH value of 7.2-7.4, however, it becomes more acidic (5.0-6.5) in the extracellular space in the endosomes and drops further to pH 4.0 in lysosomes (primary and secondary), in the tumour cells the pH values are lower by 0.5-1.0 units than in the healthy tissue as it is reported by non-invasive techniques[55, 71]. That feature could be used for selective targeting.

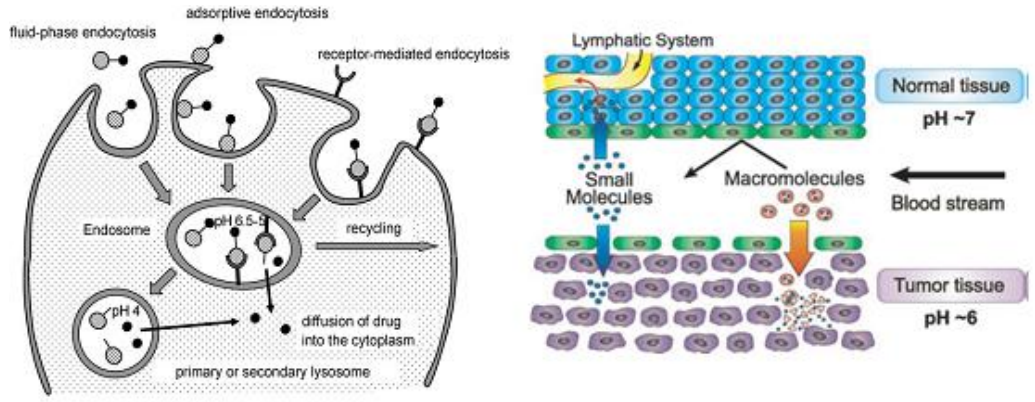

Figure 1-8 Endocytic pathway with different pH regions (left). To the right, the scheme that illustrates the normal cell and the one touched by the cancer with the possible ways for the drug delivery system migration shown [55].

As of now, only between 10-100 ppm of administered antibodies may reach their targets in vivo[72]. Therapeutics that are available now, are quite limited with their non-selective distribution in the human body that leads to high administration doses, fast excretion, poor pharmacokinetics (very fast release also called "burst effect" that may lead to the overdose at certain spots) and side effects which in case of anti-cancerous drugs might be very severe causing damage to the healthy cells[73, 74]. Nanotechnology offers some ways to overcome these challenges and has received a lot of attention in the past 20 years[72]. The nano-carriers such as polymeric structures, micelles, liposomes, iron oxide and gold encapsulated with a drug have been used for advanced therapies e.g. Abraxane and Doxil[21]. Research focused on encapsulation Fe_3O_4 nano-carriers with cisplatin and coated with Poly(D,L-Lactide) showed the ability of iron oxide to absorb the drug and release it within 70 hours from activation in PBS (phosphate buffer saline)[75]. Only recently MOFs, thanks to their interesting properties – large pores and porosity with impressive surface areas (BET) up to 6240 m^2/g[36] (MOF 210) or reported

7140 m^2/g for NU-110[76] (NU – Northwestern University), theoretically predicted to go as high as 10 000 m^2/g or greater[77, 78] and coordinative unsaturated sites upon dehydration, has turned the research world into converting them into drug delivery systems.

MOFs offer the possibility to incorporate the Mn or Gd cations in the framework that can work as imaging agent with an encapsulated cargo that the agent will enable tracing to allow for a better understanding of the targeting and delivery mechanisms. The Lin Group developed imaging agents – a nano-MOF containing Manganese with a linker terephthalic acid (BDC) or trimesic acid (BTC)[17].

A gas or small molecules can serve as a drug. Some of the gases are highly toxic in high amounts but paradoxically when dosed in a controllable way, are crucial for life processes: NO, CO and H_2S. The most recognised for its vasodilating properties is nitric oxide but the two other gases recently have caught interest with more research done on their controlled delivery[35]. The pores of MOFs are big enough to host small molecules of drugs, e.g. CPO-27 Ni (11Å). The presence of nickel makes the entire structure quite toxic for bioaplications[23] , however, it can still be used for anti-tumour drugs as they are very toxic[20]. Christian Serre's group tested their MIL materials family (MIL-53, 88A, 88B, 89, 100, 101-NH_2) for drug loading: doxorubicin, cidovir, busulfan, caffeine, azidothimidine triphosphate (antiviral for HIV)[79]. For better drug storage, derivatives of 2,5-dihydroxyterephthalic acid linkers were used that introduced different functional groups in the framework which had great impact on the size of pores leading to the formation of flexible iron (III) dicarboxylates[22, 26, 33]. This group also accomplished to synthesize a BioMOF called BioMIL based on a bioactive linker which is nicotinic acid and a non-toxic iron (LD_{50} = 30g/kg). It is important to mention that nicotinic acid is responsible in the human body for lowering LDL-cholesterol and triglyceride levels and keeping HDL-cholesterol levels high and also shows antibacterial and vasodilating properties[42], and is a precursor for NADH coenzyme in living cells. Some other MOFs based on the nicotinic acid as a linker were already reported but they all had a toxic cation in the framework (Cu)[80].

The anti-cancer drugs can be simply divided into 4 groups in regards with the mechanism they present to fight the cancer cells, these are alkylating agents, antimetabolites, anthracyclines and hormones. In this thesis, MOFs were researched as potential drug delivery systems for two drugs representing alkylating agent group – cisplatin and antimetabolites – 5- fluorouracil.

Alkylating agents have chemical groups capable of forming a covalent bond with nucleophilic substances in the cell, and such a substance is DNA. Nitrogen in guanine in the position N7 is strongly nucleophilic and as such a perfect target for alkylation, nitrogen molecules in adenine (N1, N3 positions) and in cytosine (N3) may also be a target of attack for the alkylating agents. These can bond in the intra- or inter- chain positions, leading to cross-linking, which disturbs transcription and replication of DNA, and ideally, the DNA-chain of the tumour cells. In this group, we can list the following agents cisplatin, carboplatin, busulfan hydroxycarbamide and carmustine[81].

1.3.1. Cisplatin

Already in 1968[82] cytotoxicity against cancerous cells presented by cisplatin was recognized and in numerous intensive research projects over subsequent years showed efficacy against several cancers in clinical trials[83]. Finally in 1978, it was approved by the FDA, although it has been known since 1845[74] in the world of chemistry. The mechanism of action of cisplatin is based on forming intrastrand and interstrand cross-links with nucleic acids, which causes damage because by its binding to the bases of DNA, the multiplication of DNA is impaired, leading to cell death (apoptosis) caused by inability of DNA to proliferate[84, 85].

Looking at the variety of cancers where cisplatin is used as a drug - the treatment of head, neck, ovarian, cervical[86], testicle, breast and bladder tumours[87-89], one can state that cisplatin is the most commonly used anti-cancer drug. There are some shortcomings of cisplatin therapy, as the drug affects all cells because it cannot distinguish between cancerous and healthy cells. Even though its efficacy is quite high, it comes with many side-effects: these include nephrotoxicity (kidneys damage) and neurotoxicity (toxicity in the nervous system); drug resistance of tumours also develops over time as well as may cause an acute thrombosis in patients receiving chemotherapy based on cisplatin[90, 91]. As a result, research is

ongoing in order to circumvent the drug's side-effects by introducing new ways in which cisplatin is delivered[88, 92, 93]. This is achieved by the use of a variety of drug delivery systems, designed to release the drug inside the tumour cell and to leave healthy cells untouched. Carbon nanotubes[94], liposomes[88, 95-99], polymers[88, 100] and nano-sized metal phosphates[87], oxides[75] and hyaluronic acid nanoparticles[101] are all under investigation. Recently MOFs have also begun to be explored in this regard[23, 102, 103].

Below, in the Figure 1-9, reader may find the representation of different derivatives of cisplatin that will follow the same mechanism of action in the tumour cells, namely intrastrand cross-linking of DNA.

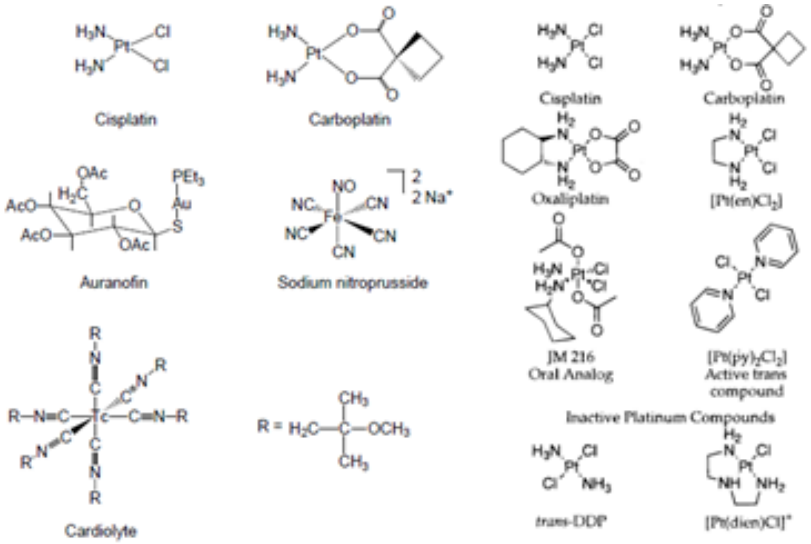

Figure 1-9 Different derivative of cisplatin reproduced from[104] (left) and[74] (right).

Only cis-platin is active in cancer treatment, as its geometric isomer trans-platin did not show this feature in the clinical trials[74]. What makes the drug efficient, it is its affinity to DNA which acts here as a target to which cisplatin is bound which causes damage to the helical structure followed by the inability for further replication and transcription. That leads to the cell apoptosis[104]. Recently it was discovered that cisplatin does not enter the tumour cells by passive diffusion but a copper transporter CTR1, which is a cell membrane protein and influences cisplatin uptake. At the same time cisplatin causes degradation of CTR1 and in this way introduces a limitation for its accumulation in the cancer tissue. The

resistance of the tumour cell against cisplatin that occurs over the course of time is linked to lack of the membrane protein in the cancer cell[105].

1.3.2. 5-Fluorouracil

Fluorouracil (5-FU) is an example of another mechanism of action which aims to replace uracil in purine biosynthesis. In contrary to uracil, 5-FU cannot be converted to thymidylate and because of this blocks DNA synthesis and cell proliferation. 5-FU is widely used mainly in topical applications to treat solid tumours, however, some drawbacks e.g. variable efficacy and toxicity limit its usage and FDA recommends not to administer 5-FU to patients with dihydropyrimidine dehydroglenase deficiency (DPD metabolic disorder).

The structure of 5-FU is depicted in Figure 1-10.

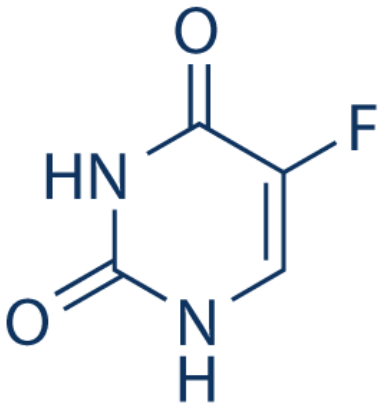

Figure 1-10 Structure of Fluorouracil, which is a derivative of uracil.

The drug was patented by Charles Heidelberg, who carried out research that showed that 5-FU was capable to stop the propagation of cancer in mice[106].

5-Fluorouracil is a hydrophilic drug what makes it challenging for preparations of formulations as its solubility in water is very sparse, and can only be enhanced in acidic or basic environments. It is though widely used as a part of therapies to treat colorectal, bladder, head and neck and breast cancers[107, 108]. Likewise cisplatin, therapies comprising 5-FU are toxic to the healthy cells and the short half-life (16 min) makes the therapy not very long-lasting with repetitions of administered doses being necessary and as such these have to be well adjusted depending on the individual[109].

A new Zn-MOF (Zn-BDC) was reportedly synthesised of a surface area of 600 m^2/g that was then used for 5-FU encapsulation with the loading achieved at

the level of 0.42 g/g. 5-FU release was monitored[110]. This piece of research did not provide any information on the drug delivery system efficacy in the *in vitro* environment. ZSM-5 zeolite has been recently investigated for its potential application as a drug delivery system for 5-FU[111].

Another approach has been presented by researcher at School of Pharmacy, UCL, to encapsulate 5-FU, by applying electro-spinning method. This technique involved a preparation of a formulation for production of electrospun fibres[112] that contained 5-FU. It has been shown that pH values had tremendous effect on the speed of drug release and at pH =1, between 40% and 80% of cargo was released and only increasing the pH value to 6.8 resulted in 100% release of the drug. The ideal drug delivery system would keep the cargo intact at pH 7 and only allow for a release at lower pH values to target the areas touched by cancer.

1.4. Adjuvants – integral part of every vaccine

First vaccination procedure that was ever reported was the one performed by Edward Jenner and this was 220 years ago. He realized that people whose job was to milk cows, were not vulnerable to smallpox. Based on this observation he inoculated a boy with a cowpox and as a result this gave him immune protection against smallpox[113, 114]. Years later, it has been researched that the protection against disease can be provided by vaccination in a form of administration live-attenuated virus, inactivated virus or a vaccines. The latter was the safest way of offering a full protection, however the immune response induced was quite insignificant. Live attenuated vaccines have a live form of the pathogen that was modified so that it is in its non-virulent form, which can still multiply in the living organism without causing the full form of the disease. The immune response is very strong and the lifetime immunity to the virus can be achieved by administration of only two doses (rubella, measles)[115, 116]. However, there is a risk associated with this type of the vaccines as the pathogen can reverse to its virulent form which would pose a danger of the infection with the disease following vaccination. The other possibility is to administer the inactivated vaccine, in which the pathogen is dead and is unable to reproduce in the body as once dead, it cannot reinstate its virulence. Inactivation is realized by use of heat, radiation or

chemicals to inactivate the pathogen and it is of great importance to monitor such a process to make sure that no live strains of pathogen was left in the vaccine. As a result, such vaccines are much safer than live attenuated ones and just to name an example is Salk polio vaccine. This type, however, can only induce relatively weak immune response when compared to the former type, and in order to achieve a long-term immune protection an administration of multiple doses is necessary[117].

Subunit vaccines contain only a part from the antigen, such as sugar of a virus which would be something the immune system would respond to and record the immune event. The antigen is either modified in a chemical or mechanical way, that damages the cellular structure or by genetic engineering where the genomic material has been removed from the pathogen[118]. Administration of such a non-virulent vaccines does not cause any infection in the organism and can be given to patients with HIV or these undergoing chemotherapy. It is worth noting that subunit vaccines as well as inactivated ones, to be efficient need to paired with an adjuvant, which is a second component added to the formulation containing antigen. "Adiuvare", the verb in Latin means to help or to aid and is where the word adjuvant originates from. It was observed and then reported by Alexander Glenny nearly 100 years ago, that the antigen (toxoid) that was precipitated with aluminium potassium sulfate was able to stimulate much stronger immune response than the antigen itself and resulted in much higher number of antibodies produced[119]. This experiment was performed *"in vivo"* on guinea pigs and proved that aluminum is capable of working as a powerful adjuvant and remained for many years the only vaccine adjuvant one approved by FDA in the USA and referred as alum and by far most widely used. Its role is to enhance the immune response, by stimulating the production of the antibodies that was initially triggered by the administration of antigen and would not reach the desired threshold to be effective[120]. It has been researched that Al-containing adjuvants induce strong immune responses[121]. So far, there is no explanation to the mechanism of such action and trials are made in order to develop other adjuvants that would contain other metals, or salts like calcium phosphate, which is used in diaphtheria/pertussis/tetanus vaccines[122].

Special cells like dendritic, macrophages, B cells and T cells are involved in creating an immune response. Dendritic Cell (DC) presents antigen to T cells which activates a specific immune response that would be conveyed by a T cell (pre-programmed by DC) to this particular pathogen that the antigen came from. What happens is the following: if an antigen is detected in the body, dendritic cell will travel to the lymph node in order to present the antigen to the T cell. Activated T cells secrete cytokines and chemokines to recruit other immune cells to fight the pathogen. By monitoring the response from the stimulated DCs, we can predict how effectively DCs will activate T cells to respond to pathogen. T cells assist other cells by speeding up the process of B cell-maturation, and are called a T-helper (CD4+) and ascribed as Th. In an event of infection, the T and B cells are "naïve", meaning that they are not efficient to fight the infection and need to adapt numerous cell proliferations must occur in the body to produce a certain number of effectively working cells, which are able to produce cytokines (protein mediators) or differentiate to cells able to secrete antibody to fight the infection (B cells). The other type of T cells, CD8+ (cytotoxic T lymphocytes) will act as a warhead to destroy infected cells, as well as tumour cells. The last type of cells, important for this thesis are the B cells, which are able to produce antibodies that are specific to the pathogen.

Generally, vaccine will stimulate one or both immune responses, recognized as Th1 and Th2. Th2 is observed during cell stimulation by alum – coordination of humoral response which is responsible for production of antibodies, and very common in case of bacterial infections [123]. Th1 response is cell-mediated and follows through activation of cytokines, which is promoting viral termination. This kind of response involves mainly T cells that displays major histocompatibility complex including cells infected by pathogens, tumour cells or transplanted cells. The function of the vaccine is to create a supply of specific B and T cells with the memory to the pathogen causing a disease, but in this case without infecting the body. Th1 cells synthesise cytokines: IL-2, IL-18, IFN-γ also promote cellular defence and inflammatory response. Th2 cells secrete the cytokines: IL-4, IL-5, IL-6 and IL-13 as well as TNF-α (tumour necrosis factor). The perfect adjuvant would be able to activate T cells to give rise to Th1 and Th2

responses in order to cover a wider spectrum of immune response and hence be universal for bacterial and viral infections.

Cytokines are small proteins playing a pivotal role in signalling to the cells the state of inflammation arising from the state of infection. Cytokines term, includes interleukins, interferons, chemokines and tumour necrosis factors. These proteins are secreted by B and T cells (lymphocytes), mast cells and macrophages. It is worth noting that each cytokine may be produced by any of the cells. They are important for immune system as they regulate cell population and maturation by keeping in balance immune responses coming from humoral (Th2) and cell-mediated (Th1) immune responses. Some can influence the way other cytokines act and as such important to host immune responses to infection, inflammation and tumour cells. Just to introduce some of the cytokines, IL-2 and IL-6 are believed to treat cancer[124], IFN-α found application to treat multiple sclerosis and hepatitis C. IL-4 activates T cells into Th2 cells. TNF-α is produced mainly by macrophages and plays crucial role in regulating the immune cells, responsible for triggering inflammatory response (fever) or capable of inducing apoptotic death. The latter action is believed to give some hope in the cancer therapies[125-127].

Many materials come to interest when it comes to search after the potent adjuvant. There was some research done, dedicated to the potential usage of Zinc oxide as an adjuvant formulated in a nanoparticles form, where after 21 days after vaccination performed on mice elevated amounts of IL-17, IL-4 and IL-5 were reported[128]. Another study performed later, where nano-sized ZnO with particles smaller than 50 nm were used, confirmed these findings especially on enhanced secretion of the following cytokines: IL-2, IL-4, IL-6, IL-17, however the production of IL-10 and TNF-α decreased[129]. Also, an interesting study was performed in the 90' to investigate the role of the surface area of the materials used. This investigated SiO_2, ZrO_2, Fe-oxides (III and II+III), SnO_2, Al_2O_3. Silica was reported to promote antibody production, Aluminium and Iron oxides triggered small response and others proved to be not effective[130].

Au-nanoparticles came to interest of researchers as potential drug carriers for Pt(IV) warheads in the cancer therapy[131]. And yet as a potential candidate for novel adjuvants especially for vaccines against HIV-1 with their modified surface

[132]. These studies showed that there are some cases for which the immune response triggered is not sufficient and as research suggests the best results, to stimulate the immune response, are obtained by introducing the second adjuvant which is alum[133].

The human immune system is highly complicated and this introduction does not aim to describe it fully and the goal is to give the reader an overview to follow the concepts of this thesis. For more detailed outlook into immunology, the reader is advised to consult the textbooks[115, 134-136].

1.5. References

1. R. J. Kuppler, D. J. Timmons, Q.-R. Fang, J.-R. Li, T. A. Makal, M. D. Young, D. Yuan, D. Zhao, W. Zhuang and H.-C. Zhou, *Coordination Chemistry Reviews*, 2009, **253**, 3042-3066.
2. S. L. James, *Chemical Society Reviews*, 2003, **32**, 276-288.
3. G. Ferey, *Chemical Society Reviews*, 2008, **37**, 191-214.
4. K. M. Thomas, *Dalton transactions*, 2009, **0**, 1487-1505.
5. P. D. C. Dietzel, V. Besikiotis and R. Blom, *Journal of Materials Chemistry*, 2009, **19**, 7362-7370.
6. K. Sumida, D. L. Rogow, J. A. Mason, T. M. McDonald, E. D. Bloch, Z. R. Herm, T.-H. Bae and J. R. Long, *Chem Rev*, 2011, **112**, 724-781.
7. K. L. Mulfort and J. T. Hupp, *J Am Chem Soc*, 2007, **129**, 9604-+.
8. D. Zhao, D. Yuan and H.-C. Zhou, *Energy & Environmental Science*, 2008, **1**, 222-235.
9. R. E. Morris and P. S. Wheatley, *Angew Chem Int Edit*, 2008, **47**, 4966-4981.
10. S. Ma and H.-C. Zhou, *Chem. Commun.*, 2010, **46**, 44-53.
11. L. J. Murray, M. Dinca and J. R. Long, *Chemical Society Reviews*, 2009, **38**, 1294-1314.
12. J.-R. Li, J. Sculley and H.-C. Zhou, *Chem Rev*, 2011, **112**, 869-932.
13. J. Lee, O. K. Farha, J. Roberts, K. A. Scheidt, S. T. Nguyen and J. T. Hupp, *Chemical Society Reviews*, 2009, **38**, 1450-1459.
14. A. Henschel, K. Gedrich, R. Kraehnert and S. Kaskel, *Chem. Commun.*, 2008, **0**, 4192-4194.
15. A. Corma, H. García and F. X. Llabrés i Xamena, *Chem Rev*, 2010, **110**, 4606-4655.
16. M. Kurmoo, *Chemical Society Reviews*, 2009, **38**, 1353-1379.
17. K. M. L. Taylor, W. J. Rieter and W. Lin, *J Am Chem Soc*, 2008, **130**, 14358-14359.
18. K. M. L. Taylor-Pashow, J. D. Rocca, Z. Xie, S. Tran and W. Lin, *J Am Chem Soc*, 2009, **131**, 14261-14263.

19. M. D. Allendorf, C. A. Bauer, R. K. Bhakta and R. J. T. Houk, *Chemical Society Reviews*, 2009, **38**, 1330-1352.
20. P. Horcajada, R. Gref, T. Baati, P. K. Allan, G. Maurin, P. Couvreur, G. Ferey, R. E. Morris and C. Serre, *Chem Rev*, 2012, **112**, 1232-1268.
21. R. C. Huxford, J. Della Rocca and W. Lin, *Current Opinion in Chemical Biology*, 2010, **14**, 262-268.
22. P. Horcajada, C. Serre, M. Vallet-Regí, M. Sebban, F. Taulelle and G. Férey, *Angewandte Chemie*, 2006, **118**, 5974-5978.
23. A. C. McKinlay, R. E. Morris, P. Horcajada, G. Ferey, R. Gref, P. Couvreur and C. Serre, *Angew Chem Int Ed Engl*, 2010, **49**, 6260-6266.
24. A. C. McKinlay, B. Xiao, D. S. Wragg, P. S. Wheatley, I. L. Megson and R. E. Morris, *J Am Chem Soc*, 2008, **130**, 10440-10444.
25. C.-D. Wu and W. Lin, *Angewandte Chemie International Edition*, 2005, **44**, 1958-1961.
26. P. Horcajada, F. Salles, S. Wuttke, T. Devic, D. Heurtaux, G. Maurin, A. Vimont, M. Daturi, O. David, E. Magnier, N. Stock, Y. Filinchuk, D. Popov, C. Riekel, G. Férey and C. Serre, *J Am Chem Soc*, 2011, **133**, 17839-17847.
27. D. Farrusseng, *Metal-Organic Frameworks: Applications from Catalysis and Gas Storage*, Wiley-VCH Verlag GmbH & Co. KGaA, 2011.
28. L. Öhrström, *RSC Publishing CrystEngComm Blog*, 2013.
29. P. Wood, *Highly Holey: MOFs with Record-Breaking Surface Areas*, 2013.
30. S. Keskin and S. Kizilel, *Ind Eng Chem Res*, 2011, **50**, 1799-1812.
31. B. F. Hoskins and R. Robson, *J Am Chem Soc*, 1989, **111**, 5962-5964.
32. C. Serre, F. Millange, C. Thouvenot, M. Noguès, G. Marsolier, D. Louër and G. Férey, *J Am Chem Soc*, 2002, **124**, 13519-13526.
33. P. Horcajada, C. Serre, G. Maurin, N. A. Ramsahye, F. Balas, M. Vallet-Regi, M. Sebban, F. Taulelle and G. Ferey, *J Am Chem Soc*, 2008, **130**, 6774-6780.
34. H. Furukawa, Y. B. Go, N. Ko, Y. K. Park, F. J. Uribe-Romo, J. Kim, M. O'Keeffe and O. M. Yaghi, *Inorganic Chemistry*, 2011, **50**, 9147-9152.

35. P. K. Allan, P. S. Wheatley, D. Aldous, M. I. Mohideen, C. Tang, J. A. Hriljac, I. L. Megson, K. W. Chapman, G. De Weireld, S. Vaesen and R. E. Morris, *Dalton transactions*, 2012, **41**, 4060-4066.
36. H. Furukawa, N. Ko, Y. B. Go, N. Aratani, S. B. Choi, E. Choi, A. O. Yazaydin, R. Q. Snurr, M. O'Keeffe, J. Kim and O. M. Yaghi, *Science*, 2010, **329**, 424-428.
37. M. Eddaoudi, J. Kim, N. Rosi, D. Vodak, J. Wachter, M. O'Keeffe and O. M. Yaghi, *Science*, 2002, **295**, 469-472.
38. H. Furukawa, K. E. Cordova, M. O'Keeffe and O. M. Yaghi, *Science*, 2013, **341**.
39. T. Chalati, P. Horcajada, R. Gref, P. Couvreur and C. Serre, *Journal of Materials Chemistry*, 2011, **21**, 2220-2227.
40. G. Férey, C. Serre, C. Mellot-Draznieks, F. Millange, S. Surblé, J. Dutour and I. Margiolaki, *Angewandte Chemie International Edition*, 2004, **43**, 6296-6301.
41. N. J. Hinks, A. C. McKinlay, B. Xiao, P. S. Wheatley and R. E. Morris, *Micropor Mesopor Mat*, 2010, **129**, 330-334.
42. S. R. Miller, D. Heurtaux, T. Baati, P. Horcajada, J.-M. Greneche and C. Serre, *Chem. Commun.*, 2010, **46**, 4526-4528.
43. R. Batten Stuart, R. Champness Neil, X.-M. Chen, J. Garcia-Martinez, S. Kitagawa, L. Öhrström, M. O'Keeffe, M. Paik Suh and J. Reedijk, in *Pure Appl Chem*, 2013, vol. 85, p. 1715.
44. J. J. Perry Iv, J. A. Perman and M. J. Zaworotko, *Chemical Society Reviews*, 2009, **38**, 1400-1417.
45. S. Huerta, S. Chilka and B. Bonavida, *International Journal of Oncology*, 2008, **33**, 909-927.
46. P. K. Allan, Chemistry, University of St Andrews, Thesis, 2012.
47. G. A. Blaise, D. Gauvin, M. Gangal and S. Authier, *Toxicology*, 2005, **208**, 177-192.
48. F. Murad, *Angewandte Chemie International Edition*, 1999, **38**, 1856-1868.

49. R. N. Anthony R Butler, *Life, Death and Nitric Oxide*, The Royal Society of Chemistry, 2003.
50. M. R. Miller and I. L. Megson, *British Journal of Pharmacology*, 2007, **151**, 305-321.
51. H. Zhu, B. Ka and F. Murad, *World J. Surg.*, 2007, **31**, 624-631.
52. K. D. Kroncke and C. V. Suschek, *Journal of Investigative Dermatology*, 2008, **128**, 258-260.
53. P. S. Wheatley, A. R. Butler, M. S. Crane, S. Fox, B. Xiao, A. G. Rossi, I. L. Megson and R. E. Morris, *J Am Chem Soc*, 2006, **128**, 502-509.
54. J. H. Shin and M. H. Schoenfisch, *Chemistry of Materials*, 2007, **20**, 239-249.
55. R. Haag and F. Kratz, *Angewandte Chemie International Edition*, 2006, **45**, 1198-1215.
56. F. DeRosa, M. R. Kibbe, S. F. Najjar, M. L. Citro, L. K. Keefer and J. A. Hrabie, *J Am Chem Soc*, 2007, **129**, 3786-3787.
57. B. Xiao, P. S. Wheatley, X. B. Zhao, A. J. Fletcher, S. Fox, A. G. Rossi, I. L. Megson, S. Bordiga, L. Regli, K. M. Thomas and R. E. Morris, *J Am Chem Soc*, 2007, **129**, 1203-1209.
58. J. R. Hickok and D. D. Thomas, *Current pharmaceutical design*, 2010, **16**, 381-391.
59. B. Brune, *Cell Death Differ*, 2003, **10**, 864-869.
60. S. Moncada and A. Higgs *New England Journal of Medicine*, 1993, **329**, 2002-2012.
61. K. D. Kröncke, K. Fehsel and V. Kolb-Bachofen, *Clinical and Experimental Immunology*, 1998, **113**, 147-156.
62. C. Nathan, *The Journal of Clinical Investigation*, **100**, 2417-2423.
63. S. Duan, S. Cai, Q. Yang and M. L. Forrest, *Biomaterials*, 2012, **33**, 3243-3253.
64. S. P. Hussain, G. E. Trivers, L. J. Hofseth, P. He, I. Shaikh, L. E. Mechanic, S. Doja, W. Jiang, J. Subleski, L. Shorts, D. Haines, V. E. Laubach, R. H. Wiltrout, D. Djurickovic and C. C. Harris, *Cancer Research*, 2004, **64**, 6849-6853.

65. D. Wei, E. L. Richardson, K. Zhu, L. Wang, X. Le, Y. He, S. Huang and K. Xie, *Cancer Research*, 2003, **63**, 3855-3859.
66. X. Le, D. Wei, S. Huang, J. R. Lancaster and K. Xie, *Proceedings of the National Academy of Sciences of the United States of America*, 2005, **102**, 8758-8763.
67. C. Vilos and L. A. Velasquez, *Journal of Biomedicine and Biotechnology*, 2012.
68. S. Gaisford and M. Saunders, in *Essentials of Pharmaceutical Preformulation*, John Wiley & Sons, Ltd, 2012, pp. 1-35.
69. S. H. van Rijt and P. J. Sadler, *Drug discovery today*, 2009, **14**, 1089-1097.
70. E. Zhang, C. Zhang, Y. Su, T. Cheng and C. Shi, *Drug discovery today*, 2011, **16**, 140-146.
71. R. Moreno-Sánchez, E. Saavedra, S. Rodríguez-Enríquez, J. C. Gallardo-Pérez, H. Quezada and H. V. Westerhoff, *Mitochondrion*, 2010, **10**, 626-639.
72. M. Ferrari, *Nat Rev Cancer*, 2005, **5**, 161-171.
73. W. R. Sanhai, J. H. Sakamoto, R. Canady and M. Ferrari, *Nat Nano*, 2008, **3**, 242-244.
74. E. R. Jamieson and S. J. Lippard, *Chem Rev*, 1999, **99**, 2467-2498.
75. S. V. Devi and T. Prakash, *Ieee Transactions on Nanobioscience*, 2013, **12**, 60-63.
76. H. Deng, S. Grunder, K. E. Cordova, C. Valente, H. Furukawa, M. Hmadeh, F. Gándara, A. C. Whalley, Z. Liu, S. Asahina, H. Kazumori, M. O'Keeffe, O. Terasaki, J. F. Stoddart and O. M. Yaghi, *Science*, 2012, **336**, 1018-1023.
77. O. K. Farha, I. Eryazici, N. C. Jeong, B. G. Hauser, C. E. Wilmer, A. A. Sarjeant, R. Q. Snurr, S. T. Nguyen, A. Ö. Yazaydın and J. T. Hupp, *J Am Chem Soc*, 2012, **134**, 15016-15021.
78. H. Furukawa, N. Ko, Y. B. Go, N. Aratani, S. B. Choi, E. Choi, A. Ö. Yazaydin, R. Q. Snurr, M. O'Keeffe, J. Kim and O. M. Yaghi, *Science*, 2010, **329**, 424-428.

79. P. Horcajada, T. Chalati, C. Serre, B. Gillet, C. Sebrie, T. Baati, J. F. Eubank, D. Heurtaux, P. Clayette, C. Kreuz, J. S. Chang, Y. K. Hwang, V. Marsaud, P. N. Bories, L. Cynober, S. Gil, G. Ferey, P. Couvreur and R. Gref, *Nature Materials*, 2010, **9**, 172-178.

80. J. Y. Lu and A. M. Babb, *Inorganic Chemistry Communications*, 2001, **4**, 716-718.

81. H. P. Rang, J. M. Ritter, R. J. Flower and G. Henderson, *Rang & Dale's Pharmacology*, 8th edn., Churchill Livingstone.

82. M. H. Greene, *J Natl Cancer Inst*, 1992, **84**, 306-312.

83. O. Rixe, W. Ortuzar, M. Alvarez, R. Parker, E. Reed, K. Paull and T. Fojo, *Biochemical Pharmacology*, 1996, **52**, 1855-1865.

84. W. H. Ang, S. Pilet, R. Scopelliti, F. Bussy, L. Juillerat-Jeanneret and P. J. Dyson, *Journal of Medicinal Chemistry*, 2005, **48**, 8060-8069.

85. D. Gibson, *Dalton transactions*, 2009, 10681-10689.

86. P. G. Rose, B. N. Bundy, E. B. Watkins, J. T. Thigpen, G. Deppe, M. A. Maiman, D. L. Clarke-Pearson and S. Insalaco, *New England Journal of Medicine*, 1999, **340**, 1144-1153.

87. A. Diaz, M. L. Gonzalez, R. J. Perez, A. David, A. Mukherjee, A. Baez, A. Clearfield and J. L. Colon, *Nanoscale*, 2013, **5**, 11456-11463.

88. H. Xiao, L. Yan, Y. Zhang, R. Qi, W. Li, R. Wang, S. Liu, Y. Huang, Y. Li and X. Jing, *Chem. Commun.*, 2012, **48**, 10730-10732.

89. R. Wang, H. Xiao, H. Song, Y. Zhang, X. Hu, Z. Xie, Y. Huang, X. Jing and Y. Li, *Journal of Materials Chemistry*, 2012, **22**, 25453-25462.

90. D. D. Fernandes, M. L. Louzada, C. A. Souza and F. Matzinger, *Current Oncology*, 2011, **18**, 97-100.

91. T. Proverbs-Singh, S. K. Chiu, Z. Liu, S. Seng, G. Sonpavde, T. K. Choueiri, C.-K. Tsao, M. Yu, N. M. Hahn, W. K. Oh and M. D. Galsky, *Journal of the National Cancer Institute*, 2012.

92. V. Pinzani, F. Bressolle, I. Johanne Haug, M. Galtier, J. Blayac and P. Balmès, *Cancer Chemother Pharmacol*, 1994, **35**, 1-9.

93. Z. H. Siddik, D. R. Newell, F. E. Boxall and K. R. Harrap, *Biochemical Pharmacology*, 1987, **36**, 1925-1932.

94. A. H. Tamsyn and M. H. James, *Nanotechnology*, 2007, **18**, 275704.

95. J. Yang, W. Mao, M. Sui, J. Tang and Y. Shen, *Journal of Controlled Release*, 2011, **152**, E108-E109.

96. H. Song, H. Xiao, Y. Zhang, H. Cai, R. Wang, Y. Zheng, Y. Huang, Y. Li, Z. Xie, T. Liu and X. Jing, *Journal of Materials Chemistry B*, 2013, **1**, 762-772.

97. A. Samad, Y. Sultana and M. Aqil, *Current Drug Delivery*, 2007, **4**, 297-305.

98. E. A. Leite, C. M. Souza, A. D. Carvalho-Junior, L. G. V. Coelho, A. M. Q. Lana, G. D. Cassali and M. C. Oliveira, *International Journal of Nanomedicine*, 2012, **7**, 5259-5269.

99. H. Chen, S. Pazicni, N. L. Krett, R. W. Ahn, J. E. Penner-Hahn, S. T. Rosen and T. V. O'Halloran, *Angewandte Chemie International Edition*, 2009, **48**, 9295-9299.

100. H. Xiao, R. Qi, S. Liu, X. Hu, T. Duan, Y. Zheng, Y. Huang and X. Jing, *Biomaterials*, 2011, **32**, 7732-7739.

101. Y.-I. Jeong, S.-T. Kim, S.-G. Jin, H.-H. Ryu, Y.-H. Jin, T.-Y. Jung, I.-Y. Kim and S. Jung, *Journal of Pharmaceutical Sciences*, 2008, **97**, 1268-1276.

102. C.-Y. Sun, C. Qin, X.-L. Wang and Z.-M. Su, *Expert Opinion on Drug Delivery*, 2013, **10**, 89-101.

103. W. J. Rieter, K. M. Pott, K. M. L. Taylor and W. Lin, *J Am Chem Soc*, 2008, **130**, 11584-11585.

104. C. X. Zhang and S. J. Lippard, *Current Opinion in Chemical Biology*, 2003, **7**, 481-489.

105. P. a. Ma, H. Xiao, X. Li, C. Li, Y. Dai, Z. Cheng, X. Jing and J. Lin, *Advanced Materials*, 2013, n/a-n/a.

106. C. Heidelberger, N. K. Chaudhuri, P. Danneberg, D. Mooren, L. Griesbach, R. Duschinsky, R. J. Schnitzer, E. Pleven and J. Scheiner, *Nature*, 1957, **179**, 663-666.

107. P. Li, Y. Wang, Z. Peng, F. She and L. Kong, *Carbohydrate Polymers*, 2011, **85**, 698-704.

108. D. B. Longley, D. P. Harkin and P. G. Johnston, *Nat Rev Cancer*, 2003, **3**, 330-338.
109. P. J. Ross, A. Webb, D. Cunningham, J. Prendiville, A. R. Norman and J. Oates, *Annals of Oncology*, 1997, **8**, 111-115.
110. Y. Zhu, Y. Wang, P. Liu, Y. Wu, W. Wei, C. Xia and J. Xie, *New Journal of Chemistry*, 2015.
111. R. A. Al-Thawabeia and H. A. Hodali, *Journal of Chemistry*, 2015, **2015**, 9.
112. U. E. Illangakoon, D.-G. Yu, B. S. Ahmad, N. P. Chatterton and G. R. Williams, *International Journal of Pharmaceutics*, 2015, **495**, 895-902.
113. M. Kool, K. Fierens and B. N. Lambrecht, *Journal of Medical Microbiology*, 2012, **61**, 927-934.
114. E. Jenner, *Harvard Classics*, 1909-14, **38**.
115. A. Clem, *Fundamentals of vaccine immunology*, 2011.
116. S. Dhillon and M. P. Curran, *Pediatric Drugs*, 2008, **10**, 337-347.
117. N. I. o. A. a. I. Diseases, *NIAID Types of vaccines*, https://www.niaid.nih.gov/topics/vaccines/Pages/typesVaccines.aspx.
118. P. M. Moyle and I. Toth, *ChemMedChem*, 2013, **8**, 360-376.
119. A. T. Glenny, C. G. Pope, H. Waddington and U. Wallace, *The Journal of Pathology and Bacteriology*, 1926, **29**, 31-40.
120. S. Calabro, M. Tortoli, B. C. Baudner, A. Pacitto, M. Cortese, D. T. O'Hagan, E. De Gregorio, A. Seubert and A. Wack, *Vaccine*, 2011, **29**, 1812-1823.
121. V. E. J. C. Schijns and E. C. Lavelle, *Expert Review of Vaccines*, 2011, **10**, 539-550.
122. N. Goto, H. Kato, J.-i. Maeyama, M. Shibano, T. Saito, J. Yamaguchi and S. Yoshihara, *Vaccine*, 1997, **15**, 1364-1371.
123. K. Murphy, *Janeway's Immunology*, Garland Science, 2011.
124. M. Rincon, *Trends in Immunology*, 2012, **33**, 571-577.
125. K. L. Honda, S. Lamon-Fava, N. R. Matthan, D. Wu and A. H. Lichtenstein, *Prostaglandins, Leukotrienes and Essential Fatty Acids (PLEFA)*, 2015, **97**, 27-34.

126. J. Zhao and M. W. Lawless, *Cytokine*, 2013, **64**, 626-637.
127. A. Macciò and C. Madeddu, *Cytokine*, 2012, **58**, 133-147.
128. M. Matsumura, M. Nagata, K. Nakamura, M. Kawai, T. Baba, K. Yamaki and S. Yoshino, *Immunopharmacology and Immunotoxicology*, 2010, **32**, 56-62.
129. R. Roy, S. Kumar, A. K. Verma, A. Sharma, B. P. Chaudhari, A. Tripathi, M. Das and P. D. Dwivedi, *International Immunology*, 2014, **26**, 159-172.
130. J. O. Naim, C. J. van Oss, W. Wu, R. F. Giese and P. A. Nickerson, *Vaccine*, 1997, **15**, 1183-1193.
131. S. Dhar, W. L. Daniel, D. A. Giljohann, C. A. Mirkin and S. J. Lippard, *J Am Chem Soc*, 2009, **131**, 14652-14653.
132. L. Xu, Y. Liu, Z. Chen, W. Li, Y. Liu, L. Wang, Y. Liu, X. Wu, Y. Ji, Y. Zhao, L. Ma, Y. Shao and C. Chen, *Nano Letters*, 2012, **12**, 2003-2012.
133. S. Parween, P. K. Gupta and V. S. Chauhan, *Vaccine*, 2011, **29**, 2451-2460.
134. M. G. A. J;, *Exploring Immunology: Concepts and Evidence* Wiley, 2012.
135. W. E. Paul, *Fundamental Immunology*, 7th edn., Lippincott Williams and Wilkins, 2012.
136. *Principles of Immunopharmacology*, 3rd edn., 2011.

Chapter 2. Aims

The main objective of this thesis was to research and investigate the potential applications of MOFs as drug delivery carriers for anticancer drugs: cisplatin and 5-Fluorouracil (5-FU). The potential double-functionality will be looked into, obtained thanks to NO (nitric oxide) loading, as the former has shown to play an important role in the human organism particularly its beneficial anti-cancer, anti-thrombotic and anti-microbial properties. It is important for anti-cancer therapies in which the treatment may suppress immune system and an extra anti-bacterial protection is crucial.

Also, this thesis will investigate several MOFs for their potential to be candidates for its use as adjuvants in novel vaccines, replacing "alum" that is commonly used in today's vaccination formulations.

The aim of this project was to synthesise MOFs which would be non-toxic to cells and able to allow for drug encapsulation or incorporation and its release in the in-vitro conditions for possible use in medicinal applications.

In the context of anti-cancer drug delivery systems research project, MOFs were chosen on the basis of their bio-compatibility, pore sizes and the availability of the functional groups to allow for incorporation of selected drugs: cisplatin and 5FU.

In terms of the selection of MOFs for candidates for adjuvants, these were selected due to the bio-compatibility criteria as well as their porosity and in the first instance the MOFs containing Al-metal were given preference as their composition be closely related to alum. In the second instance, the search would expand for MOFs with other metal centres. It is worth noting that till now the mechanism of action for alum is unknown which makes research for novel vaccines challenging.

Each chapter of the thesis gives the aims separately, to help the reader to follow the thesis.

Chapter 3 contains Experimental Section, where the experimental methods used in this thesis are described. Chapter 4 focuses on MOFs as drug carriers for cisplatin encapsulation or incorporation in the framework and viability studies of such drug carriers. Chapter 5 describes the investigations made into variety of routes to

successfully encapsulate Fluorouracil, its release up to the viability and cytotoxicity studies. Chapter 6 investigates the potential application for MOFs as adjuvants in the novel vaccines with necessary biological testing to assess the immune response signals triggered in the macrophages and dendritic cells by their stimulation with a selection of MOFs (Al- and Zr-MOFs). Chapter 7 describes the research that was conducted in order to synthesise the multifunctional drug carrier systems, capable to perform drug delivery of the anti-cancer drug coupled with the release of nitric oxide. Chapter 8 gives some indications into the future work that could follow up the investigations for medical applications of MOFs conducted in this thesis.

Appendix 1 contains the cell parameters refinements performed in CELCheck program and Appendix 2, the x-ray patterns of the Al-MOFs synthesised to test their immune response properties. It also contains the x-ray patterns from the CIF files (simulated patterns).

Chapter 3. Experimental Methods

3.1 Solvothermal and Microwave-assisted synthesis

Both methods allow to synthesise solid material. These are often crystalline materials if the conditions for crystal growth are met, which is the case for solvothermal synthesis performed in an autoclave. Such an approach gives more adjustable parameters like heating and cooling rate, dwelling time etc. that can be refined in much better way than during microwave (MW) – assisted route. The advantage of MW – assisted approach is its speed. Microwave radiation can significantly speed up reactions, and so while the control present in solvothermal is lost, the advantage of speed can compensate. For obvious reasons obtaining a crystalline material is the goal of the synthesis. If an unknown structures are predicted to result, the obtained single crystal diffraction would allow to solve this structure (that is determining its unit cell, crystal symmetry and atom coordinates). Both methods can be used to prepare single crystals or at the very least, crystalline powders.

The principle of the solvothermal synthesis method is as follows: the reagents are mixed in solvents and then heated above their normal boiling point in a closed autoclave that can withstand high pressure. The viscosity of the solvent decreases under such conditions that leads to faster mass transfer and promotes diffusion according to Fick's law. This opens up the possibility to synthesise quite a huge number of materials which would not emerge in normal conditions. The routine step is to pre-weigh a desired amount of reactant, dissolve it in the solvent (or partially) and place in a Teflon-lined autoclave which is then placed in a stainless steel paar-bomb in an oven at the desired temperature for a chosen period of time usually being a matter of hours or days. Over the recent years microwave heating has become popular due to its dramatically improved reaction times allowing to achieve results from normally time-consuming reactions, in a much shorter time. The method is based on the fact that high dielectric momentum of the polar solvents leads to locally superheated spots thanks to the efficient thermal conversion of energy resulting in fast and homogenous nucleation preferred over

the crystal growth. This method will be often used for the synthesis of biocompatible MOFs of MIL series (MIL-53, MIL-100, MIL-88A, MIL 101-NH_2)[1]. Nevertheless, this synthesis route is not best choice if a single crystal is the goal as it yields only very fine powder solids, also the equipment is quite expensive as a flow set-up and scale-up only possible if a microwave with a big vessel is in operation. This method was useful for investigations the influence of the reaction times on the material structure, and by far the best for a quick-synthesis[2].

3.2 X-ray diffraction

The crystal structure is unique for every substance and this feature gives a wide window to characterise and then identify the materials. To define the crystal structure, the smallest building unit, with the lattice parameters: length of the edges (a, b, c) and the angles between them is necessary to be determined. This unit is called the unit cell. The unit cell is the smallest unit in the crystal that contains all the symmetry elements of that structure and through translational symmetry the structure of the crystal can be obtained. The unit is defined by 3 non-planar axis a, b, c and 3 angles α, β and γ (Figure 3-1).

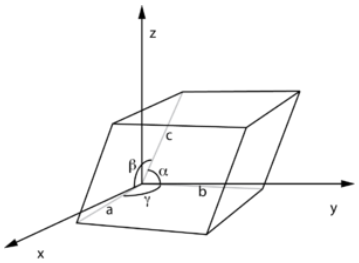

Figure 3-1 A unit cell, edges a, b and c, and angles α, β and γ.

If we added to it the symmetry of the cell then the outcome of such an operation would be the Bravais unit cell which describes the geometric arrangement of the lattice points. There are four arrangements possible: P-primitive, C-base centred, F-face-centred and I-body centred. If we repeated the unit cell in all directions, a crystal lattice will be formed. There are 7 crystallographic systems and 14 Bravais unit cells. The powder x-ray diffraction method allows for determination of the crystallinity of the material and then describes its structural properties of the sample such as inter and intra-molecular distances and the atom distribution in the

unit cell. This will lead to structure solution if single crystal material is available. If the crystals are small, a synchrotron X-rays are required to record the X-ray reflections and this will be used for solving the structure. X-rays, which are electromagnetic waves, can interact with the electrons in the specimen and the diffraction will only take place if the wavelength of the X-ray is of approximately the same size as the object they diffract on. The X-ray detector records the intensity of the X-rays being scattered by the electrons in atoms. The picture below explains what happens when X-rays are incident on a sample.

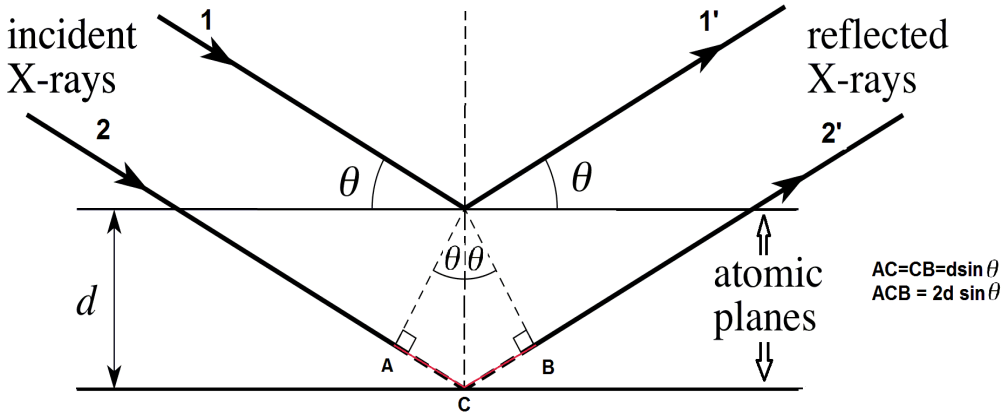

Figure 3-2 Depiction of Bragg's law[3].

X-rays are scattered by the electrons in the atoms. Figure 3-2 shows two planes of atoms that are separated by a distance d. If we consider X-ray beam numbers 1 and 2 that came in from the X-ray source, they are scattered (reflected) by the atoms to produce the diffracted beams 1' and 2'. If beams 1' and 2' are in phase there will be constructive interference and a detector will measure a large intensity. If 1' and 2' are out of phase then there will be a destructive interference and the detector will measure nothing. The condition for destructive interference is that the distance travelled by 1' and 2' must be related by a half of whole number of wavelengths, this happens when two waves are a half cycle out of phase. For example, in Figure 3-2 beam 2' travels further than 1' by a distance equal to AC+BC. Simple trigonometry means that AC+CB =2d sinθ. For constructive interference this distance must be a whole number of wavelengths giving $n\lambda = 2d \sin\theta$, this is achieved when two waves are in phase. The second beam will travel longer because the path is longer AC+CB. If Pythagorean Theorem is applied, the path can be expressed in lattice parameters d and the incident angle as diffraction angle θ in the equation (3-1).

$$AC+CB = 2d\sin\theta = n\lambda \qquad (3\text{-}1)$$

The distance AC+CB is called the path difference and must be equal, for in-phase interactions are allowed, to the wavelength (λ) multiplied by integer (n). The diffraction is described by Bragg's law: $n\lambda=2d\sin\theta$.

3.3 Microwave-Plasma – Atomic Emission Spectroscopy (MP-AES)

A liquid sample is exposed to high energy generated by microwave plasma (MP) in order to excite electrons in atoms into excited electronic states (Figure 3-3). These can then return to a lower energy state emitting energy at a characteristic set of wavelengths corresponding to the energy difference between the two levels. The portion of energy (quantum) depends on the electronic structure of that element. During the decay, photons can only transit from a high energy state to a low energy state emitting permitted wavelength and the detection of this emitted energy leads to elements' identification - both qualitatively and quantitatively. The sample is injected into the nebuliser and then sprayed in the microwave plasma chamber where electrons of the element will be excited to higher energy levels.

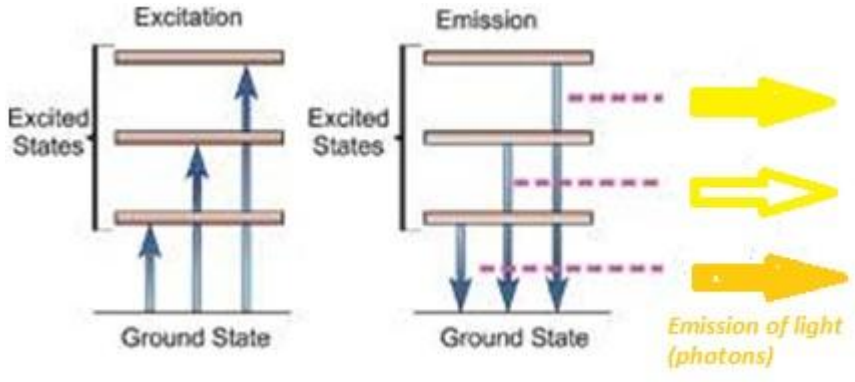

Figure 3-3 Excitation of electrons (ground state) in the atom to the excited electronic levels and the emission of the photons in a form of light (permitted wavelengths).

The MP-AES and ICP-AES (Inductively coupled plasma atomic emission spectroscopy) techniques were used to quantify the amounts of platinum encapsulated in MOF powders as well as the amounts released over time (MP-AES). The wavelength of the emission spectrum of Pt was chosen to be λ = 265.945 nm line because of its high intensity[4]. This wavelength corresponds to

emission of a quantum of energy by a photon returning from its excited state $[Xe]6s^0 4f^{14} 5d^9 6p^1$ to the ground state $[Xe]6s^1 4f^{14} 5d^9$. The orbital energy diagram for Pt atom is depicted in Figure 3-4 below.

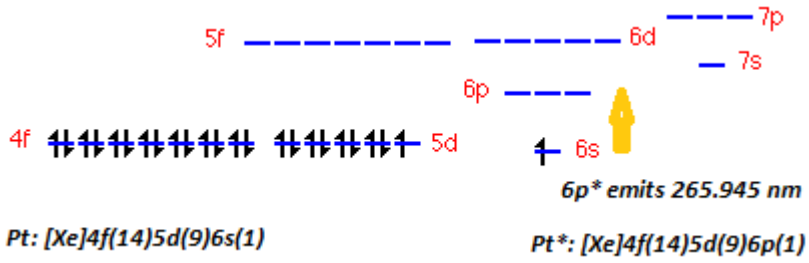

Figure 3-4 Orbital energy diagram for an Pt atom in a ground state before its excitation to $6p^1$ and the following emission of quant of energy.

In the experiments Agilent MP4100 microwave plasma – atomic emission spectrometer was used. The instrument is supplied with nitrogen from a nitrogen generator and synthetic air would only be used for an equipment start-up, making the technique more affordable than ICP, where Argon of high purity is used (min. 99.999%).

3.4. High Performance Liquid Chromatography (HPLC)

HPLC is the most broadly used analytical method in the pharmaceutical sector as it allows the separation of almost any compounds in a mixture, excluding solids. The technique is not an assay on it is own but only separates substances that can be then measured via a detector that must be carefully chosen depending on the property of the compound that will be used for characterisation (mass spectrometric, fluorescent or UV). The method relies on the fact that molecules have different retention times when they travel through different mobile phases. Here, a sample that is in a liquid form (Gas Chromatography deals with a gaseous phase) is transported in a mobile phase through a column which in this case is the stationary phase.

The analyte that is injected in the mobile phase is pumped through the column at high pressure (ca. 6000 psi = 43MPa)[5]. The retention time can be altered depending on their affinity to mobile phase, and how fast the compounds can be eluted too, high affinity of the analyte to the stationary phase is not recommended as it will make the separation impossible and will poison the column (blockage).

High-performance liquid chromatography is often used in chemical and pharmaceutical laboratories in order to separate and determine the quantities of species in a variety of materials. It uses two phases, one which is mobile and a stationary phase that is finely divided. In its humble beginnings, the method would only use solid particles as a column packing material and these were larger than 150-200 μm in order to keep the flow rate at the reasonable level. The goal of the optimisation is to separate each of the compounds in the analyte mixture giving one clear peak for each. Once the two phases are optimally selected then the separation of the species of the sample contents into the bands can be seen, with the retention times allowing for their characterization and quantity determination. The most important part of the instrument is a column and once this is damaged the measurements cannot be completed[6]. Only in the 1960' much smaller diameters of packings 3-10 μm were used, this however, required elevated pressures (200-800 atmospheres) and thus an application of a pump[7]. The purity of solvents used as a mobile phase is paramount in obtaining reliable results due to polar impurities and H_2O may seriously damage the column, also UV-absorbing impurities may lead to erroneous results when using UV-detectors[8]. The quantification method (reverse-phase HPLC) to detect 5-Fluorouracil (5-FU), was developed by Upulitha Illangakoon and performed using an Agilent 1260 Infinity instrument (Agilent Technologies) under isocratic conditions (the mobile phase consisted of 80% v/v methanol and 20% v/v acetic acid) with C18 column (00G-4326-60, Phenomenex, silica gel beads of size 3, 5, 10 μm, Pore size 100 Å, surface area 440 m^2/g, carbon load 19 %). During the measurements temperature of the column was set to 40°C, and the flow rate 1 mL/min with sample injection quantity of 10 μL for each sample and chromatograms were recorded for 10 min with UV detection at the wavelength of 266 nm, which is where the 5-FU maximum of absorption falls.

Retention time for 5-FU is ca. 3 min, however due to stabilisation of the instrument the longer run-time was required.

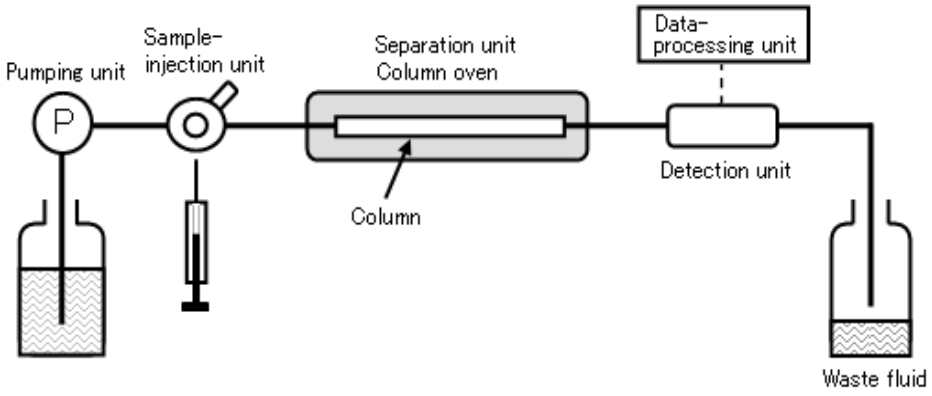

Figure 3-5 Schematic depiction of HPLC functionality

3.5 Biological Assays

3.5.1 Flow Cytometry

Apoptosis/ Necrosis and viability

The method of flow cytometry was first patented in 1953 by Mack Fulwyler[9], and is widely used for cell counting or detecting the biomarkers by measuring the fluorescence signal rising from the excited states of the organic dyes that the cells in question are labelled with. The suspended cells are passed through a nozzle that is flushed with a sheath fluid and then as they go through one by one, a laser beam is then scattered by the passing cells. The scattered light is detected by detectors and on this principle the cells are counted. The laser beam can excite the fluorescent dye on the stained cell that will emit a certain amount of energy in a form of fluorescence at a given wavelength that can be quantified by a fluorescence detector and analysed. The emitted photons are collected by sensors, the fluorescent light is filtered so each of the sensors catches only the specific wavelength. There are some channels able to detect wavelengths characteristic to fluorescence of organic dyes, these are FITC (Fluorescein isothiocyanate - a derivative of fluorescein functionalized with an isothiocyanate reactive group (N=C=S)) at 519 nm, PE (Phycoerythrin – a red protein-pigment, fluorochrome) at 575 nm and TR (Texas Red - fluorophore) at 620 nm. Fluorescence-activated cell sorting (FACS) is a special type of flow cytometry, the method was broadly developed by Len Herzenberg[10]. It provides a method for sorting a heterogeneous mixture of cells, that contains useful information to analyse the cell size and

volume. The method allows one to measure the intensity of fluorescence that arises from cell surface protein – specific monoclonal antibodies that were labelled with fluorescent dyes[11]. As such, it is quite complicated and time – consuming method, used for screening cancer cells. In the research presented in this thesis the FACS method was applied to set up a viability assay to determine apoptotic and necrotic death and the % of live cells. By labelling of cells with FITC-Annexin V, which is a biomarker for early apoptosis (a protein with a directly conjugated fluorochrome), it was possible to measure the signal on the detector. Apoptosis and necrosis are two types of cell death, the former is the programmed cell death. Cells that undergo apoptosis have their membranes changed and do not show phospholipid asymmetry that is the case for a normal cell. The human anticoagulant protein like Annexin V can bind to phospholipids in the environment rich in calcium. This can be used for determination of number of cells that are early apoptotic. At the same time using positively charged nucleic acid probe Ethidium homodimer III, the staining of necrotic cells can be realised[12]. The membrane of the live cells does not allow for binding to either of the proteins and as such offers a straight forward way of analysing live, necrotic and apoptotic cells. The cells stained with both dyes are considered and count as late apoptotic ones. This is a very important principle for anti-cancer drug delivery systems and studies of their efficacy, as not only it is important to measure viability but also the nature of the cell death because the mechanism of action should aim to induce apoptosis. Necrotic death leads to cell bursting that may contaminate other cells with the cancerous genetic material[13].

In addition, the method allows one to measure the signal on the receptors on the dendritic cells in order to assess the immune response induced by application of different stimulants, and in this research project is broadly used to verify the potential candidates for new adjuvants for novel vaccines[14].

The kit for Apoptosis/Necrosis was bought from Biotum and contained FITC-Annexin V biomarker, Ethidium Homodimer and Annexin Binding Buffer. Phosphatidylserine (PS) is translocated from the inner to the outer surface of the cell during apoptosis, which allows the dying cell to be surrounded by phagocytic cells. These cells are to protect the body by removing any harmful objects like

bacteria or dead or dying cells digesting them. Biomarker Annexin V is a Ca^{2+} - dependent phospholipid binding protein with high affinity to PS and it is labelled with fluorescein FITC (EX/EM 492/514 nm), which stains PS on the surface of apoptotic cells. Ethidium Homodimer III is a positively charge nucleic acid stain that does not show any fluorescence until bound to DNA, then it emits a fluorescence (EX/EM 528/617). It does not bind to the live or early apoptotic cells and thus stains only necrotic or late apoptotic cells. Necrosis is a result of a severe damage of the cell in which internal organelle and plasma membrane integrity are lost making it possible to be stained by the dye of high affinity to DNA. This dye is a superior alternative to PI (Propidium Iodide) or Ethidium Homodimer I as it shows much higher affinity to DNA and fluorescence quantum yield is much higher, which allows for more precise quantification. The cells stained with the dyes can be observed in the light of a fluorescent microscope as well as quantified in the flow cytometry[15].

Cytokines

Some of the immuno-assays, for accuracy and alignment with a better model, were performed on dendritic cells and Flow Cytometry was used for quantification of the signal for the protein expressed on the antigen-presenting cells providing signals for T-cells activation ($CD40^+$, CD86, $CD1a^+$).

Macrophages that in this thesis were obtained by stimulation of cancer cells THP-1 with PMA (*phorbol myristate acetate*) are also antigen presenting cells. This differentiation is much faster than the differentiation from monocytes to dendritic cells, and takes 3 days vs. 8 days in case of dendritic cells (DC) to obtain mature form of DC. Monocytes will be separated from blood cells and then stimulated with cytokines IL-4 and antibodies GM-CSF for 4 days in order to obtain immature DC, then stimulation with other cytokines (IL-4, TNF-α, IL6) and antibodies (GM-CSF, PGE_2) will transform them to mature DCs that could be stimulated with potential adjuvants and able to activate T cells, the maturation leads to increased surface expression of CD86 molecules, that would signal the T activation. The monocytes separation from the blood samples, as well as stimulation to obtain dendritic cells that were used in this thesis was performed by Dr Ilona Kubajewska.

Dendritic cells were differentiated from monocytes by incubation with polarising cytokines (rhIL-4 and rhGM-CSF) for 6 days. Monocytes were separated from PBMC (peripheral blood mononuclear cells) by magnetic sorting using EasySep Human Monocyte Enrichment kit (STEMCELL Technologies). PBMCs were isolated from human peripheral blood using gradient centrifugation method. Dendritic cells were cultured in complete RPMI 1640 medium (Roswell Park Memorial Institute). After stimulation with relevant experimental conditions (MOFs, alums: ALO(OH), $ALPO_4$, LPS (endotoxin – Lipopolysaccharides), PBS (Phosphate-buffered saline)) in 96 well plates, cells were washed with PBA buffer (PBS w/o Ca/Mg ions + 2% FBS) and stained with fluorochrome-conjugated antibodies (PE anti-human CD86 and APC anti-human CD40 by Miltenyi Biotec, PerCP-Cy5.5 anti-human CD1a by BioLegend) for 30 mins at 4°C, then fixed with 2% formaldehyde and washed 3 times with PBA. Cell suspension was resuspended in 200ul PBA and acquired by MACSQuant flow cytometry machine measuring fluorescent signal in relevant channels. Analysis was performed in MACSQuantify flow cytometry software. The dendritic cells used in the experiment were prepared by Dr Ilona Kubajewska.

3.5.2 Viability by Alamar Blue

Alamar Blue is a commercial name for a solution of rezasurin, a non-toxic compound which if applied as an assay enables pharmacokinetic studies. To contrary, assays performed with MTT (3-[4, 5-dimethylteazol-2-yl]-2,5-diphenyl tetrazolium bromide), are endpoint assays and cells are lost during the measurements. Rezasurin solution is blue in color and non-fluorescent, which upon entering cells' membrane, is reduced to resorufin by mitochondrial enzymes during cells activity, a compound that is red in color and highly fluorescent[16]. The more live cells there are, the more can convert more rezasurin into its fluorescent form resulting in a higher FL signal. The principle of the method is depicted in Figure 3-6.

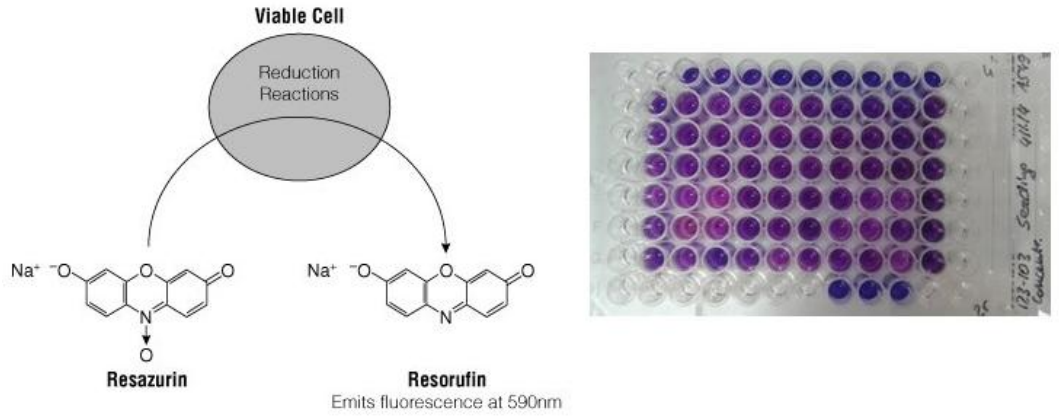

Figure 3-6 Schematic depiction of a mechanism of action of Alamar Blue viability assay and the change in colour resulting from the conversion of Resazurin (blue) into Resorufin (purple) indicating high viability of the cells.

Alamar Blue assay was performed to measure the cell viability on two different cell lines: monolayer culture A549 lung cancer cells and suspension THP-1 human leukemia (blood cancer). The incubation time for each of the two cases was optimised. Alamar Blue Assay was used to quantify the viability of A549 cells and viability of THP-1 was measured using Flow Cytometry and Necrosis/Apoptosis kit. For the viability experiments the following seeding densities were used: 500 000 cells /ml for THP-1 and 40 000 cells/ml for A549. The optimisation curves are presented below in Figure 3-7 and Figure 3-8. For A549 the incubation time based on the optimisation curve was adjusted to 4 h for all of the viability bioassays for A549 cell line and for THP-1 the optimised incubation time was 6.5 h. The incubation times were included in the drug stimulation experiments and accounted for the exposure time. Briefly, the 96-well plate with stimulated cells containing 10% by volume of Alamar Blue solution (5 mM resazurin solution in a non-completed RPMI) are incubated in the cell incubator at 37°C and environment containing 5% of CO_2. Then the plate is read in the Multiplate Reader instrument by Molecular Devices UK model m2e and the fluorescence of the product of cell activity monitored (Excitation at 555 nm and Emission at 585 nm). Fluorescence is linearly proportional to cell viability.

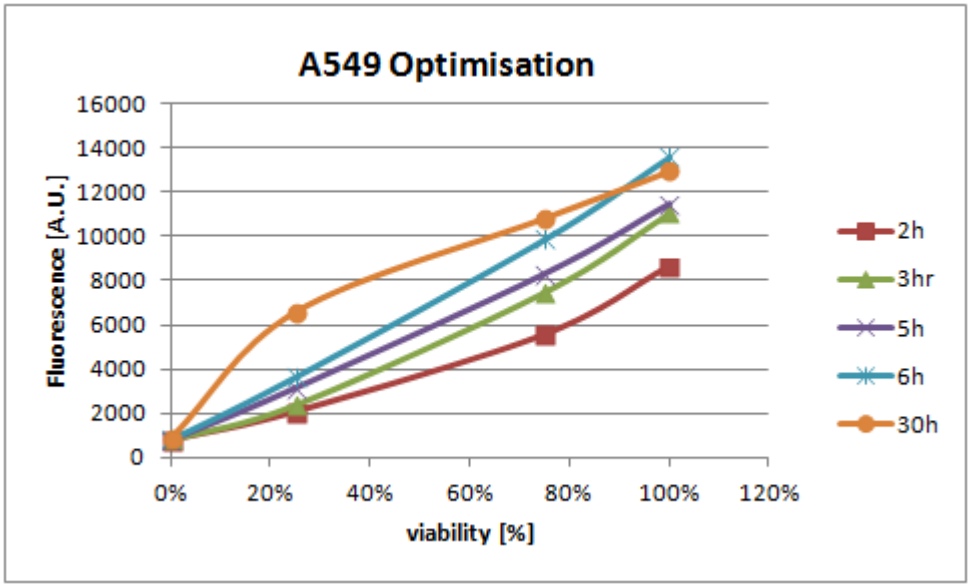

Figure 3-7 Alamar Blue bioassay optimisation for A549 cell line.

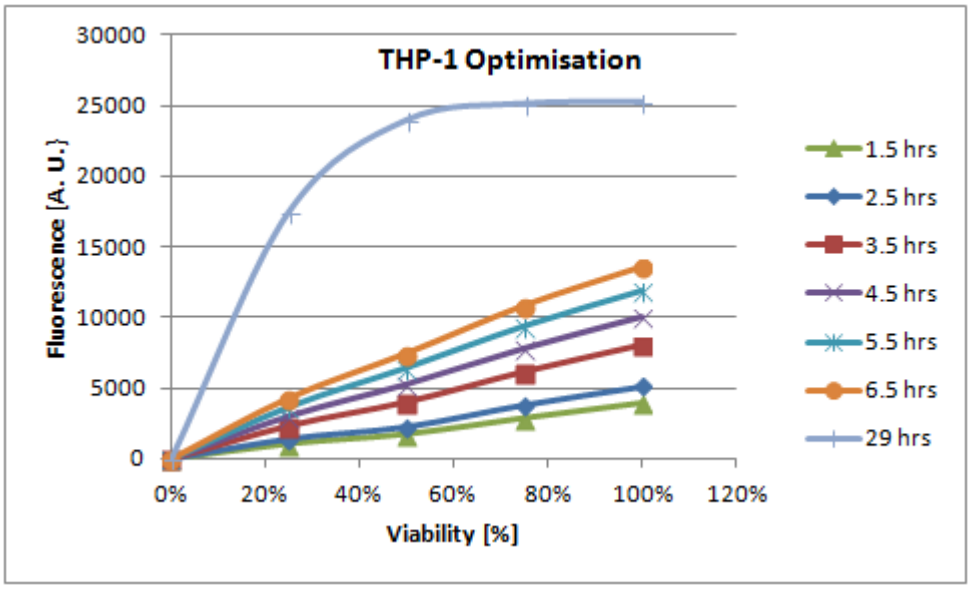

Figure 3-8 Alamar Blue bioassay optimisation for THP-1 cell line.

Cell culture of A549 monolayer cell line:

Cells were cultured in a T75 flask and incubated at 37°C (5% CO_2) and passaged once they reached the confluence level at 85-90%. The cell confluence was observed by an inverted microscope EVOS. As the cells are adherent, in order to passage them, they need to be harvested with the TrypLE Express Enzyme (1x; Life Technologies), which is a derivative of trypsine enzyme that is harmless to cells and detachment from the flask bottom takes only 10 minutes. Briefly, the media was discarded from the flask and the flask rinsed with 5 ml of PBS that does not contain Ca, Mg ions. To such prepared flask 3 ml of Trypsin (TrypLE

Express) was added and the flask placed in the incubator for 10 min, after which it was removed and examined in the microscope if the cells detached from the bottom. Then trypsin would be deactivated by an addition of 6 ml of complete growth media. The growth media for cell culture was Gibco RPMI 1640 supplemented with penicillin (100 µg/mL), streptomycin (100 µg/mL), L-glutamine (292 µg/mL), all from Life Technologies supplier and 10% v/v heat-inactivated fetal bovine serum (FBS, Gibco). This is hence referred to as "complete RPMI" or 10% RPMI. The cell suspension (9 mL) was transferred with a serological pipette and placed in the 15 ml tube and then centrifuged for 5 min at 1000 rpm so the cells would form a pellet. The cells were re-suspended in 10% RPMI 1640 growth media for cell counting and splitting. For cell seeding, cells were resuspended in 2% RPMI media, i.e. 2% FBS v/v was added instead of 10% FBS. This serves as a growth limiting step for the seeded cells. The cells were seeded on the 96-well plate. For all the experiments performed in this thesis the seeding density was 4000 cells/well (40 000/mL) which corresponded to 100 µL of cell suspension volume per well. Cell counting was accompanied by Trypan Blue exclusion test. Trypan Blue is a blue dye that permeates membranes of dead cells and thus stains them in blue and does not enter the viable cells. Therefore, live and dead cells can be distinguished.

Cell culture of suspension THP-1 cell line:

The steps for subculturing the suspension cell line are similar to above, only there is no need to use trypsin for cell passage. The growth media for subculturing and seeding was 10% completed RPMI 1640 and the seeding density was 100k/well (500 000 cells/mL) which corresponded to 200 µL of cell suspension volume per each well. Such subcultured cells were used in the cell stimulation experiment with cisplatin and 5-Fluorouracil to determine apoptosis/necrosis cell death.

3.5.3 Cytokines' secretion by ELISA

The enzyme-linked immunosorbent assay is a technique based on antibodies and a colour change arising from enzyme linking performed in a plate and designed for detection of antigen (peptides, proteins, hormones) or antibodies and their quantification. It relies on a basic concept that any antigen will bind to its specific antibody. Measurement of the absorbance at the maximum of the characteristic

wavelength of the dye and constructing a calibration curve allows for quantification of secreted cytokines.

For the purpose of this thesis the ELISA assays were performed to quantify cytokines: IL-6 and TNF-α, using commercially available kits purchased from BioLegend. In this work Sandwich ELISA method was used for detecting and quantifying cytokines that were secreted by macrophages and dendritic cells[17, 18].

For the sandwich ELISA, the 96-well plates were used. The plate was coated by a capture antibody solution (60µL in 11.94 ml of Coating Buffer – 8.4 g $NaHCO_3$, 3.56 g Na_2CO_3 in 1L of deionised H_2O, 100µL per each well), specific to the antigen of interest and incubated overnight at 4°C. Then the plate was washed with a wash buffer (9.6g PBS in 1L deionised H_2O and 0.5mL of Tween 20 added) from excessive amount of coating antibody and nonspecific binding sites were blocked with assay diluent (0.5 g bovine serum albumin in 50 ml deionised H_2O). This step also helped reducing the background. The plate prepared in this way was then sealed and incubated for 1 hour. Thereafter, it was washed again on the plate washer and to as prepared plate, the antigen-containing samples were added. This included the reference protein standards which were then used for a standard curve. Then the plate was sealed and incubated for 2 hours. A cytokine - IL-6 or TNF-α, was bound to the immobilised capture antibody if any was secreted by the macrophages. A specific primary antibody (detection antibody) was added to the samples and followed by the labelled horseradish peroxidise enzyme (Avidin HRP), producing an antibody-antigen-antibody sandwich. Then the plate was again sealed and incubated for 1 hour. Unbound antibody–enzyme conjugates were washed off. This step was quite important as any excessive amounts of enzyme-conjugates could corrupt the results. Next, TMB substrate (3,3′,5,5′-Tetramethylbenzidine) was added and enzymatically converted to a substance that can be quantified and was proportionate to the concentration of IL-6 or TNF-α present in the sample, the plate was sealed and incubated for 30 min. TMB developed a blue reaction product whose absorption was quantified at 370 or 655 nm. The reaction followed according to the scheme (Figure 3-9), colourless TMB is transferred to 3,3',5,5'-tetramethylbenzidine diimine yielding a product, blue in colour as it is a hydrogen donor for the reduction of hydrogen peroxide

upon detecting HRP and catalysed by HRP-enzyme[19]. Because this reaction can proceed with no limits, for endpoint assays, it is important to add, a so called "stop solution" (e.g 0.16 M sulphuric acid) that would denature the enzyme in the pH value, forming a yellow product with maximum of absorption at 450 nm.

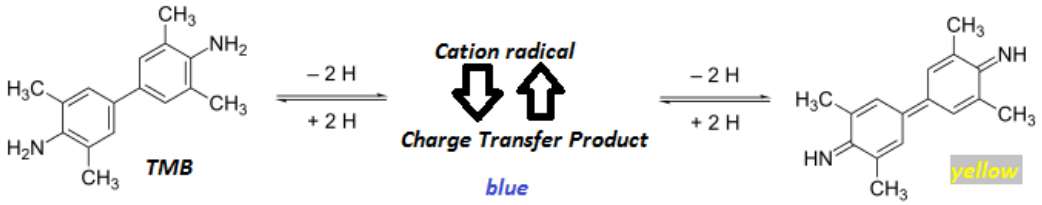

Figure 3-9 TMB oxidation process. A blue charge transfer product is formed with diamine and diimine oxidation products, an addition of a stop solution shifts the equilibrium into formation of diimine.

Differentiation of the human monocytic cell line THP-1 into macrophage-like cells was performed by stimulation with PMA (phorbol myristate acetate, 100 nM, purchased from Sigma Aldrich).

It is worth noting that differentiation of THP-1 cells to macrophages is sometimes not 100%, however serves as a model for antigen presenting cells to T-cells. The mechanism of action of ELISA kit by Biolegend is depicted in Figure 3-10 below.

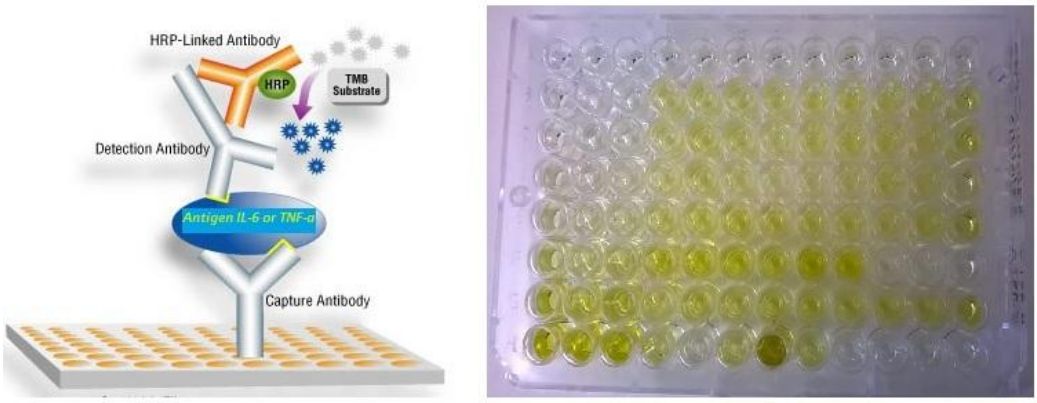

Figure 3-10 Mechanism of ELISA assay. Left image was adopted from Biolegend commercial materials. Right image is an outcome of the ELISA assay prepared by the author of this thesis.

Stimulation THP-1 cells with PMA for macrophages differentiation

For the PMA stimulation a cell suspension prepared contained 500 000 cells/mL and the seeding volume of 200 µL of cell suspension (Seeding density 100 000 cells/well). Concentration of PMA used for stimulations was 2.5 µL per well (100nM/well) and 12.5 µL/mL. Differentiation continued for 72 h and after this time the cells were stimulated with MOF powders (10 µL of a dispersion

10 mg/mL, corresponding to 500μg/mL). Lipopolysaccharides **(**LPS) – gram-positive bacteria and used as a positive control (5 μL, an eq. of 100 ng/mL), PBS – used as a negative control (w/o Ca, Mg ions 10 μL) and commercially used alums: Al-OH and Al-PO (10 μL per well of each). The macrophages were exposed to stimulants for 24 h after which time the plate was centrifuged and aliquots harvested on other two plates, for quantification of the cytokines IL-6 and TNF-α by ELISA (100 μL taken up from each well).

3.6. Nitric Oxide chemiluminescence

NO release measurements were performed in order to quantify the amount of NO being released by the MOF samples loaded with anti-cancer drugs: 5-Fluorouracil and cisplatin. Briefly, NO loading was performed in a schlenk tube in the experiment very similar to procedure for powder dehydration. In order to activate (remove solvent from) the MOF powders (0.015 g per glass vial), they were first placed under vacuum (2.3 ×10-3 bar) during which time ca. 30% of the mass was lost. They were then heated to 120°C while still under dynamic vacuum and held at this temperature overnight, leaving a fully activated material accessible for NO adsorption. The samples were subsequently cooled to room temperature and exposed to ca. 2 atm of dry NO (99.5%, Air Liquide) for 45 min. The vials were next evacuated and exposed to dry argon, before being flame sealed. This cycle of evacuation and argon flushing was repeated three times in order to remove any residual physisorbed NO from the surfaces of the MOF and glassware. To measure the release, the Sievers 280 i chemiluminescence NO analyser was used. This instrument is equipped with high-sensitivity detector that measures nitric oxide content based on chemiluminescent reaction between ozone and nitric oxide, equations 3-2 and 3-3.

$$NO + O_3 \rightarrow NO_2^* + O_2 \qquad (3\text{-}2)$$

$$NO_2^* \rightarrow NO_2 + h\nu \qquad (3\text{-}3)$$

The signal comes from the excited NO_2^* that is in the near-infrared and is measured by the photomultiplier tube detector sensitive in the red. The calibration of the instrument was made by setting up a zero for NO signal by letting air pass and then 93.2 ppm NO calibration gas (Air Products, balance nitrogen) was

passed. The nitrogen flow was set up at 200 ml/min with a cell pressure of 8.5 torr and an oxygen pressure of 6.1 psig. The nitrogen supply, before it enters the sample chamber is flowing through the flask containing LiCl saturated solution which provides relative humidity at the level of 11 % (15 mg in 12 ml of H_2O)[20], to replace NO bound to the metal open sites with H_2O molecules coming from the moisture passed through the nitrogen gas. Below (Figure 3-11), there is a picture of the experimental set-up.

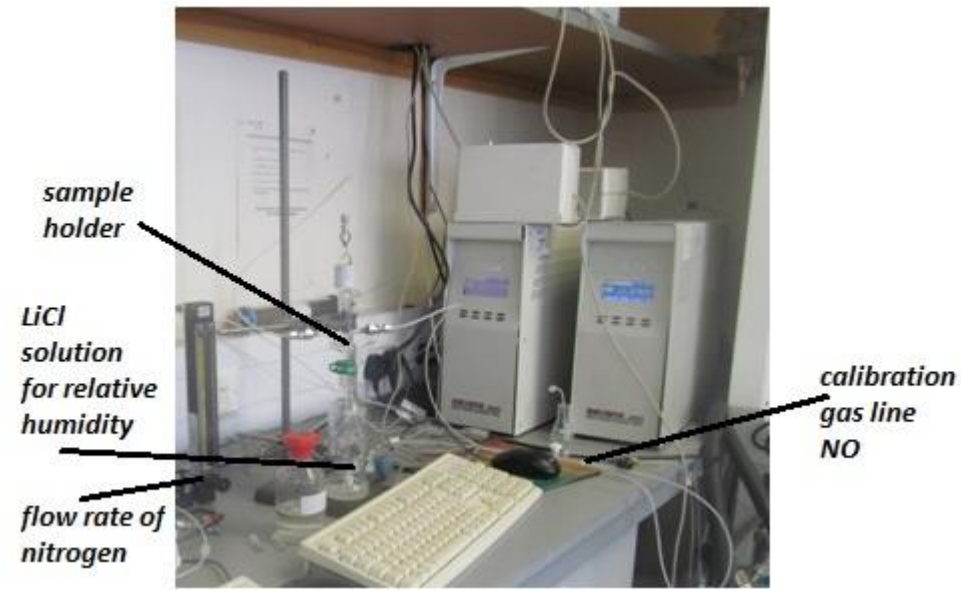

Figure 3-11 Nitric Oxide analyser experimental set up.

3.7 Fourier transform infrared spectroscopy (FTIR)

Molecules have vibrational modes, which are associated with vibrations of functional groups and bonds. This property of compounds is very useful for their identification and widely used with developed spectroscopic methods, one of which is Fourier Transform Infra Red Spectroscopy. In this method, light (polychromatic radiation) that covers full range 4000-400 cm^{-1} is produced by a light source e.g. a high pressure mercury lamp, (wavelengths from 2.5 to 25μm) is split into two beams, one of them always travels a longer path than the other. This is achieved by installing a set of mirrors, one in a fixed position and the other moving and a beam-splitter (Michelson interferometer), see (Figure 3-12) for FTIR instrument scheme. Ideally the beam-splitter would transmit half of the radiation to the stationary mirrors and another half would be reflected to hit the moving mirror, this allows to generate an optical path difference. The recombined

beams would pass through the sample and some of the radiation will be absorbed by the sample. The signal of the recombined beams, which would vary in optical path length will be transferred onto detector, which measures a difference of intensities as a function of difference of optical paths[21].

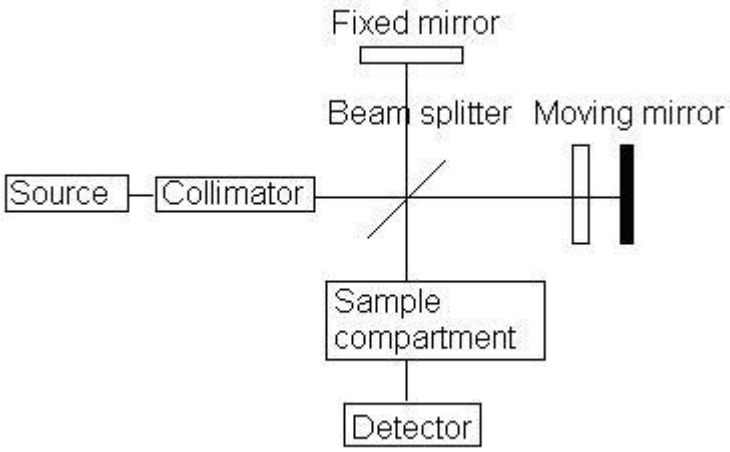

Figure 3-12 Simplified diagram of an FTIR spectrometer.

If a mathematical operation - Fourier transform (FT) is now applied to this spectrum, which is called interferogram and contains all the frequencies as a plot of their intensities versus time, it will be transferred into a new function, which is a commonly known as a plot of absorption against a wave number. The relation between the function of time f(t) and a function of wave number F(v) that is changing in time, is described by the equation (3-4):

$$f(t) = \frac{1}{\sqrt{2\pi}} \int_{-\infty}^{\infty} F(v) \cos(2\pi v t) dt \qquad (3\text{-}4)$$

The FTIR instrument is capable of acquiring an interferogram in seconds and as such allows to plot results with much better signal-to-noise ratio as many scans can be taken in a very little time. Spectra allow to analyse vibrations of the bonds and functional groups that are characteristic for chemical compounds[22]. Not all of the molecules would absorb infra red radiation but only these with bonds having a diapole moment[23]. Region below 1500 cm^{-1} is called a fingerprint region and contains spectra of many bending vibrations from within the molecule, which are quite complex to analyse due to the fact of complicated series of absorptions, however this region is very unique to every compound and allows to identify the substance, once we have a known spectra of this compound.

3.8 References

1. G. A. Tompsett, W. C. Conner and K. S. Yngvesson, *ChemPhysChem*, 2006, **7**, 296-319.
2. S. Bauer, C. Serre, T. Devic, P. Horcajada, J. r. m. Marrot, G. r. Férey and N. Stock, *Inorganic Chemistry*, 2008, **47**, 7568-7576.
3. http://serc.carleton.edu/research_education/geochemsheets/BraggsLaw.html.
4. NIST, *Basic atomic spectroscopic data*, http://physics.nist.gov/PhysRefData/Handbook/Tables/platinumtable1.htm.
5. S. Gaisford and M. Saunders, in *Essentials of Pharmaceutical Preformulation*, John Wiley & Sons, Ltd, 2012, pp. 1-35.
6. H. H. Willard, L. L. Merritt and J. A. Dean, *Instrumental Methods of Analysis*, 3th ed. edn., Van Nostrand, 1958.
7. F. J. Holler, S. R. Crouch, D. A. Skoog and D. M. West, *Fundamentals of Analitycal Chemistry*, 9th Edition edn., 2014.
8. G. Jeffery, J. Bassett, J. Mendham and R. C. Denney, *Quantitative Chemical Analysis*, Longman Scientific & Technical, 1989.
9. M. Fulwyler, *Particle Separator, USA Pat.*, 1953.
10. M. H. Julius, T. Masuda and L. A. Herzenberg, *Proceedings of the National Academy of Sciences of the United States of America*, 1972, **69**, 1934-1938.
11. H. M. Shapiro, *Practical Flow Cytometry*, John Wiley and Sons Ltd 2003.
12. H. Lecoeur, M.-C. Prévost and M.-L. Gougeon, *Cytometry*, 2001, **44**, 65-72.
13. C. Dive, C. D. Gregory, D. J. Phipps, D. L. Evans, A. E. Milner and A. H. Wyllie, *Biochimica et Biophysica Acta (BBA) - Molecular Cell Research*, 1992, **1133**, 275-285.

14. J. P. Robinson, Z. Darzynkiewicz, P. Dean, L. Dressler, H. Tanke and L. Wheeless, *Handbook of Flow Cytometry Methods*, 1993.
15. S. Martin, at al., *J Exp Med.*, 1995, **182**, 1545-1556.
16. J. O'Brien, I. Wilson, T. Orton and F. Pognan, *European Journal of Biochemistry*, 2000, **267**, 5421-5426.
17. E. Dobrovolskaia, A. Gam and J. E. Slater, *Clinical & Experimental Allergy*, 2006, **36**, 525-530.
18. S. D. Gan and K. R. Patel, *J Invest Dermatol*, 2013, **133**, 12.
19. P. D. Josephy, T. Eling and R. P. Mason, *Journal of Biological Chemistry*, 1982, **257**, 3669-3675.
20. EU-Project, *Use of salt solutions for assuring constant relative humidity conditions in contained environments*, PTDC/ECM/099250/2008, 2008.
21. F. Daniels, J. W. Williams, P. Bender, R. A. Alberty, C. D. Cornwell, J. E. Harriman and McGraw-Hill, *Experimental Physical Chemistry*, 7th edn., 1970.
22. D. H. Williams and I. Fleming, *Spectroscopic Methods in Organic Chemistry*, 5th edn., 1995.
23. D. L. Pavia, G. M. Lampman, G. S. Kriz and J. A. Vyvyan, *Introduction to Spectroscopy*, 5th edn., 2014.

Chapter 4. MOFs as drug delivery carrier for cisplatin

4.1. Aims

Cisplatin, *cis*-[$Pt(NH_3)_2Cl_2$], is one of the most successful and researched anti-cancer drugs with its use accounting for nearly 50% of all anti-cancer therapies for a variety of cancers[1, 2]. Despite its high toxicity (the first generation drug), cisplatin is used in the treatment of head, neck, ovarian, cervical, testicle, breast and bladder tumours[3-5]. The toxicity of cisplatin against cancerous cells was first recognized in 1968[6]. Over subsequent years of intensive research, it showed high efficacy against many cancer types in clinical trials[7] and was finally approved as an anti-tumour drug by the FDA (Food and Drug Administration) in 1978[8]. Cisplatin is capable of forming intra- and inter-strand cross-links with nucleic acids of DNA. This leads to cell death (apoptosis) due to the resultant inability of DNA to replicate[9]. Cancer is one of the most feared diseases known to mankind. Therefore, the development of new and more efficient drugs has continuously attracted a great deal of attention. This chapter will explore MOFs (CPO-27 Mg, CPO-27 Ni, UiO66 and UiO66-NH_2) for their potential application as drug delivery systems for cisplatin. This is thanks to utilising their high surface areas, high porosity and non-toxic character. It should be mentioned that CPO-27 Ni shows toxicity, however, as anti-cancer drugs are much more toxic than Ni, this MOF was qualified for the testing phase. Different encapsulation strategies: physical encapsulation and conjugation, will be presented, and these assessed in terms of their efficacy by a variety of bio – assays *in vitro* (Alamar Blue and Flow Cytometry) and resulting in the choice for the best strategy for cisplatin delivery. Encapsulation of a variety of active pharmaceutical ingredients is a broadly known way of developing drug carrier systems and some MOFs with their relatively large voids have been investigated. A good example was given by Christian Serre's group with their range of MIL materials[10-13]. Zr-MOFs have been previously researched for their potential application as drug delivery carriers for caffeine[14]. According to the literature, conjugation technique has been

successfully applied to some MOFs, by activating an amine group on the organic ring of the MOF framework, this including Mn-MOF and MIL-101[15, 16]. Due to the fact that the MOFs listed have not yet been approached for their applicability for cisplatin, and that encapsulation and conjugation proved to be a good way of obtaining particles showing cytotoxic character, this chapter will describe the research conveyed.

4.2. Synthesis

Four MOFs were chosen to serve as the best candidates because of their relatively non-toxic character (excluding CPO-27-Ni), simplicity of synthesis and large cages that could accommodate a molecule of cisplatin. Each of the materials was prepared in a large batch in order to reduce heterogeneity of different batches and stable parameters of the powders. Briefly the synthesis was the following:

UiO66

A mixture of zirconium (IV) chloride (82 mg, 0.35 mmol) and 1,4-benzenedicarboxylic acid (58 mg, 0.35 mmol) in dimethyl formamide (DMF; 5 mL) was acidified using HCl (37 wt%, 805 μL, 9.7 mmol). The solution was sealed inside a 23 ml Teflon-lined steel autoclave and heated at 220°C under autogenous pressure for 24 hours[17]. The UiO66 product was collected by vacuum filtration, washed with DMF and dried in vacuum. The reaction has been scaled up in order to obtain ca. 4 g of the MOF powder and the reaction was carried out in a 600 mL autoclave[18].

UiO66 –NH_2

A mixture of zirconium (IV) chloride (82 mg, 0.35 mmol) and 2-amino-1,4-benzenedicarboxylic acid (63 mg, 0.35 mmol) in DMF (5 mL) was acidified using HCl (37wt%, 805 μL 9.7 mmol) and acetic acid (concentrated, 605 μL, 10.57 mmol). The solution was sealed inside a 23 ml Teflon-lined steel autoclave and heated at 120°C under autogenous pressure for 24 hours. The UiO66-NH_2 product was collected by vacuum filtration, washed with DMF and then with MeOH and dried in vacuum. The yield was 130 mg, efficiency 90%.of The reaction was scaled up, in order to obtain enough powder to cover all of the experiments once

the material has been characterised. The amounts obtained were 1.774 g, 87.7%, scale up of the reaction was 14 times according to the procedure in literature[17, 19]. Successful preparation of the MOFs was confirmed by X-ray diffraction, with the patterns of the obtained materials being identical to those reported in the literature. The particle size of the Zr-MOFs was assessed by SEM to be around 250-300 nm (Figure 4-1).

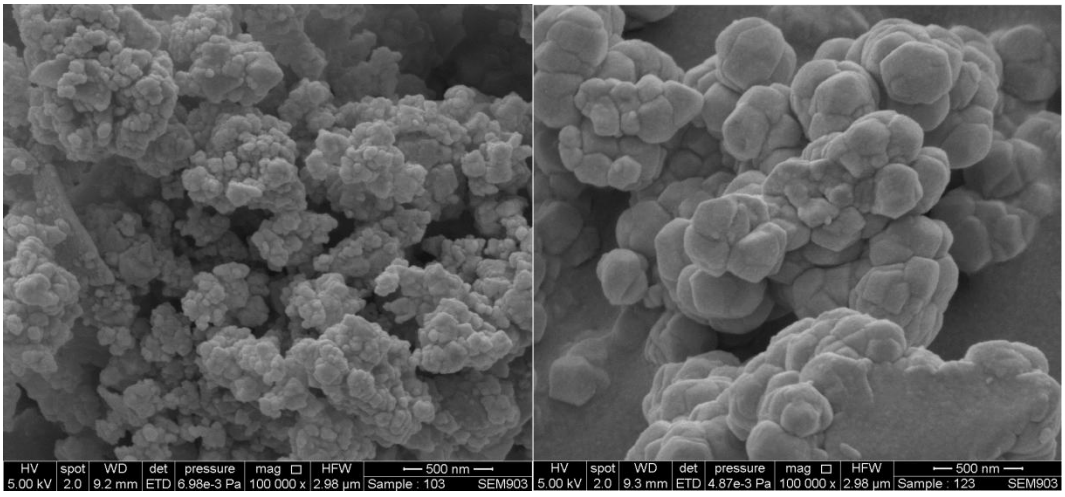

Figure 4-1 SEM images of UiO66-NH_2 (left) and UiO66 (right).

CPO-27 MOFs have been synthesised in the hydro-solvothermal process in autoclaves[20]. In this synthesis, which eliminates toxic organic solvents like DMF, the reactants (metal salt and an organic linker) are dissolved in a solution which is a mix of 50:50 (v/v) of water and THF for CPO-Ni and 3:10 (v/v) for CPO-Mg. The solvothermal reaction is carried out at 110 ºC. The synthesis time according to Dietzel et al. recommendation should be 3 days[21]. The MOF powder after its synthesis was kept in a water bath in order to perform the ion exchange and remove THF from the pores of the material. It was noted that the formation of the final product can be achieved in 24 hours in the autoclave, even in case of a 25-times scale-up. Some trials were made to apply microwave assisted synthesis process as this method offers a rapid formation of the MOF powders, in just 60-120 min versus 24-hour cycle. The only drawback of following this method being the size of the vials which in our case, only allowed for preparing small quantities of the powder that is 58 mg if small vials (5ml) are used or 115 mg yield 83% if larger vials are used (12 ml). The microwave-aided syntheses enables to verify the reaction conditions quicker before dedicating longer time intervals if the

solvothermal process is used (reaction in the autoclave). The aim for this thesis was to use the same batch for all of the experiments to avoid any batch-related discrepancies in the surface properties: porosity, BET which are crucial for development of drug delivery systems. The method originally published by Dietzel et al. was adapted and it was observed that it gave satisfying results[22].

Briefly:

CPO-27-Mg

A mixture of an organic linker 2,5-dihydroxyterephthalic acid (99 mg, 0.5 mmol) and metal salt $Mg(NO_3)_2 \cdot 6H_2O$ (257 mg, 1.0 mmol) were dissolved in a solution of THF (7 mL), NaOH (2 mL, 1 M), and water (3 mL) under stirring. The given above quantities were scaled up 25 times to 6.425 g (25 mmol) of $Mg(NO_3)_2 \cdot 6H_2O$, 2.475 g (12.5 mmol) of dhtp and volume of solvent: 175 ml of THF, 75 ml of H_2O and 50 ml of 1M NaOH, in order to obtained higher yield of the MOF powder. The mixture was then sealed in a 600 mL Teflon-lined autoclave and heated in an oven at 110 °C for 24 hours. The product $Mg_2(dhtp)(H_2O)_2 \cdot 8H_2O$ was collected by filtration as a light-yellow substance. Ca. 2 g was obtained, 38 %. The reaction is depicted in Figure 4-2 below.

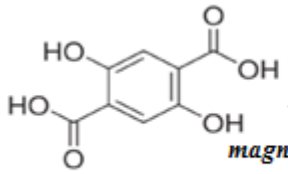

$+ 2Mg(NO_3)_2 \cdot 6H_2O + NaOH \rightarrow Mg_2(C_8O_6H_2) \cdot 7H_2O + 4NO^-_3 + 2Na^+ + 2H^+$

magnesium nitrate hexahydrate

2,5-dihydroxyterephthalic acid

Figure 4-2 Simplified equation of the reaction of synthesis of CPO-27 Mg.

CPO-27-Ni

2,5-dihydroxyterephthalic acid (2.972 mg, 15 mmol) was dissolved in THF (50 mL), $[Ni(OCOCH_3)_2] \cdot 4H_2O$ (7.466 mg, 30 mmol) was dissolved in H_2O (50 mL), both solutions were mixed together[23] and stirred until homogenous. The amounts were scaled up 3 times, which gave 22.398 g of $[Ni(OCOCH_3)_2] \cdot 4H_2O$, 8.916 g of dhtp and 150 ml of THF and 150 ml of H_2O. After being stirred, all the reactants were transferred to a 600 ml Teflon-lined autoclave and heated in an oven at 110°C for 24 h. Dark yellow powder $Ni_2(C_8O_6H_2)(H_2O)_2 \cdot 8H_2O$ was collected after filtering and dried under vacuum. 4 g was obtained, 54.3%.

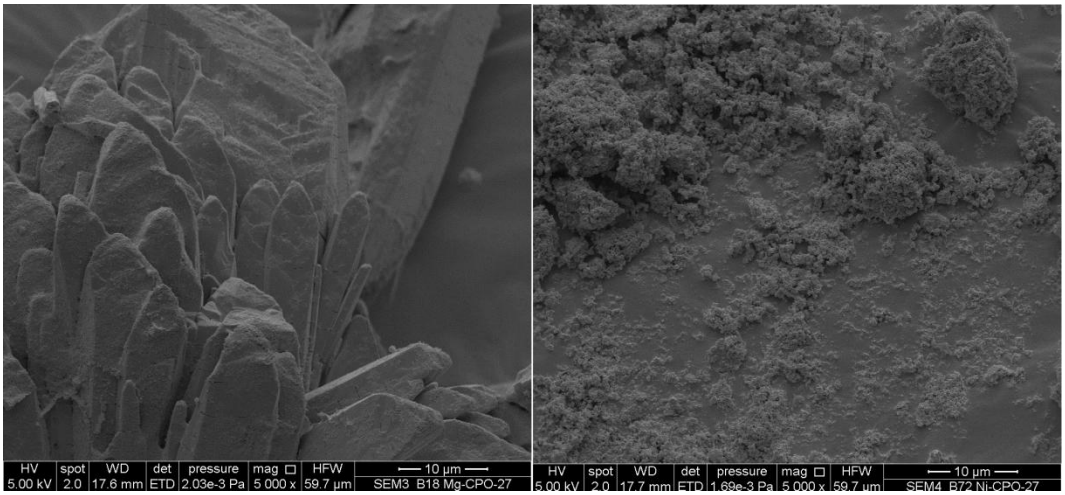

Figure 4-3 SEM images of CPO-27 Mg (left) and CPO-27 Ni (right).

The size of particles of CPO-27 Mg was assessed to be ca. 10 µm and CPO-27 Ni between 400-600 nm.

4.2.1 One pot synthesis

A one-pot route was pursued to synthesise the MOF powders with cisplatin that would be already entrapped in the pores and cages of the materials.

For Zr-MOFs, two syntheses were performed: in 50 ml autoclaves (solvothermal) and in 12 ml glass vials (microwave-assisted synthesis), the protocols were adopted and the amounts of cisplatin were added according to the Table 4-1. The reaction time for a synthesis in autoclaves was set to be 24 hours at 120°C for UiO66-NH_2 and 220°C for UiO66, for microwave-radiation aided synthesis, reaction time was shorter and set to be 40 min, same temperature conditions applied.

For CPO Mg and CPO Ni only a hydro-solvo-thermal method was exploited, and the reaction time was set to be 24 hours and temperature 110 °C for both MOFs. The quantities of cisplatin added to the mixture of the reagents were adjusted based on cisplatin's solubility in a solvent at the level of 80% (2.53 mg/mL of H_2O)[24].

MOF	Linker [mg]	Metal-Salt [mg]	Solvents [mL]	Cisplatin [mg]
CPO-27 Mg	99 (0.5 mmol)	257 (1 mmol)	7 THF, 3 H_2O, 2 1M NaOH	10 (0.033 mmol)
CPO-27 Ni	594 (6mmol)	1493 (6mmol)	10 THF, 10 H_2O	20 (0.066 mmol)
UiO66	58 (0.35mmol)	82(0.35mmol)	5 DMF, 0.807 HCl, 0.6 acetic acid	52 (0.17 mmol)
UiO66-NH_2	63(0.35mmol)	82(0.35mmol)	5 DMF, 0.807 HCl, 0.6 acetic acid	52(0.17 mmol)

Table 4-1 Synthesis summary of the chemicals used in the MOF synthesis.

4.2.2 Encapsulation

The high surface areas and quite big cages of 11-12 Å[23] for CPO -27 (Mg and Ni) and 11 Å and 8.5 Å in case of Zr-MOFs (UiO66)[25, 26] are a foundation for the idea of exploiting a method of physical entrapment of an anticancer drug. The procedure was as follows: MOF powders (ca. 350 mg) were dehydrated under dynamic vacuum overnight and then immersed in a solution of cisplatin, cis-$[Pt(NH_3)_2Cl_2]$, (35 mL, saturation with cisplatin at 80%, 2mg/mL, (6.66 mM) in deionised water). This corresponded to a theoretical loading of 30 mg of cisplatin per 100 mg of dehydrated MOF. The encapsulation continued for 48 hours under stirring at room temperature. The samples were centrifuged and allowed to dry in air. There was an effort made to measure the quantity of cisplatin that did not migrate into the pores of materials, however, the signal coming from cisplatin was masked by the one coming from the MOF (UV-VIS spectroscopy).

4.2.3. Conjugation

An alternative route to encapsulation, conjugation, was explored. According to this strategy, a war head attached to the MOF via functionalised amine group into a “peptide bond” could release its cargo “on demand” when in the proximity of a cancer cell where oxygen concentration is lower and hence would reduce Pt(IV) to Pt(II) allowing for a more targeted action as all the cargo is kept intact and only realised at its destination. In order to create such a drug delivery system, a modified version of cisplatin was synthesised. The prerequisite for this route is presence of available amine groups in the framework, which then could be

functionalised in an amide coupling reaction. Thus, this method cannot be applied to just any MOF.

A prodrug of cisplatin, *cis,cis,trans*,-[$Pt^{IV}(NH_3)_2(Cl)_2(O_2CCH_2CH_2CO_2H)(OH)$] (see Figure 4-2), was synthesised in the following procedure (schematic reaction depicted in Figure 4-5). A suspension of cisplatin (0.4 g, 1.33 mmol) in H_2O (12 mL) at 60 °C was oxidized with H_2O_2 (20 mL) added dropwise. The reaction was kept running for 4 hours, and then the resultant bright yellow solution left to cool overnight. Yellow crystals (yield: 234 mg, 53%) were recovered by filtration and washed with ice cold water. A more detailed procedure can be found in the literature[1, 27]. The product (Complex 1, 202 mg, 0.6 mol) was then reacted with succinic anhydride (60 mg, 0.6 mol) at 70°C in a DMF (5 mL) suspension for 24h under stirring and then cooled to room temperature. DMF was removed under vacuum and the residual suspension (1 mL) was dissolved in acetone, and precipitated with diethyl ether to give a pale yellow solid with yield: 180 mg, 70% (Complex 2).

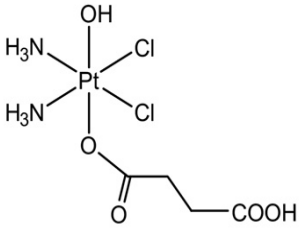

Figure 4-4 The structure of the cisplatin prodrug used in this work.

The prodrug was conjugated to UiO66—NH_2 using the EDC/NHS method in an aqueous solution. A detailed procedure can be found in the literature [28, 29]. In brief, 1-ethyl-3-(3-dimethylaminopropyl)carbodiimide (EDC·HCl 0.038 g, 0.20 mmol) and N-hydroxysuccinimide (NHS 0.023 g, 0.20 mmol) were dissolved in de-ionized water (15 mL) under stirring. Next, the prodrug (0.70 g, 0.16 mmol) was added into the aqueous solution. After the solution became clear, UiO66-NH_2 (0.140 g, 0.0798 mmol) was added and the reaction mixture (ratio 1 mol Pt to 3 mol amine groups) stirred at room temperature for 24 hours. Finally, the solid product was recovered by vacuum filtration, washed with water and left to dry in air.

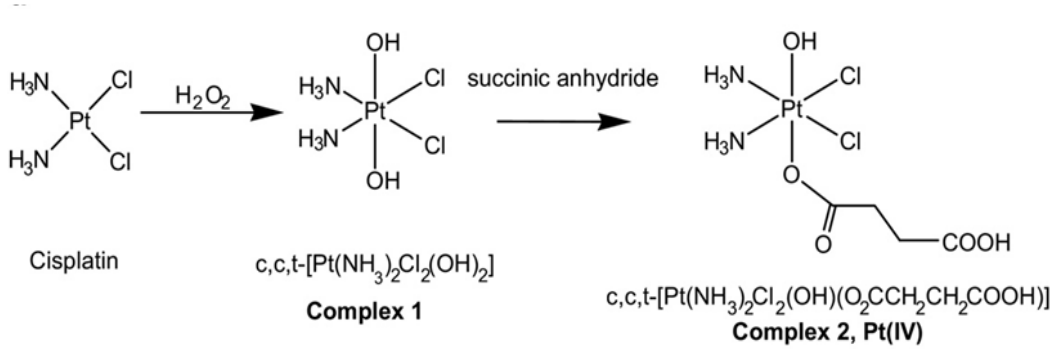

Figure 4-5 Schematic depiction of cisplatin modification 2-step reaction to obtain the non-toxic derivative of cisplatin Pt (IV) able to be reduced "in vitro".

4.3. Results

4.3.1 Quantification of cisplatin content

In order to quantify the amount of Pt in the MOF powders EDX (Energy-Dispersive X-ray Spectroscopy) technique was used in the first instance. The EDX method is a good estimate for metal concentration in the sample, however, it is not analytical and quantitative. A high number of scans must be taken from the samples to provide good statistical distribution and more precise results. Two data sets have been discarded from analysis – max and min read-outs to provide better averaging. This dramatically changed results, which are shown in Table 4-2 also including Pt:Zr ratios. For each analysis, the number of scans was no smaller than 8 for MOF samples encapsulated with cisplatin and 6 for UiO66NH_2-prodrug. This limitation was due to the time constraints. For the simplicity of calculations of the content of cisplatin expressed in %wt, the molecular weights of MOFs used are following, CPO-27 Ni (491.5 g/mol), CPO-27 Mg (422.7 g/mol) for $M_2(dhtp)(H_2O)_2 \cdot 8H_2O$, UiO66 (1664 g/mol) and UiO66NH_2 (1754 g/mol) and an assumption that perfect crystals with no defects in their structure are obtained.

For Zr-MOF with a conjugated prodrug, the estimation of Pt content was made based on the EDX read-outs for weight% of Pt in the sample. Looking at the range of the results for Pt content estimates based on EDX data, it is not sufficient to conclude regarding cisplatin and another analytical method for Pt quantification was necessary to be applied.

MOF	Pt: Metal ratio (Mol) All data sets	Corresponds to Cisplatin loading wt.% Value in brackets corresponds to data with discarded data	Pt: Metal ratio (Mol) max 1data set discarded
UiO66-NH_2-prodrug	1:1.76	21 Pt wt % (17 Pt wt%)	1:2.50
UiO66-NH_2 encapsulated	1:15.9	7.0 (6.1)	1:13.6
UiO66 encapsulated	1:17.4	5.9 (1.6)	1:66.1
CPO Mg encapsulated	1:24.4	5.5 (5.4)	1:25.1
CPO Ni encapsulated	1:20.4	5.7 (5.8)	1:19.7

Table 4-2 Summary of the estimation of cisplatin contents utilizing EDX measuring technique.

The digested powders of CPO-Mg, CPO-Ni, UiO66 and UiO66-NH_2 loaded with cisplatin in the encapsulation method and UiO66NH_2 with a conjugated prodrug were analysed by ICP-AES/MP-AES. The digestion of CPO-Mg and CPO-Ni with 37% HCl overnight, was successful, whereas the other MOFs were stable in HCl solution and digestion must have been carried out using aqua regia 3:1 vol. HCl:HNO_3. Despite a lot of attempts made to digest the powders – an amount of 4 ml of the acid solution has been added to each volumetric flask containing 1.5 - 6 mg Zr-MOF powders, and treated for an hour before diluting up to 100 mL with deionised water, there were no signs of reaction and powders were seemingly left unchanged. Nevertheless, the aliquots were taken for analysis under assumption that aqua regia solution should be penetrating the pores of material bringing Pt amounts stuck in the pores into the analyte solution. The prodrug that is conjugated to the amine group of the UiO66-NH_2 MOF is a derivative of cisplatin, and as such with a different structure, however it is stipulated that *"in vivo"* conditions Pt(IV) will be reduced to release Pt(II), a cytotoxically active part of cisplatin as the peptide bond will be cleaved [27]. The results are shown in Table 4-3. Surprisingly, the amount of cisplatin encapsulated in the pores of UiO66 was very low when compared with those encapsulated in UiO66-NH_2.

MOF	Pt content wt%±SEM	Cisplatin content wt%±SEM	Method
CPO-27 Mg-encapsulated	1.64±0.016	2.53±0.03	ICP-AES
CPO-27 Ni-encapsulated	0.91±0.004	1.39±0.01	ICP-AES
UiO66-encapsulated	1.00±0.01	1.54±0.02	MP-AES
UiO66-NH_2-encapsulated	2.32±0.03	3.58±0.04	MP-AES
UiO66NH_2-conjugated	4.40±0.04	6.77±0.06	MP-AES

Table 4-3 Summary of results obtained using MP-AES and ICP techniques.

In order to measure the cisplatin content encapsulated and conjugated in Zr-MOF powders, which were very robust and hard to digest, a quantification on ICP-MS has been performed at University of Warsaw, that included a novel method of samples mineralisation in School of Chemistry in Prof. Ewa Bulska Lab, which is dedicated to spectroscopic techniques of elements quantification. The method applied by Warsaw University group was based on mineralisation of the samples (ca. 5 mg) with 1mL of the solution obtained by mixing two acids HNO_3:HCl (vol 1:3) and then the samples were digested aided with a microwave radiation (Milestone UltraWave). The following program was applied: both, temperature and pressure were gradually increasing to values 270°C and 140 bar respectively over the time of 15 minutes. The microwave-aided heating program has been repeated twice. This method has been developed by Prof. Bulska's group and used to mineralise samples obtained by e.g. NASA – this was communicated to me when meeting in person Prof. Bulska during World Chemistry Congress in Busan, Aug 2015. The digested samples were then diluted with deionised water by weight, and the proportions for dilutions were adjusted based on the quantity of Pt in the sample to match the range of the calibration curve. The quantification of the Pt content in the samples was performed on ICP-MS NexION 300D (Perkin Elmer) with the following parameters: Cyclonic Spray Chamber, Plasma Power 1200 W, Argon gas flow rate 18 L/min, zero gas flow rate 1.2 L/min. Calibration curve has been constructed by measuring the signal of 3 points in the range 0-100 µg/L (blank, 10 µg/L and 100 µg/L), the standard used was Multi-element Ultra Scientific ICP MS Calibration Standard #3, with Pt content 10 mg/L. The Pt contents is shown in the Table 4-4 below.

MOF	Pt content wt%±SEM	Cisplatin content wt%±SEM	Method
UiO66-encapsulated	4.6 ± 0.2	7.07 ± 0.4	ICP-MS
UiO66-NH_2-encapsulated	6.8 ± 0.3	10.46 ± 0.5	ICP-MS
UiO66NH_2-conjugated	6.5 ± 0.3	10.00 ± 0.5	ICP-MS

Table 4-4 Pt and cisplatin quantification by ICP-MS, with an application of a microwave aided digestion method.

The cisplatin content in the sample was calculated according to the equation 4-1.

$$\%wt\ cisplatin = wt\%\ Pt \cdot \frac{M_{mol\ cisplatin}}{M_{mol\ Pt}} = 1.538 \cdot wt\%\ Pt \qquad 4\text{-}1$$

These results show that digestion with cold aqua regia was not efficient and the MOF porous structure withheld cisplatin quantities in its framework as there is still some Pt retained in the MOF structure and not in the solution with aqua regia. Especially, striking is the difference in Pt-content in UiO66 accounting for 5.59 %, and 6.92 % for UiO66-NH_2 but only 3.23 % for UiO66-NH_2 with conjugated prodrug which may be due to the fact that the peptide bond connecting a prodrug to the amine group, may be broken by aqua regia. For EDX estimates, if one of the read-outs in a data set is discarded then based on the same calculations, we find 1.3 wt% and 5.2 wt% for UiO66 and UiO66-NH_2 respectively, which by far is close to the MP-AES analysis.

TGA analysis of the unloaded and loaded samples was performed to estimate the cisplatin content. The cisplatin will decompose at 270 °C in the thermal process to Pt, which is indicated in the TGA plot showing a weight loss of 65 % of the mass. The composition of MOF that underwent the thermal process may be affected and in a result a mixture of oxides can be formed, and this composition is not stable in time, which is leading to uncertainty of the cisplatin/ Pt content that was initially incorporated in the sample. However, the attempt was made to estimate the amount of cisplatin by comparing the differences in the solvent content between loaded and unloaded MOFs based on the TGA plots. The free space in the pores of the framework should be filled up by H_2O/DMF and in the encapsulation process will be taken and is occupied by cisplatin molecules instead.

The water content in the MOF-cisplatin loaded samples was read out from the TGA plots (weight loss at 110°C), and was found for CPO Mg to be 2.5 wt% (from 27.5 wt%), for CPO Ni by 1.5 wt% (from 24.6 wt%). In case of Zr-MOFs,

as for their synthesis DMF is used, which is then partially exchanged with water in the solvent exchange process, the solvent content (water + DMF) was read out from the TGA plots as a weight loss at the 160 °C. The following changes were noticed loaded vs. unloaded samples: a drop by 6.6 wt% (from 23.1 wt%) in case of UiO66 and by 8.2 wt% (from 21.7 wt%) in case of UiO66NH_2, this is based on TGA results obtained in St Andrews, the feed gas used was air. The amount of solvent content for each of the MOFs that drops after the encapsulation may be a good estimate of the cisplatin quantity that was successfully encapsulated in the porous framework, as the TGA results match closely the results of ICP/MP.

MOF	"Drop" in a solvent content	Cisplatin content by ICP/MP
CPO Mg	2.4 wt%	2.53 wt%
CPO Ni	1.5 wt%	1.39 wt%
UiO66	6.6 wt%	7.07 wt%
UiO66-NH_2	8.2 wt%	10.5 wt %

Table 4-5 Comparison between results obtained in ICP-MP analysis and TGA solvent losses.

It should be noted that comparing the differences in a weight loss between loaded and unloaded MOFs can be misleading as to the cisplatin or Pt content emerging from the fact that Pt is a very heavy molecule (M_{mol} = 195.084 g/mol) when compared to metal molecules in MOFs: Mg (24.305 g/mol), Ni (58.693 g/mol) or Zr (91.224 g/mol) that are the remaining product or their oxides of the combustion process, the composition of these product may not be stoichometric and may vary depending on many conditions. For simulation purposes the Table 4-6 was compiled to depict probable outcomes for combustion products based on the assumption that there will be a preference for oxide formation (NiO, MgO, ZrO_2), no oxide formation or half oxide formation (eg. 3 Zr + 3 ZrO_2). This is due to the fact of a limited knowledge of the product composition once their combustion is completed. MOFs can absorb various amount of solvents in their pores depending on the conditions, some of the pores may remain empty. During the combustion process different products are formed, depending on the framework. Thus, it is very challenging to predict the drug content in the situation that the drug will not be completely burned out, and in the case of cisplatin, most probably Pt or PtO are formed.

Remaining product in wt% (100% = dehydrated MOF compensated by solvent content from TGA plot)			Remaining product in wt% 100% = Structural MOF formula as given in literature			Experimental results in wt%
No oxides	oxides	Half oxides	No oxides	oxides	Half oxides	
16%	26%	21%	11 %	19%	15%	**20.7%**
30%	38%	34%	24%	30%	27%	**26.2%**
26%	37%	32%	34%	44%	39%	**33%**
27%	35%	31%	32%	42%	37%	**31%**

Table 4-6 Simulation of the possible products forming during TGA combustion of MOFs.

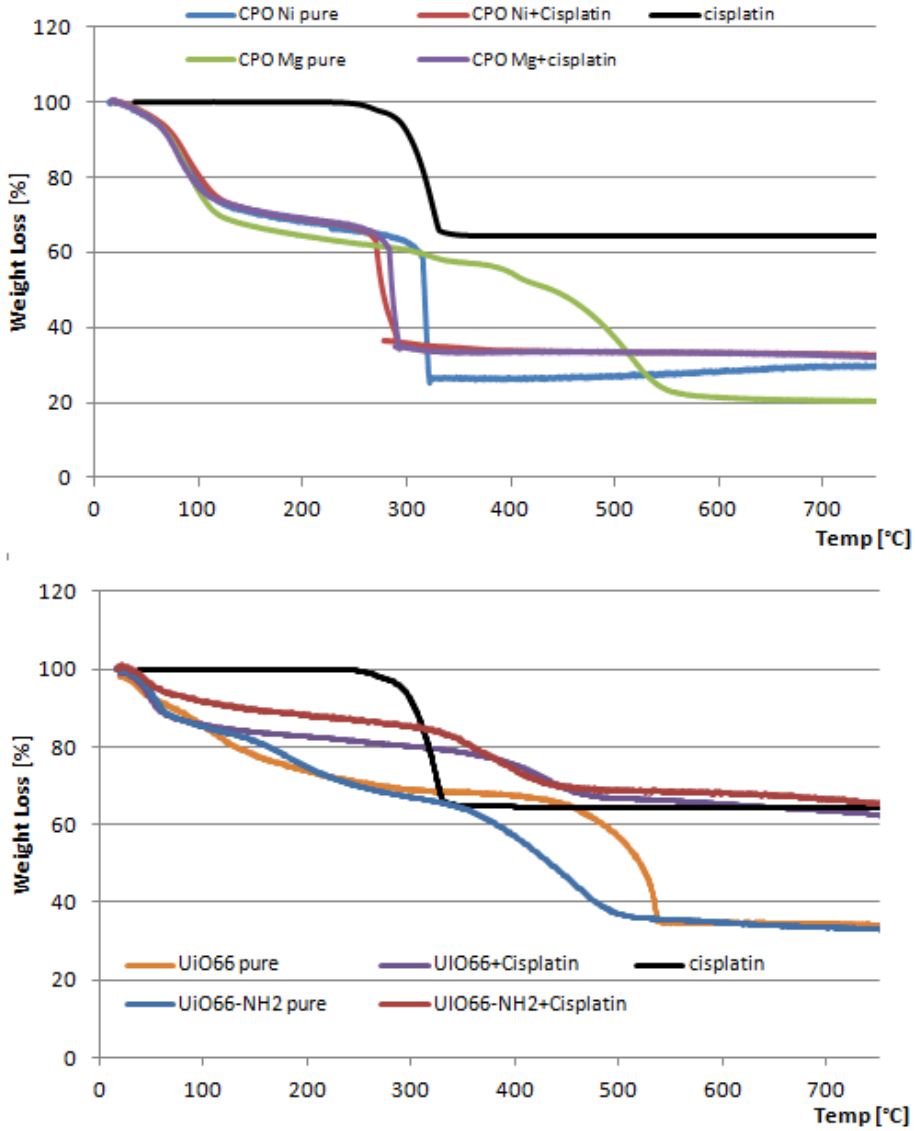

Figure 4-6 TGA of MOFs loaded and unloaded with cisplatin, cisplatin marked in black for a reference.

By combining the results obtained from ICP/MP-AES analysis and TGA plots (weight loss of solvents), the calculations on the Pt:Metal ratio were conducted. In

the TGA process, the solvent evaporates first. Each of the samples contains a known amount of cisplatin. Let's calculate the "dry" mass of the MOF: 100% – [solvent] % – [cisplatin] % = dry pure MOF. These masses are then calculated into mols of substance, for MOFs this will be the dehydrated structure with no water molecules (UiO66 = 1664 – 36 g/mol, UiO66NH_2 = 1754 – 36 g/mol, CPO Mg = 242 g/mol, CPO Ni = 311 g/mol). Based on this assumption, we obtained the following ratio of Pt: Metal, CPO Mg [Pt:Mg = 1:68.4], CPO Ni [Pt:Ni = 1:102.4], UiO66 [Pt:Zr = 1:10.7], and UiO66NH_2 [Pt:Zr = 1:6.6].

For UiO66NH_2 with a conjugated prodrug, the synthesis conditions will have 6 amine groups available to be functionalised and only 2 prodrug groups (reaction 1 mol of MOF on 2 mols of Pt-prodrug) based on the ICP result for Pt content of 6.5 wt%, we can form an equation (Eq.4-2), describing the number of moles of Pt per 1 mol of the MOF:

$$\frac{195.084 \cdot x}{(1754-a)+417 \cdot x} = 0.065 \qquad 4\text{-}2$$

Where x is the number of moles (prodrug or Pt) being conjugated to the amine group of Zr-MOF and a equals either 0 (unsuccessful), 1 or 2 (if all the available amine groups set by synthesis conditions are conjugated, every 3rd amine group). Solving this equation, we obtain x = 0.6783±0.12%, by rounding it up 0.68. So the ratio Pt: Zr = 1:8.82, meaning that roughly every 8th-9th amine group will be conjugated to Pt-prodrug. If the entire amount of Pt was successfully conjugated to the amine group, then the Pt wt% would be 15.09 wt% (Table 4-7). The max incorporation of prodrug functionalising all the 6 amine groups would require the dose of 210 mg per 140 mg of Zr-MOF.

No. of functionalised amine groups	1	2	3	4	5	6
Pt wt%	9	15	19	23	25	28

Table 4-7 Pt wt% content in the MOF depending on the number of amine groups successfully functionalised.

Some attempts were made to adapt UVVIS analysis for the purpose of cisplatin content determination. However, the MOF samples gave the signal at the cisplatin maximum of Absorbance at 301 nm masking it and setting up a new cut off at around 300 nm. This was noticed for CPO Mg and CPO Ni and UiO66 samples and made the application of this method for determination of cisplatin quantity,

impossible. MOFs' own absorbance masks completely the spectra coming from cisplatin. Due to the fact that molar absorption coefficient for cisplatin for its maximum at 301 nm is 0.130 $mM^{-1}cm^{-1}$, giving A = 0.2 for the concentration of 0.49 mg/ml, the further dilution of the samples would lead to reaching the undetectable limit of cisplatin concentration. In case of UiO66-NH_2, this "feature" of the powder was only observed when a dissolution studies were performed on the control sample (pure UiO66-NH_2) and the test sample (loaded with cisplatin). The control sample would give absorbance signal that would gradually be raising with higher t > 0 min, excluding the application for UV-VIS method (Figure 4-7).

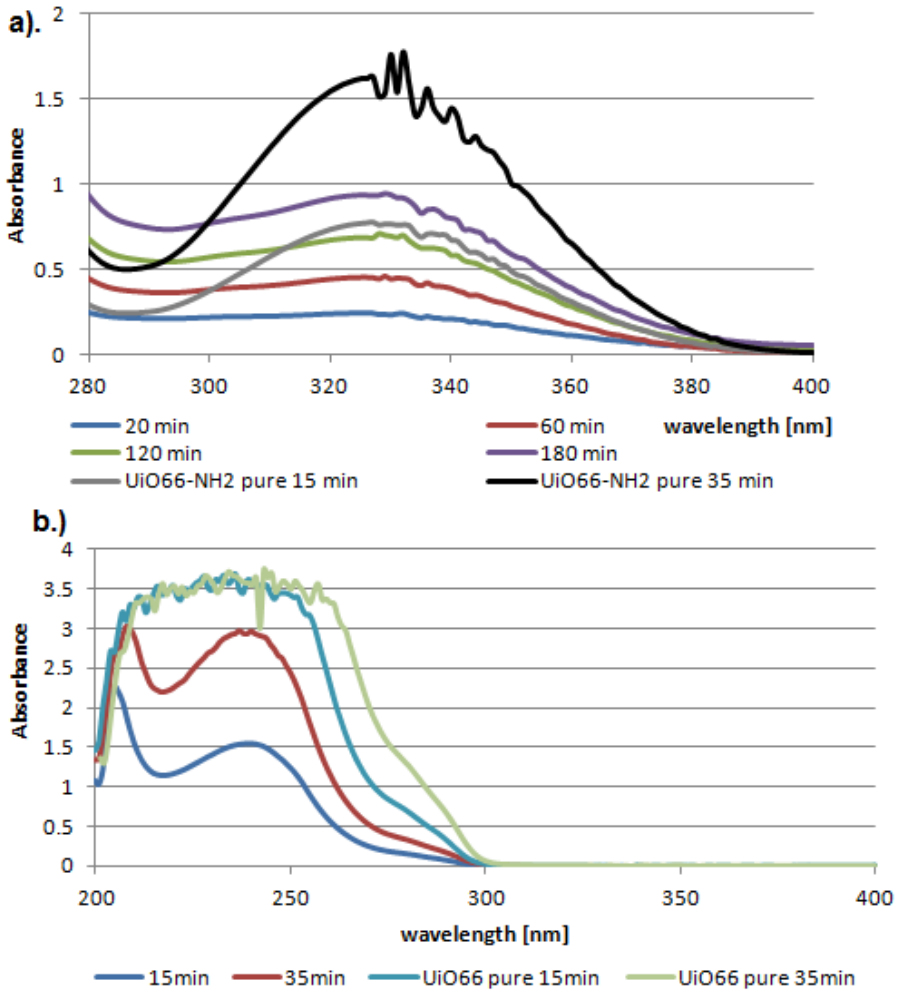

Figure 4-7 Results for the cisplatin quantification by application of UVVIS. A.) shows the release measured for UiO66NH_2, over 180 min and after 15 and 35 min on the test samples B.) release measured for UiO66. Experiment used the pelletised material.

4.3.2 Cisplatin Release

The quantification of the cisplatin in samples was performed utilising ICP-AES and ICP-MS, and MP-AES technique was used to assess how much cisplatin (wt%) has been released over time from the drug – loaded MOF.

For the release experiment, MOF powder (CPO Ni, CPO Mg, UiO66 and UiO66-NH_2) was prepared in a form of a pellet ca. 20 mg each, containing 25% of a drug-loaded MOF and the remaining 75% being Teflon. In each experiment, two pellets of 20 mg were added to 10 mL of TRIS buffer of pH 7.4, the release was carried out at 37 °C. TRIS buffer was prepared in a following way: 100 mL 0.1M TRIS (2-Amino-2-hydroxymethyl-propane-1,3-diol), 84 mL 0.1 M HCl, and 12 mL deionised H_2O), it is an organic compound widely used in biochemistry, here it was used in order to keep the solution free of Na^+ and K^+ ions, to protect the torch of MP-AES. Aliquots of 0.5 mL were removed in the following time points: 15 min, 30 min, 1 h, 2, h, 3 h, 4 h, 5 h and 24 h. Cisplatin release was quantified as expressed in Pt amounts in solution and then the cisplatin content calculated based on Pt content. Experiments were performed in duplicate. All calculations for the extent of release are related to the amount of the active powder in a pellet and not to the mass of a pellet. Also, a pellet preparation technique was applied in order to examine the feasibility of adjusting the percentage of drug (active powder) in a pellet, replacing 75% of its weight with a non-toxic material such as Teflon (patient dependent dose). The results are shown in the Figure 4-8 below.

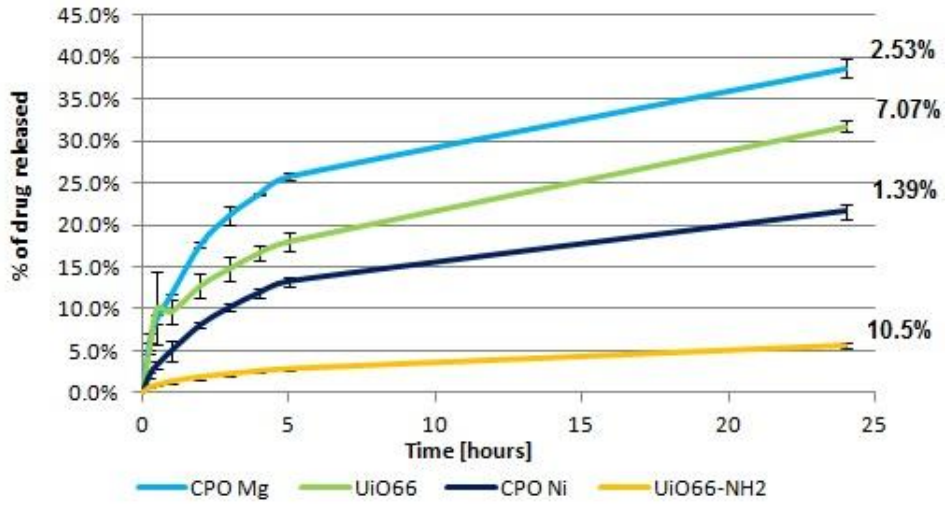

Figure 4-8 Plot depicts cisplatin release from the MOF pellets (25wt% of the pellet is an active MOF-powder) over 24 hours.

The plot shows that the release of cisplatin from CPO Mg powder (cisplatin loading at the level of 2.53 wt%) is reaching nearly 40 % of the incorporated cargo, and is the highest from the given MOF. UiO66-NH_2 releases only above of 5% of its cargo, which is the lowest, even though the ICP analysis showed that the cisplatin loading is the highest. It must be noted that the drug loading content for this diagram for CPO Mg and CPO Ni are based on the digestion in concentrated HCl and analysed by MP-AES and for the Zr-MOFs a special digestion technique was applied and analysis performed on ICP-MS, thus the comparison should be made between CPO Mg and CPO Ni, pointing out that CPO Mg is a better candidate for a drug delivery carrier for cisplatin than CPO Ni is. It should also be stressed that cisplatin content is expressed in weight units and CPO Ni is much heavier than CPO Mg which may lead to this conclusion. Conversely, analysis of the released cisplatin quantities by UiO66 and UiO66-NH_2 points out that the former is a better candidate for drug delivery system for cisplatin. It should be noted that the release was carried out over a limited time which is 24 hours, and the curves are still far away from reaching a plateau, apart from performance of UiO66-NH_2. The quantities of released cisplatin are reaching 38.6 % in case of CPO Mg, 31.8 % for UiO66, 21.6 % for CPO Ni and only 5.6 % for UiO66-NH_2. The poor release of cisplatin obtained from UiO66-NH_2, despite its high drug loading of 10.5wt %, may be linked to the interaction between the amine group and Pt in cisplatin, most probably ruled by the very same mechanism that is involved in Pt-binding at the N7 sites of Guanosine (Guo) and Adenosine in DNA. Cisplatin binds much more strongly to guanosine due to the fact of amine binding to the oxygen on guanosine [30, 31]. The diagram Figure 4-9 below shows the release of a drug expressed in Pt quantities in μg per each mg of MOF powder.

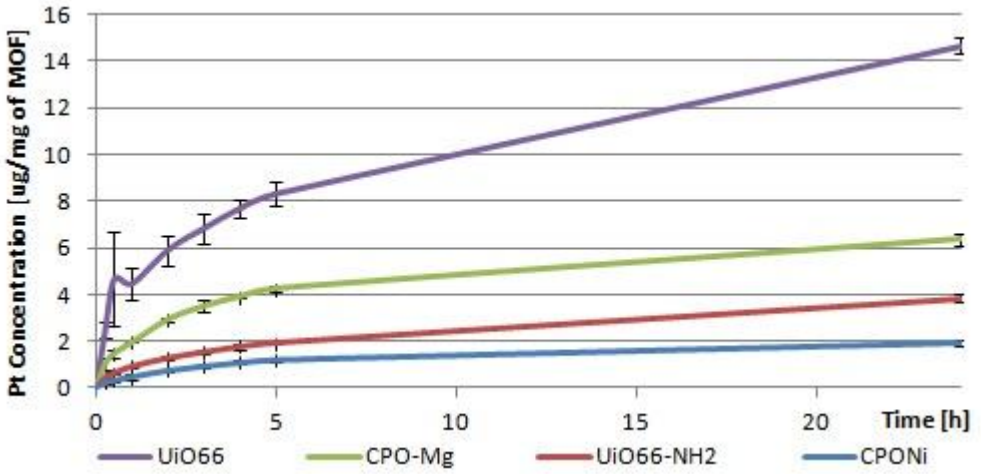

Figure 4-9 Release of cisplatin from the MOF powders expressed in quantities of Platinum [µg] per MOF weight unit [mg]. The pellets used contained 25% wt of cisplatin loaded MOF powder.

If we looked at the release of Pt expressed in µg per mg of MOF, the one carrying the highest amount of Pt is UiO66, with 14.66 µg/mg, Pt release of others is inferior with UiO66-NH_2, carrying 3.82 µg Pt per each mg of MOF and CPO Ni with only 1.96 µg. This may be due to the poor loading achieved or blockage of the encapsulated quantities in case of amine-Zr MOF. The content of cisplatin in the samples was calculated based on the Pt concentration, by multiplying it by a factor 300.01/195.08, which corresponds to molecular weight of cisplatin to molecular weight of Pt.

To normalise the results and accommodate the differences in molecular weight of the MOF compounds, Pt or cisplatin release profile and drug loading, were expressed in µg cisplatin per mol of MOF. This allows for a direct comparison of drug loading potential. The molecular formula of UiO66 is $Zr_6O_4(OH)_4(CO_2C_6H_4CO_2)_6$ and molecular weight 1664 g/mol thus one gram of is equivalent to 0.60 mmol [32], UiO66NH_2 is $Zr_6O_4(OH)_4(CO_2C_6NH_5CO_2)_6$ and molecular weight 1754 g/mol and similarly 1 g an equivalent of 0.57 mmol. For CPO-27 the molecular formula is $M_2(C_8O_6H_2)(H_2O)_2{\bullet}8H_2O$ [23] the molecular weights are: 491 g/mol and 423 g/mol, with 1 g equivalents of 2 mmol and 2.36 mmol for CPO Ni and CPO Mg respectively. This approach is simplified and does not compensate for H_2O and DMF presence in the pores of the material. The results are shown in Figure 4-10.

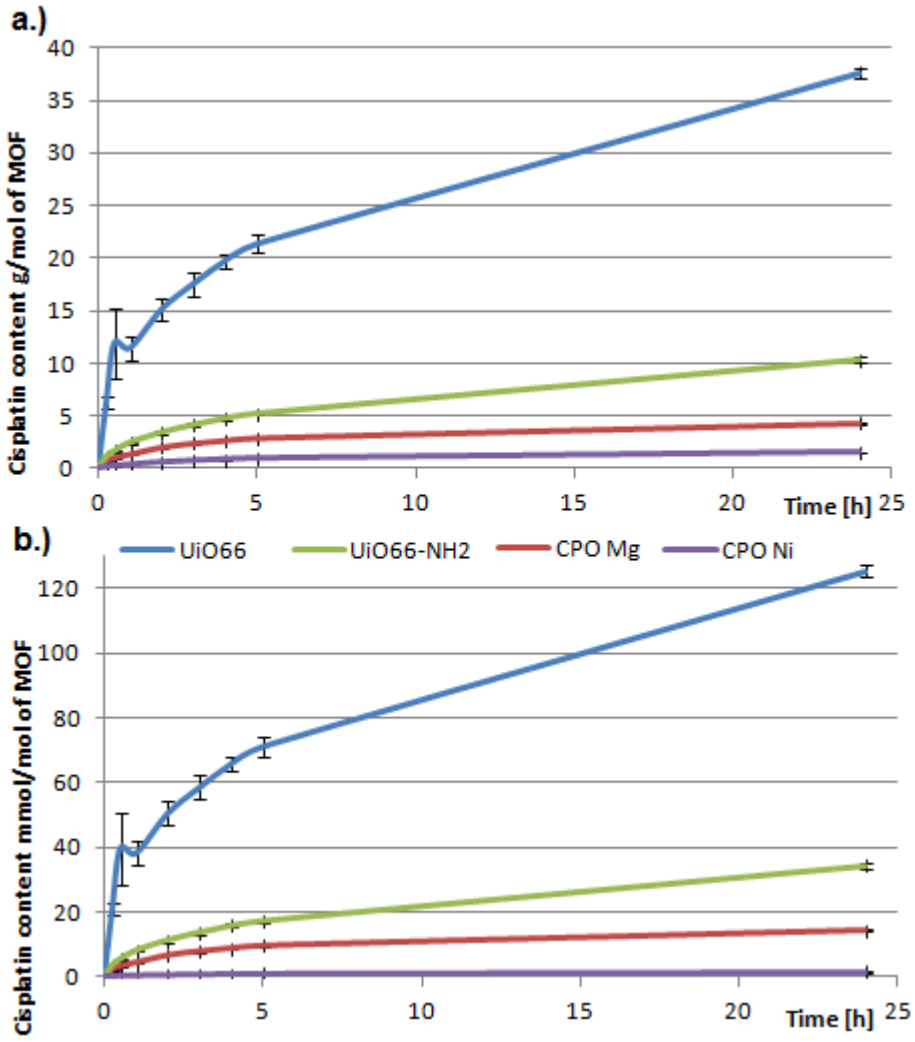

Figure 4-10 Release of cisplatin, depiction of a normalised release of cisplatin to mol of MOF, a.) g of cisplatin per mol of MOF and b.) mmol of cisplatin per mol of MOF.

The same results were calculated to express the quantity of cisplatin per 1 mol of metal in the MOF. In all of the depictions UiO66 is the best performing MOF for the release of cisplatin and CPO Ni is not performing so well.

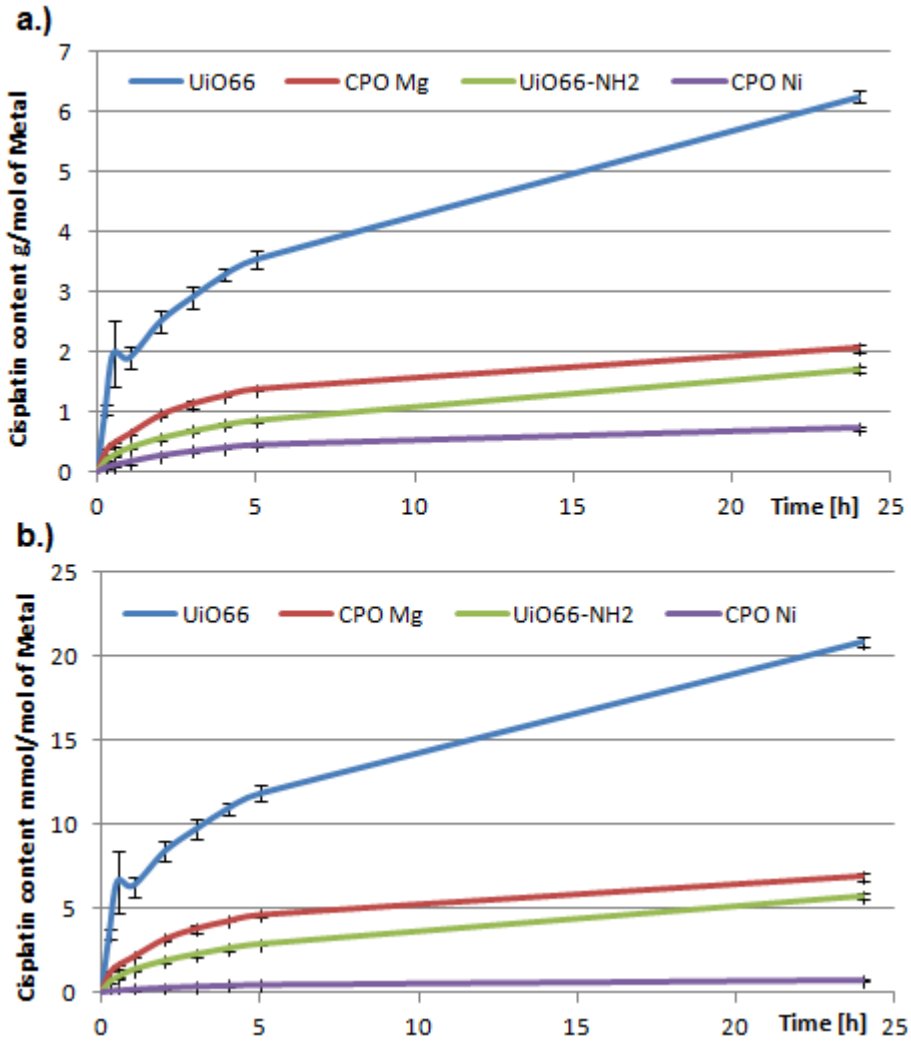

Figure 4-11 Cisplatin released quantities per 1 mol of Metal ion, a.) in g of cisplatin and b.) in mmol of cisplatin.

In order to check if the Teflon content may have influenced the release profile of the drug, a pellet containing 100% active powder of CPO Ni was prepared. CPO Ni was chosen as it was the option with very low cisplatin release, the experiment was run in a duplicate and release carried over 48 h. Also, this was carried on the best performing MOF, UiO66, over 24 hours. The results are shown in the Figure 4-12 below. All the calculations relate to mass of active MOF powder used in that experiment.

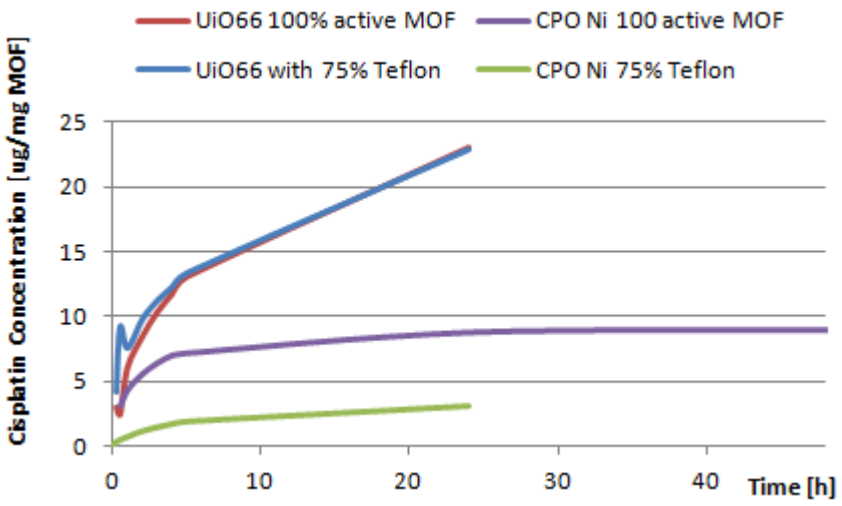

Figure 4-12 Cisplatin release profile from pellets containing 100% of active powder and only 25%, the rest being Teflon.

The values obtained indicate a possible Teflon influence on the cisplatin release profile from pellets prepared with 25% of active powder (CPO-27 Ni, UiO66). The difference is 5.7 μg/mg active MOF, 3.00 μg/mg vs. 8.7 μg/mg (CPO-27 Ni). This is not the case for UiO66 though. This may be due to entrapment of cisplatin in the MOF structure when the pressure is applied to form a pellet and the Teflon presence may work as a release-block. The Zr-MOF with a conjugated prodrug of cisplatin has not been tested for the release profile as it is envisaged that the release mechanism will be activated by reducing environment in the cancer cells in which $[Pt^{IV}(NH_3)_2(Cl)_2(OH)(O_2CCH_2CH_2CO\text{-}NH\text{-}UiO66)]$ will be reduced to $[Pt^{II}(NH_3)_2]Cl_2$ which in the solution will form a radical $[Pt^{II}(NH_3)]^{2-}$ that easily interacts with nitrogen (N7) of guanine on double-stranded DNA chain[3, 28, 33, 34]. It has been proven that Pt(IV) – prodrug compound does not have the ability to cleave the DNA chain by intercalation of Pt to guanine or adenine and only cisplatin Pt(II) moiety shows such a behaviour[35, 36].

4.3.3 Viability assays

Viability assays were set up and performed in order to assess the efficacy of the two proposed methods for cisplatin incorporation in the MOF framework. One being physical encapsulation and the other conjugation of a modified cisplatin prodrug to an amine group of Zr-MOF. These assays used Resazurin dye (Alamar Blue assay) and Flow Cytometry (FACS) techniques. The latter method also

allowed to assess the kind of death, the cell undergoes by cell staining with the markers such as FITC-Annexin V to quantify early apoptosis and Ethidium Homodimer III (superior to Propidium Iodide) for necrosis. The mechanism was described in Chapter 3 Experimental Methods.

4.3.3.1. Viability of cells : Conjugation vs. Encapsulation method

Alamar Blue assays, as well as FACS, were used to quantify the viability of cells that were exposed to drug delivery systems, for 24 hours. Both viability assays were performed using different passage number and different cells, Alamar Blue tested viability on A549 lung cancer whereas FACS – THP-1 human leukemia cancer. The FACS instrument is designed to work with suspension cells and if adherent cell culture should be investigated, the cells must be treated with trypsin so they could flow freely and be counted. This may though influence the results and may block the instrument, this is why only THP-1 cells were tested with the FACS technique for the purpose of this thesis. The prodrug of cisplatin $[Pt^{IV}(NH_3)_2(Cl)_2(OH)(O_2CCH_2CH_2CO_2H)]$ that was used in the conjugation reaction was analysed by Elemental Analysis showing that values found during the analysis, [C] 10.77 %, [H] 2.67 % and [N] 6.61 % agree with expected content 11 wt%, 2.76 wt% and 6.45 wt% respectively. Cisplatin as well as two modified compounds, oxoplatin and prodrug were analysed using ATR spectroscopic technique showing the vibrations of characteristic bonds, this indicates that 2-step cisplatin modification reaction was successful. In a prodrug spectra a very broad band of O-H stretch can be seen in a range of 3300-2500 cm^{-1}, C=O stretch 1760-1690 cm^{-1} and C-O stretch 1320-1210 cm^{-1}. ATR infrared spectroscopy (Figure 4-13) shows bands at around 1580 and 1730 cm^{-1} corresponding to amide groups, proving a peptide bond formation between the Pt(IV) prodrug and the amine group of UiO66-NH_2. Small bands corresponding to amine groups can also be seen, as not all available amine groups on the MOF were involved in the conjugation. The band at 1750 cm^{-1} in the MOF, completely disappeared after conjugation, which supports the hypothesis of a successful conjugation.

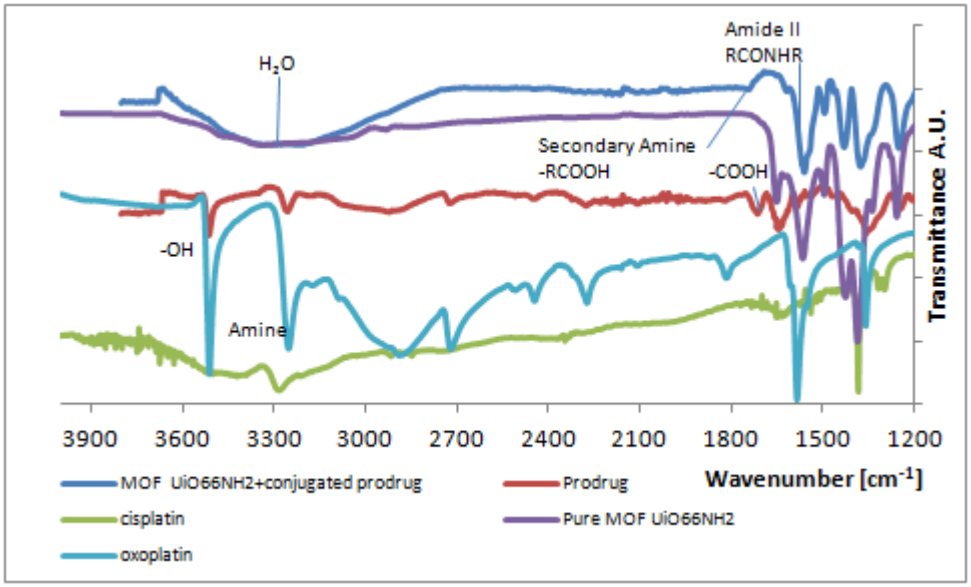

Figure 4-13 FTIR spectra of modified cisplatin products and Zr-MOF.

TGA analysis of cisplatin, prodrug, UiO66-NH_2 and Zr-MOF with a conjugated prodrug indicates that the compounds are different to cisplatin. Cisplatin TGA curve shows that this compound starts to decompose at 270 °C with a weight loss of 37.6 % which indicates that metallic Pt is a combustion product. The TGA analysis (Figure 4-14) was performed with nitrogen as a feed gas so no oxides can be formed. In case of prodrug, the weight loss amounts to 52.8 wt% which also indicates that a prodrug is burned to metallic Pt. The difference in weight loss between the Zr-MOF with conjugated prodrug and pure Zr-MOF is ca. 4 wt%, which is due to the Pt quantities in the burned material.

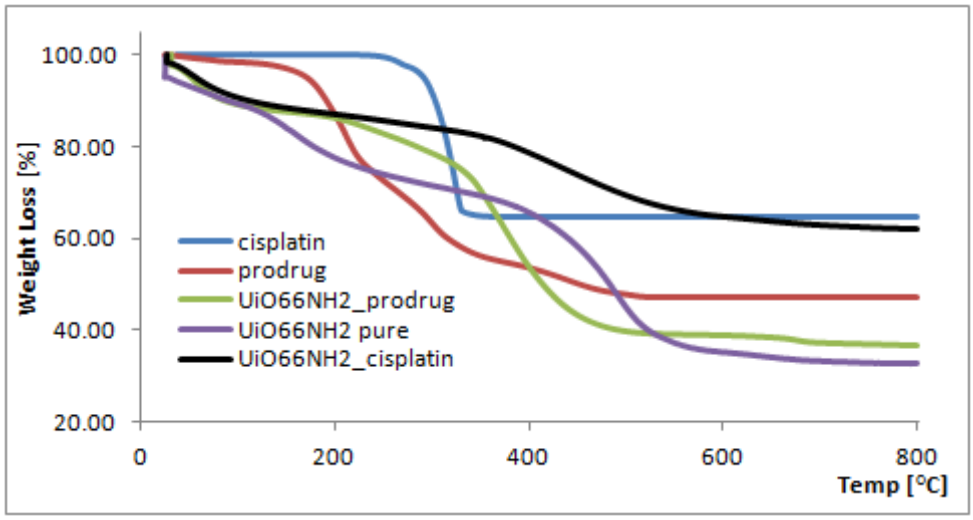

Figure 4-14 TGA results for Zr-MOF, cisplatin and a prodrug.

The results obtained from TGA in oxygen free environment for the Zr-MOF encapsulated with cisplatin is not clear as it indicates the Pt content at the level of 29.3 % wt and ICP-MS showed that Pt weight content is at the level of 6.5 %wt. This may be due the formation of an oxide product that is stable in temperatures of more than 800°C. In the MOF framework, there is oxygen available for this new compound formation. There was an idea to analyse the product that was left after TGA analysis with X-ray radiation, however, the quantities were very small.

The amide-coupling reaction allows for the direct incorporation of a non-toxic Pt(IV) prodrug to the MOF amine group. The Pt(IV) prodrug can be easily reduced in an environment poor in oxygen, resulting in cytotoxic Pt(II)-containing cisplatin. This reduction can be realized by biological reducing agents such as glutathione[28, 37]. The MOF integrity was retained after the coupling process. No impurities are evident in the PXRD pattern, which is shown in (Figure 4-15). Some attempts were made to reduce the Pt(IV) prodrug with ascorbic acid[27] and quantify the amount of cisplatin released by ^{195}Pt NMR, however the signal to noise ratio was low and the results therefore inconclusive.

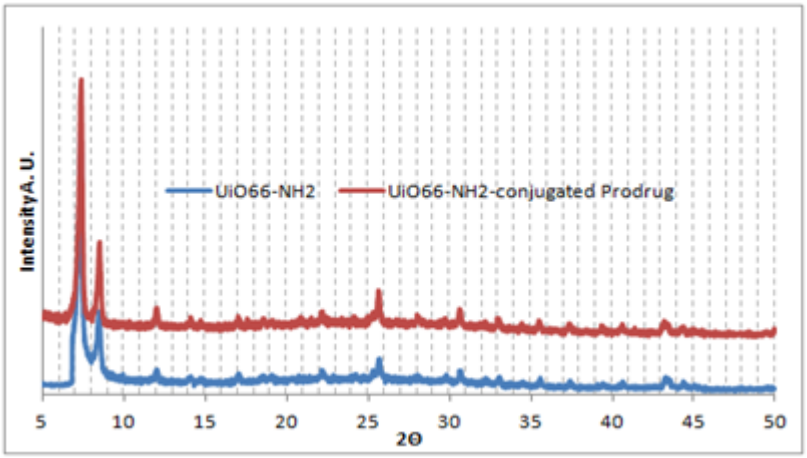

Figure 4-15 PXRD of UiO66-NH_2, phase pure (blue) and with a cisplatin prodrug conjugated (red).

The lung cancer cell line A549 was stimulated with different MOF formulations and cell viability was examined after 24h exposure using the Alamar Blue assay. This cell line was selected for *in vitro* studies because cisplatin is commonly used to treat lung cancer. The data are presented as mean ± SEM (standard error of the mean) from two independent experiments, with each set of conditions run in triplicate for each experiment. Suspensions of the MOF formulations were

prepared with a concentration of 1mg/100μL and aliquots of 10, 30 and 50 μL were used to stimulate the cells. MOF powders were ground in the mortar with a pestle before preparing the suspensions so to avoid big agglomerates of the powder. This corresponded to 100 μg, 300 μg and 500 μg of MOF per well respectively. Complete RPMI was added to even up the volume in wells to 150 μL. A cisplatin solution was prepared as a positive control, with a concentration of 1 mg/ml (3.33 mM). The aliquots used for cell stimulations were the same as those for MOF powders: 10 μL (cisplatin concentration 222 μM), 30 μL (cisplatin concentration 666 μM) and 50 μL (cisplatin concentration 1110 μM). Statistical analysis was performed by Repeated Measures ANOVA and Sidak's multiple comparisons test using GraphPad Prism v6.05 software. Differences between means were considered statistically significant when $P < 0.05$ (*), $P < 0.01$ (**), $P < 0.001$ (***), or $P < 0.0001$ (****). "P" is the probability of obtaining the observed effect purely due to chance. $P < 0.05$ is the conventional threshold for a statistically significant result, and indicates that there is only a 5% of chance that the conclusion drawn is in fact false. Subsequent levels of significance commonly used in statistics are $P < 0.01$, $P < 0.001$, $P < 0.0001$, which denote 1%, 0.1% and 0.01% chance, respectively. The lower the P value obtained, the higher the level of significance of the observed effect and, consequently, the greater our confidence that it is true. Statistical analysis was performed by Dr Ilona Kubajewska. The cytotoxic efficacy of UiO66-NH_2 with encapsulated cisplatin and UiO66-NH_2 conjugated with the cisplatin prodrug are compared in Figure 4-16. It appears that the latter performed better in inducing cell death, particularly at higher concentrations where statistically significant outcomes were observed. This is expected to be a result of the higher drug accessibility "on demand" in the conjugated system, as well as the binding between cisplatin and the amine groups of UiO66-NH_2 quenching the release. The conjugated UiO66-NH_2 system shows approximately the same cytotoxicity as the cisplatin itself at higher concentrations, but is less effective at low concentrations. In all cases, there is a distinct dose-dependent effect observed of the drug-loaded MOFs on cell viability. It is clear that these systems are biologically functional, and thus have potential as drug delivery systems.

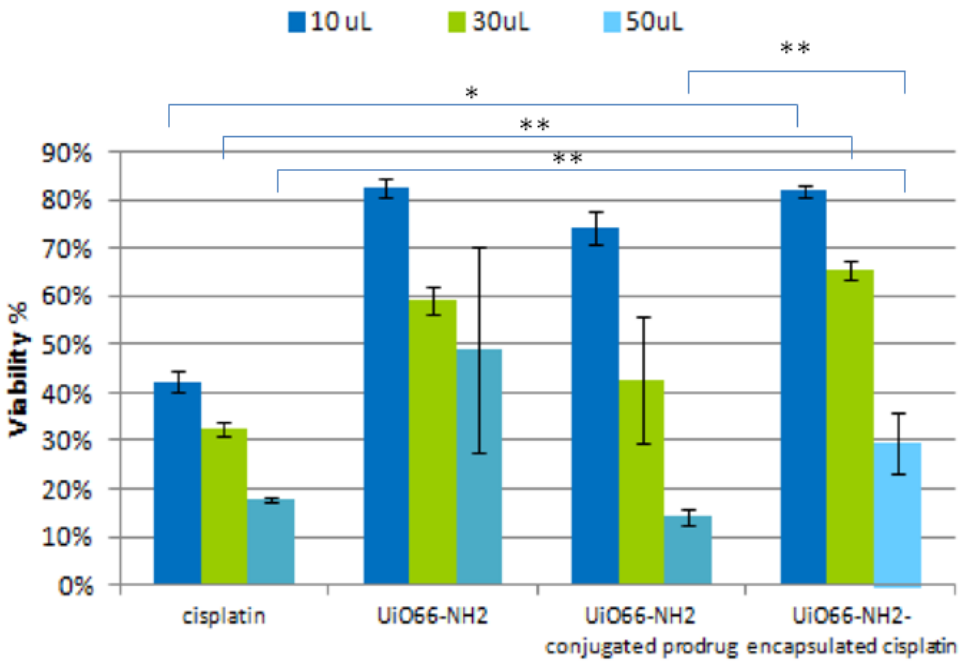

Figure 4-16 Cell viability (A549) after 24h exposure to UiO66-NH_2 with encapsulated cisplatin and conjugated with the prodrug. Results are from two separate experiments, each of them conducted in triplicate, shown as mean ± SEM. *, refer to the p values of statistical significance P<0.05 (*) and P<0.01 (**). 10, 30 and 50 µL are the volumes of aliquots added to the cell suspension correspond to a concentration of encapsulated cisplatin that can be found in Table 4-8 and 4-9. Cisplatin stimulating solution 1mg/ml was added as the same aliquot volumes with concentrations corresponding to 222, 666 and 1110 µM respectively for 10, 30 and 50 µL added.**

The situation is pretty similar for THP-1 cells stimulated with Zr-MOF formulations. The volume of the cells being stimulated was 200 µL and added aliquots were 50 µL (1 mg / 100 µL). The results (Figure 4-17) show that prodrug stimulation induces much higher apoptotic death than cisplatin does. The Zr-MOF with a conjugated cisplatin prodrug is showing slightly higher efficacy (viability at the level of 76 %) than the formulation prepared in the encapsulation route (viability 81.5 %). The percentage of cells undergoing the necrotic death induced by drug delivery systems based on UiO66-NH_2 with incorporated cisplatin, is very small and the result show that it is not a main mechanism for cell death. It is worth noting that no matter how diligently the powders were ground and milled before preparation of suspensions for cells stimulations, the formulation was not 100% homogenous. This may have caused a disruption and influenced the results obtained as it cannot be excluded that bigger or smaller chunks of material may

have been pipetted during cell stimulation experiment. The possible way to address this could be separation of MOF powders into the fractions using a sieve, however, it may not solve the problem and the sieve could retain cisplatin particles on its metal surface or making them in a nanoparticles size.

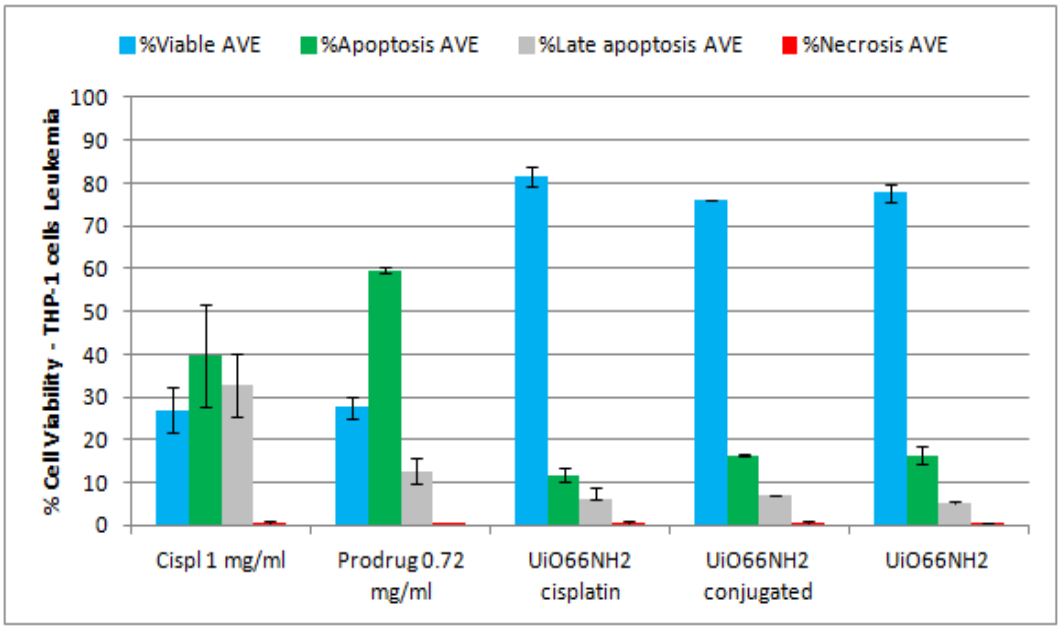

Figure 4-17 THP-1 cell viability (blue) by FACS, differentiating between the cell death: apoptosis (green), late apoptosis (gray) and necrosis (red). The error bars are SD (standard deviation) of results taken from duplicates. 24h stimulation. Concentration of MOF stimulant 2 g/L (500 µg/250 µL).

Amounts of encapsulated cisplatin may be bound to the amine group which would impair or even stop the drug release, the ICP (Inductively coupled plasma) quantified cisplatin loading is slightly higher (10.5 wt%) for a carrier with encapsulated drug, however, the efficacy is lower as shown by the results in the two viability assays. In case of a conjugation technique, the release of the prodrug is not influenced by the amine group.

4.3.3.2. Viability of cells: Zr-MOFs (UiO66 and UiO66-NH_2) and CPO-27 (Ni and Mg) as an example of drug delivery carriers in encapsulation route

Four MOF materials have been selected for carriers of cisplatin, and these systems were prepared by the encapsulation route. Their efficacy against cancer was tested on 2 types of cell lines: A549 lung cancer and THP-1 human leukemia. MOFs were chosen due to their non-toxic character, large pores and simplicity of the

synthesis route[22, 25, 26, 38]. Alamar Blue assay was used to assess viability of A549 cells and the cells' viability was monitored in two time points, after 24 and after 48 hours. The FACS allowed assessment of viability and conclude the kind of cell death that the used formulation may induce. Table 4-8 presents the relations between added material and the concentration of MOF powder in the well. The cell concentration for both cell lines were not the same, and the seeding density adjusted to the type of the cells, in case of A549 cells in the given volume of 100 µL, 4 000 cells were seeded and in case of THP-1, 200 000 cells were seeded per 200 µL (100 000 per 100µL).

Aliquots added[µL], all MOFs	MOF quantity added to cells[µg]	A549 cell line 100 µL MOF concentration [g/L]	THP-1 cell line 200 µL MOF concentration [g/L]
10	100	0.9	0.5
20	200	1.7	0.9
30	300	2.3	1.3
40	400	2.9	1.7
50	500	3.3	2.0

Table 4-8 Amount of aliquots of MOF suspension used for cell stimulations.

The cisplatin concentration based on the ICP measurements has been found to be 1.39 wt% for CPO Ni, 2.53 wt% for CPO Mg, 7.1 wt% for UiO66 and 10.5 wt% for UiO66-NH_2. By multiplying the MOF powder quantities pipette in the well by these values, the cisplatin concentration can be found and expressed in [g/L], and this can be further calculated to express this concentration in mM, see tables Table 4-9 and Table 4-10. Cisplatin solution 1 mg/mL used as a standard (aliquot of 50 µL) corresponds to the concentration of 200 mg/L, 0.67 mM for THP-1 cells stimulation and 333 mg/L, 1.11 mM for A549.

A549 cell line 100 µL MOF concentration [g/L]	CPO Mg Cisplatin concentration (mg/L) [mM]	CPO Ni Cisplatin concentration (mg/L) [mM]	UiO66 Cisplatin concentration (mg/L) [mM]	UiO66-NH_2 Cisplatin concentration (mg/L) [mM]
0.9	(23.0) [0.08]	(12.6) [0.04]	(64.5) [0.22]	(95.5) [0.32]
1.7	(42.2) [0.14]	(23.2) [0.08]	(118.3) [0.39]	(175.0) [0.58]
2.3	(58.4) [0.19]	(32.1) [0.11]	(163.8) [0.55]	(242.3) [0.81]
2.9	(72.3) [0.24]	(39.7) [0.13]	(202.9) [0.68]	(300.0) [1.00]
3.3	(84.3) [0.28]	(46.3) [0.15]	(236.7) [0.79]	(350.0) [1.17]

Table 4-9 Concentration of cisplatin (mg/L) and (mM), stimulated A549 cells.

THP-1 cell line 200 µL MOF concentration [g/L]	CPO Mg Cisplatin concentration (mg/L) [mM]	CPO Ni Cisplatin concentration (mg/L) [mM]	UiO66 Cisplatin concentration (mg/L) [mM]	UiO66-NH_2 Cisplatin concentration (mg/L) [mM]
0.5	(12.0) [0.02]	(6.6) [0.02]	(33.8) [0.11]	(50.0) [0.17]
0.9	(23.0) [0.04]	(12.6) [0.04]	(64.5) [0.22]	(95.5) [0.32]
1.3	(33.0) [0.11]	(18.1) [0.06]	(92.6) [0.31]	(137.0) [0.46]
1.7	(42.2) [0.14]	(23.2) [0.08]	(118.3) [0.39]	(175.0) [0.58]
2.0	(50.6) [0.17]	(27.8) [0.09]	(142.0) [0.47]	(210.0) [0.70]

Table 4-10 Concentration of cisplatin (mg/L) and (mM), stimulated THP-1 cells.

This indicates that formulation UiO66-NH_2 with its high drug loading, in the dose, that is introduced in the cell media and brings in slightly more cisplatin in the well, should have the same or higher efficacy as 1 mg/ml cisplatin solution and the viability should be same after treatment with cisplatin solution and by stimulation with Zr-MOF.

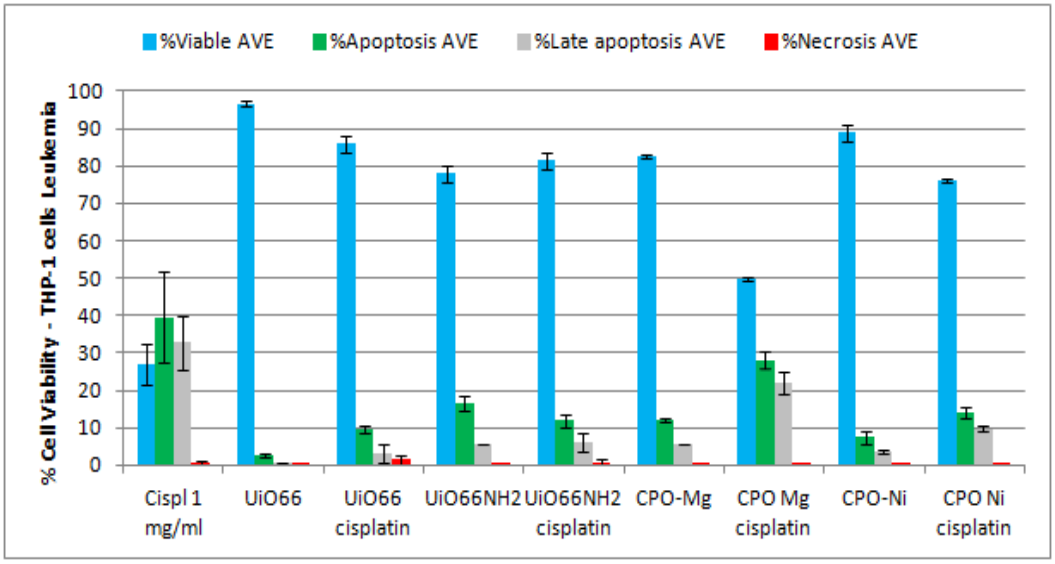

Figure 4-18 Viability results by Flow Cytometry, THP-1 stimulation over 24 h exposure. Fluorescent staining allows to recognise the cell death mechanism. The error bars are SD (standard deviation) of results taken from duplicates. Concentration of MOF stimulant 2 g/L (500 µg/250 µL).

Nevertheless, the results do not seem to support this (Figure 4-18). There is no significant difference between the viability of the cells stimulated with UiO66-NH_2 and the MOF containing cisplatin. This, may be connected with the retention of cisplatin in the MOF framework due to the interaction of amine group with Pt in the cisplatin and also the imperfection of a suspension as is not homogeneous.

UiO66 does not effects the viability of cells (97 %) and when loaded with a anti-cancer drug cargo decreases cells' survival (86 %). CPO Ni shows surprisingly high viability (89 %), and when encapsulated with cisplatin this viability will be decreased (76 %), same is observed for CPO Mg (82 %), however here, the % surviving cells is significantly lower ca. 50 % when cells are treated with the MOF carrying a drug cargo. Results depend on the homogeneity of the suspension as well as the condition of the cells used in the experiment (passage number). Below an example of a FACS cell viability analysis performed on cells of lower passage number (Figure 4-19) is presented. Unfortunately, the instrument got clotted and it was not possible to unblock it to finish the run including all the test samples in duplicate, that is why only those that were measured in duplicate are shown. Once the cells have been stimulated and the fluorescent dyes added there is a small time window for performing the analysis and the material cannot be preserved in the e.g. fridge for further investigations.

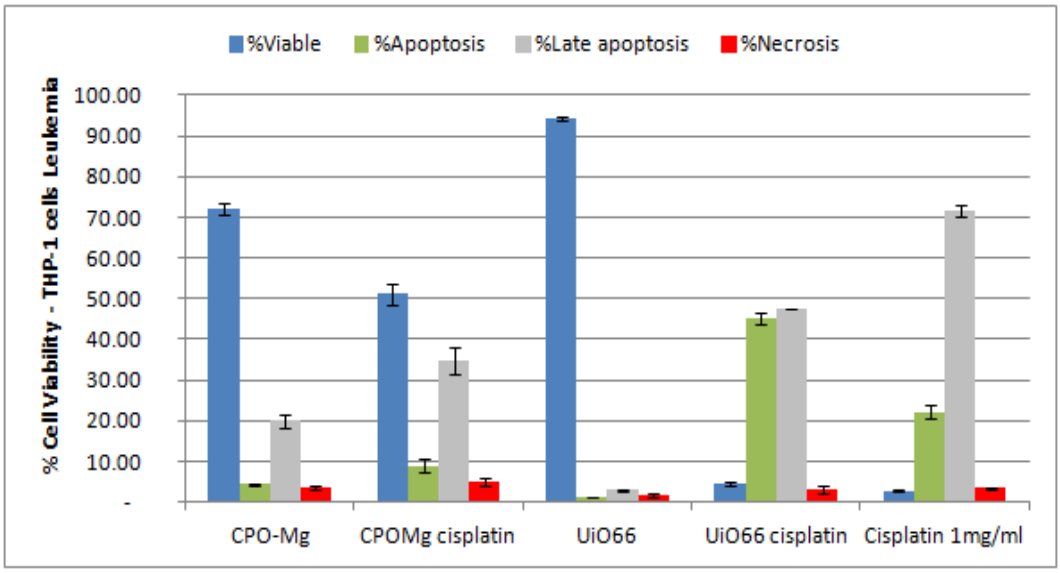

Figure 4-19 FACS analysis of THP-1 cell viability performed on lower passage number. The error bars are SD (standard deviation) of results taken from duplicates. 24h stimulation. Concentration of MOF stimulant 2 g/L (500 µg/250 µL).

We can see that viability of the cells treated with pure UiO66 MOF is not compromised and is dramatically lower when treated with cisplatin-loaded UiO66, its efficacy is very high and is comparable to cisplatin, which could be concluded from the calculations of a dose being used to stimulate cell material (see Table 4-10).

Let's take a look at the results obtained by stimulation of a different cell culture, A549 lung cancer, where cisplatin finds its application in various therapies[1, 39, 40]. The stimulation of cells was carried out for 24 h and 48 h and the results are depicted below (Figure 4-20) and (Figure 4-21). The number of the cell passage used for these experiment was 36 in case of 24 h and 37 in case for 48 h stimulations. The data shown come from two independent experiments (two well plates), in duplicate for each formulation. For each of the experiment, there was a viability calibration curve run along with the stimulations allowing to assess the viability. The standard curve was constructed as follows: fluorescence of untreated cells corresponded to 100 % and 0 % cells (RPMI media alone) to 0 % viability, with additional calibration points at 75 %, 50 % and 25 %. The amount of aliquots used for this experiment are listed in Table 4-9. The results show that after 24 h cancer cells stimulation with CPO Mg with encapsulated cisplatin, the cell viability drops, however there is no significant difference if this MOF contained cisplatin or not. To contrary, when stimulated with CPO Ni, the drop in viability for MOF carrying cisplatin cargo is noticeable.

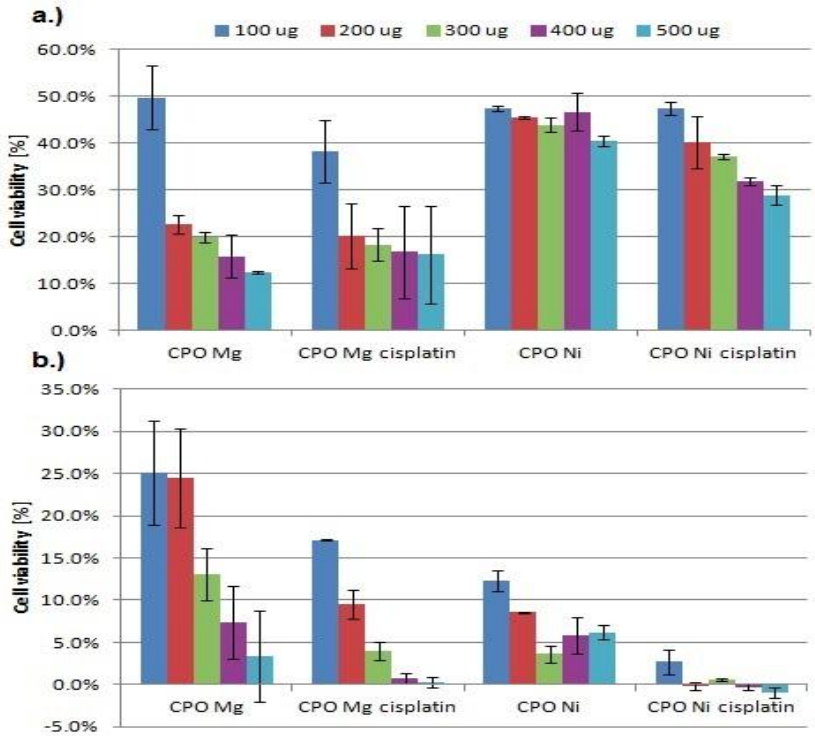

Figure 4-20 A549 cells viability testing, CPO Mg and CPO Ni used as a stimulant with/without encapsulated cisplatin a.) 24 hours and b.) 48 hours exposure. Concentration depicted in the legend refers to the quantity of added MOF in the aliquot. Please refer to Table 4-8, 4-9 and 4-10.

The situation changes for stimulations carried out for a longer time of 48 h. Here, we can see that viability of cells drops to 0 when CPO-27 Ni containing cisplatin is used. For CPO-27 Mg, there is a noticeable drop in cell viability after stimulation with the MOF containing cisplatin, which may be elucidated with the fact of delayed cisplatin release or the lack of homogeneity of the formulation. Particles size of CPO-27 Mg is 10 μm and CPO-27 Ni is 500-600 nm and this may be too big to migrate into the cell to release the cargo (see Figure 4-3).

In case of Zr-MOF, the results show that viability of cells treated with UiO66 containing cisplatin drops rapidly and at the same time the pure MOF is not cytotoxic to the cells when exposure is 24h. For UiO66-NH_2, there is a slight decrease of the viability (drug carrier), however, pure MOF is not harmless to cells. The cisplatin loading is the highest achieved in this group of MOFs but the expected high cytotoxic effect is not observable. This is caused by interaction of amine group in the aromatic carbon ring of the framework with Pt of cisplatin. If the exposure time is increased to 48 hours, UiO66 is showing higher cytotoxicity towards the cells, however the UiO66 loaded with cisplatin does not kill the cells completely, which would be an indication that the cargo carried by the MOF has been released within 24 hours after stimulation.

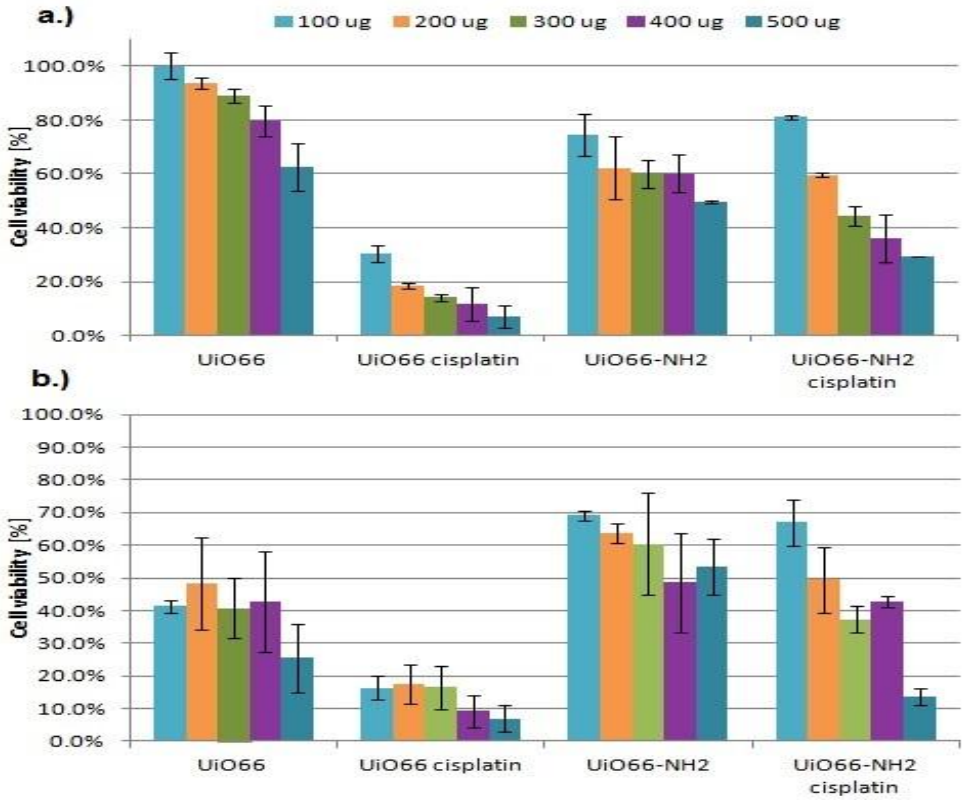

Figure 4-21 A549 cells viability test, UiO66 and UiO66-NH_2 used as a stimulant with/without encapsulated cisplatin a.) 24 hours b.) 48 hours exposure. Concentration depicted in the legend refers to the quantity of added MOF in the aliquot. Please refer to Table 4-8, 4-9 and 4-10.

It can be concluded based on viability tests performed that the best candidate for the MOF-based drug delivery system prepared in the encapsulation route, is UiO66. The dose of cisplatin typically used in anti-cancer therapy is 20 mg/m^2 per day for 5 days in case of testicular cancer, and 75 – 100 mg/m^2 administered once every 4 weeks for ovarian cancer[41]. According to the Boyd formula[42], an average male of 175 cm weighing 80 kg has a body surface area of 1.99 m^2 Applying the same formula to an average female of 165 cm weighing 58 kg results in 1.63 m^2. This would mean that in order to use the cisplatin-loaded MOFs in these therapies, an amount of ca. 1.7 g – 2.3 g (4 week treatment) would be necessary to treat ovarian cancer, and approx. 0.56 g for testicular cancer (a day).

4.3.4 NPs of metallic Platinum as a result of one – pot synthesis.

A synthesis aiming at cisplatin encapsulation in the one-step route in the variety of MOFs: CPO Mg and Ni as well as Zr-MOFs: UiO66 and UiO66-NH_2, resulted in formation of metallic nanoparticles of Pt incorporated in the MOF framework.

This is quite an interesting aspect because it can open up the new potential application in photo catalysis and catalysis[43-45]. Some attempts have been made to immobilise nanoparticles of Pt in the voids of the UiO66-NH_2 cages to use it as a platform for a catalyst[46]. The average size of the particles obtained in a one-step synthesis, was estimated to be 80 Å based on X-ray pattern analysis and application of the Scherrer equation[47], see Eq. 4-3, where **k** is a constant, wavelength of radiation (**λ**), width at half maximum of the peak (**β**) and the Bragg angle (**θ**) in radians at which x-rays are scattered from the crystal lattice.

$$\vartheta = \frac{k\lambda}{\beta \cos\theta} \qquad 4\text{-}3$$

The calculations were confirmed for UiO66 by TEM, Figure 4-22. Unfortunately, the MOF framework had been destroyed during this process and only the Pt can be seen here.

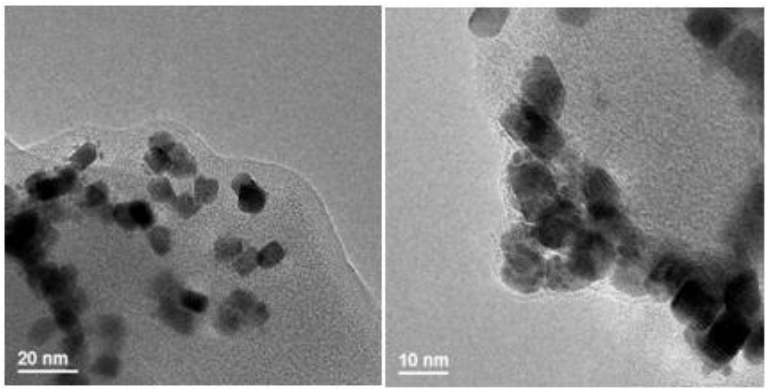

Figure 4-22 TEM of the UiO66 with Pt particles inside.

Incorporation of metallic Pt occurred during the microwave and autoclave routes of synthesis of UiO66 and UiO66-NH_2. A comparison of the PXRD patterns of the pure MOF powders and those containing Pt nanoparticles are shown below in Figure 4-23. The broad peaks coming from metallic Pt can be seen in the PXRD pattern at 2θ of 39.76° (111) and 46.23° (200) with d of 2.265 Å and 1.962 Å respectively. These peaks have the highest intensities and thus are characteristic to Pt[48, 49]. In case of CPO Ni, the Pt is not noticable in the PXRD pattern, in case of CPO Mg, there are two broad peaks coming at the stated above 2θ values. However, when compared with a PXRD pattern of a pure MOF, these peaks are there too. It might lead to a conclusion that the peaks from Pt crystal latice and CPO-27 crystal lattices overlap.

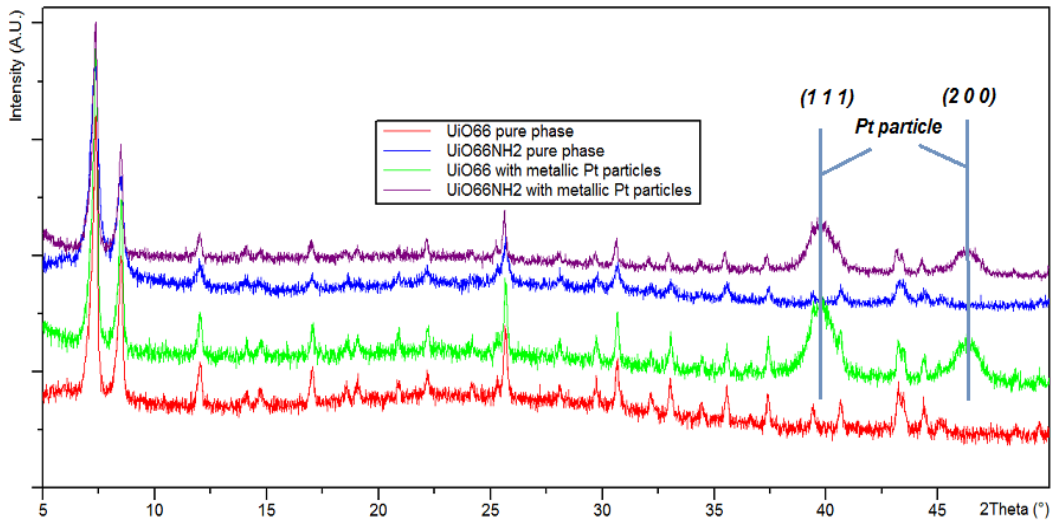

Figure 4-23: PXRD of Zr-MOFs, phase pure UiO66 (red) and UiO66-NH_2 (blue) and containing Pt nanoparticles – UiO66 (green) and UiO66-NH_2 (purple).

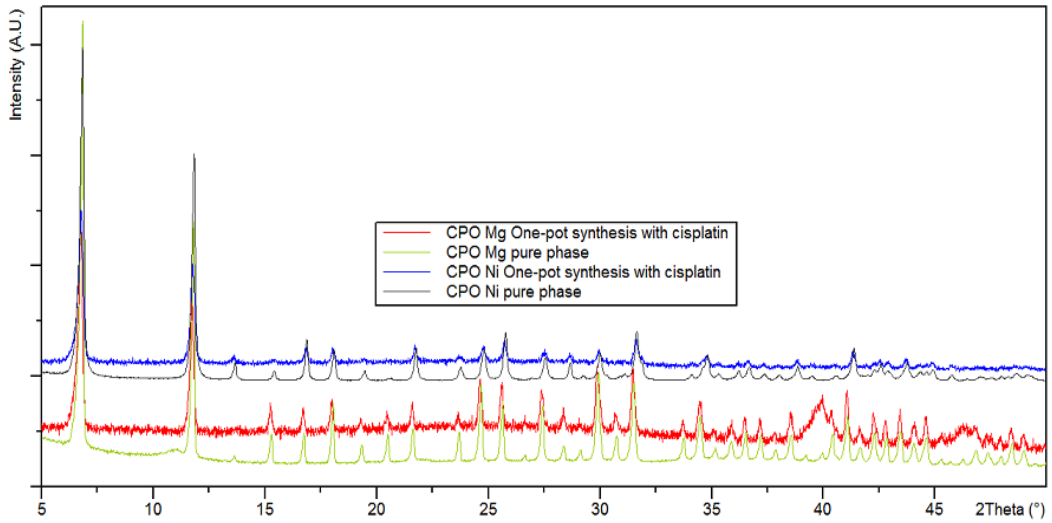

Figure 4-24 PXRD of CPO-27 MOFs, phase pure CPO Mg (green) and CPO Ni (gray) and after one-step synthesis with cisplatin CPO Mg (red) and CPO Ni (blue).

The reaction temperatures used (120 °C and 220 °C for UiO66NH_2 and UiO66 respectively and 110 °C for CPO-27) which is much lower than the cisplatin decomposition temperature (270 °C), it is assumed that the reduction of the cisplatin to metallic platinum is driven either by the increased pressure in the sealed reaction vessel, or by reaction with acetic acid or formaldehyde produced by thermal decomposition of DMF. EDX shows that the Pt nanoparticles are homogeneously distributed throughout the MOF powders, with Zr : Pt ratios of 1:2.6 and 1 : 1.5 (% Atomic) for UiO66 and UiO-NH_2 respectively. For CPO Ni

EDX analysis is showing Pt : Ni ratio to be 1 : 115 (% Atomic), and for CPO Mg this relation is 1 to 29. The EDX analysis supports the argument that metallic Pt particles are entrapped in the CPO Mg structure.

TGA measurements showed that nanoparticles of Pt in the structure do not significantly influence the robustness of the network, the decomposition temperature of the UiO66-NH_2 remains effectively unchanged whilst that of the UiO66 decreases from 420 °C to approx. 400 °C upon inclusion of the Pt nanoparticles. The Pt-content, made on the basis of TGA, is estimated at the level of 9 % for both MOFs UiO66 and UiO66-NH_2, see Figure 4-25.

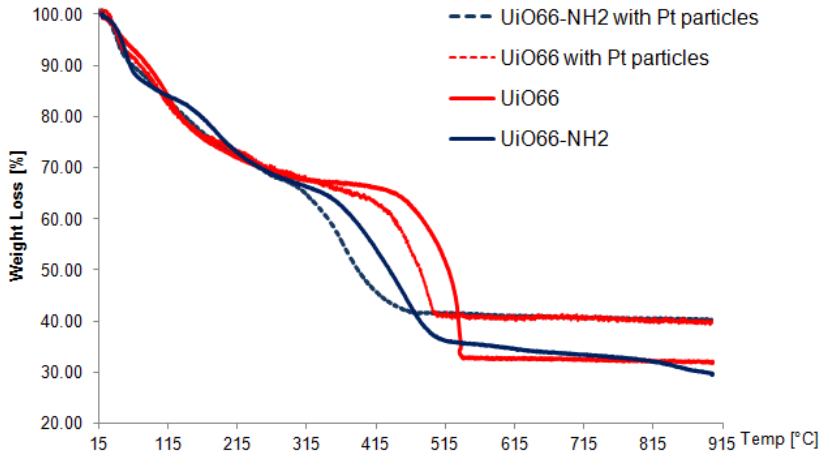

Figure 4-25 TGA analysis of Zr-MOFs with metallic Pt particles.

4.4. Conclusions and Summary

This chapter illustrated different synthesis strategies of the potential drug delivery systems for cisplatin and investigated potential usefulness of four MOFs for this purpose: CPO Ni, CPO Mg, UiO66 and UiO66-NH_2. In case of the latter MOF, a conjugation technique of the Pt-prodrug (obtained by cisplatin modification) to the amine group by activating a formation of a peptide bond was researched. Results show that efficacy of such a drug carrier is better when compared with the system utilising the same MOF but prepared in the encapsulation route.

The encapsulation route allowed for preparation a drug delivery systems that is a strong candidate – UiO66. This Zr-MOF releases cisplatin successfully and as consequence decreases the viability of the cancer cells. The experiments showed that the viability of cells decreased to 86% for THP-1 and 5% when performed on the lower passage number which can be compared with cisplatin efficacy (blood

cancer). Viability of A549 cells (lung cancer) when stimulated with UiO66 MOF dropped to 25% after the 24h exposure to drug delivery system and 16% after 48h exposure. This was the best result achieved in the group of MOFs being tested. This may be due to large pores in the structure of the UiO66 MOF. High porosity is also one of the properties of UiO66-NH_2, however here, there is another mechanism coming to fore – an interaction of cisplatin with amine groups in the structure of this MOF. As a consequence, high loading of 10.46 wt% of cisplatin does not give rise to increased efficacy and UiO66 appears to be a better candidate with only 7.07 wt% cisplatin loading. Such a comparison is viable for both MOFs show very similar molecular weights.

When comparing two cisplatin – loaded CPO-27 MOFs, according to the obtained results the efficacy of CPO Mg measured as a function of cell viability (lung and blood cancer cells) is higher than shown by cisplatin – loaded CPO Ni, and CPO Mg is considered as a non-toxic MOF in contrary to CPO Ni which contains Ni. However, if we only compared results obtained from viability assays performed on the lung cancer, it becomes obvious that after 48h exposure to the drug being released over time from CPO Ni system, the cell viability is less than 3%. It is worth mentioning that MOF powder showed tendency to form aggregates when suspended in the growth media during formulation preparations that were unable to break into smaller pieces, the pipetting of the given doses of stimulants is not error – free. In order to prevent this, a more optimised way of stimulants aliquots must be designed.

The one-pot synthesis for preparation of MOFs with incorporated cisplatin did not lead to a formation of drug delivery systems, however, allowed to prepare MOFs (UiO66 and UiO66NH_2) with metallic particles of nano – Pt trapped in their pores. This might be an interesting method of synthesis of a subnano-catalytic system with a MOF serving here as a carrier platform.

TGA measurements proved to be not the best route to assess the cisplatin content. This may be caused by the presence of water molecules in the material that in the due course of cisplatin encapsulation are exchanged with cisplatin which is much heavier. Even though, the known amounts of MOF powders were used for encapsulation and concentration solution used for encapsulation and its volume

was also known, it proved not to give a precise cisplatin content in the loaded material but only an indication that there was a change of mass.

The EDX method was used for crude estimates of cisplatin content, again the lack of knowledge on the exact molecular weight of material and operating only with approximation allowed for qualitative analysis and determination of regions in the sample with higher concentration of Pt. The method of choice when it comes to Pt content analysis should be ICP-AES/ICP-MP or MP-AES as these can give precise results for element content in the material as long as it is straight forward to perform mineralisation of the sample, which in the case of Zr-MOFs proved to be a complicated task and aqua regia solution was not able to dissolve the MOF structure. It was believed that this strong acid could allow for extraction of Pt from the pores of the material, however, once the microwave – based laser method, developed at the University of Warsaw in the group of Prof. Ewa Bulska, was applied to perform the dissolution of Zr-MOFs, the ICP –MP analysis returned higher Pt content.

It was hypothesised that encapsulation of anti – cancer drugs in the delivery system may increase the efficacy of the anti – cancer therapy. The MOFs were thought to be a good candidate for a host with their large pores and availability of variety of structures. Nevertheless, it seems to be very hard to control the release of the drug that is loaded in the carrier system and remotely navigate the cargo to the tumour lesions sparing the healthy cells. As it was showed in this chapter, the high drug loading and release do not guarantee high efficacy and selectivity that is needed to fight the cancer. The author believes that another solution for anti – cancer therapies will emerge and this will be based on personalised medicine route[50], relying on the cancer immunology of the human body[51] employing monoclonal antibodies[52] as drug carriers and exploring targets in cancer metabolism to design better delivery systems.

4.5. References

1. M. Reithofer, M. Galanski, A. Roller and B. K. Keppler, *European Journal of Inorganic Chemistry*, 2006, **2006**, 2612-2617.
2. P. a. Ma, H. Xiao, X. Li, C. Li, Y. Dai, Z. Cheng, X. Jing and J. Lin, *Advanced Materials*, 2013, n/a-n/a.
3. A. Diaz, M. L. Gonzalez, R. J. Perez, A. David, A. Mukherjee, A. Baez, A. Clearfield and J. L. Colon, *Nanoscale*, 2013, **5**, 11456-11463.
4. H. Xiao, L. Yan, Y. Zhang, R. Qi, W. Li, R. Wang, S. Liu, Y. Huang, Y. Li and X. Jing, *Chem. Commun.*, 2012, **48**, 10730-10732.
5. R. Wang, H. Xiao, H. Song, Y. Zhang, X. Hu, Z. Xie, Y. Huang, X. Jing and Y. Li, *Journal of Materials Chemistry*, 2012, **22**, 25453-25462.
6. M. H. Greene, *J Natl Cancer Inst*, 1992, **84**, 306-312.
7. O. Rixe, W. Ortuzar, M. Alvarez, R. Parker, E. Reed, K. Paull and T. Fojo, *Biochemical Pharmacology*, 1996, **52**, 1855-1865.
8. E. R. Jamieson and S. J. Lippard, *Chem Rev*, 1999, **99**, 2467-2498.
9. W. H. Ang, S. Pilet, R. Scopelliti, F. Bussy, L. Juillerat-Jeanneret and P. J. Dyson, *Journal of Medicinal Chemistry*, 2005, **48**, 8060-8069.
10. P. Horcajada, T. Chalati, C. Serre, B. Gillet, C. Sebrie, T. Baati, J. F. Eubank, D. Heurtaux, P. Clayette, C. Kreuz, J. S. Chang, Y. K. Hwang, V. Marsaud, P. N. Bories, L. Cynober, S. Gil, G. Ferey, P. Couvreur and R. Gref, *Nature Materials*, 2010, **9**, 172-178.
11. A. C. McKinlay, R. E. Morris, P. Horcajada, G. Ferey, R. Gref, P. Couvreur and C. Serre, *Angew Chem Int Ed Engl*, 2010, **49**, 6260-6266.
12. P. Horcajada, R. Gref, T. Baati, P. K. Allan, G. Maurin, P. Couvreur, G. Ferey, R. E. Morris and C. Serre, *Chem Rev*, 2012, **112**, 1232-1268.
13. P. Horcajada, C. Serre, M. Vallet-Regí, M. Sebban, F. Taulelle and G. Férey, *Angewandte Chemie*, 2006, **118**, 5974-5978.
14. D. Cunha, C. Gaudin, I. Colinet, P. Horcajada, G. Maurin and C. Serre, *Journal of Materials Chemistry B*, 2013, **1**, 1101-1108.
15. K. M. L. Taylor-Pashow, J. D. Rocca, Z. Xie, S. Tran and W. Lin, *J Am Chem Soc*, 2009, **131**, 14261-14263.

16. K. M. L. Taylor, W. J. Rieter and W. Lin, *J Am Chem Soc*, 2008, **130**, 14358-14359.
17. A. Schaate, P. Roy, A. Godt, J. Lippke, F. Waltz, M. Wiebcke and P. Behrens, *Chemistry – A European Journal*, 2011, **17**, 6643-6651.
18. C. Zlotea, D. Phanon, M. Mazaj, D. Heurtaux, V. Guillerm, C. Serre, P. Horcajada, T. Devic, E. Magnier, F. Cuevas, G. Ferey, P. L. Llewellyn and M. Latroche, *Dalton transactions*, 2011, **40**, 4879-4881.
19. M. Kandiah, M. H. Nilsen, S. Usseglio, S. Jakobsen, U. Olsbye, M. Tilset, C. Larabi, E. A. Quadrelli, F. Bonino and K. P. Lillerud, *Chemistry of Materials*, 2010, **22**, 6632-6640.
20. N. Nijem, J. F. Veyan, L. Kong, H. Wu, Y. Zhao, J. Li, D. C. Langreth and Y. J. Chabal, *J Am Chem Soc*, 2010, **132**, 14834-14848.
21. P. D. C. Dietzel, P. A. Georgiev, J. Eckert, R. Blom, T. Strassle and T. Unruh, *Chem. Commun.*, 2010, **46**, 4962-4964.
22. P. D. C. Dietzel, R. Blom and H. Fjellvåg, *European Journal of Inorganic Chemistry*, 2008, **2008**, 3624-3632.
23. P. D. C. Dietzel, V. Besikiotis and R. Blom, *Journal of Materials Chemistry*, 2009, **19**, 7362-7370.
24. C. M. Riley and L. A. Sternson, in *Analytical Profiles of Drugs*, 1985, vol. 14, p. 77.
25. X. Zhu, J. Gu, Y. Wang, B. Li, Y. Li, W. Zhao and J. Shi, *Chem. Commun. (Cambridge, U. K.)*, 2014, **50**, 8779-8782.
26. X. Zhu, J. Gu, J. Yang, Z. Wang, Y. Li, L. Zhao, W. Zhao and J. Shi, *Journal of Materials Chemistry B*, 2015, **3**, 4242-4248.
27. Y. Shi, S.-A. Liu, D. J. Kerwood, J. Goodisman and J. C. Dabrowiak, *Journal of Inorganic Biochemistry*, 2012, **107**, 6-14.
28. H. Song, H. Xiao, Y. Zhang, H. Cai, R. Wang, Y. Zheng, Y. Huang, Y. Li, Z. Xie, T. Liu and X. Jing, *Journal of Materials Chemistry B*, 2013, **1**, 762-772.
29. S. Dhar, W. L. Daniel, D. A. Giljohann, C. A. Mirkin and S. J. Lippard, *J Am Chem Soc*, 2009, **131**, 14652-14653.
30. J. Reedijk, *Platinum Metals Review*, 2008, **52**, 2-11.

31. R. Jan, in *Medicinal Inorganic Chemistry*, American Chemical Society, 2005, vol. 903, pp. 80-109.
32. C. Wang, X. Liu, J. P. Chen and K. Li, *Scientific Reports*, 2015, **5**, 16613.
33. L. Ellis, H. Er and T. Hambley, *Australian Journal of Chemistry*, 1995, **48**, 793-806.
34. K. S. Lovejoy and S. J. Lippard, *Dalton transactions*, 2009, 10651-10659.
35. J. F. Vollano, E. E. Blatter and J. C. Dabrowiak, *J Am Chem Soc*, 1984, **106**, 2732-2733.
36. E. E. Blatter, J. F. Vollano, B. S. Krishnan and J. C. Dabrowiak, *Biochemistry*, 1984, **23**, 4817-4820.
37. R. J. Brandon and J. C. Dabrowiak, *Journal of Medicinal Chemistry*, 1984, **27**, 861-865.
38. F. Bonino, S. Chavan, J. G. Vitillo, E. Groppo, G. Agostini, C. Lamberti, P. D. C. Dietzel, C. Prestipino and S. Bordiga, *Chemistry of Materials*, 2008, **20**, 4957-4968.
39. V. B. Cetintas, A. S. Kucukaslan, B. Kosova, A. Tetik, N. Selvi, G. Cok, C. Gunduz and Z. Eroglu, *Cell Biology International*, 2012, **36**, 261-265.
40. D. Wang and S. J. Lippard, *Nat Rev Drug Discov*, 2005, **4**, 307-320.
41. Drugs.com.
42. *WWW Source: http://cancerguide.org/drugdosing.html*.
43. D. Sun, W. Liu, Y. Fu, Z. Fang, F. Sun, X. Fu, Y. Zhang and Z. Li, *Chemistry – A European Journal*, 2014, **20**, 4780-4788.
44. H. Liu, L. Chang, L. Chen and Y. Li, *Journal of Materials Chemistry A*, 2015, **3**, 8028-8033.
45. R. J. Kuppler, D. J. Timmons, Q.-R. Fang, J.-R. Li, T. A. Makal, M. D. Young, D. Yuan, D. Zhao, W. Zhuang and H.-C. Zhou, *Coordination Chemistry Reviews*, 2009, **253**, 3042-3066.
46. Z. Guo, C. Xiao, R. V. Maligal-Ganesh, L. Zhou, T. W. Goh, X. Li, D. Tesfagaber, A. Thiel and W. Huang, *ACS Catalysis*, 2014, **4**, 1340-1348.
47. J. I. Langford and A. J. C. Wilson, *J. Appl. Crystallogr.*, 1978, **11**, 102-113.
48. S. Krehula and S. Musić, *Croat. Chem. Acta*, 2011, **84**, 465–468.

49. J. Čejka, N. Žilková and P. Nachtigall, *Molecular Sieves: From Basic Research to Industrial Applications* 2005.
50. S.-H. Cho, J. Jeon and S. I. Kim, *Journal of Breast Cancer*, 2012, **15**, 265-272.
51. V. Bruttel and J. Wischhusen, *Frontiers in Immunology*, 2014, **5**.
52. A. M. Scott, J. P. Allison and J. D. Wolchok, *Cancer Immunity*, 2012, **12**, 14.

Chapter 5. MOFs as a drug delivery carrier for Fluorouracil (5-FU).

5.1. Aims

5-Fluorouracil (5-FU) is used to treat solid tumours administered either as an injection/infusion[1] or topical as an ointment to treat skin cancers[2], it is classified as anti-metabolite, which disrupts bioprocesses. The mechanism of action arises from the ability to inhibit thymidylate synthase (interfering with pyrimidine metabolic pathway) and the intercalation of fluoronucleotides in DNA and RNA chains which efficiently stops their synthesis that would lead to p53 dependent apoptotic death of a cancer cell[3, 4]. Such a treatment can cause several unpleasant symptoms when administered, just to name a few: nausea, vomiting and dermatological toxic effects, as it leads to a rapid absorption of the drugs through the cells. 5-FU has very short biological half-life of 8-14 minutes[5], that is why there is a need for a carrier that could transport the drug through the body[6] and release it after reaching its destination. There are some concepts of utilizing polymeric materials as the drug carriers[7-9]. Also, fluorouracil is not easily soluble in water which makes it challenging when it comes to preparation of drug formulations and high efficacy achieved by them. 5-FU can be easily dissolved in acids and basic solutions. Also high solubility is achieved in organic solvents like DMSO or DMF, these, however, are toxic and would be of hazard for bio-applications. Metal organic frameworks with their high porosity and large pores able to accommodate guest molecules, came to interest as potential drug delivery systems for 5-FU encapsulation. There are some ongoing trials for incorporation of the drug, utilizing metal organic frameworks, serving as a host and carrier for the drug[10, 11], liposomes are also used to serve this purpose[12] as well as polymers[13].

In this chapter, two routes of encapsulations were investigated, one in methanol and the other in a solution comprising 50/50 v/v Methanol/Formic acid (MeOH/FA) to enhance the solubility of 5-FU and to increase amount of drug in the solution used for encapsulation. Four MOFs have been tested for their

retention and release of the drug: CPO-27 – Mg and Ni and Zr-MOFs – UiO66 and UiO66-NH_2. In order to assess efficacy of the obtained systems, biological testing was performed to evaluate viability of the cells that were treated with formulations as well as the type of death they induce. The released quantities and the achieved loading were measured using HPLC with a UV detector.

5.2. Encapsulation MOFs with 5-FU (UiO66, UiO66-NH_2, CPO Mg, CPO Ni)

Physical encapsulation, also called impregnation, is one of the commonly used technique for incorporation of drugs into porous structures[14-18]. Based on this, it has been chosen for the investigation of its potential for 5-Fluorouracil. For these encapsulations, the MOFs previously synthesised for the cisplatin encapsulation were used Zr-MOFs and CPO-27. The details of their synthesis are described in Chapter 3.

Two encapsulation solutions were prepared, one was pure methanol and the other was a mix v/v 50/50 of formic acid and methanol. The concentration of 5-FU in each of the solutions was adjusted according to the solubility data and kept at the level of 80% of max. solubility that could be achieved for that solvent. This gave the following limits: 40 mg/ml for Fluorouracil dissolved in Formic Acid and 0.8 mg/ml for Methanol. The data was acquired from product specification sheet by one of the manufacturers[19]. The volume of the encapsulation solution was set to be 5 mL for each of the routes, and the amount of MOF powder was ca. 100 ±5% mg in case of MeOH and 200 ± 5% mg in case of the 50/50 mix. The max amount of 5-FU in MeOH solutions was 4 mg, and 102 mg in 50/50 solutions. Hence, the maximal achievable drug loading in this encapsulation was 3.8 wt%[$\frac{4}{4+100}$] for the former and 33.8 wt% [$\frac{102}{102+200}$] for the latter case. The amounts of MOF powder were chosen based on the fact that some MOF quantities could be lost due to the centrifugation procedure and dissolving in the encapsulation media. The MOF powders were kept in the encapsulation solution under stirring for a period of 48h and recovered by centrifugation and left to dry. The experiment was prepared in duplicate.

5.3. Results

5.3.1. MOF framework stability – X-ray of 5-FU encapsulated powders.

The MOF's stability was tested in a 50/50 v/v solution containing MeOH and formic acid (FA) to test if the framework can endure such a treatment. The duration of immersion under stirring was set to be 48 hours to recreate the conditions of drug encapsulation.

The x-ray diffraction patterns recorded by the author, show that in case of UiO66-NH_2 the framework is kept intact. A presence of a new phase is observed for CPO-27 Ni which may be due to structure collapse or these extra peaks would signal the presence of 5-FU at the surface and not in the pores of material. In the case of the CPO-27 Mg, the peaks shift towards higher theta values that indicates the crystal lattice contraction, some peaks disappeared from the x-ray pattern which may indicate that this structure is digested over time by formic acid. For reference, the simulated x-ray diffraction pattern of 5-FU can be found in Appendix 2 p.170. After immersion in the solution, it was noticeable that some peaks disappeared from the x-ray pattern of UiO66. Here, due to the number of peaks missing, it is not possible to say which way they might have shifted. The x-ray diffraction patterns are depicted in Figure 5-1 and Figure 5-2.

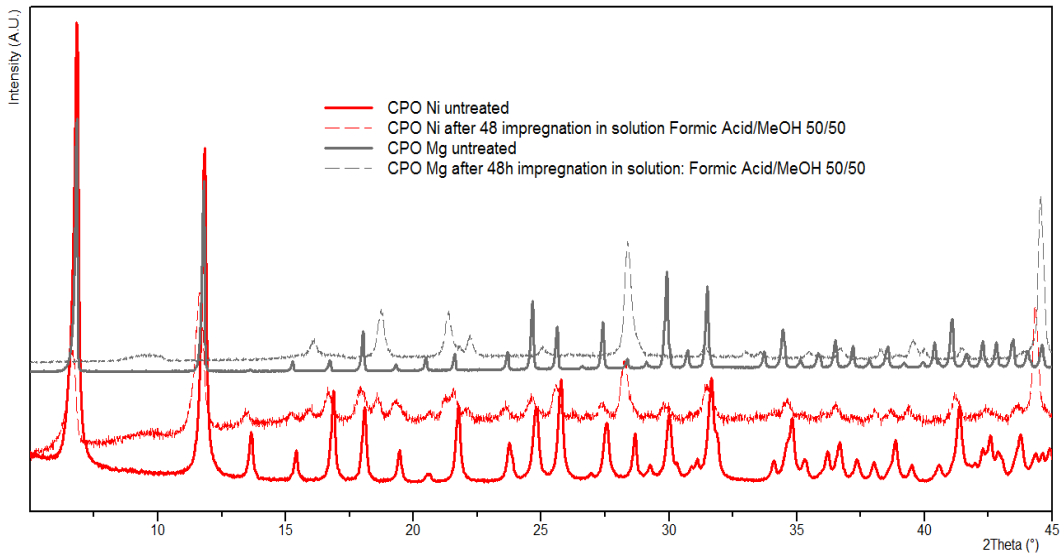

Figure 5-1 X-ray diffraction patterns of CPO Mg and CPO Ni, untreated and after immersion in the solution of MeOH/FA.

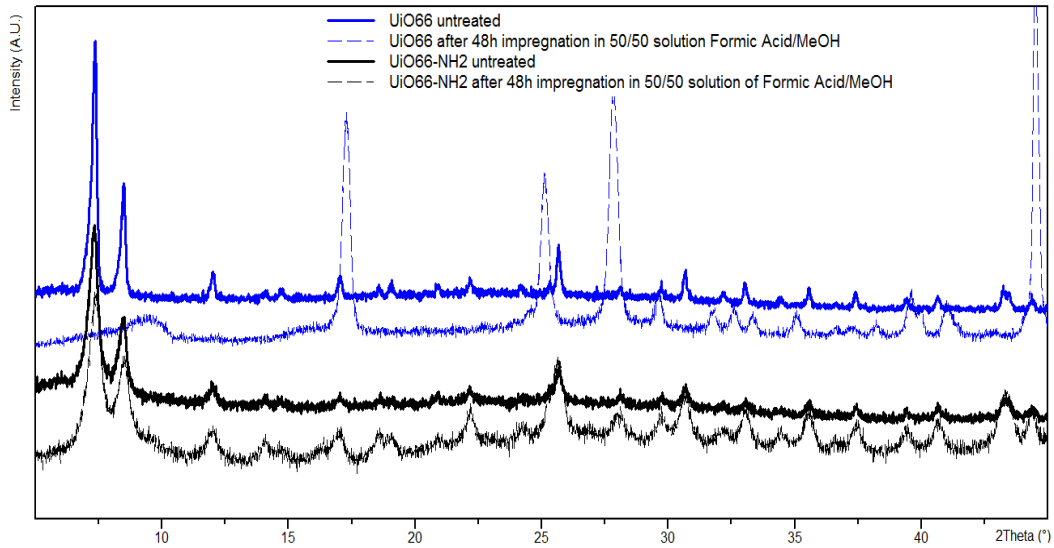

Figure 5-2 X-ray diffraction patterns of UiO66 and UiO66-NH_2, untreated and after immersion in the solution of MeOH/FA.

After 5-FU encapsulation, the MOF structures were characterised by PXRD, in order to assess the integrity of the frameworks and the recorded x-ray patterns showed that the peaks were shifting. Cell parameter refinement was performed, using the CELREF software. The CIF files of the previously synthesised and reported MOFs were used as models for indexing the peaks of the MOF-powders that were used in the encapsulation experiment. This allowed to compensate for any changes in the cell parameters between the powders used and the CIF files. Based on this, an indexed framework of CPO-27 Ni, CPO-27 Mg and UiO66 were created and indexation operation was repeated using these indexed structures to determine the parameters of the cell that underwent encapsulation. It was expected that the cell unit should become slightly bigger, to accommodate the 5-FU molecules. This property has already been noticed in the case of MIL MOFs and described as a "breathing effect" and is connected with the expansion of the cell parameters to accommodate the guest molecules making MOFs potential candidates for drug encapsulation e.g. ibuprofen[15, 20-22]. This effect can be huge for MILs[22, 23] but it is seemingly much smaller in the case of the MOFs author has chosen for 5-FU encapsulation. The peak indexing operation allowed to confirm that peaks are shifting, and the results of the cell parameters refinement are shown in Table 5-1 below.

CPO Ni R-3, α=β=90° ɣ=120°, a=b ≠c	Pure V=3893 Å^3	5-FU in MeOH V=3966 Å^3	5FU (FA/MeOH) V=3893 Å^3
a=b	25.9279	26.1189	25.9234
c	6.6881	6.7130	6.6894
CPO Mg R-3, α=β=90° ɣ=120°, a=b ≠c	Pure V=3957 Å^3	5-FU in MeOH V= 4018 Å^3	5FU (FA/MeOH) V= 4083 Å^3
a=b	25.9997	26.1296	26.2902
c	6.7597	6.7966	6.8214
UiO66 FM-3M, α=β= ɣ= 90°, a=b=c	Pure V= 8881 Å^3	5-FU in MeOH V=9106 Å^3	5FU (FA/MeOH) V=8889 Å^3
a=b=c	20.7089	20.8825	20.7156

Table 5-1 Cell parameters refinement results obtained in CELREF software. Peaks coming from 5-FU were subtracted from the diffraction patterns of encapsulated powders by indexing 5-FU peaks based on its CIF file.

Interestingly, the crystal lattice parameters expand when the encapsulation is performed in methanol (MeOH), and in case of MeOH/FA solution, this effect is only observed for CPO Mg. However, this cell parameter refinement is based on 4 peaks that could be associated with the MOF framework, as other peaks are coming from 5-FU, indicating that the MOF framework did not kept intact. The peaks associated with 5-FU presence are showing up in the x-ray pattern, some already in MeOH encapsulation, though 5-FU peaks are especially noticeable in MeOH/FA encapsulation route. Each unit cell of 5-FU contains 8 molecules of the drug (Z=8 in the CIF file that was used)[24], meaning that each molecule takes up 125 Å^3, at the same time the pore volume per unit in CPO Mg based on CCDC 668974 (Z=18) is 2843.18 Å^3 which when recalculated per each individual Mg gives ca. 158 Å^3. This leads to a conclusion that per each Mg atom, 1.26 5-FU molecules can be successfully encapsulated. During the encapsulation in MeOH, the unit cell volume of CPO Mg expands by 61 Å^3 which would maximally allow ca. 1.29 5-FU per each Mg atom (2.4% increase), in case of MeOH/FA this expansion is bigger and maximum molecule load is thus ca. 1.32 5-FU molecules per each Mg atom (5% increase). In case of UiO66, the pore volume per unit cell equals 7845 Å^3, which corresponds to 2.6 5-FU molecules per each Zr atom (24 of these in the unit cell). With changing cell parameters during MeOH encapsulation process this ratio will increase up to 2.7 (ca. 4% increase). UiO66-NH_2 peaks

were not indexed due to the fact of a missing CIF file of the crystallographic structure. All the refined cell parameters are filed in Appendix 1 of this Thesis.

Below, the x-ray patterns of the loaded/unloaded MOF materials (Figure 5-3, Figure 5-4) are depicted. At around 28° (2θ), in case of CPO Mg, CPO Ni and UiO66, there is a peak which is very characteristic for 5-FU presence in the structure. It has been observed that the peaks after the encapsulation with 5-FU in MeOH are shifting to the left, and that the encapsulation in FA/MeOH was quite detrimental for some of the MOFs, as not all of the peaks are present in the pattern (CPO Mg, UiO66) with the only MOF that "survived" encapsulation $UiO66NH_2$ as its structure remained intact.

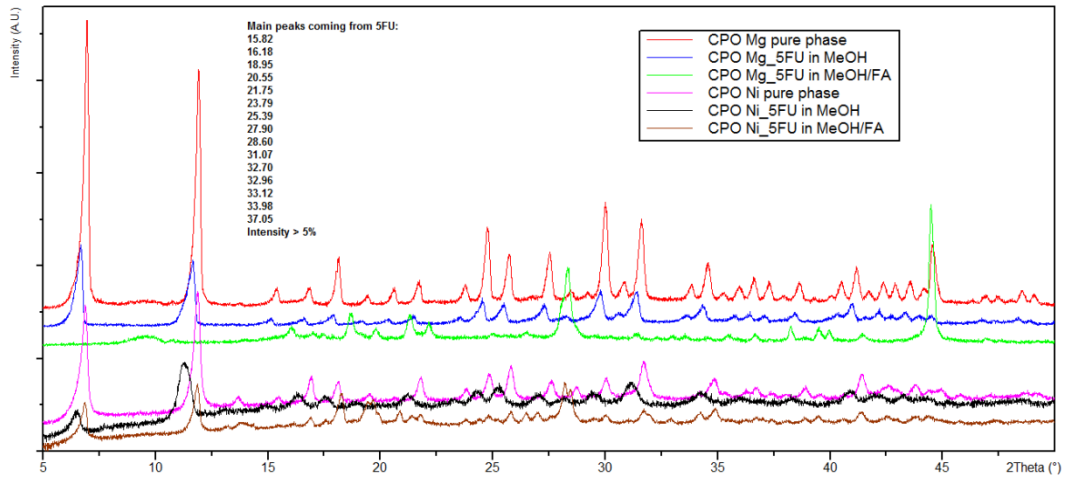

Figure 5-3 X-ray diffraction pattern of CPO Mg and CPO Ni, unloaded/loaded with 5-FU encapsulated in MeOH or MeOH/FA.

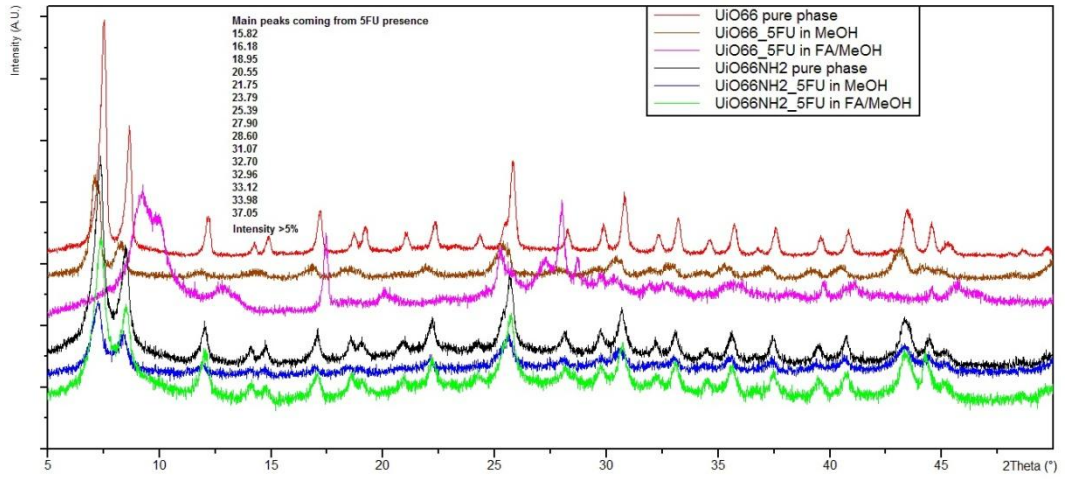

Figure 5-4 X-ray diffraction pattern of UiO66 and $UiO66NH_2$, unloaded/loaded with 5-FU encapsulated in MeOH or MeOH/FA.

The shift into lower angles is an indication that the cell parameters are changing and the crystal unit expanding to accommodate the drug in the MOF framework and we observe a slight "breathing effect".

5.3.2. Presence of 5FU in the pores of MOFs

5.3.2.1. Changing BET

The TRISTAR surface area and porosity analyser was employed to measure the pore volume as well as the BET surface area in order to compare these properties of the drug loaded and unloaded MOFs.

MOF/encapsulation route	Evacuation temp [°C]	Pore Volume BJH Desorption [cm^3/g]	Surface area BET m^2/g
UiO66-NH_2	140	0.257	559.6 ± 13.4
in MeOH	100	0.187	690.1 ± 17.2
in MeOH/FA	100	0.186	284.2 ± 6.5
UiO66	120	0.058	852.2 ± 3.8
in MeOH	100	0.044	818.9 ± 22.3
in MeOH/FA	100	0.008	1.6 ± 0.01
CPO Mg	140	0.058	18.4 ± 0.23
in MeOH	100	0.064	17.5 ± 0.23
in MeOH/FA	100	0.007	2.9 ± 0.023
CPO Ni	140	0.178	274.4 ± 6.8
in MeOH	100	0.135	103.1 ± 2.4
in MeOH/FA	100	0.027	4.2 ± 0.04

Table 5-2 Adsorption properties of MOFs, BET, pores volume, pore size.

The evacuation temperature was a bit higher for the pure MOFs because there was a concern that the 5-FU encapsulated in the pores may be destroyed by exposure to higher temperature under vacuum. This may lead to inaccuracies when the comparisons are made, for the surface area of the pure MOFs and their pore volume, as it was proven that these properties are highly dependent on the evacuation temperature[25]. On the other hand, if the evacuation temperature of the pure MOF, would match the one with the encapsulated drug, then the host (DMF, H_2O) could still be in the pores leading to misleading results. The BET surface areas are decreasing for almost all MOFs tested, for the MeOH/FA encapsulation BET areas are dramatically low, which may be the effect of the partially destroyed structure depicted by x-ray diffraction patterns.

UiO66-NH_2 structure according to x-ray patterns is perfectly intact, for MeOH/FA encapsulation there is a decrease of BET from 559 m^2/g (pure MOF) to 284 m^2/g, which is a loss of ca. 50%. The difference in the BET for 5-FU encapsulated in MeOH method (690 m^2/g) and MeOH/FA method is huge, almost 3-fold, and it must be noted that in this case the evacuation temperatures were the same for both cases, 100°C.

In CPO Ni, the specific pore volume of the pure MOF is 0.178 cm^3/g measured at 140°C. If we compared this with the unit cell parameters from CIF file, CCDC 28847 comprising of 18 Ni Z=18 which corresponds to 2 molecules, we find the void area be 2809.6 $Å^3$. Per each molecule it would be 312.2 $Å^3$, and 156 $Å^3$ per each Ni. It seems that "a guest" is taking up 0.043 cm^3/g in MeOH encapsulation, 5-FU molecule takes up 125 $Å^3$ which corresponds to $344•10^{18}$ Fluorouracil molecules per gram of the powder, likewise 0.151 cm^3/g drop (MeOH/FA) takes it to $1208•10^{18}$ 5-FU molecules. Incorporating the Avogadro's number to calculate the mol quantities, we get 0.057 mmol (7.41 mg) and 0.2 mmol (26 mg) for the second case for a gram of the powder.

In UiO66, we find 0.058 cm^3/g in the pure material, dropping to 0.044 cm^3/g for the MeOH route and to 0.008 cm^3/g for MeOH/FA route. In a CIF file CCDC 73358, we have 54 Zr atoms which corresponds to 9 molecules comprising 6 Zr atoms each, for this unit cell the void area is 7845.3 $Å^3$ which gives per molecule 871.7 $Å^3$ and 145 $Å^3$ per each Zr. Again, the void volume drop of 0.016 cm^3/g (MeOH) may correspond to $128•10^{18}$ molecules of 5-FU, and 0.05 cm^3/g (MeOH/FA) to $400•10^{18}$ 5-FU molecules. In moles quantities, we find here 0.021 mmol (2.7 mg) and 0.066 mmol (8.6 mg) respectively, per each gram of the powder. These calculations may only be taken as the first approximation of the 5-FU content and for a final confirmation another analytical technique should be involved, e.g. HPLC.

5.3.2.2. FTIR spectra (ATR)

The MOF powders were analysed using FTIR (ATR): Attenuated Total Reflectance method, because it offers a relatively straightforward and easy way for the sample analyses and eliminates the preparation of KBr discs. 5-FU structure is presented in Figure 5-5 .

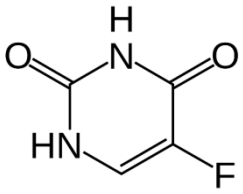

Figure 5-5 Structure of 5-Fluorouracil.

The recorded spectra, 5-FU and pure MOFs can be compared with the ones of the MOFs loaded with 5-FU in two encapsulation routes.

The broad band 3300-2700 cm^{-1} can be assign to NH-stretching vibrations in 5-FU and the stretching at 1647 cm^{-1} attributed to carbonyl group stretching (C=O), the peak at 1242 cm^{-1} arises from C-F bond stretching. These peaks can be found in the spectra of UiO66-NH_2 encapsulated with 5-FU in MeOH/FA route, which can be seen in Figure 5-6. In case of 5-FU loaded UiO66, the peak coming at 748 cm^{-1} in both of encapsulation routes that overlaps with stretching in the 5-FU spectra can serve as a proof of drug presence in the MOF framework (Figure 5-7).

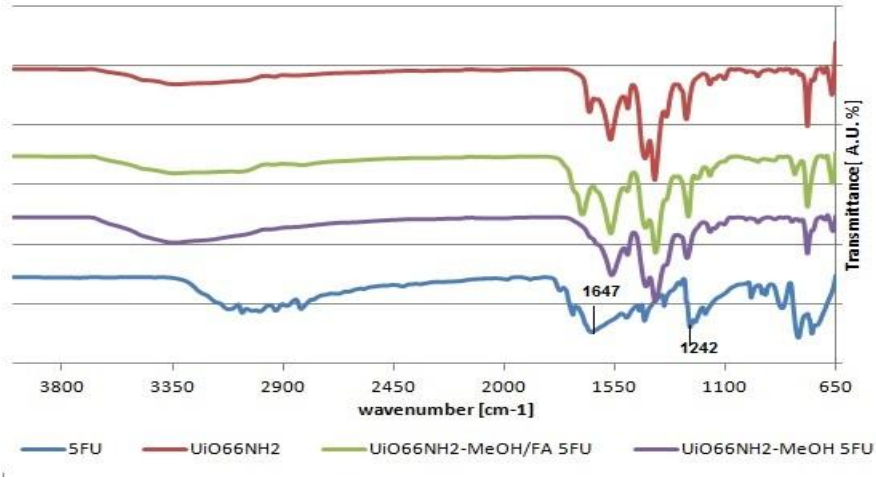

Figure 5-6 FTIR ATR spectra of UiO66NH_2, 5-FU unloaded/loaded in two encapsulation routes. Red-marked is pure MOF.

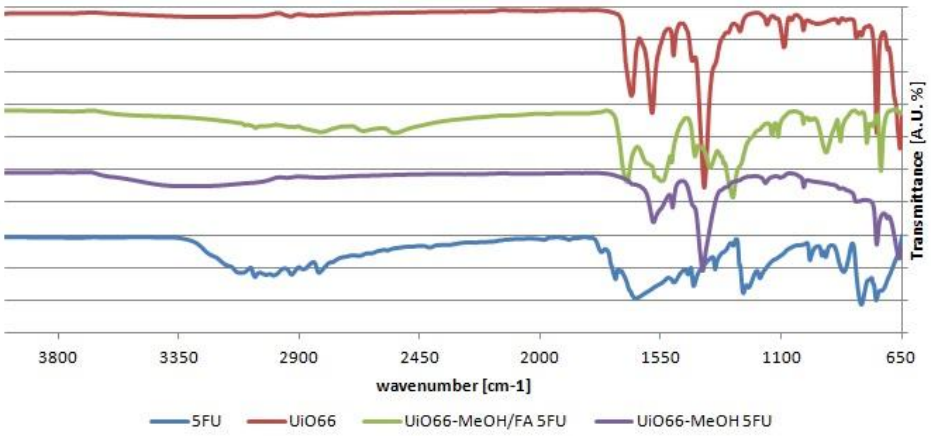

Figure 5-7 FTIR ATR spectra of UiO66, 5-FU unloaded/loaded in two encapsulation routes. Red-marked is pure MOF.

In case of CPO Mg, the spectra analysis concluded that MeOH encapsulation was not as efficient as the one aided with addition of formic acid.

The spectra of a 5-FU loaded MOF bears similar features to the spectra of the drug (Figure 5-8).

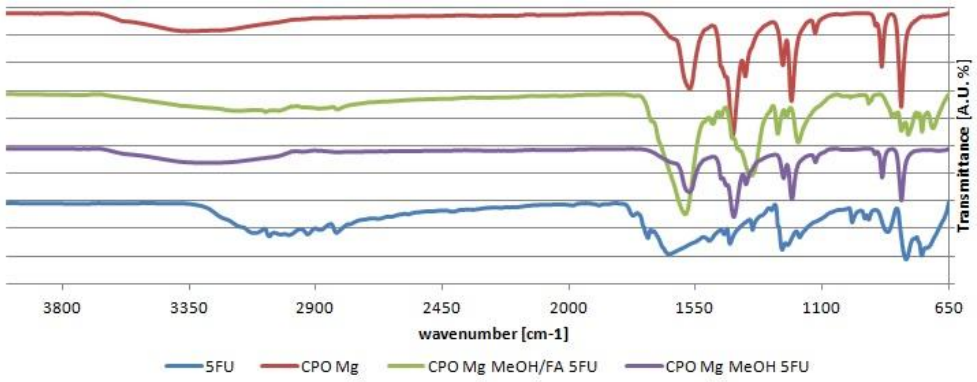

Figure 5-8 FTIR ATR spectra of CPO Mg, 5-FU unloaded/loaded in two encapsulation routes. Red-marked is pure MOF.

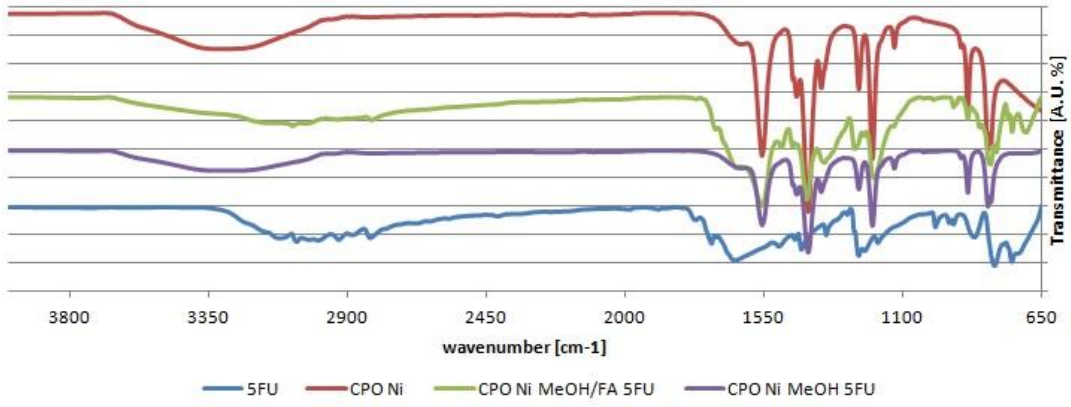

Figure 5-9 FTIR ATR spectra of CPO Ni, 5-FU unloaded/loaded in two encapsulation routes. Red marked is pure MOF.

The spectra of MOFs prepared in MeOH/FA encapsulation route seem to show the stretching bands similar to the ones in the 5-FU spectra. Especially the bands at 725-817 cm^{-1} indicating the vibrations of CF=CH group.

5.3.2.3. Drug release and challenges to measure it (HPLC/UV-VIS)

For the determination of the 5-FU quantities and its release profile encapsulated in the MOFs, HPLC method was applied. 5-FU calibration curve 0-250 µg/ml was constructed, based on 9 points, each measured 3 times (Figure 5-10).

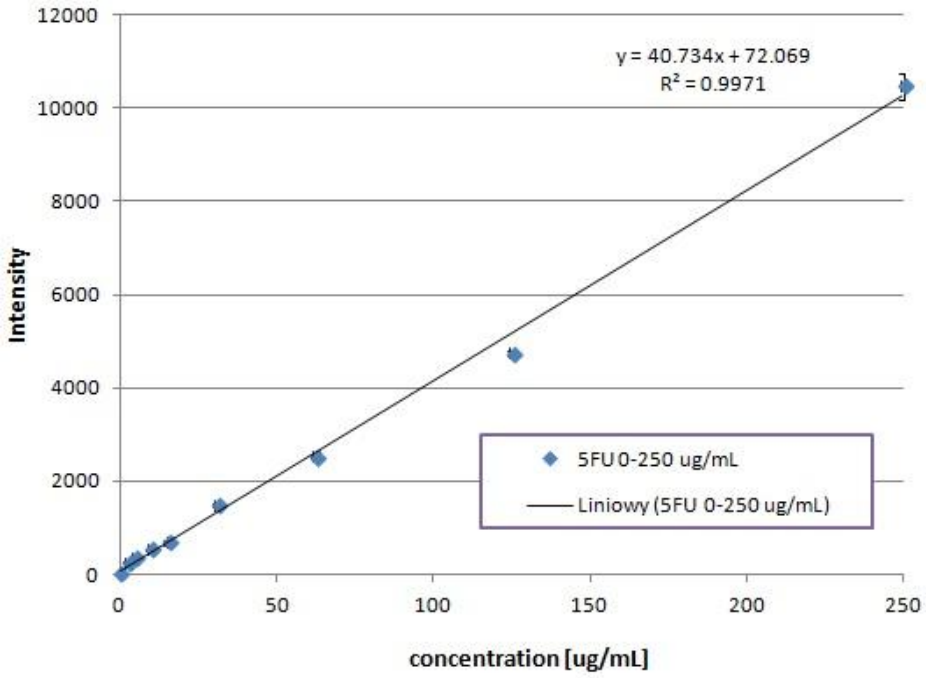

Figure 5-10 Calibration plot of 5-FU in a range 0-250 µg/mL.

The aliquots (0.5 mL) were harvested during the 48h release experiment (time points 0.25, 0.5, 1, 2, 3, 4, 24 and 48h) and then diluted 5x and then filtered with a 0.22 µm Micropore filter and transferred to the HPLC brown-coloured vials in order to keep them light-protected. Dilution was applied to perform a UV-VIS measurements for 5-FU quantities in a 2.5 mL cuvette. However, the spectra were masked by the MOFs inner-absorbance and another method of separation had to be applied. HPLC was the most appropriate.

The CPO- Mg and Ni based samples (ca. 18 mg) were digested in a concentrated HCl (0.8 mL, 37%wt) and left overnight. Zr-based MOFs proved to be very robust and the digestion was not performed based on the previous experience with cisplatin. The following 5-FU quantities were found in the MOF powders:

MOF	MeOH/FA encapsulation [µg 5-FU/mg powder]	MeOH encapsulation [µg 5-FU/mg powder]
CPO Mg	115.2 ± 1.4% (11.5 wt%)	10.8 ± 0.4% (1.08 wt%)
CPO Ni	151.4 ± 0.3% (15.1wt%)	21.1 ± 21.1% (2.1 wt%)

Table 5-3 Quantities of 5-FU determined with HPLC UV-detector 266 nm, in drug-loaded MOF powders: CPO Mg and CPO Ni.

It has been observed that CPO Ni has a higher loading capacity of the encapsulated drug. Taking into account the amounts of 5-FU introduced in the solutions used for the two encapsulation routes that were followed, 4 mg (MeOH) and 102 mg (MeOH/FA), hence the theoretical loading was 3.8wt% and 33.8wt% respectively, and for CPO Mg was achieved in 28% (MeOH) and 34% (MeOH/FA), for CPO Ni to 55% and 45% respectively. The HPLC was used to quantify the amount of 5-FU in the aliquots (Figure 5-11).

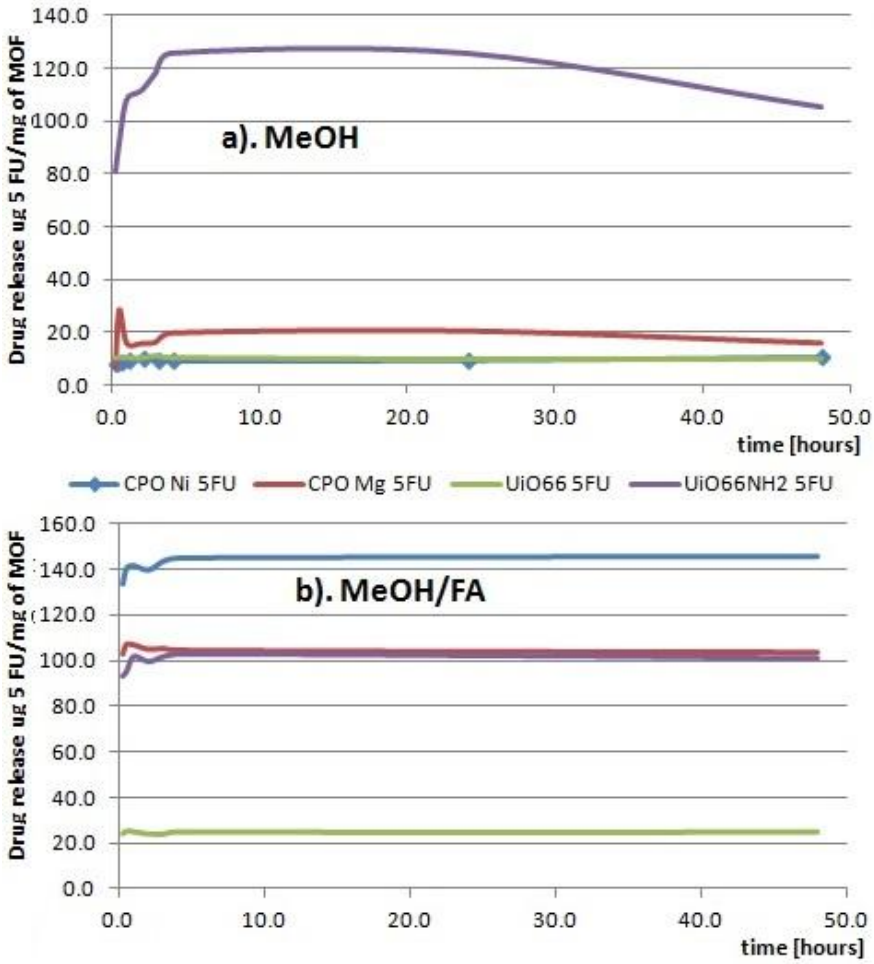

Figure 5-11 Release profiles for 5-FU [µg/mg MOF] encapsulated in MOFs (CPO Ni, CPO Mg, UiO66, UiO66NH$_2$) in two encapsulation routes a). MeOH and b). MeOH/FA.

All the MOFs do not show a drug retention and the release is observable almost immediately. This may be due to the fact that the 5-FU was only adsorbed at the surface and did not penetrate the pores of the material. Only UiO66-NH_2 in MeOH encapsulation releases the cargo gradually. It must be noted that some peaks arising from MOF itself could be wrongly assigned to 5-FU, with retention time is ca. 3.098 min detected at 266 nm, even though all the aliquots were filtered before the measurement to avoid recording the signal from MOF and to prevent the column from clogging.

UV-VIS was initially applied to estimate the content of absorbed 5-FU during the encapsulation process. The aliquots were taken from the encapsulation mixture, just before the end of the encapsulation – 48 h, 50 µL from MeOH solutions and 3 µL from MeOH/FA encapsulation solution, and diluted 60 and 1000 times respectively to match the Absorbance not exceeding 1. The concentration of remaining 5-FU in the encapsulation solution was calculated based on Absorbance UV-VIS measurements, and the amount absorbed was calculated as a difference between the remaining 5-FU and the concentration of encapsulation solution prepared that was 21.018 mg/mL for MeOH/FA and 0.788 mg/mL for MeOH. Based on these calculations the % of absorbed available drug was calculated (Table 5-4).

Encapsulation solution/48 hours	CPO Mg	CPO Ni	UiO66	UiO66NH_2
MeOH (% of absorbed 5-FU)	42.0	41.1	44.5	40.2
MeOH/FA (% of absorbed 5-FU)	19.7	56.6	43.4	41.9

Table 5-4 % of absorbed 5-FU from the encapsulation solution after the process was stopped after 48 h.

The results obtained are not far off the ones obtained from the HPLC measurements of the two MOFs: CPO Mg and CPO Ni.

The release experiment was performed and aliquots harvested in order to perform UV-VIS analysis. This proved to be unsuccessful due to the absorbance coming from the MOF powders. The figure 5-12 a.) depicts the measured absorbance from the release experiment from CPO Mg in MeOH/FA, formic acid spectra and 5-FU own spectra are also included. The CPO Mg own absorbance is masking the one arising from 5-FU. The sample was diluted 3 – 100 times and the recorded spectra still did not allow for quantification of 5-FU content. Figure 5-12 b.)

shows the Absorbance spectra from the aliquot harvested after 24 hours for MOFs encapsulated in MeOH/FA and after 48 hours in case of MeOH. The 266 nm absorbance is marked with a line. The result is the same, MOFs inner absorbance at 266 nm overlaps with absorbance arising from 5-FU which eliminates this method as a quantifier of 5-FU content (Figure 5-12).

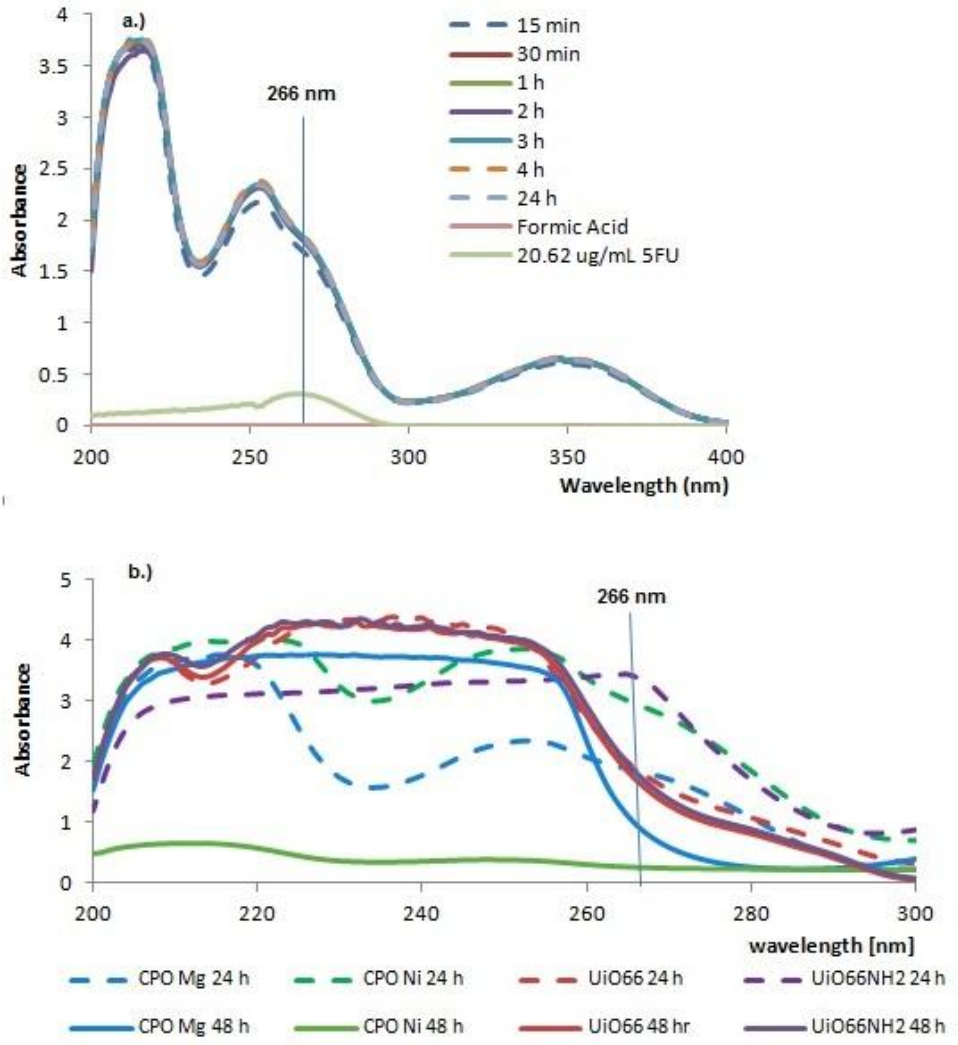

Figure 5-12 Absorbance spectra recorded in UV-VIS method. Fig. a.) shows CPO Mg spectra recorded in different time points, encapsulation was performed in MeOH/FA. Fig. b.) shows recorded UV-VIS spectra for MOFs in one particular time point, 24 hours (MeOH/FA –dotted line) and 48 hours (MeOH –solid line).

HPLC was selected to be the method that would troubleshoot the above mentioned challenging issue.

5.3.2.4. Traces of 5-FU in the NMR spectra

Another technique that was utilized in order to verify the presence of 5-FU in the MOF powders was liquid NMR (Bruker 500 MHz), a 4 min ^{1}H scan was performed. The powder samples ca. 20 mg were suspended in 10 ml of PBS and the aliquots were taken after 48h (CPO Mg, UiO66) and 24h (CPO Ni, $UiO66NH_2$), and control sample was a 0.75 mg/ml solution of pure 5-FU. The NMR chemical shifts are shown in Figure 5-13.

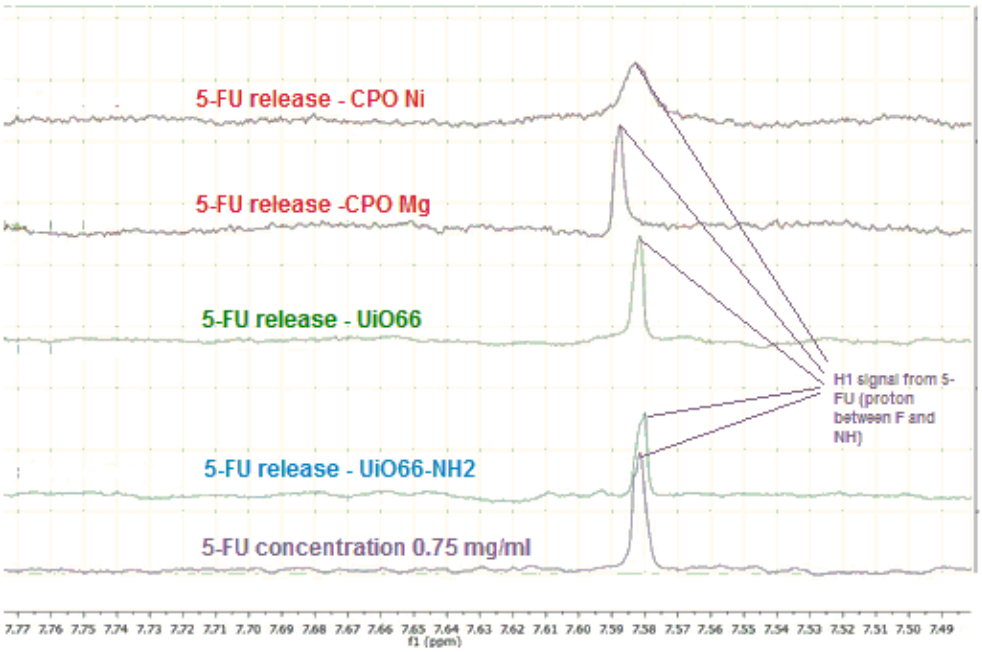

Figure 5-13 NMR chemical shifts acquired @500MHz Bruker, aliquots in D_2O solvent, harvested after 24h/48h release. MOF encapsulated in MeOH/FA. From the bottom – 5-FU, $UiO66NH_2$, UiOO66, CPO Mg and top is CPO Ni.

The same procedure was repeated after leaving the samples for a week to release 5-FU, here as a control sample a 0.253 mg/ml 5-FU solution was used. D_2O was used as an NMR solvent. The NMR shifts are shown in Figure 5-14. In both cases, there is a peak with the chemical shift at 7.59 ppm coming from the ^{1}H proton, that is bound to a carbon. ChemDraw Professional program predicts the ^{1}H signal coming from the ^{1}H (between –F and –NH groups) at 7.01 in DMSO and for the other two ^{1}H protons bound to N atom should give a doublet at 11.32 ppm and 11.01, this signal is much weaker though and was not observed. Prediction of chemical shifts in D_2O was not in ChemDraw database.

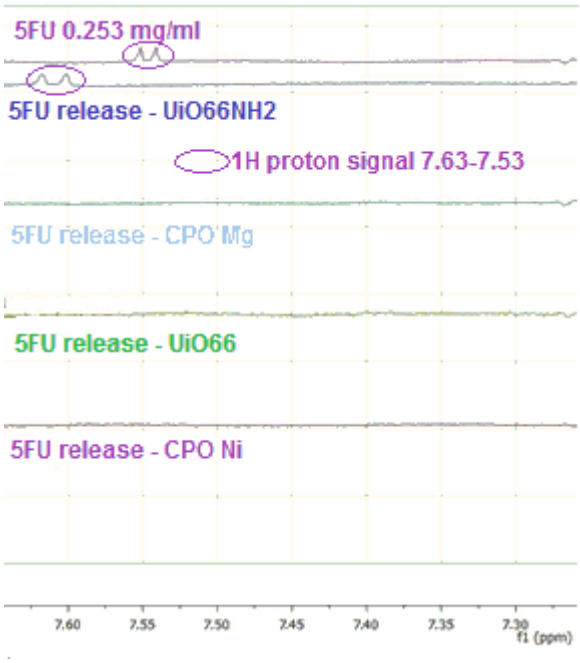

Figure 5-14 NMR shifts acquired @500 MHz Bruker, aliquots in D_2O solvent, harvested after 1 week release –test 2. MOFs encapsulated in MeOH. From the top – 5-FU, UiO66NH_2, CPO Mg, UiO66 and bottom is CPO Ni.

Results show that only UiO66NH_2 encapsulated in MeOH shows some traces of 5-FU in the released aliquot, the remaining MOFs do not show any traces when detected on NMR. MOF powders that were encapsulated with the drug in MeOH/FA solution show presence of 5-FU in the released aliquots. This confirms the FTIR results.

5.3.3. Biological testing: Viability and Efficacy

Alamar Blue (rezasurin) and Flow Cytometry (FACS) assays were prepared to assess the efficacy of stimulation of cancer cells with MOF powders loaded with 5-FU. Flow cytometry allowed to test the drug formulation on the THP-1 cells in terms of cell viability and type of cell death mechanism (necrosis or apoptosis), assay based on resazurin allowed for testing the same formulations on A549 lung cancer cell line. It must be mentioned that as A549 cells are the adherent type of cells, the well surface is important for their proliferation and growth. The MOF drug carrier systems could deposit on that surface when falling on the well bottom, thus not permitting for the cells' growth. The Alamar Blue assay was constructed to test the cells' viability after 28h and 48h drug exposure, FACS – 24h, apoptosis can be measured up until 24h after stimulation, later it is only late

apoptosis. This experiment was prepared in duplicate (two wells). There was an attempt to run 2 independent experiments, however, the instrument got blocked and only recorded measurements from one of the wells. MOF powders prepared as a formulation in suspension with RPMI or PBS form clots that FACS is very sensitive to. In order to keep the instrument unblocked, a "hot bleach" rinsing technique must be applied after each 2 samples to prevent clogging. The cell culture preparation and the overview of the techniques are described in the Chapter 3, Experimental Methods.

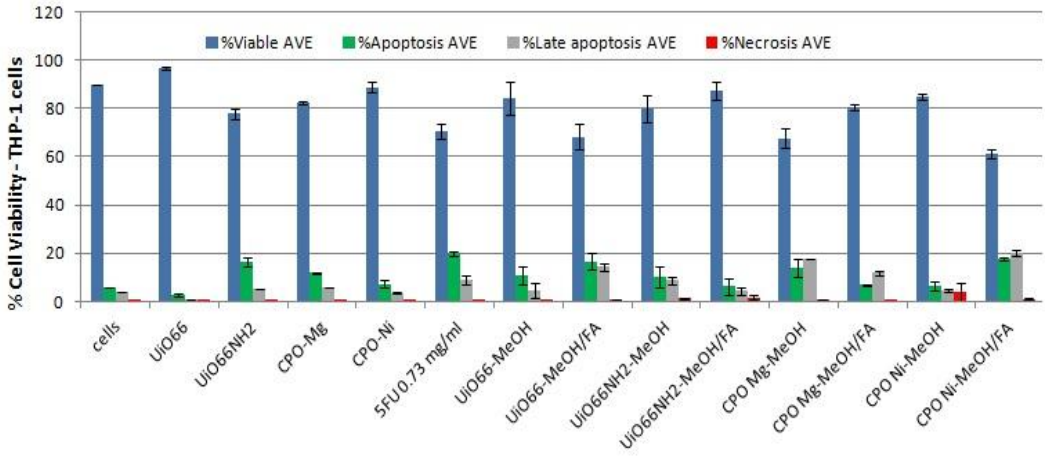

Figure 5-15 FACS measurements to test the cell viability and type of cell death measured after the 24 h exposure to the drug formulations. Error bars are SD, results from duplicates.

The dose of drug formulations used for cell stimulations was 50 µL per well. This corresponded to 500 µL of loaded/unloaded MOF sample, with a concentration reaching 2 g/L as the cell suspension volume was 200 µL per well,. The control stimulant with a concentration of 0.73 mg/mL 5-FU (36.5 ug in 50 µL, 0.146 g/L or 1.1 mM) was adjusted to support the idea that the 5-FU loading in the MOFs may be reaching ca. 7 wt%. The results showed high cell viability when the cells were stimulated with UiO66 and CPO Ni (96% and 89% respectively) and slightly lower if stimulated with CPO Mg and UiO66-NH_2 (82% and 78% respectively), the control sample (untreated cells) showed viability at the level of 90%. Cells stimulated with 5-FU 0.73 mg/mL solution showed viability of 71%. The cell viability drops to 84% when stimulated with UiO66 loaded with 5-FU in methanol and further to 68% if the cells are exposed to UiO66 loaded with 5-FU in a MeOH/FA route, where theoretical loading was higher per gram of MOF. Also

the dominating mechanism of cell death is apoptosis, and ca. 30% cells would undergo this type of death (16% early +14% late apoptosis). It is worth mentioning that the % of cells that underwent necrosis is very low and can be neglected. The stimulation with 5-FU loaded CPO Ni has effect on cells and their viability drops to 85% (MeOH) and 61% (MeOH/FA) which by far shows the best efficacy for the tested range of MOFs. For stimulations performed with CPO Mg and UiO66-NH_2, the results are not showing any particular trend, stimulation with 5-FU loaded UiO66-NH_2 gives 80% viability (MeOH) and 87% (MeOH/FA), likewise 5-FU loaded CPO Mg shows cell viabilities at the levels 68% (MeOH) and 81% (MeOH/FA). These values are very close to the ones obtained after stimulation with the pure MOF. This may lead to a conclusion that the amount of 5-FU stored in the MOF material is not enough to dramatically lower viability, also 5-FU is a drug whose efficacy is reported to increase over time and only the exposure times of 48-72 h would allow to spot the difference.

The further testing was performed on A549 cell line, applying Alamar Blue viability assay. The drug exposure time was 28h and 48h, two doses were used, either 10 μL (containing 100 ug MOF) or 50 μL (containing 500 ug MOF). Cell suspension of 100 μL per well was normalized with 2% RPMI growth media to 150 μL after stimulation and incubated for the given time, after which Alamar Blue solution was added (15 μL, 10% per volume, per well) and the plates were incubated for another 4 hours after which the fluorescence at EX/EM 555/585 nm was recorded. The 5-FU dose of 10 μL per well corresponded to 0.16 g/L (1.23 mM) concentration and 50 μL to 0.032 g/L (0.25 mM). This corresponded to drug loading of 8 wt% (8 μg per 100 μg, and 40 μg per 500 μg). Two independent experiments were prepared (2 plates) for each of the exposure times, each well was prepared in duplicate. Figure 5-16 shows results of a 24h-stimulation of A549

cells with two different doses, 100 μg and 500 ug of MOFs (10 and 50 μL).

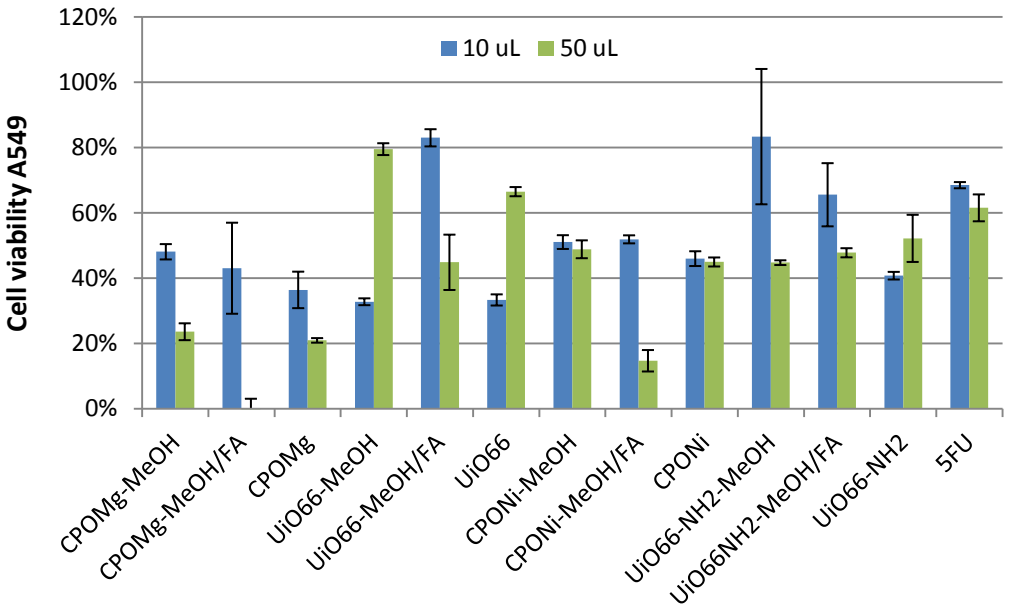

Figure 5-16 Results of lung cancer cells stimulation for 24h with MOFs and 5-FU control solution. Error bars are SEM (standard error of mean) from the 2 independent experiments each in duplicate.

The results are showing quite a high deviation from the average values and the SD (standard deviations) are high, so it might be that the stimulation dose of 10 μL may be too small for the accurate administration. Nevertheless, the trend can be identified for almost all of the MOFs (apart from UiO66-MeOH, UiO66 pure). With addition of more formulation to the cell suspension, the cell proliferation and growth is visibly inhibited and cell viability drops. The MOF powders has the tendency to deposit at the bottom of the well and may block the available surface for cells' growth. MOF powders suspended in RPMI are unfortunately not a perfectly homogenous suspension comprising of nano particles (200-500 nm) and some form aggregates and these could have been injected in the cell suspension without a proper dose control resulting in a higher stimulation dose. With a higher dose of 50 μL, the SDs are much smaller, however, loaded UiO66-NH_2 does not seem to act any different to the pure MOF, the same holds for CPO Mg. There is a noticeable decrease in cell viability, when comparing UiO66 pure and 5-FU loaded in MeOH/FA and the same can be observed for CPO Ni. Surprisingly, CPO Ni should be toxic to the cells on its own due to the presence of Ni metal in

its structure, the results show that it is less cytotoxic to THP-1 and A549 than e.g. CPO Mg.

Below, Figure 5-17 shows the results of cells' stimulation with MOFs, with a drug exposure of 48 hours.

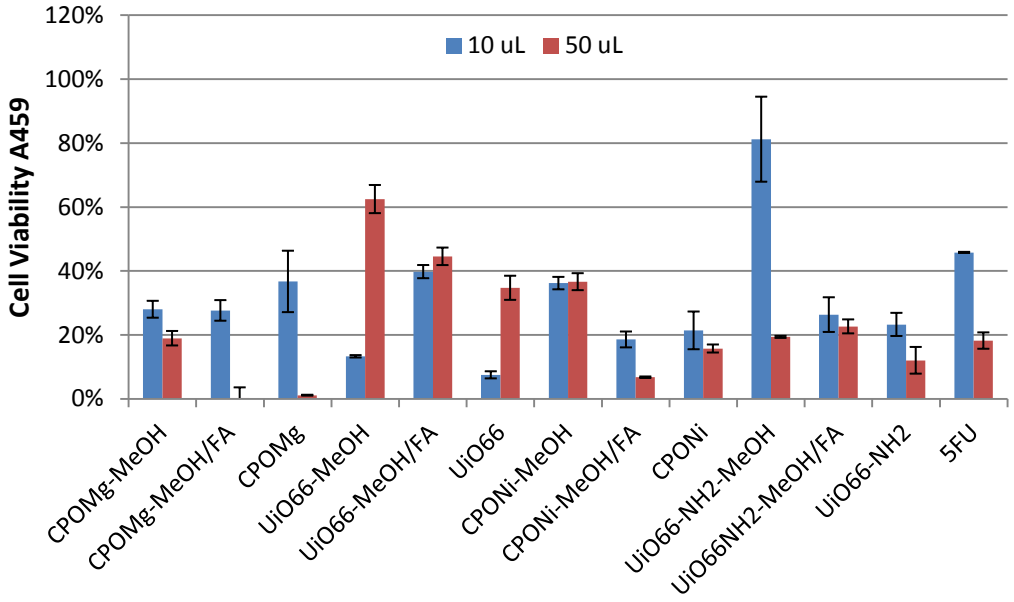

Figure 5-17 Results of 48h lung cancer cells stimulation with MOFs and 5-FU control solution. Resazurin assay. Error bars are SEM (standard error of mean) from the 2 independent experiments each in duplicate.

The cells stimulated with formulation containing 5-FU at the concentration of 0.37 mM (10 µL) and 1.87 mM (50 µL) in the well (150 µL), showed the decreased viability when compared with the 24 h drug exposure, from 68% down to 46% and from 62% to 18% respectively. From the results obtained the conclusion can be derived that the efficacy of the drug delivery system prepared in MeOH/FA encapsulation method is higher than the MeOH, which may be due to the fact that the 5-FU concentration in the encapsulation solution was much higher. Also, it cannot be excluded that some amounts of Formic acid could retain in the MOF pores/ structure and thus be toxic to the cells. The MOF powders after encapsulation were centrifuged and not rinsed with H_2O in order to prevent the drug being pushed out from the pores of the material. It was also noticed that results are dose-dependent only in some cases(10 µL vs 50 µL). This may be due to the inaccuracy of the pipetting of a non-homogeneous suspension containing MOF's aggregates. Some attempts were made to resolve this issue: by grinding

the MOF materials and by exposing the prepared suspensions to ultrasound vibrations.

5.4. Conclusions

5-FU is one of the anti-cancer drugs that has been used in formulations to treat various cancers e.g. colon, breast, pancreas, ovarian and head[4, 26] and lung cancer[27]. However, it is causing severe side effects if administered in bigger quantities and that is why there is a need to design a drug delivery system that would capture the drug and slowly release it in the patient's organism. It has been reported that 5-FU encapsulation was successfully performed using MOF material Zn-BDC[28], however no cytotoxic studies were performed, only release studies. Viability studies are very important in assessing efficacy of MOFs as potential drug delivery systems. The loading and release may be low but still sufficient to decrease the viability of the cancer cells. Hence, the attempt to run these tests for the purpose of this thesis. This included the viability testing for determination of viability and the type of death cells undergo – apoptosis or necrosis (FACS), and AlamarBlue assay based on redox potential and equilibrium between Resazurin and Resorufin. The results of the examination show that there is a potential to utilize the MOFs as delivery system for 5-FU. The encapsulation that was performed in MeOH showed that the MOF frameworks stayed intact when compared to formic acid route, however the achieved loading was much lower due to the low solubility of 5-FU in polar solvents. Generally, viability studies showed that cancer cell stimulation (lung cancer A549) with MOFs with encapsulated drug cargo was more efficient than of these stimulated with 5-FU only. In case of THP-1, the induced apoptotic death was observed to be higher than triggered by 5-FU only when the stimulations were performed with CPO Ni and UiO66 for encapsulation in MeOH/FA and for CPO Mg, for encapsulation route in MeOH (see Figure 5-15). Frameworks have the ability to encapsulate the drug and release it, however more research is needed to learn how to control the drug release better and also to investigate some other encapsulation techniques to achieve higher drug loading. The next step could be to unify the size of the MOF particles used for preparation of suspensions.

5.5. References

1. Drugs.com, https://www.drugs.com/pro/fluorouracil-injection.html.
2. B. J. Thompson, M. Ravits and D. N. Silvers, *The Journal of Clinical and Aesthetic Dermatology*, 2014, **7**, 35-37.
3. H. P. Rang, J. M. Ritter, R. J. Flower and G. Henderson, *Rang & Dale's Pharmacology*, 8th edn., Churchill Livingstone.
4. D. B. Longley, D. P. Harkin and P. G. Johnston, *Nat Rev Cancer*, 2003, **3**, 330-338.
5. M. Richard L. Schilsky, *Oncology*, 1998, **12**, 13-18.
6. M. Olukman, O. Sanli and E. K. Solak, *Journal of Biomaterials and Nanobiotechnology*, 2012, **3**, 469-479.
7. R. L. Sastre, R. Olmo, C. Teijón, E. Muñíz, J. M. Teijón and M. D. Blanco, *International Journal of Pharmaceutics*, 2007, **338**, 180-190.
8. V. R. Babu, M. Sairam, K. M. Hosamani and T. M. Aminabhavi, *International Journal of Pharmaceutics*, 2006, **325**, 55-62.
9. E. Fournier, C. Passirani, A. Vonarbourg, L. Lemaire, N. Colin, S. Sagodira, P. Menei and J. P. Benoit, *International Journal of Pharmaceutics*, 2003, **268**, 31-35.
10. J.-Q. Liu, X.-F. Li, C.-Y. Gu, J. C. S. da Silva, A. L. Barros, S. Alves-Jr, B.-H. Li, F. Ren, S. R. Batten and T. A. Soares, *Dalton transactions*, 2015, **44**, 19370-19382.
11. C.-Y. Sun, C. Qin, C.-G. Wang, Z.-M. Su, S. Wang, X.-L. Wang, G.-S. Yang, K.-Z. Shao, Y.-Q. Lan and E.-B. Wang, *Advanced Materials*, 2011, **23**, 5629-5632.
12. C. A. M. d. C. a. Â. M. Moraes, *Acta Scientiarum. Technology* 2003, 51-63.
13. Pedro Pires Goulart Guimarães, Sheila Rodrigues Oliveira, Gabrielle de Castro Rodrigues, Savio Morato Lacerda Gontijo, Ivana Silva Lula, Maria Esperanza Cortés, Ângelo Márcio Leite Denadai and R. D. Sinisterra, *Molecules*, 2015, **20**, 879-899.
14. S. R. Miller, D. Heurtaux, T. Baati, P. Horcajada, J.-M. Greneche and C. Serre, *Chem. Commun.*, 2010, **46**, 4526-4528.

15. P. Horcajada, C. Serre, M. Vallet-Regí, M. Sebban, F. Taulelle and G. Férey, *Angewandte Chemie*, 2006, **118**, 5974-5978.
16. P. Horcajada, T. Chalati, C. Serre, B. Gillet, C. Sebrie, T. Baati, J. F. Eubank, D. Heurtaux, P. Clayette, C. Kreuz, J. S. Chang, Y. K. Hwang, V. Marsaud, P. N. Bories, L. Cynober, S. Gil, G. Ferey, P. Couvreur and R. Gref, *Nature Materials*, 2010, **9**, 172-178.
17. P. Li, Y. Wang, Z. Peng, F. She and L. Kong, *Carbohydrate Polymers*, 2011, **85**, 698-704.
18. C.-Y. Sun, C. Qin, X.-L. Wang and Z.-M. Su, *Expert Opinion on Drug Delivery*, 2013, **10**, 89-101.
19. http://www.enzolifesciences.com/ALX-480-099/5-fluorouracil/.
20. D. Cunha, M. Ben Yahia, S. Hall, S. R. Miller, H. Chevreau, E. Elkaïm, G. Maurin, P. Horcajada and C. Serre, *Chemistry of Materials*, 2013, **25**, 2767-2776.
21. P. Horcajada, F. Salles, S. Wuttke, T. Devic, D. Heurtaux, G. Maurin, A. Vimont, M. Daturi, O. David, E. Magnier, N. Stock, Y. Filinchuk, D. Popov, C. Riekel, G. Férey and C. Serre, *J Am Chem Soc*, 2011, **133**, 17839-17847.
22. P. Horcajada, C. Serre, G. Maurin, N. A. Ramsahye, F. Balas, M. Vallet-Regi, M. Sebban, F. Taulelle and G. Ferey, *J Am Chem Soc*, 2008, **130**, 6774-6780.
23. T. Devic, P. Horcajada, C. Serre, F. Salles, G. Maurin, B. Moulin, D. Heurtaux, G. Clet, A. Vimont, J.-M. Grenèche, B. L. Ouay, F. Moreau, E. Magnier, Y. Filinchuk, J. Marrot, J.-C. Lavalley, M. Daturi and G. Férey, *J Am Chem Soc*, 2009, **132**, 1127-1136.
24. A. T. Hulme, S. L. Price and D. A. Tocher, *J Am Chem Soc*, 2005, **127**, 1116-1117.
25. J. Kahr, R. E. Morris and P. A. Wright, *CrystEngComm*, 2013, **15**, 9779-9786.
26. O. Ş. Merve Olukman, Ebru Kondolot Solak, *Release of Anticancer Drug 5-Fluorouracil from Different Ionically Crosslinked Alginate Beads*, 2012, **3**, 469-479.

27. X. Pan, X. Zhang, H. Sun, J. Zhang, M. Yan and H. Zhang, *PLoS ONE*, 2013, **8**, e56679.
28. Y. Zhu, Y. Wang, P. Liu, Y. Wu, W. Wei, C. Xia and J. Xie, *New Journal of Chemistry*, 2015.

Chapter 6. MOFs as potential vaccine adjuvants

6.1. Aims

This research work aimed at opening an avenue for novel potential applications for MOFs, as adjuvants – an important part of a vaccine. In this section, I would like to recap on the topic of vaccines and immunology in a more detailed way to help the reader follow this chapter. The brief introduction into this topic was given in Chapter 1.

Vaccination is the most effective medical intervention ever developed saving some millions lives per year[1] by preparing an individual to develop effective biological defence mechanisms (immunity) against "danger" thanks to pattern recognition receptors able to recognise pathogens – infectious agents and thus to protect against an infectious disease[2] and has been used for more than 100 years[3]. Vaccine is also considered as a potential protection against cancer and this direction of development is also increasingly targeted[4]. A vaccine contains a small amount of a material which resembles a disease – causing agent (the "antigen" – a viral, microbial or tumour component). The antigen comprises of a subunit or an inactivated form of the pathogen, and hence should not itself cause infection. The vaccine stimulates the body's immune system to recognize the antigen as unwanted and destroy it, but also to generate memory in cells which can rapidly respond to a subsequent infection, thereby conferring effective immunity against the pathogen. In order to ensure that robust immunity is inoculated, an "adjuvant" is usually added to vaccines to mimic the danger signals that naturally trigger immune responses. At present, inorganic compounds known as 'alums' (usually either AlO(OH) or amorphous aluminium hydroxyphosphate) are used as adjuvants in the majority of cases. "Alum" can lead to strong immunity to microbes and larger parasites, but does not provoke the necessary immune response to overcome viral infections or the majority of cancers. Only alum and a new adjuvant containing alum (AS04) are currently licensed by the FDA[5]. These often do not provoke the precise pattern of immune responses needed to most

effectively target a particular disease, which has led to problems in developing vaccines against, for instance, malaria[6].

The Alum adjuvant that is an Al-based mixture of hydroxides or phosphates has been doing the trick of boosting the immune response; however, its action is limited to inducing Th2 responses[7]. In immunology, there are two types of immune responses recognized, one is Th1 type, which is a cell – mediated response, and could kill intracellular bacterium and viruses, whereas Th2 response (induced by pathogen) stimulates a humoral immunity leading to production of antibodies, and as such to elimination of extracellular bacterial infections[8]. Up until now, the mechanism of how adjuvants are working has not been fully explained. And some empirical tests identified their ability to stimulate the immune response when administered along with an antigen[9].

Hence, there is a need to develop more powerful adjuvant material that would hopefully outperform alum and hopefully leading to elucidation of the mechanism of action of adjuvants, which is unknown.

A total of 9 MOFs were tested for their ability stimulate to dendritic cells (DCs) to maturation and secretion of cytokines. This feature was assessed in terms of cytokine secretion (IL-6 and TNF-α), and the expression of the surface markers CD1a, CD40 and CD86 on dendritic cells. Dendritic cells (DCs) are capable to detect and recognise antigens and present them through MHC (major histocompatibility complex to helper T cells (T-cell receptors) which activate a specific immune response against the particular pathogen that the antigen came from [10]. Once the antigen has been recognise, DCs would move towards the lymph nodes. At this point DCs are mature, and lose their ability for antigen uptake and only can express the co-stimulatory molecules[11]. By monitoring the response from the stimulated DCs, we can get an idea how effectively DCs will activate T cells to respond to pathogen.

Briefly, cytokines are small peptides that are released by cells in order to induce an immune response and enable for communication between the cells. Mainly, they are secreted by macrophages or T cells. The measuring of secreted cytokines level responsible for pro-inflammatory action like IL-6 and TNF-α could allow for screening of the potential candidates for the novel adjuvants in new anti-cancer

prevention programmes. Also, the screening of the cell viability level after the stimulation allow to eliminate the toxic compounds. There is a variety of cytokines and for the purpose of this research, the testing was performed on the secretion of interleukin family (IL-6) and tumour necrosis factor family (TNF-α), the former one can promote different actions dependent on the interleukin and the role of the latter is to regulate inflammatory and immune responses[12].

Surface markers CD1a, CD40 and CD86, are expressed on the surface of the antigen – presenting cells like DCs. CD1a is a cell surface glycoprotein[13], related to presenting a lipid antigen to T cells, CD40 (cluster of differentiation) is a protein that belongs to TNF-receptor family, and is expressed by B cells, DCs, and macrophages[14], which are the antigen-presenting cells but it is also expressed on cancer cells (bladder, ovary, cervix). The antigens are presented to T cells. CD86 is a protein and activation marker for antibody producing cells (B cells), and DCs stimulated with chemical allergens would respond by increased level of co-stimulatory molecule[15]. The wider description of the key cells in immunity is given in Chapter 1, Section 1.4.

This chapter is a continuation of a concept presented by Dr Gareth Williams and aims to investigate other materials than double layered hydroxides (LDHs) as these showed promising results to be the candidate to replace alum and potent enough to be taken into consideration[16] . As such, research extends over the range of MOFs to be explored as adjuvants. Based on these results, it was proposed that MOFs could be even better candidates due to the fact of their wide range of structures, quite high surfaces areas and pores and these can be used for hosting of an antigen, a variety of different linkers used and metal anions which gives almost limitless number of combinations, that can be tested for immune response, catalogued and leading to establishment of a model of the optimally working adjuvant. The target of this concept, is to develop an adjuvant model, that would allow to predict the immune response triggered by the material based on its property – this however, it is not the aim of this thesis.

6.2. Synthesis

The Zr-MOF powders assessed to have potential for a possible application as adjuvants for novel vaccines were synthesised according to the procedures found in the literature[17, 18]. Briefly, these synthesis routes are to be found in Chapter 4, in the section 4.2, dedicated to synthesis.

The Al-MOFs were chosen based on the simplicity of the synthesis procedures found in the literature and the fact that they have Al-metal in their frameworks, and thus can be compared with the commercially used Al-containing "alum" adjuvants. There was a hypothesis that MOF materials with Al-cation may over perform alum for its stimulation of cytokines secretion, especially TNF-α and IL-6, given the fact that the organic linker may also contribute to the immunologic stimulation. Also, in scope of this research was a bold idea to investigate if it would be possible to control the immune response by changing the metal/linker, thus giving us a wide range of tuneable adjuvant candidates. These results could be a foundation for a data base to develop an adjuvant model and then to design an adjuvant with the desired properties as to inducing the desired immune responses.

The following MOFs were chosen: Al-MIL 53, Al-MIL 53_NH_2, MIL 96, DUT 5, MIL 120, MIL 122, MIL 101_NH_2.

MIL-53 AL

A mixture of terephthalic acid (288 mg, 1 mmol) and metal salt $Al(NO_3)_3 \cdot 9H_2O$ (1.3 g, 0.5 mmol) were dissolved in a solution of distilled water (5 ml) and left under stirring for 30 min. The mixture was then transferred to a Teflon-lined autoclave (23 ml) sealed, and placed in the oven for 72 hours at 220 °C. The product was collected by filtration as a white substance, ca. 370 mg was obtained. This synthesis followed the protocol found in the literature[19].

MIL-101 Al-NH_2

$AlCl_3 \cdot 6H_2O$ (514 mg, 1 mmol) was dissolved in DMF (30 ml) in a 50 ml Teflon liner. Under stirring 2-aminoterephthalic acid (562 mg, 1.5 mmol) was added and the mixture was stirred for 30 min. Then the liner was placed in an autoclave), sealed and placed in the oven for 72 hours at 130°C. The collected powder was

yellowish and the yield was 845 mg. The procedure was in accordance to the one in literature[20],[21].

MIL-96 and MIL-96 ("pure phase")

The synthesis route was exactly the same as mentioned in the literature[22]. Two MOFs were synthesised, one reported as MIL-96 and the other as MIL-96 "pure phase" by the scientific paper that established the synthesis route. Briefly, for this "pure phase" synthesis $Al(NO_3)_3 \cdot 9H_2O$ (1.314 g, 3.5 mmol) was dissolved in distilled water (5 ml) and to this solution, trimethylbenzenetricarboxylate was added (0.44 g, 1.75 mmol). The organic linker is quite powdery and it was challenging to disperse it in water as it floated on its surface. The autoclave was sealed and placed in the oven for 24 hours at 210°C. The collected powder was white and the yield was 549 mg. For MIL-96 which is not noted as "phase pure" by literature[22], the only difference was the linker being used, and in this case it was trimesic acid. The synthesis conditions were same as for the "pure phase" with only different amounts of reagents: $Al(NO_3)_3 \cdot 9H_2O$ (1.314 g, 3.5 mmol) was dissolved in distilled water (5 ml) and to this solution trimesic acid (105 mg, 0.5 mmol) was added. Yield: 205 mg

MIL-120

$Al(NO_3)_3 \cdot 9H_2O$ (3.2 g, 8.5 mmol) was dissolved in 20 ml of distilled H_2O and left under stirring. Pyromellitic acid (benzene-1,2,4,5-tetracarboxylic acid, 0.5 g, 2 mmol) was dissolved in 4M NaOH (3.4 ml, 13.6 mmol) and left under stirring. The two solutions were transferred into a Teflon-lined autoclave (50 ml) and stirred for 30 min before being placed in the oven for 24 hours at 210°C. The collected white powder was washed with H_2O under reflux for 10 hours at 100°C. Yield: 189 mg. The synthesis procedure can be found in literature[23].

MIL-122

$Al(NO_3)_3 \cdot 9H_2O$ was dissolved in 5 ml of distilled water (342 mg, 0.9 mmol) and left under stirring. Then 276 mg (0.9 mmol) of the organic linker 1,4,5,8-naphthalenetetracarboxylic acid was added to the metal salt solution. The Teflon-lined autoclave (50 ml) was then sealed and placed in an oven for 24 hours at 210°C. The product was collected by filtration and the yield was 149 mg. The synthesis route followed the protocol[24].

DUT-5

A mixture of $Al(NO_3)_3 \cdot 9H_2O$ (0.52 g, 1.4 mmol) was dissolved in 30 ml DMF. 4,4-biphenyldicarboxylic acid (0.26 g, 1.07 mmol) was added and the reagents were left under stirring for 30 min, then the solution was transferred to an autoclave (50 ml) and placed in the oven for 24 hours at 120°C. The product was a white powder that was washed with DMF 3 times. The yield was 443 mg. The method can be found in the literature[25].

These MOFs all contained Al- or Zr-cation in their structure and the linker was different every time (see Table 6-1). The linkers used are characterised in the table below. This allowed to spot different patterns for immune responses and in the next step would help to build a model. This, however, was not the aim of this thesis.

MOF	Linker	Linker Structure	Metal cation
UiO66	Terephthalic acid	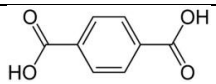	Zr
MIL 53			Al
UiO66-NH_2	2-aminoterephthalic acid	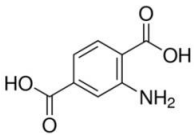	Zr
MIL-101-NH_2			Al
MIL-96	Trimesic acid	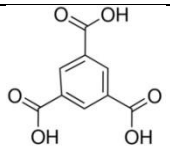	Al
MIL-96 "pure phase"	trimethyl benzenetricarboxylate	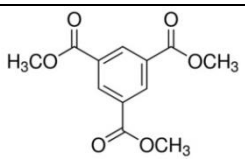	Al
MIL-120	pyromellitic acid	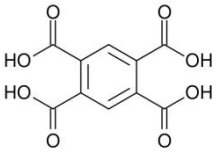	Al
MIL-122	1,4,5,8-napthalenetetracarboxylic acid	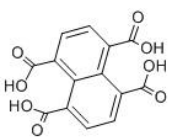	Al
DUT-5	biphenyldicarboxilic acid	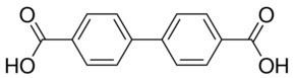	Al

Table 6-1 Organic linkers used for the MOFs synthesis.

6.3.Results

6.3.1.X-ray patterns

The characterisation was performed by X-ray on RIGUKU and by comparing the location of the peaks from crystal lattices. The X-ray diffraction patterns are to be found in Appendix 2. All of the 7 Al-containing MOFs were successfully synthesised and the peak patterns compared to these from the literature.

6.3.2.Immune responses measured by ELISA

The immune responses induced by the presence of MOF particles in macrophages and dendritic cells were measured with ELISA and flow cytometry (FACS). The principles of the two methods are described in the Experimental Section 3.5, Chapter 3. FACS was performed to verify the quantity of the receptors activated on the dendritic cells surfaces, with CD40, CD86 and CD1a quantified. ELISA was a pivotal experiment to measure the secretion of two cytokines IL-6 and TNF-α. They regulate the body temperature to stop infections and relaxing blood vessels in order to allow leucocytes to permeate to the centre of infection. It is stipulated that they may play a vital role in fighting the cancer by making healthy cells immune to tumour-genesis and tumour-proliferation.

IL-6 is secreted by macrophages or T cells to give rise to immune response. It has been recently associated with presence of cancer in human tissues as elevated concentrations of this cytokine are found in human blood diagnosed with an advanced cancer. It is stipulated that the higher levels of IL-6 cytokines can fight the cancer cells. It can be released in response to microbial molecules/pathogens.

The main role of TNF-alpha (tumour necrosis factor alpha)is to regulate the immune cells and induce inflammation in order to reduce the viral replication and cancer growth.

Macrophages were obtained through the THP-1 cells differentiation, and dendritic cells from the differentiation of primary human monocytes, as detailed in Chapter 3, Section 3.5.3. The levels of secreted cytokines were compared with the ones induced by a commercial alum: ALHYDROGEL (Aluminium Hydrohide Gel, CAS No. 21645-51-2, Al content 10mg/ml) and Adju – Phos (Aluminimum Phosphate Gel, $AlPO_4$ content 2%, CAS No. 7784-30-7), both purchased from

Brenntag, Denmark, which is commonly used for variety of vaccines. It must be pinpointed that "alum" does not have a defined structure or composition and immunologists refer to all of the adjuvants containing Aluminium in the gel as "alum". Chemists, however, refer to materials having a formula $KAl(SO_4)_2 \cdot 12H_2O$ and alternatively $NH_3(aq)Al(SO_4)_2$, as "alum" which causes a lot of uncertainty and definitely has its influence on the possibility to compare the properties of variety of alums. In the immunology world, AlO(OH) "alum" is a crystalline layered material in a suspension and $Al(OH)_x(PO_4)_y$ is an amorphous material containing hydroxyl and phosphate groups[26].

Three independent experiments with at least three replicates in each experiment, were performed for each of the parameters and the results obtained averaged. Al-MOFs' performance as the potential adjuvant were assessed against the commercial alum, and results were compared within all of the tested MOFs containing Al-cation in the network. Another experiment was performed to test the performance of the two Zr-MOFs against the two commercial alums: Aluminium-phosphate and Aluminium-hydroxite containing commercial alums. LPS (bacterial lipopolysaccharide), which is an endotoxin was used as a positive control since it is known to induce a strong immune response. The differentiation of THP-1 cells to macrophages was performed to enable secreting cytokines. Such an approach has been demonstrated in literature[27].

6.3.2.1.Immune response: Al-MOFs

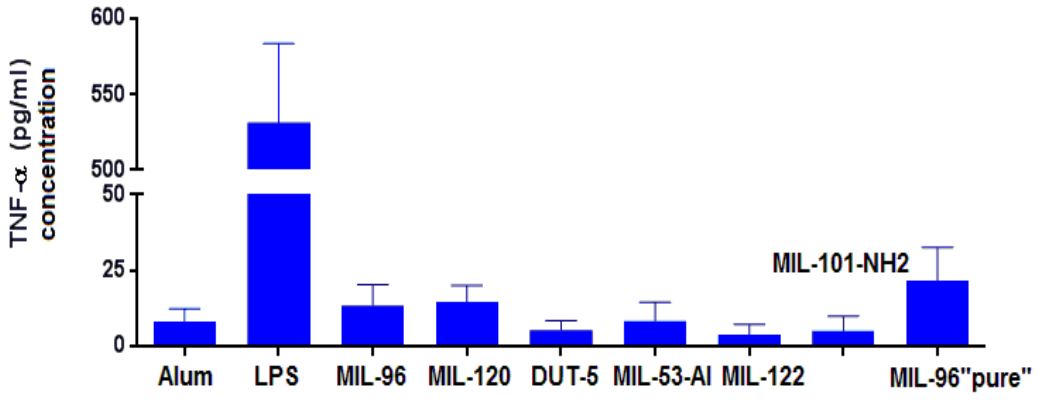

Figure 6-1 TNF-α levels secreted by macrophages (THP-1) after 24h stimulation with Al-MOFs and alum, measured by ELISA. The error bars refer to SEM (standard error of mean).

Figure 6-1 shows the quantities of TNF-α secreted (tumour necrotic factor α). TNF-α regulates immune cells and induces inflammation in order to reduce viral replication and cancer growth[28]. Hence, it is hypothesised that it may play a vital role in anti-cancer therapies, including vaccines[4, 29].

Obtained results (Figure 6-2) show that some MOFs perform better than alum, MIL-96 and MIL-120 and MIL-96 "pure" lead to concentrations of TNF-α three times greater than induced by stimulation with alum. MIL-53 Al induces similar levels of secretion of TNF-α to alum. The levels of another cytokine, IL-6 (interleukin-6), were also quantified.

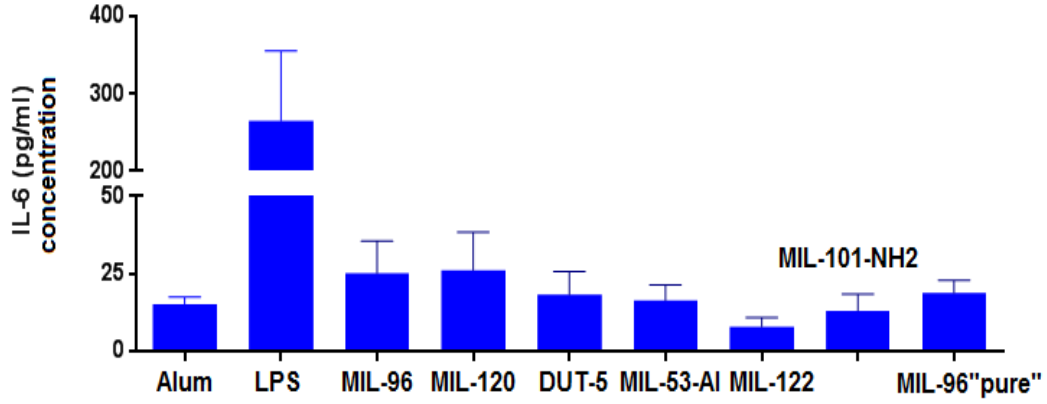

Figure 6-2 IL-6 levels secreted by macrophages (THP-1) after 24h stimulation with Al-MOFs and alum, measured by ELISA. The error bars refer to SEM (standard error of mean).

In terms of the amount of secreted cytokine IL-6 by the stimulated macrophages, commercially available alum performs better than MIL-122 and MIL-101-NH_2, other tested Al-MOFs show more promising results though. MIL-96 and MIL120, followed by MIL-96 "pure phase" and DUT 5 and MIL-53 Al show increased levels of IL-6. This could be a result of the contribution of the linkers to the enhancement of immune response triggered. Also morphology of the samples and the size of the particles may play a role here. However, the latter is more challenging to claim, as upon introduction of the MOF powder into the PBS (phosphate buffered saline) in order to prepare a suspension for cell stimulation, the MOF particles tend to clamp and form aggregates that are very difficult to disintegrate. PBS was used as a carrier phase due to the fact that it is neutral to viability and cytokine' secretion. To address this issue, a method for preparation of the homogeneous suspension with similar particle sizes should be further

investigated. If successful, this could lead to commercialisation of new adjuvants for novel vaccines.

Figure 6-3 depicts the SEM image taken of the two MOFs prepared with different linkers, these are both MIL-96 structures. The shape of the particles is different, which may have a tremendous effect on the ability of the MOF powder to induce the immunological signal in the cells.

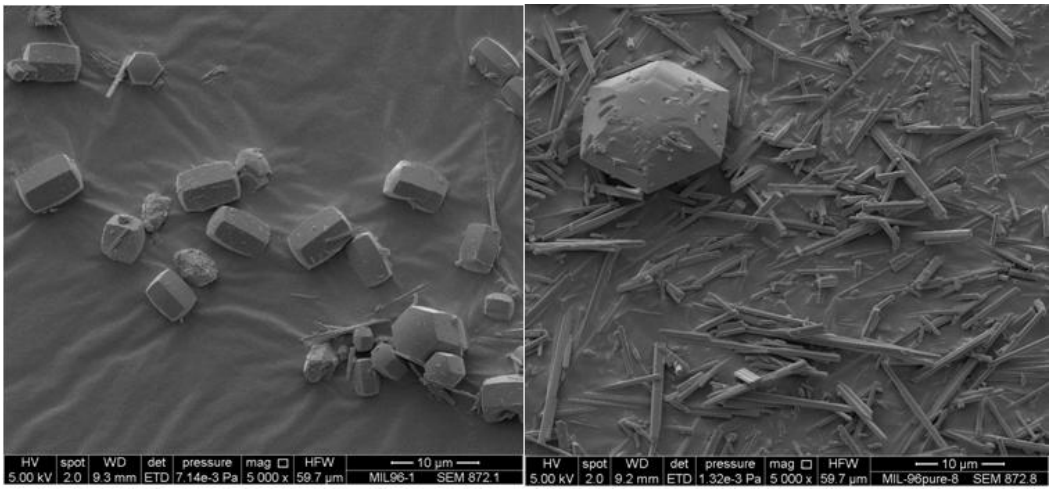

Figure 6-3 SEM image of MIL-96 (left) and MIL-96 "pure phase" (right). The difference in the morphology of the samples is noticeable.

6.3.2.2. Immune response: Zr-MOFs

The ELISA tests were performed to investigate the ability of Zr-MOFs (UiO66 and UiO66-NH_2) for secretion of cytokines TNF-α and IL-6. This was done in two independent experiments and each condition within was done in triplicate. The obtained results are presented below, TNF-α (Figure 6-4) and IL-6 (Figure 6-5).

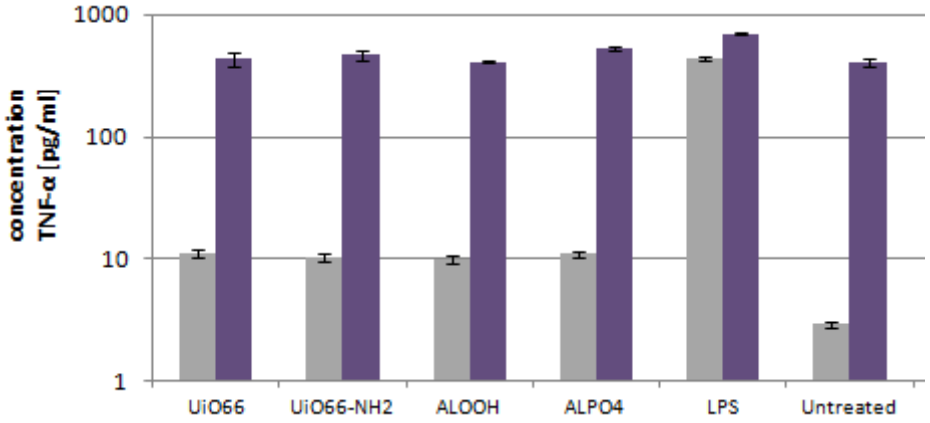

Figure 6-4 TNF-α levels secreted by macrophages THP-1 after 24h stimulation with Zr-MOFs and alums, measured by ELISA. Two independent experiments (grey and purple columns), error bars are a standard deviation (SD) between results, in triplicates.

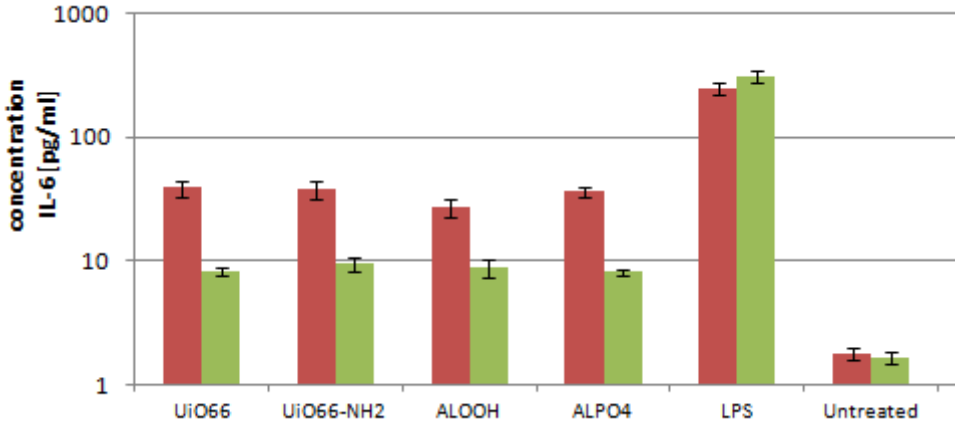

Figure 6-5 IL-6 levels secreted by macrophages THP-1 after 24h stimulation with Zr-MOFs and alums, measured by ELISA. Two independent experiments (red and green columns), error bars are a standard deviation (SD) between results, in triplicates.

Based on the results obtained, we can assume that the performance of Zr-MOFs is only slightly better when compared to AlO(OH) alum and achieving the same results when compared to $AlPO_4$ (aluminium hydroxyphosphate). Macrophages stimulated with LPS show elevated levels of secreted cytokines, while untreated cells produce only low levels.

There was an attempt to investigate the correlation of the induced immune-response (IL-6) with the amount of the stimulant added to the cell suspension. The following quantities were chosen 10µL (476 µg MOF/ml), 20 (910 µg/ml)and 30µL (1300 µg/ml).

The amount of IL-6 secretion slightly increased with the increased quantities of Zr-MOFs added, but remained rather stable in case of alums. This is an important finding, as the quantity of adjuvant must be adjusted to its optimum depending on the material being used to boost the immune response.

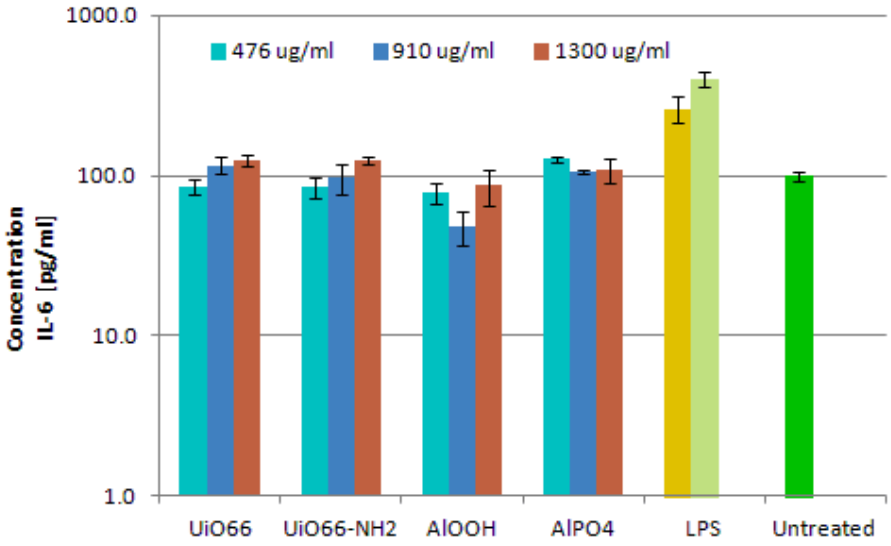

Figure 6-6 IL-6 concentration secreted by macrophages THP-1 after 24h stimulation with Zr-MOFs and alums, measured by ELISA. Increasing concentration of stimulants Zr-MOFs and alums, LPS concentration 100 ng/ml (yellow) and 200 ng/ml (fair green).Results based on experiment from one plate in duplicates. Error bars refer to standard deviation (SD) between the results measured from two wells.

As shown by the results, the highest levels of IL-6 were obtained when stimulated with the highest dose of Zr-MOFs, however in case of alums the dose seemed not to play a crucial role. This could stipulate that a higher concentration of MOF powder is potentially needed in order to induce much more pronounced immune response. For alums, there is no special trend being observed and it looks like 910 mg/ml dose induces lower immune response.

To summarise the ELISA experiments, we can conclude that Al-MOFs look more promising than Zr-MOFs to be candidates for the novel adjuvants.

6.3.3.Immune responses measured by Flow Cytometry

Flow Cytometry equipment was used to measure the concentration of the surface proteins on the dendritic cells following exposure to the MOFs. The dendritic cells were kindly provided by Dr Ilona Kubajewska.

The activity of three receptors on cell surface of dendritic cells (DCs) were measured when stimulated with Al-MOFs, these were: CD40, CD1a and CD86.

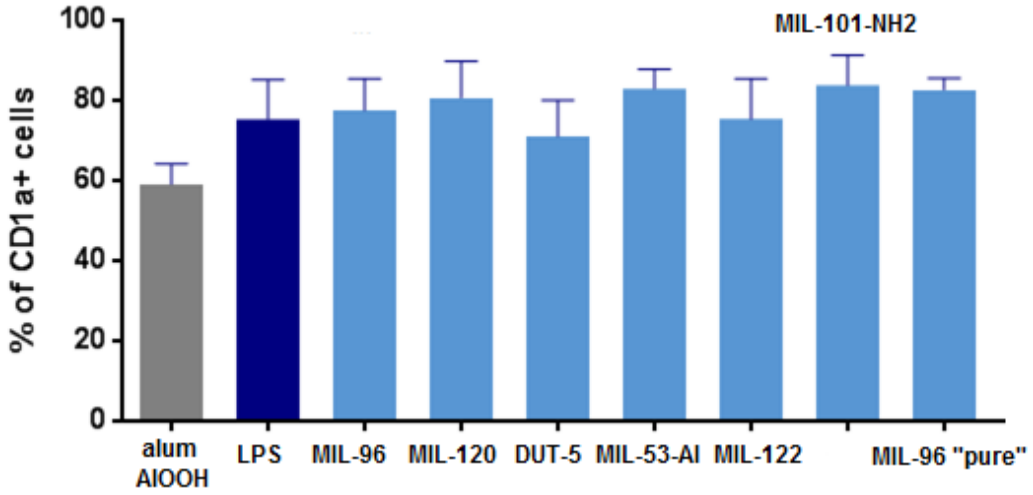

Figure 6-7 CD1a expression on dendritic cells after 24h stimulation with Al-MOFs and alum, measured by FACS. Error bars are SEM (standard error of mean) from three independent experiments.

The above results (Figure 6-7) show that MIL-101-NH_2 is the best candidate to successfully activate the CD1a receptor, with MIL-96 "pure phase" followed by MIL-120 and MIL-53-Al in terms of the percentage of cells expressing this co stimulatory molecule.

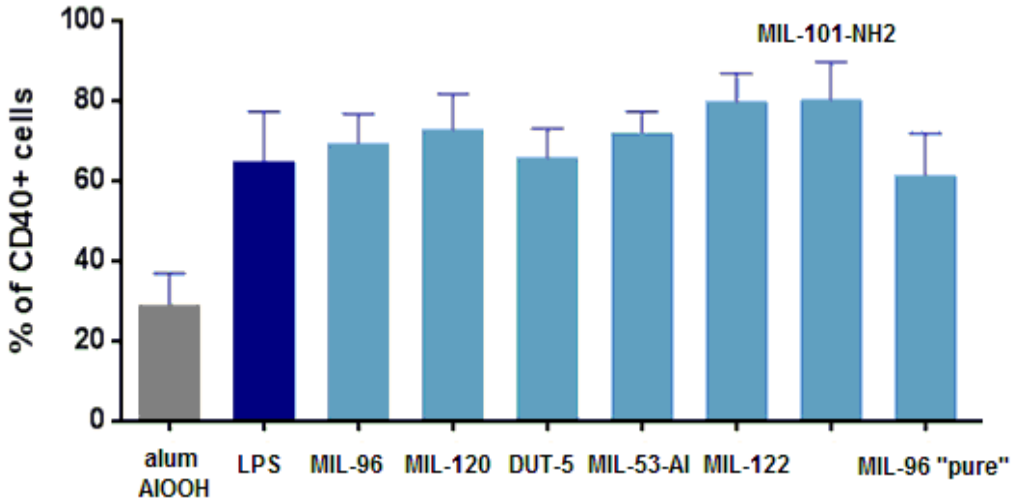

Figure 6-8 CD40 expression on dendritic cells after 24h stimulation with Al-MOFs and Alum, measured by FACS. Error bars refer to SEM (standard error mean), experiments performed over 3 plates, each in duplicates. FACS measurement performed by and courtesy of Dr Kubajewska.

Again, as we can see (Figure 6-8), MIL-101-NH_2 is the best performing MOF when it comes to activation of the CD40 receptor, followed by MIL-122. Based

on the results obtained, MOFs are showing better ability to induce higher immune response than alum. This opens door to further investigations to test the performance of MOF powders, in order to assess their efficiency *in vivo*.

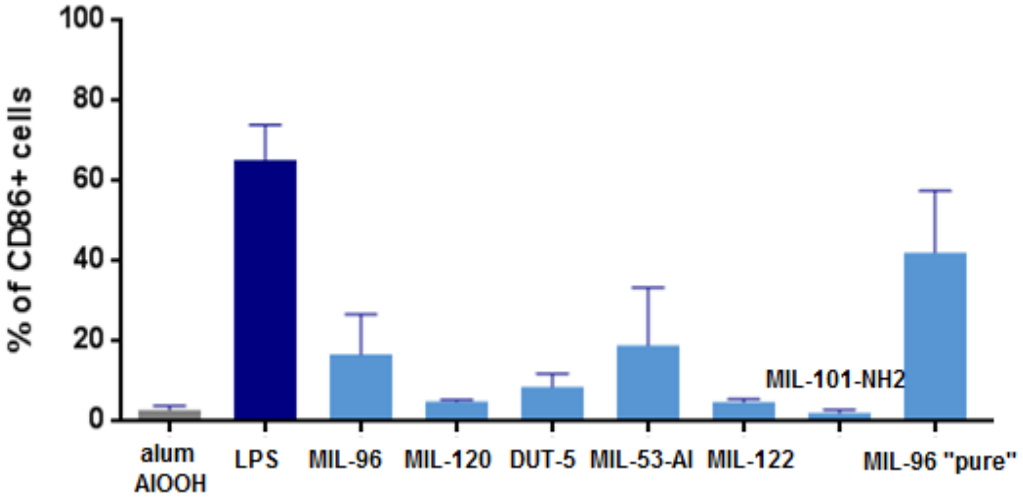

Figure 6-9 CD86 expression on dendritic cells after 24h stimulation with Al-MOFs and Alum, measured by FACS, courtesy of Dr Kubajewska. Error bars refer to SEM (standard error of mean), results obtained over 3 independent experiments with duplicates.

In terms of CD86 expression (Figure 6-9), alum shows low levels of expression and MIL-96 "pure phase" stimulation is leading to the production of more CD86 receptors in a comparison made over all the tested MOFs. MIL-53-Al, which also leads to up – regulated expression of CD86 receptor, could also be taken into account as a candidate for a new adjuvant.

To summarise, different MOFs can up-regulate expression of the surface markers, what was observed in case of MIL-96"pure" for CD86 (outperformed alum), however, when CD40 expression was monitored, this MOF did not induce a significant level of response and MIL-122 and MIL-101-NH_2 took the lead. The MOF, which gives the best results over the data sets obtained is MIL-96 "pure". It is not always the best in its class, however, the response induced for secretion of TNF-α, and elevated levels of expressions CD1a and CD86, gives it the lead and as such this MOF should be taken for further experiments *in vitro* as well as *in vivo*.

6.3.4.Viability tests - Dendritic Cells and THP-1 differentiated macrophages

It is vital to assess the viability of the cells when these are stimulated with a certain substance. It is important to observe elevated signal from the receptors, and elevated cytokine expression, however, the potential adjuvant cannot be too toxic because the cells would be terminated which is not desired, some cell death is not a bad outcome though as it sends signals and stimulates the immune response. The viability testing was performed with Alamar Blue assay for Zr-MOFs, and by FACS for Al-MOFs.

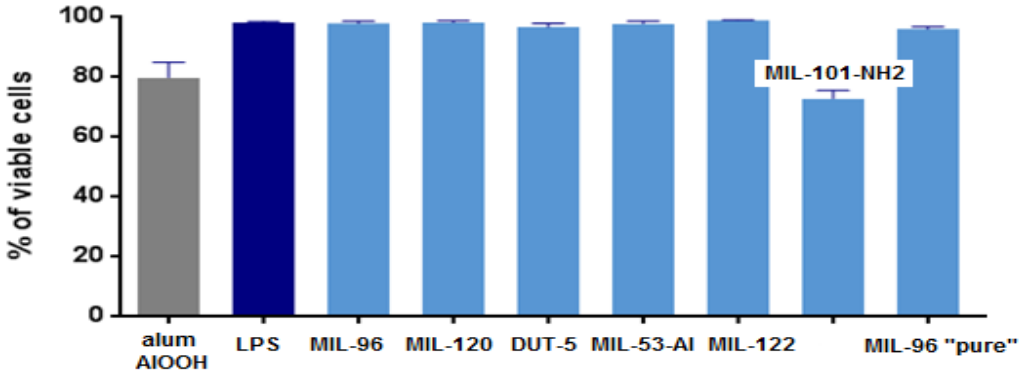

Figure 6-10 Viability of dendritic cells after exposure to Al-MOFs and alum for 24h, measured by FACS based on Annexin V/PI staining. Results were averaged based on 3 independent experiments, courtesy of Dr Kubajewska. Error bars are SEM (standard mean of error).

Based on the results obtained (Figure 6-10) for the viability screening, almost all the MOFs, except MIL-101-NH_2 can be regarded as non-toxic and do not compromise the safety of the living system - the cells. MIL-101-NH_2 decreases viability to70 % and when compared with different tested MOFs, may show higher toxicity, due to the presence of amine group. Alum shows the viability at the level of 80%.

Similar experiments were performed to measure the viability of macrophages when stimulated with Zr-MOFs. After the 24-hour simulation was completed, the aliquots of cells suspension containing secreted cytokines were harvested. Please refer to Chapter 3 Section 3.5.2. for a detailed description of the procedure.

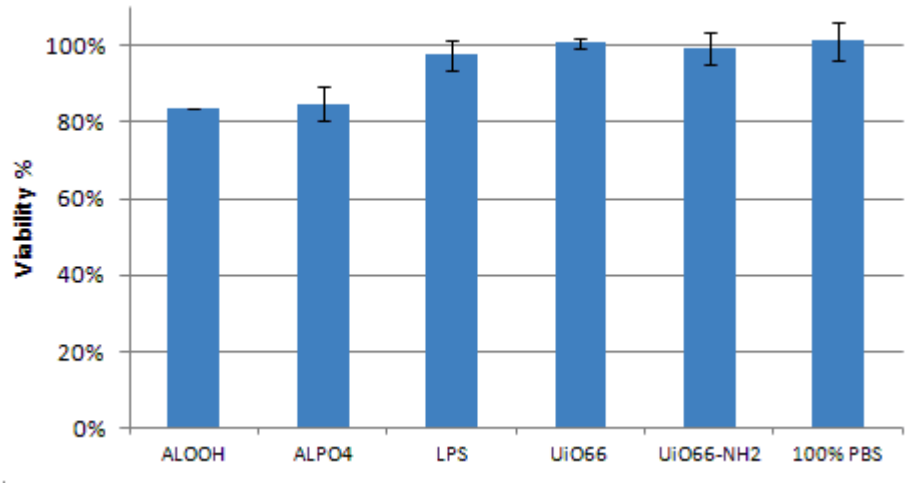

Figure 6-11 Viability of macrophages (THP-1 cells) after 24-hour stimulation with Zr-MOFs and alums AlOOH and ALPO4, measured by Alamar Blue assay. Error bars refer to SEM (standard error of mean), results from 2 independent experiments, each in duplicate.

The viability results show that the stimulation with Zr-MOFs did not compromise the cell viability, as opposed to the alum samples (AlO(OH) and $ALPO_4$), which decreased the number of live cells down to 84-85%. Control wells, stimulated with PBS solution or LPS (100 ng/ml) show that LPS decreases the viability slightly, PBS stimulation does not harm the cells. The results obtained, viability testing on dendritic cells and macrophages, show that Zr-MOF and Al-MOF, apart from MIL-101-NH_2, are non-toxic to the cells and could be potentially used as adjuvants. The obtained results show that generally MOFs do not compromise cells' viability. This property of MOFs combined with the data showing the induction of higher immune responses based on the levels of IL-6 and TNF-α cytokines and the expression of cell receptors on the dendritic cells responsible for the stimulation of T cells, suggests that MOFs might be strong candidates for novel adjuvants in vaccines. Recently, some attempts were made to synthesise biocompatible MOFs with lower toxicity, especially the ones containing Fe in their framework[30-32], the MOFs containing Cr and Co cations in their framework show the highest toxicity[33, 34], but still can be used as drug carriers for anti-cancer drugs as the latter are very toxic anyway.

6.4. Conclusions

The concept of providing a more potent adjuvant to replace alum was the foundation of this research project. It is strongly believed that Al (Aluminium) may be the key to triggering the immune responses[3], and with the new class of MOF materials allowing to play around with variety of their structures and linkers with an exact composition, showed a promising route to follow as MOFs are seen as potential candidates for variety of applications, with some in medicine[35-37]. There have been a lot of vaccines invented over the years for variety of diseases, with the idea to immunize the organism with the pathogen's subunit and induce specific immune response against it. Likewise, the idea that links the immune system with the cancer prevention emerged, and there were some trials made to design a vaccine for cervical cancer that led to Gardasil invention[38].

In this chapter, a series of Al- and Zr-containing MOFs were synthesised and their immunogencity explored in the *in vitro* studies. Experiments were performed to probe the maturation of macrophages and dendritic cells, looking at the levels of cytokines secreted by the macrophages and surface protein expression by the dendritic cells. The results show that MOFs containing Al-metal in their framework were more potent in provoking cytokine secretion than a commercially used alum or MOFs with a Zr-metal, and leading to increased concentrations of TNF-α and IL-6. The cell viability levels were also higher in the case of Al-MOFs, than those measured for alum, and it may be concluded that alum led to decreased viability. Upon stimulation with Al-MOFs, higher percentages of dendritic cells (DCs) expressed signal from CD40, CD86 and CD1a receptors and thus are expected to be able to activate T-cells more effectively than alum[39]. The results obtained with Zr-MOFs showed the levels of cytokines secreted were only slightly higher than these obtained after stimulation with alum. The viability studies showed that Zr-MOFs are non-toxic to the cells and the viability levels are sustained at nearly 100%.

Overall, the data collected indicated that Al-containing MOFs could be potent vaccine adjuvants. To prove this, further studies must be performed to link different parameters of the substances e.g. shape of grains, size of particles, zeta-potential, distances between Metal-carbon chemistry of the compounds to their

immunogenic properties. This would allow to build an adjuvant model and predict the potentially best match for an adjuvant. Such modelling was performed by Dr Williams showing promising results for LDH (layered double hydroxides) to link their chemistry to their performance as adjuvants[16]. The *in vivo* results were promising. However, in case of MOFs, in order to prove the model, some more *in vitro* studies are needed and ultimately some *in vivo*, also taking into consideration further MOF structures.

6.5. References

1. B. Pulendran, S. Li and H. I. Nakaya, *Immunity*, 2010, **33**, 516-529.
2. R. Medzhitov, *Immunity*, **30**, 766-775.
3. M. Kool, K. Fierens and B. N. Lambrecht, *Journal of Medical Microbiology*, 2012, **61**, 927-934.
4. C. A. Klebanoff, N. Acquavella, Z. Yu and N. P. Restifo, *Immunological reviews*, 2011, **239**, 27-44.
5. FDA, *Common Ingredients in U.S. Licensed Vaccines*, http://www.fda.gov/BiologicsBloodVaccines/SafetyAvailability/VaccineSafety/ucm187810.htm.
6. C. R. Alving, K. K. Peachman, M. Rao and S. G. Reed, *Current Opinion in Immunology*, 2012, **24**, 310-315.
7. J. M. Brewer, M. Conacher, A. Satoskar, H. Bluethmann and J. Alexander, *European Journal of Immunology*, 1996, **26**, 2062-2066.
8. K. Murphy, *Janeway's Immunology*, Garland Science, 2011.
9. V. E. J. C. Schijns and E. C. Lavelle, *Expert Review of Vaccines*, 2011, **10**, 539-550.
10. J. Banchereau and R. M. Steinman, *Nature*, 1998, **392**, 245-252.
11. M. Idzko, H. Hammad, M. van Nimwegen, M. Kool, M. A. M. Willart, F. Muskens, H. C. Hoogsteden, W. Luttmann, D. Ferrari, F. Di Virgilio, J. C. Virchow and B. N. Lambrecht, *Nat Med*, 2007, **13**, 913-919.
12. *Principles of Immunopharmacology*, 3rd edn., 2011.
13. S. Porcelli, M. B. Brenner, J. L. Greenstein, C. Terhorst, S. P. Balk and P. A. Bleicher, *Nature*, 1989, **341**, 447-450.
14. A. Chatzigeorgiou, M. Lyberi, G. Chatzilymperis, A. Nezos and E. Kamper, *BioFactors*, 2009, **35**, 474-483.
15. B. C. Hulette, C. A. Ryan, L. A. Gildea and G. F. Gerberick, *Toxicology and Applied Pharmacology*, 2005, **209**, 159-166.
16. G. R. Williams, K. Fierens, S. G. Preston, D. Lunn, O. Rysnik, S. De Prijck, M. Kool, H. C. Buckley, B. N. Lambrecht, D. O'Hare and J. M. Austyn, *The Journal of Experimental Medicine*, 2014, **211**, 1019-1025.

17. M. J. Katz, Z. J. Brown, Y. J. Colon, P. W. Siu, K. A. Scheidt, R. Q. Snurr, J. T. Hupp and O. K. Farha, *Chem. Commun.*, 2013, **49**, 9449-9451.
18. A. Schaate, P. Roy, A. Godt, J. Lippke, F. Waltz, M. Wiebcke and P. Behrens, *Chemistry – A European Journal*, 2011, **17**, 6643-6651.
19. T. Loiseau, C. Serre, C. Huguenard, G. Fink, F. Taulelle, M. Henry, T. Bataille and G. Férey, *Chemistry – A European Journal*, 2004, **10**, 1373-1382.
20. P. Serra-Crespo, E. V. Ramos-Fernandez, J. Gascon and F. Kapteijn, *Chemistry of Materials*, 2011, **23**, 2565-2572.
21. 0183
22. T. Loiseau, L. Lecroq, C. Volkringer, J. Marrot, G. Férey, M. Haouas, F. Taulelle, S. Bourrelly, P. L. Llewellyn and M. Latroche, *J Am Chem Soc*, 2006, **128**, 10223-10230.
23. C. Volkringer, T. Loiseau, M. Haouas, F. Taulelle, D. Popov, M. Burghammer, C. Riekel, C. Zlotea, F. Cuevas, M. Latroche, D. Phanon, C. Knöfelv, P. L. Llewellyn and G. Férey, *Chemistry of Materials*, 2009, **21**, 5783-5791.
24. C. Volkringer, T. Loiseau, N. Guillou, G. Férey and E. Elkaïm, *Solid State Sciences*, 2009, **11**, 1507-1512.
25. I. Senkovska, F. Hoffmann, M. Fröba, J. Getzschmann, W. Böhlmann and S. Kaskel, *Micropor Mesopor Mat*, 2009, **122**, 93-98.
26. S. Allan, *Nat Rev Immunol*, 2008, **8**, 320-320.
27. K. L. Honda, S. Lamon-Fava, N. R. Matthan, D. Wu and A. H. Lichtenstein, *Prostaglandins, Leukotrienes and Essential Fatty Acids (PLEFA)*, 2015, **97**, 27-34.
28. A. Macciò and C. Madeddu, *Cytokine*, 2012, **58**, 133-147.
29. J. van der Weijden, L. E. Paulis, M. Verdoes, J. C. M. van Hest and C. G. Figdor, *Chemical Science*, 2014, **5**, 3355-3367.
30. S. Rojas, E. Quartapelle-Procopio, F. J. Carmona, M. A. Romero, J. A. R. Navarro and E. Barea, *Journal of Materials Chemistry B*, 2014, **2**, 2473-2477.

31. S. R. Miller, D. Heurtaux, T. Baati, P. Horcajada, J.-M. Greneche and C. Serre, *Chem. Commun.*, 2010, **46**, 4526-4528.
32. A. C. McKinlay, R. E. Morris, P. Horcajada, G. Ferey, R. Gref, P. Couvreur and C. Serre, *Angew Chem Int Ed Engl*, 2010, **49**, 6260-6266.
33. R. K. S. S. K. G. P. S. J. S. Duhan, Springer, 2014, pp. 190-191.
34. R. C. Huxford, J. Della Rocca and W. Lin, *Current Opinion in Chemical Biology*, 2010, **14**, 262-268.
35. S. Keskin and S. Kizilel, *Ind Eng Chem Res*, 2011, **50**, 1799-1812.
36. P. Horcajada, C. Serre, M. Vallet-Regí, M. Sebban, F. Taulelle and G. Férey, *Angewandte Chemie*, 2006, **118**, 5974-5978.
37. P. Horcajada, T. Chalati, C. Serre, B. Gillet, C. Sebrie, T. Baati, J. F. Eubank, D. Heurtaux, P. Clayette, C. Kreuz, J. S. Chang, Y. K. Hwang, V. Marsaud, P. N. Bories, L. Cynober, S. Gil, G. Ferey, P. Couvreur and R. Gref, *Nature Materials*, 2010, **9**, 172-178.
38. NHS, *HPV vaccine*, http://www.nhs.uk/conditions/vaccinations/pages/hpv-human-papillomavirus-vaccine.aspx.
39. T. L. Flach, G. Ng, A. Hari, M. D. Desrosiers, P. Zhang, S. M. Ward, M. E. Seamone, A. Vilaysane, A. D. Mucsi, Y. Fong, E. Prenner, C. C. Ling, J. Tschopp, D. A. Muruve, M. W. Amrein and Y. Shi, *Nat Med*, 2011, **17**, 479-487.

Chapter 7. MOFs as multifunctional drug delivery systems – nitric oxide release

7.1. Aims

This chapter explores the possibilities of utilizing MOFs as multifunctional drug delivery systems. MOFs were encapsulated with selected anti-cancer drugs: cisplatin or 5-FU, and engaging the open metal sites as well as available amine sites to serve as the capture point for NO absorption was investigated. In case of cisplatin treatment, anticancer therapy may lead to thrombosis[1-3] – the formation of blood clots that may cause hypoxia and in extreme cases tissue death, heart attacks and strokes. Entrapment of nitric oxide (NO) – known for its anti-thrombosis, anti-inflammatory and anti-bacterial effects[4-6] – in the cisplatin-loaded MOFs, could mitigate this risk. Previous studies have shown that NO can be stored and released on demand by the MOFs HKUST-1, CPO-27-Mg and CPO-27-Ni[7-9]. It must be mentioned that nitric oxide itself has also been reported to cause cancer cell death[10]. Thus, preparing MOFs loaded with cisplatin and NO should permit the production of dual-functionality systems mitigating the risk of thrombosis as well as maximising the anti-cancer efficacy, and when co-loaded with 5FU also maximising anti-cancer treatment results.

7.2. Nitric Oxide loading

7.2.1 MOFs encapsulated with 5FU or Cisplatin

All four MOFs: CPO-27 Mg CPO-27 Ni and UiO66 and UiO66-NH_2 loaded either with cisplatin or with 5FU were previously examined. Because MOFs have a strong affinity and high capacity for NO, the release experiments can take a very long time until the NO concentration drops below biologically active levels, time constraints meant, the experiments could only be done in duplicate. The amount of released NO from the MOF containing anticancer drug was compared against the amount in the pure MOF, which was also run in duplicate. The NO loading was performed using the procedure described in Chapter 3 of this thesis and was applied for all the samples tested.

7.2.2 Zr-MOF with a conjugated prodrug

The aim of this section was to investigate if the conjugation of the cisplatin prodrug to the amine group of UiO66NH_2 would affect the release of NO and the storage capacity for this gas.

7.3. Results

During the previous experiments with CPO-27 MOFs, it has been discovered that due to the presence of open metal sites in the structure, so-called "unsaturated metal sites", NO entrapment is possible as these sites are able to chemically retain NO and release it in a controllable way[5, 11]. To trigger this "on demand" process, a replacement of nitric oxide molecule by another is necessary. It is done by placing the MOF powder in an environment of a controlled moisture level so that the H_2O will compete with NO for the open metal site occupancy and as a result will trigger NO release[7, 8, 12]. UiO66 shows poor NO release, although its porosity is high as the structure lacks of NO binding sites. On the other hand, the presence of the cisplatin and fluorouracil in the pores of the material enhances the NO release. This indicates that the presence of the unsaturated sites like amine groups or nitrogen in the aliphatic chain is crucial when it comes to gas storage by chemisorptions and prolonged release. It might well be that concentration of NO in the pores is quite high initially, but is released too quickly for NO to be measured. For the targeted application, the property is not very useful. UiO66-NH_2 shows better results for NO release, due to the presence of the NH_2 group which can form the diazeniumdiolate group (NONOate)[13] in combination with the NO.

7.3.1 NO release: UiO66-NH_2 with a conjugated prodrug.

The release of NO was measured from the pure UiO66-NH_2 and with a conjugated cisplatin prodrug in order to check if the presence of a prodrug affected the release profile. The amounts of NO released are quite high and similar, this would prove that functionalisation of the amine group with a prodrug of cisplatin in amide-coupling reaction did not affect the ability of UiO66-NH_2 for NO storage and release. Conversely, UiO66, showed very poor ability to release NO over time. This shows the difference between two sorption processes, the

physisorbed NO in UiO66 versus chemisorbed in UiO66-NH_2. There are no anchor points in the big voids of the UiO66 material for NO, hence immediately after the vial was cracked NO was released very quickly and by the time the probe was introduced in the analyser the amounts were very low and the release was completed within 100 sec.

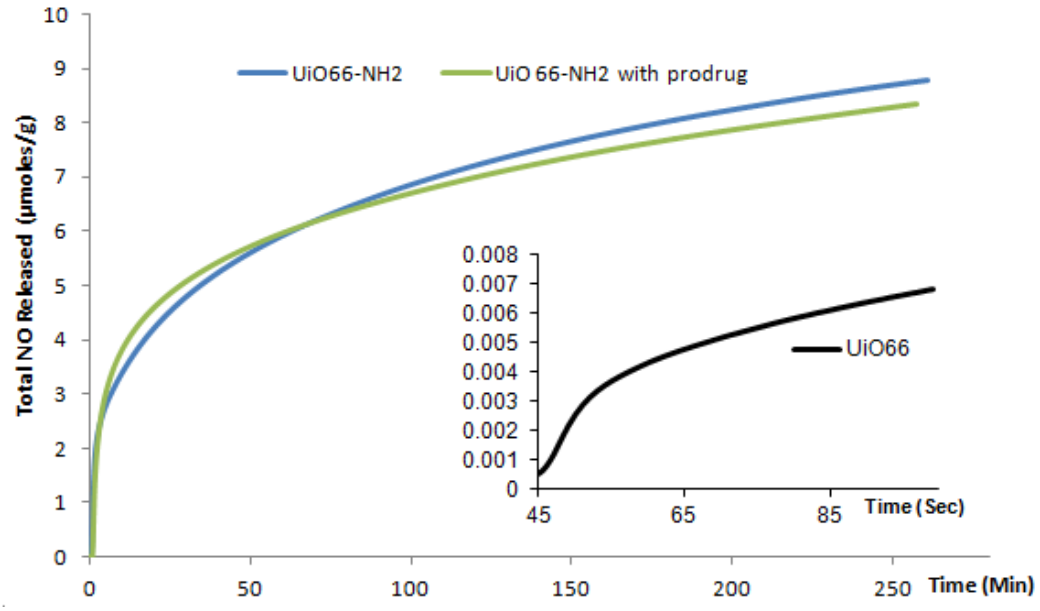

Figure 7-1 Total NO released monitored over time. Blue line indicates pure MOF UiO66-NH_2 whereas green the same MOF with conjugated prodrug. In the inset, there is a depiction of a NO release profile registered for UiO66. The vertical axis has same units as the main Y axis.

The plot above shows registered total NO release, it is worth noting that the conjugation did not influence the amount of NO that is released which can serve as a proof for a successful double functionalisation of the drug carrier. The Table 7-1 below shows the Total quantities of NO that were measured to be released by Zr-MOFs.

MOF	UiO66-NH_2 pure	UiO66-NH_2-conjugated	UiO66 pure
Total NO release [µmoles]	13.2 ± 3.22	7.69 ± 0.43	0.01 ± 0.0019

Table 7-1 Total NO released by different Zr-MOFs containing in the ring a conjugated prodrug, amine group or no functional group at all.

The difference between the amount of the released NO from UiO66-NH_2 in a pure or in its conjugated form does not vary a lot. The monitoring for NO release was carried out up until the moment NO concentration detected by analyser was

20 ppb (cut – off point). The concentration at that level is still biologically active and stays active down to the values of ca. 2-3 ppb. However, as the NO release measurements are a time consuming process taking a long time to achieve the NO parts drop down to that concentration, the cut-off was set to be 20 ppb. This way, it was still possible to compare obtained results.

It has been stipulated that the elevated concentration of NO in tumours makes them more susceptible to therapies (radio and chemo) and what is more, be able to induce apoptotic death in cancer cells[4, 14]. Recent studies performed on lung fibroblast cells investigated the relation between NO concentration and cisplatin cytotoxicity, concluding that NO enhances the action of the latter on the tumour cells[15].

7.3.2 NO release from Mg-MOFs encapsulated with cisplatin and fluorouracil drugs.

The two drugs were chosen to be encapsulated in the CPO-27 Mg-MOF carriers as they are both used in anti-cancer treatments, however, both have some shortcomings. The multifunctional carrier action was identified as interesting for investigations and some attempts were made to load the MOFs, previously encapsulated with drugs, with nitric oxide (NO). CPO-27 Mg, has been known for its ability to entrap NO and to allow for a controlled release[16] that is triggered by the H_2O molecules that are contained in the moisture saturated nitrogen /air flow. The plot below shows the result of the release experiment.

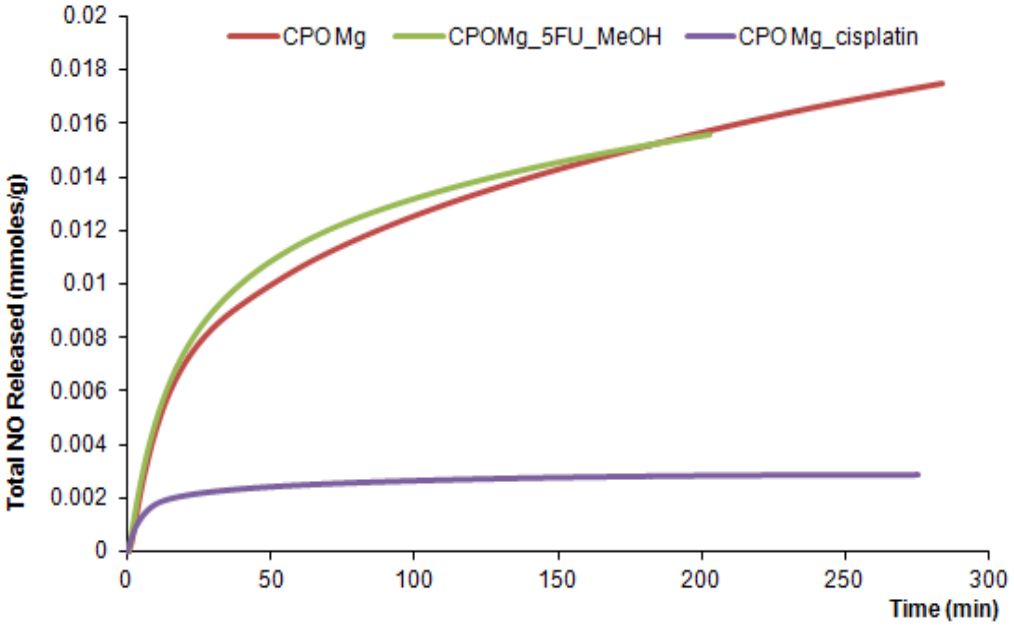

Figure 7-2 Total NO released from CPO-27 Mg MOF, pure (red), encapsulated with fluorouracil in Methanol (green) and encapsulated with cisplatin (purple).

Results show that the encapsulation with 5-FU of the pores of CPO-27 Mg in methanol solution, does not compromise the ability of the MOF to entrap NO on its open metal sites, and the capacity for NO loading remains at the same level as it seems 5-FU does not block the open metal sites. This may be elucidated with the presence of N-groups in the 5-FU drug that have a potential to (2 unpaired electrons) chemically bind NO and hence prolong its release. The quantity of the drug in the pores of MOF structure was not very high, please refer to Chapter 5. Another explanation for this, would be that 5-FU is not migrating into the pores of material and stays at the surface which allows for binding of NO to metal open sites. The other route for encapsulation was investigated, utilising 50/50 v/v solution of formic acid and methanol in which 5-FU was diluted reaching 80% of saturation. CPO-27 Mg structure was not fully intact, showing some evidence of damage, the total released NO was measured to be 0.21 μmol/g. The value for CPO-27 Mg encapsulated with cisplatin was 2.05 μmol/g, and 13.5 μmol/g for the amount of NO being released from CPO-27 Mg encapsulated with 5-FU in methanol and for the pure MOF it was measured to be 16.7 μmol/g. The presence of cisplatin in the pores dramatically decreased the release of nitric oxide, it might be due to the fact that two amine groups on cisplatin block the open metal sites

and this mechanism makes them unavailable to NO entrapment, reducing the release of the gas 8 x when compared to the release that is achieved with the pure MOF.

7.3.3. NO release from Ni-MOFs encapsulated with cisplatin and fluorouracil drugs.

CPO-27 Ni proved to be one of the MOFs with very high NO release which is triggered upon exposure to moisture reaching the delivery of ca. 7 mmol/g of material[8]. This feature would make it a good candidate for a multifunctional carrier as the results in Chapter 4 showed its high capacity and ability for cisplatin release. Below, in the Figure 7-3, the total NO release from CPO-27 Ni is depicted. Extraordinary behaviour of CPO-27 Ni to entrap nitric oxide for its prolonged release is partially compromised by the presence of 5-FU drug in the pores of the material, this is further impaired when cisplatin is encapsulated, similar as in case of CPO-27 Mg.

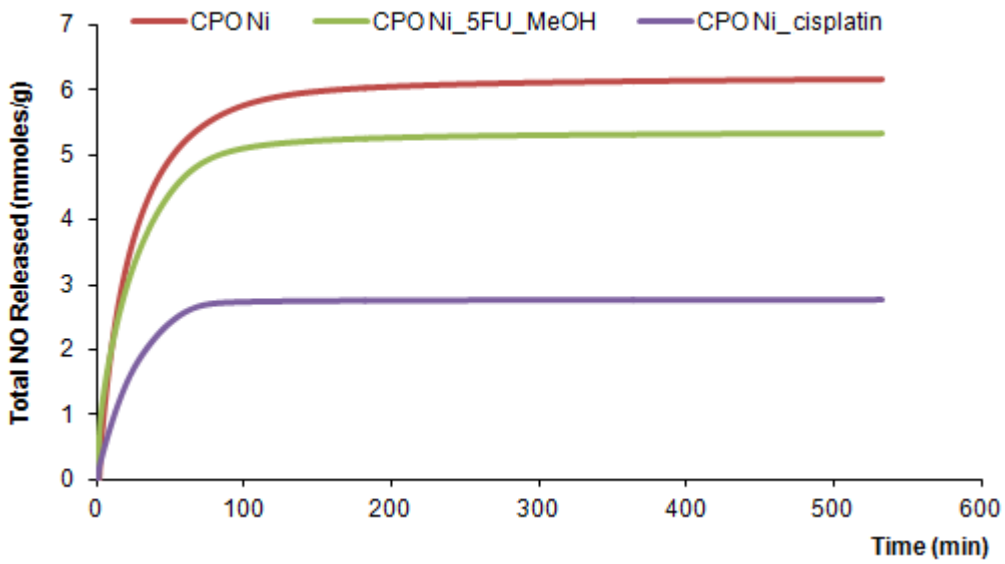

Figure 7-3 Total NO released from CPO-27 Ni MOF, pure (red), encapsulated with fluorouracil in Methanol (green) and encapsulated with cisplatin (purple).

The average release of nitric oxide from CPO-27 Ni was measured to be 6.09 ± 0.1 mmol/g, based on two samples. The average amount released from CPO-27 Ni with encapsulated 5-FU showed 5.15 ± 0.1 mmol/g, and with cisplatin only 2.61 ± 0.11 mmol/g. These amount, even though lower than in case of the pure MOF are still significant to provide desired level of NO concentration. The

mechanism behind this causing such a drop in the released amount of nitric oxide is similar that is observed for CPO-27 Mg and must be due to the interaction between amine groups of cisplatin and open metal sites of Ni in the MOF structure. It should be mentioned that such a nitric oxide cargo would still play its role in preventing thrombosis in patients under anti-cancer treatment.

7.3.4. NO release from Zr-MOFs encapsulated with cisplatin and fluorouracil drugs.

It was observed that encapsulating UiO66-NH_2 with cisplatin increases the amount of NO being released. This is due to the presence of additional amine groups on the cisplatin that can entrap NO.

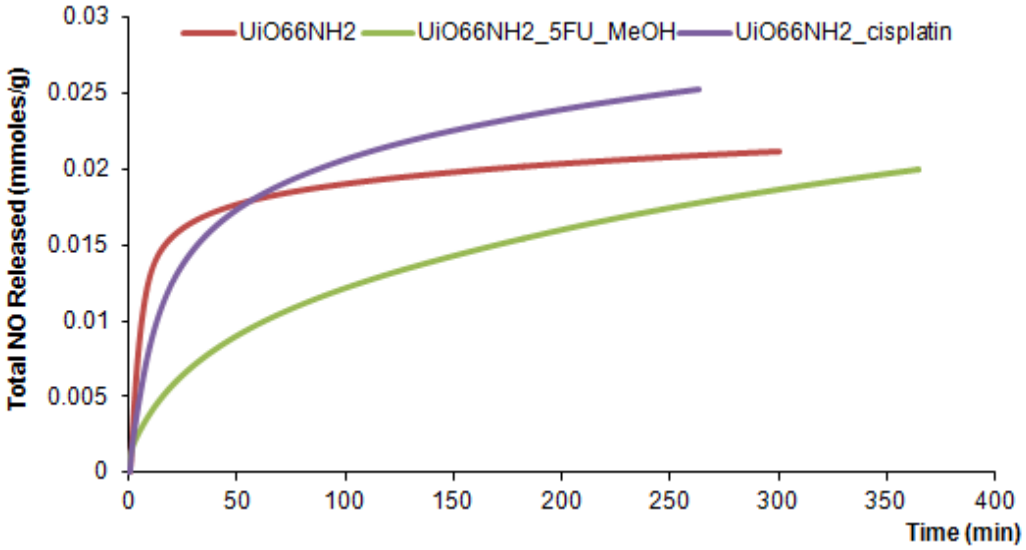

Figure 7-4 Total NO released from UiO66-NH_2, pure (red), encapsulated with 5FU in Methanol (green) and encapsulated with cisplatin (purple).

UiO66-NH_2 with encapsulated fluorouracil (5-FU) performs slightly worse than the pure MOF and the MOF encapsulated with cisplatin. This may be due to the interaction between amine groups on the functionalised organic linker of the MOF and the 5-FU molecule. The measured released quantity (cut-off concentration for NO at 20 ppm) was 13.2±3.2 μmol/g and for encapsulated cisplatin this was 22.7±1.45 μmol/g and finally for MOF with encapsulated 5-FU was 11.8±1.5 μmol/g, see Figure 7-4. The experiment that aimed at achieving higher loading of 5-FU in the MOF with encapsulation in a solution of 50/50 v/v MeOH and Formic acid, resulted in obtaining a MOF sample with NO release to be 1.88±0.04 μmol/g. This low result obtained for NO release can be elucidated by the fact of

partial MOF structure collapse during the encapsulation, or affecting the amine groups on the linker that were not able to support the NO entrapment.

UiO66 ability to retain and then release NO is rather poor, and this can be explained by the fact that there are no open sites for NO to form a bond. The MOF with encapsulated 5-FU shows almost the same results for NO release as the quantity of 5-FU in the pores is low. This is then dramatically different if the encapsulation of 5-FU is done in 50/50 v/v solution MeOH/Formic acid saturated with fluorouracil. Here, the main vehicle for NO capturing is 5-FU itself. The amount of the released NO measured for UiO66 is 0.013 μmol/g and goes up to 0.45 μmol/g for UiO66 encapsulated with 5-FU in MeOH/Formic acid solution. This is a 400-fold increase. The NO release curves are depicted in Figure 7-5.

The evidence shows that cisplatin increases release of NO in UiO66 but not in CPO-27, we can thus conclude that open metal sites play an important role in the NO storage and release mechanism. We can conclude that by introducing cisplatin in the pores of the MOF material without any open metal sites, the NO release will be enhanced when compared with the pure MOF e.g. UiO66.

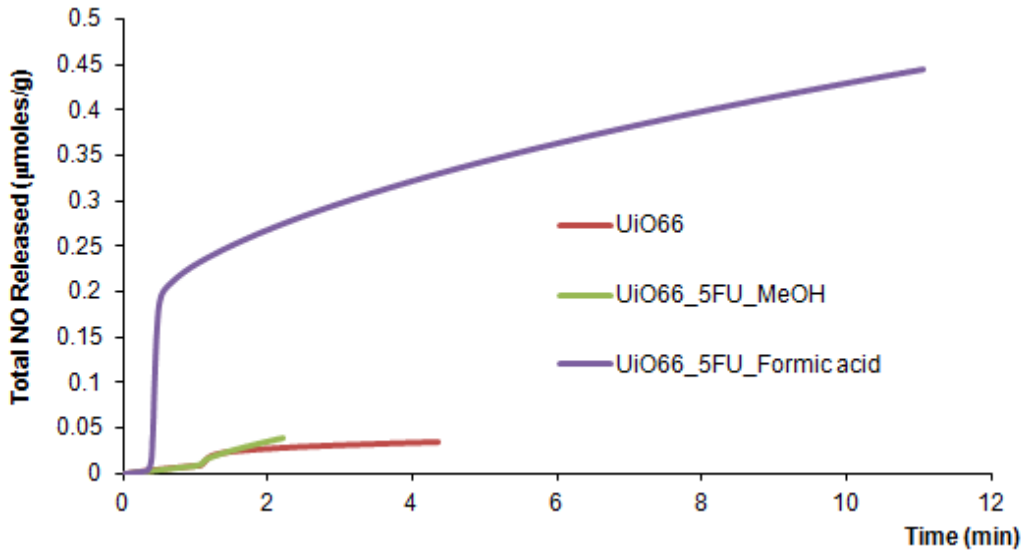

Figure 7-5 Total NO released from UiO66, pure (red), encapsulated with 5FU in MeOH (green) and encapsulated with 5FU in 50/50 v/v MeOH/Formic A. (purple).

For clarity, as the amount of NO released from UiO66 encapsulated with cisplatin was measured to be much higher than from the unloaded MOF, this is depicted on the separate plot, see Figure 7-6. Again, the reason behind is assigned to the

presence of cisplatin in the pores of the material and the interaction between NO and amine groups of cisplatin. The amount of nitric oxide measured was 16.5±4.2 μmol/g which is almost as high as the results obtained for UiO66-NH_2 encapsulated with cisplatin and can be attributed to the presence of cisplatin.

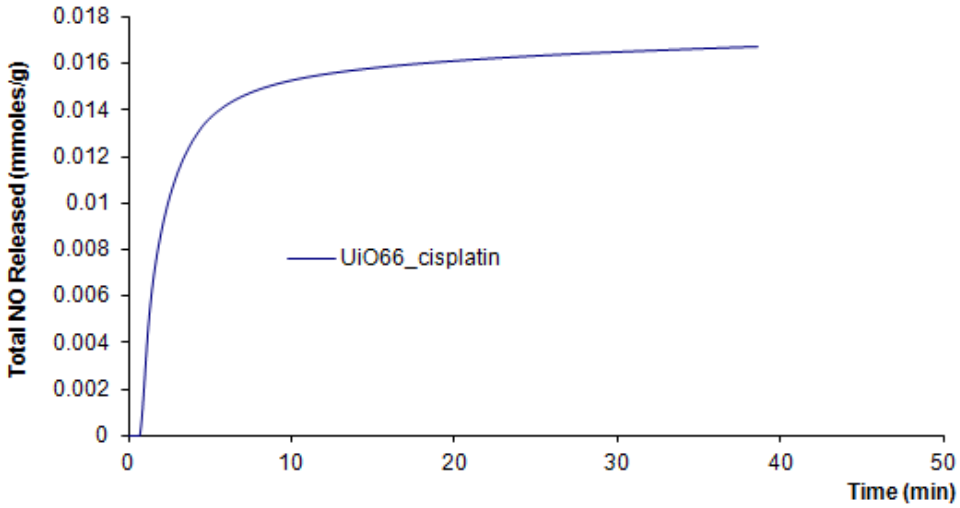

Figure 7-6 Total NO released from UiO66 Zr MOF, encapsulated with cisplatin.

This result shows that not only the MOF should necessarily show the ability to entrap NO but also there is a possibility for increased NO uptake if the encapsulated drug will have open sites.

7.4. Conclusions

The performed experiments were to investigate the possibilities for co-entrapment of two therapeutic agents, an anti-cancer drug and nitric oxide to capitalize on anti-tumor properties and to utilize NO anti- thrombotic properties. Thrombosis can be a threat during anti-cancer therapies offered to the patients. The results show that CPO-27 Ni has the superior properties when it comes to entrapping NO and then releasing it on demand. Ni in the MOF, however, is toxic and may be questioned for its choice. All of the anti cancer drugs and therapies, however, are far more toxic than Ni, and as such CPO-27 Ni application as a drug delivery system for cisplatin and 5-FU with the entrapped nitric oxide can be justified. CPO-27 Mg performs worse than CPO-27 Ni in terms of its entrapment ability for nitric oxide, but on the other hand, its toxicity is very low. Still, CPO-27 Mg loaded with cisplatin seems to release less nitric oxide, which is due to the fact

that the open metal sites were occupied by the electron pair from the amine group coming from cisplatin blocking it to accessible by nitric oxide. This is also the mechanism for CPO-27 Ni. UiO66, when encapsulated with cisplatin shows a pronounced surge in the amount of a released nitric oxide thanks to its interaction with amine groups on the anti-cancer drug. When unloaded, UiO66 ability to retain the gas in its structure was negligible. The quantities of cisplatin that could be stored and then released leading to the decreased viability of the cancer cells were quite substantial. This would make UiO66 the best candidate for the multifunctional drug delivery systems. As for UiO66-NH_2, the nitric oxide uptake is still the same for the MOF with a conjugated prodrug, where cytotoxicity can be switched on demand when in the proximity of tumour environment. The conjugated moiety did not completely block the amine group interaction but also offered the amine groups on the prodrug to compensate for the amine groups on the linker engaged in the peptide bond and hence inactive for nitric oxide capturing. The unloaded MOF has the ability to entrap nitric oxide, to contrary to its non-functionalised form UiO66 thanks to the amine groups able to interact with nitrogen of nitric oxide.

To conclude, MOFs with big pores and cages could make excellent drug delivery systems for anti-cancer drugs as they can be host drug molecules. The nitric oxide loading of these MOFs, which do not necessary offer metal open sites, can be increased and optimized by encapsulation of drugs that could offer open sites for nitric oxide to bind to and then be released in a controlled process. This can be observed for cisplatin-loaded UiO66, in which the released amount of nitric oxide measured is 16.5 μmol/g and is by far 1000 times higher than for the unloaded MOF.

7.5. References

1. T. Proverbs-Singh, S. K. Chiu, Z. Liu, S. Seng, G. Sonpavde, T. K. Choueiri, C.-K. Tsao, M. Yu, N. M. Hahn, W. K. Oh and M. D. Galsky, *Journal of the National Cancer Institute*, 2012.
2. M. Jafri and A. Protheroe, *Anti-Cancer Drugs*, 2008, **19**, 927-929.
3. D. D. Fernandes, M. L. Louzada, C. A. Souza and F. Matzinger, *Current Oncology*, 2011, **18**, 97-100.
4. S. Huerta, S. Chilka and B. Bonavida, *International Journal of Oncology*, 2008, **33**, 909-927.
5. N. J. Hinks, A. C. McKinlay, B. Xiao, P. S. Wheatley and R. E. Morris, *Micropor Mesopor Mat*, 2010, **129**, 330-334.
6. A. C. McKinlay, R. E. Morris, P. Horcajada, G. Ferey, R. Gref, P. Couvreur and C. Serre, *Angew Chem Int Ed Engl*, 2010, **49**, 6260-6266.
7. F. Bonino, S. Chavan, J. G. Vitillo, E. Groppo, G. Agostini, C. Lamberti, P. D. C. Dietzel, C. Prestipino and S. Bordiga, *Chemistry of Materials*, 2008, **20**, 4957-4968.
8. A. C. McKinlay, B. Xiao, D. S. Wragg, P. S. Wheatley, I. L. Megson and R. E. Morris, *J Am Chem Soc*, 2008, **130**, 10440-10444.
9. E. Garrone, B. Fubini, E. Escalona Platero and A. Zecchina, *Langmuir*, 1989, **5**, 240-245.
10. S. Duan, S. Cai, Q. Yang and M. L. Forrest, *Biomaterials*, 2012, **33**, 3243-3253.
11. A. C. McKinlay, Chemistry, University of St Andrews, Thesis, 2010.
12. A. C. McKinlay, J. F. Eubank, S. Wuttke, B. Xiao, P. S. Wheatley, P. Bazin, J. C. Lavalley, M. Daturi, A. Vimont, G. De Weireld, P. Horcajada, C. Serre and R. E. Morris, *Chemistry of Materials*, 2013, **25**, 1592-1599.
13. A. Lowe, P. Chittajallu, Q. Gong, J. Li and K. J. Balkus Jr, *Micropor Mesopor Mat*, 2013, **181**, 17-22.
14. D. Hirst and T. Robson, *Curr. Pharm. Des.* , 2010, **16**, 411-420.
15. D. A. Wink, J. A. Cook, D. Christodoulou, M. C. Krishna, R. Pacelli and S. Kim, *Nitric Oxide*, 1997, **1**, 88-94.

16. P. Horcajada, R. Gref, T. Baati, P. K. Allan, G. Maurin, P. Couvreur, G. Ferey, R. E. Morris and C. Serre, *Chem Rev*, 2012, **112**, 1232-1268.

Chapter 8. Further Work

The research depicted in this thesis covers a wide spectrum of potential biological applications where metal organic frameworks could be successfully implemented. This includes the investigation of possible MOF applications in medicine as drug delivery systems for two anti-cancer drugs: cisplatin and fluorouracil as well as new adjuvants for novel vaccines. It is worth noting that many aspects of chemistry and biochemistry have been addressed ranging from material synthesis, characterisation to immune response testing and conducting the viability studies in order to assess chosen MOFs in terms of their efficiency.

Not every aspect could have been addressed in this thesis due to the time constraints as well as the wide variety of MOF structures available and thus there is a potential for continuation of the work described.

First of all, for cisplatin encapsulation, some other MOFs with huge pores and ideally without unsaturated metal sites, as it has been observed that this feature prevents the cisplatin cargo from being released with the drug remaining trapped in the pores. The other MOFs could be tested for their loading and release of cisplatin e.g. MIL-125[1]. The interesting idea recently being researched is to encapsulate cisplatin in a protein called ferritin in one of the nanocages as it is biocompatible and capable of cisplatin delivery to targeted sites[2]. As a potential candidate for prodrug conjugation platform MIL-53-NH_2, MIL-101-NH_2 and MIL-125-NH_2 could be good candidates due to their availability of amine group in the structure. Also, in order to double the amount of cargo, a synthesis of a MOF structure with 2,5-diaminoterephthalic acid as a linker would be suitable, e.g. UiO66-$(NH_2)_2$[3]. Once the prodrug of cisplatin will be incorporated in the MOF structure, it might be used for co-encapsulation of 5-Fluorouracil, creating a multifunctional drug delivery system. Cisplatin prodrug would not take up the space in the material voids, anchored to the amine functional groups and allowing for such a double co-encapsulation.

The cytotoxicity tests to assess the efficacy of the prepared formulations, were only performed on A549 lung cancer cells, and THP-1 human leukaemia and author's wish would be to perform some more tests on HeLa cell line (cervical

cancer cells) for cisplatin and colorectal cancer e.g. HCA-7 Colony 29 for 5-Fluorouracil.

Some other drugs like heparin could be loaded in the MOF structure, ideally in the MOF with unsaturated metal sites to allow for a nitric oxide co-loading to top up the potential release of antithrombotic cargo available. The MOF/heparin/NO formulation could be used as a patch offered to women on birth control pills as it is commonly known that it poses a higher risk of platelets clotting that may lead to heart attack, especially for those who smoke. The risk of arterial thrombosis was 1.6 times higher for women on oral contraceptive pill when compared to those not using this form of birth control[4].

In case of Fluorouracil encapsulation, the further investigation may follow to optimise the encapsulation route, which would require a set-up of other encapsulation system, different to the one used in this thesis (MeOH or MeOH/formic acid) that would increase 5-FU solubility without compromising the MOF structure during encapsulation. Other MOFs as candidates for these encapsulation routes should be tested, e.g. MIL materials used for ibuprofen loading – MIL-53-Fe with ca. 20% wt, and MIL-101-Fe with ca. 1.4 g ibuprofen/g of material released after 6 days, or MIL-88 with its impressive pore sizes of 6 to 16 Å and showing a breathing effect of 85-230% in volume[5].

New routes are being followed to investigate other options for drug delivery systems, just to name a few: electrospun - nanofibers obtained in an electrospinning process[6] containing 5-Fluorouracil[7] or 3D printing for personalised medicine[8], or different proteins and antibodies[9]. With the amount of research conducted into various potential drug delivery systems, MOFs may not be seen as the first league candidates due to the fact that there is an issue with biocompatibility and excretion from the human body.

From the perspective of this thesis, the most hopes still lie in taking further steps to explore the efficiency of MOFs as novel adjuvants, as this area has never been researched before and for the first time it has been disclosed in this thesis. Metal oxides[10, 11] and double layered hydroxides (LDHs)[12] proved to have a potential to outperform alum in their ability to stimulate cells to secrete elevated concentration of cytokines. It is worth mentioning that still little is known about the mechanism

behind the immunisation by adjuvants and it is not yet fully understood[13], hence researchers perform screening of many materials for their immune response inducing properties without knowing what triggers this mechanism.

In the group of tested MOFs, some showed great potential in inducing the immune response, these were Al-containing MOFs. Hence, it is recommended to undertake some further studies *in vitro*, investigating the levels of other cytokines being secreted and also expression of the receptors on dendritic cells and finally a move towards *in vivo* testing should be made. Some other MOFs like CPO-27: Mg, Ni, Co and Zn were also qualified as potential candidates, and the tests are on-going but not in the scope of this thesis. The next steps would involve a set-up of some immuno-assays for MOFs having in their structure different metal ions and the same linker, and then performing the same experiment for MOFs with the same metal ion in the building unit, it was done in the case of Al, and different linkers. The data collection and analysis would allow for modelling of properties, which would lead to defining a model for a super-adjuvant.

This work however, would require a tandem of skills of an immunologist and a chemist in order to perform necessary synthesis, powder characterisation and investigation of biological properties – cytokines secretion, surface cell receptors and in vivo response and these involving a design of immuno-assays aided by FACS, ELISA, and also multiplex Luminex that allows to simultaneously detect and quantify the concentration of multiple cytokines in just one experiment, which is a great help to speed up the screening process. Author would see that help from a mathematician would also be necessary in order to run some computer simulations and build a model.

8.1. References

1. H. Guo, F. Lin, J. Chen, F. Li and W. Weng, *Applied Organometallic Chemistry*, 2015, **29**, 12-19.
2. N. Pontillo, F. Pane, L. Messori, A. Amoresano and A. Merlino, *Chem. Commun.*, 2016, **52**, 4136-4139.
3. M. J. Katz, Z. J. Brown, Y. J. Colon, P. W. Siu, K. A. Scheidt, R. Q. Snurr, J. T. Hupp and O. K. Farha, *Chem. Commun.*, 2013, **49**, 9449-9451.
4. R. E. J. Roach, F. M. Helmerhorst, W. M. Lijfering, T. Stijnen, A. Algra and O. M. Dekkers, *Cochrane Database of Systematic Reviews*, 2015.
5. P. Horcajada, C. Serre, G. Maurin, N. A. Ramsahye, F. Balas, M. Vallet-Regi, M. Sebban, F. Taulelle and G. Ferey, *J Am Chem Soc*, 2008, **130**, 6774-6780.
6. Y. J. Son, W. J. Kim and H. S. Yoo, *Archives of Pharmacal Research*, 2014, **37**, 69-78.
7. U. E. Illangakoon, D.-G. Yu, B. S. Ahmad, N. P. Chatterton and G. R. Williams, *International Journal of Pharmaceutics*, 2015, **495**, 895-902.
8. A. Goyanes, A. B. M. Buanz, G. B. Hatton, S. Gaisford and A. W. Basit, *European Journal of Pharmaceutics and Biopharmaceutics*, 2015, **89**, 157-162.
9. G. Y. Berguig, A. J. Convertine, S. Frayo, H. B. Kern, E. Procko, D. Roy, S. Srinivasan, D. H. Margineantu, G. Booth, M. C. Palanca-Wessels, D. Baker, D. Hockenbery, O. W. Press and P. S. Stayton, *Mol Ther*, 2015, **23**, 907-917.
10. R. Roy, S. Kumar, A. K. Verma, A. Sharma, B. P. Chaudhari, A. Tripathi, M. Das and P. D. Dwivedi, *International Immunology*, 2014, **26**, 159-172.
11. J. O. Naim, C. J. van Oss, W. Wu, R. F. Giese and P. A. Nickerson, *Vaccine*, 1997, **15**, 1183-1193.
12. G. R. Williams, K. Fierens, S. G. Preston, D. Lunn, O. Rysnik, S. De Prijck, M. Kool, H. C. Buckley, B. N. Lambrecht, D. O'Hare and J. M. Austyn, *The Journal of Experimental Medicine*, 2014, **211**, 1019-1025.
13. S. AWATE, L. A. Babiuk and G. Mutwiri, *Frontiers in Immunology*, 2013, **4**.

List of Abbreviations used in this Thesis

MOF	metal-organic frameworks
UiO66	Universitetet i Oslo (University of Oslo)
CPO	Coordination polymer of Oslo
5-FU	5-Fluorouracil
ELISA	enzyme-linked immunosorbent assay
PMA	phorbol myristate acetate
HRP	horseradish peroxidase
TMB	3,3′,5,5′-Tetramethylbenzidine
IL-6	interleukin 6 (cytokine)
TNF-α	tumor necrosis factor (cytokine)
NO	nitric oxide
XRD	X-ray diffraction
PXRD	powder X-ray diffraction
FTIR	Fourier Transform Infra red
NMR	Nuclear Magnetic Resonance
THF	Tetrahydrofuran
DMF	Dimethylformamide
BET	Brunauer, Emmett and Teller (surface area)
THP-1	cancer cell line human leukemia
A549	cancer cell line lung cancer
HPLC	High-pressure Liquid Chromatography

Appendix 1 ChekCELL cell refinement program

Refinements performed on MOF cells, that were used in the 5-Fluorouracil encapsulation in order to monitor the MOF "breathing effect": CPO Ni, CPO Mg, UiO66, UiO66-NH_2.

The conclusions derived from these cell refinements are described in Chapter 5.

CHEKCELL is a modified version of CELREF for analysing the solutions given by the CRYSFIREprogram. The cell parameters refinement program from powder diffraction diagram was used, which is not as powerful as GSAS, however allows for cell refinement. The program was developed at the Laboratoire des Matériaux et du Génie Physique Ecole Nationale Supérieure de Physique de Grenoble (INPG) Domaine Universitaire by Jean Laugier and Bernard Bochu.

The below results are the reports from the program with the refined parameters of the cell.

```
5-Fluorouracil in UiO66 (encapsulation v/v 50/50 Formic
acid/Methanol CELREF Version 3.  2/22/2016 6:13:32 PM
------------------------------------------------------------
-----------



Initial values    : (Refinement keys on 2nd line)
--------------    :
  Zero     Lambda       a        b        c       alpha  beta
gamma   volume
   0.000 1.54190    9.2200   12.6600   12.6700   89.70   43.90
98.60   1000.08
   0       0          1        1        1         1       1
1

    H       K       L       2Th(obs)  2Th_obs-shift  2Th(Calc)
diff.

    0    -1     1     13.3463       13.3463     13.4167     -
0.0704
    2     0      2      19.5757         19.5757      19.4773
0.0984
    0     1      2      20.6263         20.6263      20.5770
0.0493
    2     1     2     21.6851       21.6851     21.7758     -
```

```
0.0907
   -1      2      1      24.4027         24.4027      24.3178
0.0849
    1      2      3      25.8509         25.8509      25.7929
0.0580
   -1     3     1     27.9826       27.9826     28.0211     -
0.0385
    2      0      0      28.7143         28.7143      28.6356
0.0787
   -1     -2      1      29.7118         29.7118      29.6211
0.0907
    1    -3     3     32.7695       32.7695     32.7972     -
0.0277
   -2     2     1     36.6889       36.6889     36.7654     -
0.0765
    2     1     5     36.8779       36.8779     36.8898     -
0.0119
    3      3      4      39.7359         39.7359      39.7325
0.0034
    3    -3     5     41.6667       41.6667     41.6773     -
0.0106
    4     -2      2      44.5520         44.5520      44.5180
0.0340
    4      1      6      45.7554         45.7554      45.7207
0.0347
    3      3      1      46.8101         46.8101      46.7944
0.0157
   -1    -5     1     47.5812       47.5812     47.6173     -
0.0361
    5     -1      5      49.4351         49.4351      49.4305
0.0046

Sqrt(Sum(2Th O-C)**2)/(Nref-Npar)) : 0.0694
Sqrt(Sum(2Th O-C)**2)/Nref       ) : 0.0574

Final values      : (Standard errors on 2nd line)
------------
  Zero     Lambda       a        b        c       alpha  beta
gamma   volume
   0.000 1.54190    9.2170   12.6874   12.6627   89.74   43.87
98.67   1000.51
  0.0000 0.00000   0.0276   0.0318   0.0348   0.292  0.083
0.185    5.295


    H      K      L      2Th(obs)  2Th_obs-shift  2Th(Calc)
diff.

    0    -1     1     13.3463       13.3463     13.4201     -
```

```
0.0738
    2      0      2      19.5757         19.5757      19.4873
0.0884
    0      1      2      20.6263         20.6263      20.5960
0.0303
    2     1     2     21.6851        21.6851     21.7866     -
0.1015
   -1      2      1      24.4027         24.4027      24.3212
0.0815
    1      2      3      25.8509         25.8509      25.7979
0.0530
   -1     3     1     27.9826        27.9826     28.0019     -
0.0193
    2      0      0      28.7143         28.7143      28.6695
0.0448
   -1     -2      1      29.7118         29.7118      29.6381
0.0737
    1    -3     3     32.7695        32.7695     32.7795     -
0.0100
   -2     2     1     36.6889        36.6889     36.7923     -
0.1034
    2     1     5     36.8779        36.8779     36.9187     -
0.0408
    3      3      4      39.7359         39.7359      39.7344
0.0015
    3     -3      5      41.6667         41.6667      41.6561
0.0106
    4     -2      2      44.5520         44.5520      44.5360
0.0160
    4      1      6      45.7554         45.7554      45.7443
0.0111
    3     3     1     46.8101        46.8101     46.8211     -
0.0110
   -1    -5     1     47.5812        47.5812     47.5869     -
0.0057
    5    -1     5     49.4351        49.4351     49.4479     -
0.0128

Sqrt(Sum(2Th O-C)**2)/(Nref-Npar)) : 0.0650
Sqrt(Sum(2Th O-C)**2)/Nref       ) : 0.0538

CELREF Version 3.  2/22/2016 5:34:55 PM
------------------------------------------------------------
-----------

CPO Mg MeOH peaks omitted 5FU.dif

Initial values    : (Refinement keys on 2nd line)
--------------    :
```

Zero	Lambda	a	b	c	alpha	beta	gamma	volume
0.000	1.54190	25.9997	25.9997	6.7597	90.00	90.00	120.00	3957.26
0	0	1	0	1	0	0	0	

H	K	L	2Th(obs)	2Th_obs-shift	2Th(Calc)	diff.
1	1	0	6.6070	6.6070	6.7998	-0.1928
3	0	0	11.6520	11.6520	11.7915	-0.1395
1	0	1	13.6740	13.6740	13.6780	-0.0040
0	2	1	15.0890	15.0890	15.2894	-0.2004
2	1	1	16.6520	16.6520	16.7499	-0.0979
1	3	1	19.1960	19.1960	19.3514	-0.1554
3	3	0	20.3570	20.3570	20.4965	-0.1395
3	2	1	21.3840	21.3840	21.6530	-0.2690
5	2	0	24.5090	24.5090	24.6933	-0.1843
1	2	2	28.1700	28.1700	28.4147	-0.2447
7	1	0	29.6880	29.6880	29.9624	-0.2744
7	1	0	29.8210	29.8210	29.9624	-0.1414
5	4	1	33.7500	33.7500	33.8026	-0.0526
9	0	0	35.7140	35.7140	35.8962	-0.1822
8	2	0	36.3390	36.3390	36.5780	-0.2390
0	0	3	39.8660	39.8660	40.0162	-0.1502
6	5	1	40.4460	40.4460	40.4812	-0.0352
6	6	0	41.6520	41.6520	41.6883	-0.0363
5	7	1	43.7950	43.7950	44.0763	-0.2813

```
Sqrt(Sum(2Th O-C)**2)/(Nref-Npar)) : 0.1892
Sqrt(Sum(2Th O-C)**2)/Nref       ) : 0.1790

Final values      : (Standard errors on 2nd line)
------------
  Zero     Lambda       a        b        c       alpha  beta
gamma   volume
   0.000 1.54190   26.1296   26.1296    6.7966   90.00   90.00
120.00   4018.73
  0.0000 0.00000    0.0359    0.0000    0.0042    0.000  0.000
0.000    6.058


    H       K       L       2Th(obs)  2Th_obs-shift  2Th(Calc)
diff.

    1     1     0      6.6070        6.6070      6.7660     -
0.1590
    3     0     0     11.6520       11.6520     11.7327     -
0.0807
    1      0      1      13.6740         13.6740      13.6038
0.0702
    0     2     1     15.0890       15.0890     15.2077     -
0.1187
    2     1     1     16.6520       16.6520     16.6612     -
0.0092
    1     3     1     19.1960       19.1960     19.2502     -
0.0542
    3     3     0     20.3570       20.3570     20.3935     -
0.0365
    3     2     1     21.3840       21.3840     21.5403     -
0.1563
    5     2     0     24.5090       24.5090     24.5686     -
0.0596
    1     2     2     28.1700       28.1700     28.2589     -
0.0889
    7     1     0     29.6880       29.6880     29.8101     -
0.1221
    7      1      0      29.8210         29.8210      29.8101
0.0109
    5      4      1      33.7500         33.7500      33.6271
0.1229
    9      0      0      35.7140         35.7140      35.7118
0.0022
    8     2     0     36.3390       36.3390     36.3898     -
0.0508
    0      0      3      39.8660         39.8660      39.7895
0.0765
    6      5      1      40.4460         40.4460      40.2692
```

```
0.1768
    6      6      0      41.6520         41.6520      41.4715
0.1805
    5      7      1      43.7950         43.7950      43.8438      -
0.0488

Sqrt(Sum(2Th O-C)**2)/(Nref-Npar)) : 0.1073
Sqrt(Sum(2Th O-C)**2)/Nref       ) : 0.1015

CELREF Version 3.  2/13/2016 12:26:05 PM
------------------------------------------------------------
-----------
CPO Mg encapsulated in Formic acid/MeOH with 5-FU


Initial values    : (Refinement keys on 2nd line)
--------------    :
  Zero     Lambda       a         b         c        alpha   beta
gamma    volume
   0.000 1.54190   25.9997   25.9997    6.7597   90.00   90.00
120.00   3957.26
   0       0          1         0         1         0       0
0

    H       K       L       2Th(obs)  2Th_obs-shift  2Th(Calc)
diff.

    1      3      1      18.7054         18.7054      19.3514      -
0.6460
    3      2      1      21.2946         21.2946      21.6530      -
0.3584
    1      2      2      28.3482         28.3482      28.4147      -
0.0665
    9      0      0      35.5357         35.5357      35.8962      -
0.3605

Sqrt(Sum(2Th O-C)**2)/(Nref-Npar)) : 0.5832
Sqrt(Sum(2Th O-C)**2)/Nref       ) : 0.4124

Final values      : (Standard errors on 2nd line)
------------
  Zero     Lambda       a         b         c        alpha   beta
gamma    volume
   0.000 1.54190   26.2902   26.2902    6.8214   90.00   90.00
120.00   4083.15
  0.0000 0.00000    0.2539    0.0000    0.0553    0.000   0.000
0.000    51.474
```

```
    H       K       L       2Th(obs)  2Th_obs-shift  2Th(Calc)
diff.

    1     3     1     18.7054       18.7054     19.1536     -
0.4482
    3     2     1     21.2946       21.2946     21.4270     -
0.1324
    1      2      2      28.3482         28.3482      28.1443
0.2039
    9      0      0      35.5357         35.5357      35.4862
0.0495

Sqrt(Sum(2Th O-C)**2)/(Nref-Npar)) : 0.3622
Sqrt(Sum(2Th O-C)**2)/Nref       ) : 0.2561

CELREF Version 3.  2/22/2016 5:06:57 PM
------------------------------------------------------------
-----------

CPO Ni encapsulation in Formic acid/MeOH with 5-FU

Initial values    : (Refinement keys on 2nd line)
--------------    :
  Zero     Lambda       a        b        c       alpha  beta
gamma   volume
   0.000 1.54190   25.9279   25.9279    6.6881   90.00   90.00
120.00   3893.75
   0       0          1         0         1         0       0
0

    H       K       L       2Th(obs)  2Th_obs-shift  2Th(Calc)
diff.

    1      1      0       6.8816          6.8816       6.8186
0.0630
    3      0      0      11.8766         11.8766      11.8242
0.0524
    2      2      0      13.7179         13.7179      13.6616
0.0563
    0      2      1      15.4925         15.4925      15.4219
0.0706
    2      1      1      16.9236         16.9236      16.8788
0.0448
    4      1      0      18.1153         18.1153      18.1050
0.0103
    1      3      1      19.5374         19.5374      19.4771
0.0603
    3      2      1      21.7841         21.7841      21.7779
0.0062
```

```
    0     5     1     23.8398       23.8398     23.8676     -
0.0278
    2      4      1      24.8576         24.8576      24.8502
0.0074
    5      1      1      25.8196         25.8196      25.7977
0.0219
    4      3      1      27.6024         27.6024      27.6016
0.0008
    1      2      2      28.7286         28.7286      28.6941
0.0345
    7      1      0      30.0520         30.0520      30.0474
0.0046
    6      2      1      31.7176         31.7176      31.6985
0.0191
    4     2     2     34.0606       34.0606     34.1385     -
0.0779
    1      5      2      34.8541         34.8541      34.8540
0.0001
    2     7     1     35.3250       35.3250     35.3672     -
0.0422
    4      6      1      37.4271         37.4271      37.4164
0.0107
    0      7      2      38.9210         38.9210      38.9065
0.0145
    4     5     2     41.4015       41.4015     41.4200     -
0.0185
    3     0     3     42.3006       42.3006     42.3023     -
0.0017
    7     2     2     42.6224       42.6224     42.6307     -
0.0083
    9     2     1     43.0421       43.0421     43.0647     -
0.0226
    1     8     2     43.7618       43.7618     43.8143     -
0.0525
    6     4     2     44.3946       44.3946     44.3966     -
0.0020
    2    10      1      47.1140         47.1140      47.0726
0.0414

Sqrt(Sum(2Th O-C)**2)/(Nref-Npar)) : 0.0385
Sqrt(Sum(2Th O-C)**2)/Nref       ) : 0.0371

Final values      : (Standard errors on 2nd line)
------------
  Zero     Lambda       a        b        c       alpha  beta
gamma   volume
   0.000 1.54190   25.9234   25.9234    6.6894   90.00   90.00
120.00   3893.16
  0.0000 0.00000    0.0157    0.0000    0.0009    0.000  0.000
```

0.000 2.423

H	K	L	2Th(obs)	2Th_obs-shift	2Th(Calc)	diff.
1	1	0	6.8816	6.8816	6.8198	0.0618
3	0	0	11.8766	11.8766	11.8263	0.0503
2	2	0	13.7179	13.7179	13.6640	0.0539
0	2	1	15.4925	15.4925	15.4203	0.0722
2	1	1	16.9236	16.9236	16.8779	0.0457
4	1	0	18.1153	18.1153	18.1082	0.0071
1	3	1	19.5374	19.5374	19.4771	0.0603
3	2	1	21.7841	21.7841	21.7787	0.0054
0	5	1	23.8398	23.8398	23.8691	-0.0293
2	4	1	24.8576	24.8576	24.8519	0.0057
5	1	1	25.8196	25.8196	25.7997	0.0199
4	3	1	27.6024	27.6024	27.6041	-0.0017
1	2	2	28.7286	28.7286	28.6898	0.0388
7	1	0	30.0520	30.0520	30.0527	-0.0007
6	2	1	31.7176	31.7176	31.7020	0.0156
4	2	2	34.0606	34.0606	34.1365	-0.0759
1	5	2	34.8541	34.8541	34.8524	0.0017
2	7	1	35.3250	35.3250	35.3716	-0.0466
4	6	1	37.4271	37.4271	37.4213	0.0058
0	7	2	38.9210	38.9210	38.9063	0.0147
4	5	2	41.4015	41.4015	41.4207	-0.0192
3	0	3	42.3006	42.3006	42.2949	

```
0.0057
    7     2     2     42.6224       42.6224     42.6318     -
0.0094
    9     2     1     43.0421       43.0421     43.0710     -
0.0289
    1     8     2     43.7618       43.7618     43.8158     -
0.0540
    6     4     2     44.3946       44.3946     44.3982     -
0.0036
    2    10     1     47.1140       47.1140     47.0798
0.0342

Sqrt(Sum(2Th O-C)**2)/(Nref-Npar)) : 0.0384
Sqrt(Sum(2Th O-C)**2)/Nref       ) : 0.0370

CELREF Version 3.  2/22/2016 5:20:16 PM
------------------------------------------------------------
-----------

CPO Ni encapsulated in MeOH with 5-FU, indexed omitted 5FU
peaks.lst

Initial values    : (Refinement keys on 2nd line)
--------------    :
  Zero     Lambda       a        b        c       alpha  beta
gamma   volume
   0.000 1.54190   25.9279   25.9279    6.6881   90.00   90.00
120.00   3893.75
   0       0          1         0         1         0       0
0

    H       K       L       2Th(obs)  2Th_obs-shift  2Th(Calc)
diff.

    1     1     0      6.5110        6.5110      6.8186     -
0.3076
    3     0     0     11.2550       11.2550     11.8242     -
0.5692
    0     2     1     15.0500       15.0500     15.4219     -
0.3719
    4     1     0     17.7730       17.7730     18.1050     -
0.3320
    1     3     1     19.1340       19.1340     19.4771     -
0.3431
    3     2     1     21.8570       21.8570     21.7779
0.0791
    2     4     1     24.5380       24.5380     24.8502     -
0.3122
    5     1     1     25.4460       25.4460     25.7977     -
```

```
0.3517
    1     2     2     28.2920       28.2920     28.6941     -
0.4021
    1     6     1     28.8290       28.8290     29.3029     -
0.4739
    7     1     0     29.4480       29.4480     30.0474     -
0.5994
    3      1      2      30.4380         30.4380      30.3393
0.0987
    3      1      2      30.4380         30.4380      30.3393
0.0987
    0      4      2      31.1390         31.1390      31.1323
0.0067
    5     5     0     34.2330       34.2330     34.5963     -
0.3633
    1     5     2     34.4390       34.4390     34.8540     -
0.4150
    8     2     0     36.4190       36.4190     36.6829     -
0.2639
    1     1     3     40.7100       40.7100     41.0837     -
0.3737
    6     6     0     41.6170       41.6170     41.8091     -
0.1921
    7     2     2     42.3180       42.3180     42.6307     -
0.3127
    9     2     1     42.9790       42.9790     43.0647     -
0.0857
    3     7     2     44.8760       44.8760     44.9729     -
0.0969
    3     3     3     45.7620       45.7620     45.8000     -
0.0380
    0    11     1     46.3950       46.3950     46.5166     -
0.1216
    7     7     0     49.1140       49.1140     49.2001     -
0.0861

Sqrt(Sum(2Th O-C)**2)/(Nref-Npar)) : 0.3274
Sqrt(Sum(2Th O-C)**2)/Nref       ) : 0.3141

Final values      : (Standard errors on 2nd line)
------------
  Zero     Lambda       a        b        c       alpha  beta
gamma   volume
   0.000 1.54190   26.1189   26.1189    6.7130   90.00   90.00
120.00   3966.03
  0.0000 0.00000    0.0858    0.0000    0.0042    0.000  0.000
0.000   13.264
```

H	K	L	2Th(obs)	2Th_obs-shift	2Th(Calc)	diff.
1	1	0	6.5110	6.5110	6.7687	-0.2577
3	0	0	11.2550	11.2550	11.7375	-0.4825
0	2	1	15.0500	15.0500	15.3497	-0.2997
4	1	0	17.7730	17.7730	17.9715	-0.1985
1	3	1	19.1340	19.1340	19.3662	-0.2322
3	2	1	21.8570	21.8570	21.6464	0.2106
2	4	1	24.5380	24.5380	24.6918	-0.1538
5	1	1	25.4460	25.4460	25.6311	-0.1851
1	2	2	28.2920	28.2920	28.5713	-0.2793
1	6	1	28.8290	28.8290	29.1064	-0.2774
7	1	0	29.4480	29.4480	29.8226	-0.3746
3	1	2	30.4380	30.4380	30.1991	0.2389
3	1	2	30.4380	30.4380	30.1991	0.2389
0	4	2	31.1390	31.1390	30.9838	0.1552
5	5	0	34.2330	34.2330	34.3354	-0.1024
1	5	2	34.4390	34.4390	34.6679	-0.2289
8	2	0	36.4190	36.4190	36.4052	0.0138
1	1	3	40.7100	40.7100	40.9201	-0.2101
6	6	0	41.6170	41.6170	41.4893	0.1277
7	2	2	42.3180	42.3180	42.3688	-0.0508
9	2	1	42.9790	42.9790	42.7504	0.2286
3	7	2	44.8760	44.8760	44.6883	0.1877
3	3	3	45.7620	45.7620	45.5839	0.1781

```
    0    11      1      46.3950         46.3950      46.1719
0.2231
    7     7      0      49.1140         49.1140      48.8168
0.2972

Sqrt(Sum(2Th O-C)**2)/(Nref-Npar)) : 0.2469
Sqrt(Sum(2Th O-C)**2)/Nref       ) : 0.2368

CELREF Version 3.  2/5/2016 3:27:49 PM
------------------------------------------------------------
-----------
UiO66 encapsulation in Formic acid/MeOH with 5-FU
indexed peaks UiO66 FA MeOH 5FU eliminated.lst

Initial values    : (Refinement keys on 2nd line)
--------------    :
  Zero     Lambda       a        b        c       alpha  beta
gamma   volume
   0.000 1.54190   20.7089   20.7089   20.7089   90.00   90.00
90.00   8881.19
   0       0          1         0         0         0       0
0

    H       K       L      2Th(obs)  2Th_obs-shift  2Th(Calc)
diff.

    0      0      4      17.4420         17.4420      17.1277
0.3143
    3     1     3     18.5750       18.5750     18.6777     -
0.1027
    2     2     4     20.8860       20.8860     21.0167     -
0.1307
    1      1      5      22.3820         22.3820      22.3075
0.0745
    1     3     5     25.2820       25.2820     25.4467     -
0.1647
    2     4     4     25.7800       25.7800     25.8138     -
0.0338
    3      3      5      28.3180         28.3180      28.2597
0.0583
    4     4     4     29.8140       29.8140     29.8937     -
0.0797
    7      3      3      35.5690         35.5690      35.4831
0.0859
    5      1      7      37.6530         37.6530      37.6167
0.0363
    2      6      6      38.0610         38.0610      37.8761
0.1849
    4      0      8      38.9680         38.9680      38.8991
```

```
0.0689
    6     4     6     40.7350       40.7350     40.8803     -
0.1453
    3     1     9     41.4600       41.4600     41.6031     -
0.1431
    6     6     6     45.4480       45.4480     45.5215     -
0.0735
    0      4     10      47.3510         47.3510      47.2761
0.0749
    4      2     10      48.2120         48.2120      48.1349
0.0771
    0     8     8     49.7990       49.7990     49.8190     -
0.0200

Sqrt(Sum(2Th O-C)**2)/(Nref-Npar)) : 0.1275
Sqrt(Sum(2Th O-C)**2)/Nref       ) : 0.1240

Final values      : (Standard errors on 2nd line)
------------
  Zero     Lambda       a        b        c       alpha  beta
gamma   volume
   0.000 1.54190   20.7156   20.7156   20.7156   90.00   90.00
90.00   8889.75
  0.0000 0.00000    0.0622    0.0000    0.0000    0.000  0.000
0.000   26.709

    H       K       L       2Th(obs)  2Th_obs-shift  2Th(Calc)
diff.

    0      0      4      17.4420         17.4420      17.1222
0.3198
    3     1     3     18.5750       18.5750     18.6716     -
0.0966
    2     2     4     20.8860       20.8860     21.0099     -
0.1239
    1      1      5      22.3820         22.3820      22.3002
0.0818
    1     3     5     25.2820       25.2820     25.4384     -
0.1564
    2     4     4     25.7800       25.7800     25.8054     -
0.0254
    3      3      5      28.3180         28.3180      28.2504
0.0676
    4     4     4     29.8140       29.8140     29.8839     -
0.0699
    7      3      3      35.5690         35.5690      35.4713
0.0977
    5      1      7      37.6530         37.6530      37.6042
0.0488
```

```
    2      6      6      38.0610         38.0610      37.8635
0.1975
    4      0      8      38.9680         38.9680      38.8861
0.0819
    6     4     6     40.7350        40.7350     40.8666     -
0.1316
    3     1     9     41.4600        41.4600     41.5891     -
0.1291
    6     6     6     45.4480        45.4480     45.5061     -
0.0581
    0      4     10      47.3510         47.3510      47.2600
0.0910
    4      2     10      48.2120         48.2120      48.1185
0.0935
    0     8     8     49.7990        49.7990     49.8019     -
0.0029

Sqrt(Sum(2Th O-C)**2)/(Nref-Npar)) : 0.1284
Sqrt(Sum(2Th O-C)**2)/Nref       ) : 0.1248

CELREF Version 3.  2/22/2016 5:47:08 PM
------------------------------------------------------------
UiO66 encapsulation in MeOH with 5-FU
peaks_uio66_MeOH_eliminated 5FU.lst

Initial values    : (Refinement keys on 2nd line)
--------------    :
  Zero     Lambda       a        b        c       alpha   beta
gamma   volume
   0.000 1.54190   20.7089   20.7089   20.7089   90.00   90.00
90.00   8881.19
   0       0          1         0         0         0       0
0

    H       K       L      2Th(obs)  2Th_obs-shift  2Th(Calc)
diff.

    0     0     2      8.2245         8.2245      8.5399     -
0.3154
    0     2     2     11.8297        11.8297     12.0885     -
0.2588
    2     2     2     14.5786        14.5786     14.8192     -
0.2406
    0     0     4     17.0572        17.0572     17.1277     -
0.0705
    3     1     3     18.3640        18.3640     18.6777     -
0.3137
    0     2     4     18.9949        18.9949     19.1674     -
0.1725
```

```
    1     3     5     25.3490       25.3490     25.4467     -
0.0977
    2     4     4     25.6645       25.6645     25.8138     -
0.1493
    2     4     6     32.1087       32.1087     32.3520     -
0.2433
    1      3      7      33.2804         33.2804      33.2317
0.0487
    6     0     6     36.5701       36.5701     36.8291     -
0.2590

Sqrt(Sum(2Th O-C)**2)/(Nref-Npar)) : 0.2276
Sqrt(Sum(2Th O-C)**2)/Nref       ) : 0.2170

Final values      : (Standard errors on 2nd line)
------------
  Zero     Lambda       a        b        c       alpha  beta
gamma   volume
   0.000 1.54190   20.8825   20.8825   20.8825   90.00   90.00
90.00   9106.44
  0.0000 0.00000   0.1552   0.0000   0.0000   0.000  0.000
0.000   67.686

    H       K       L       2Th(obs)  2Th_obs-shift  2Th(Calc)
diff.
    0     0     2      8.2245        8.2245      8.4688     -
0.2443
    0     2     2     11.8297       11.8297     11.9876     -
0.1579
    2     2     2     14.5786       14.5786     14.6953     -
0.1167
    0      0      4      17.0572         17.0572      16.9843
0.0729
    3     1     3     18.3640       18.3640     18.5210     -
0.1570
    0     2     4     18.9949       18.9949     19.0066     -
0.0117
    1      3      5      25.3490         25.3490      25.2316
0.1174
    2      4      4      25.6645         25.6645      25.5955
0.0690
    2      4      6      32.1087         32.1087      32.0757
0.0330
    1      3      7      33.2804         33.2804      32.9475
0.3329
    6      0      6      36.5701         36.5701      36.5120
0.0581
Sqrt(Sum(2Th O-C)**2)/(Nref-Npar)) : 0.1619
Sqrt(Sum(2Th O-C)**2)/Nref       ) : 0.1544
```

Appendix 2 X-ray pattern of 5-Fluorouracil/Chapter 5

X-ray diffraction pattern of 5-FU, generated from the CIF file, Crystal maker.

{Hulme et al., JACS, 2005, 127, 1116}

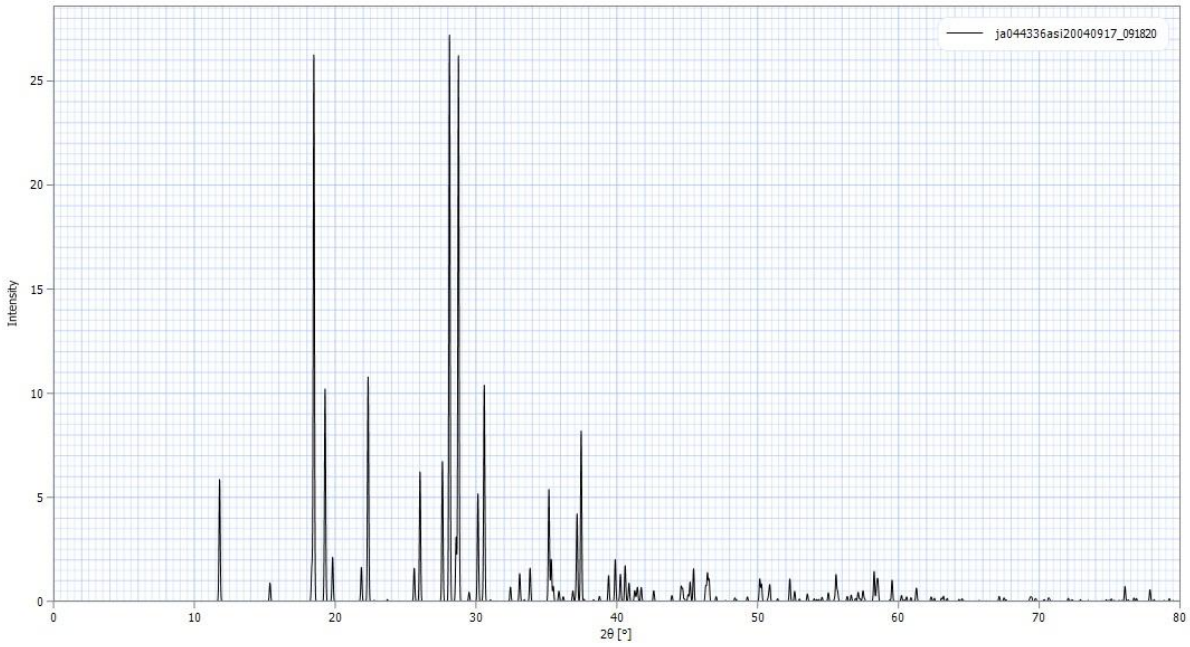

Appendix 3 X-ray patterns of Al-MOFs/Adjuvants/Chapter 6

X-ray diffraction patterns of the Al-MOFs that were synthesised for the Adjuvant project.

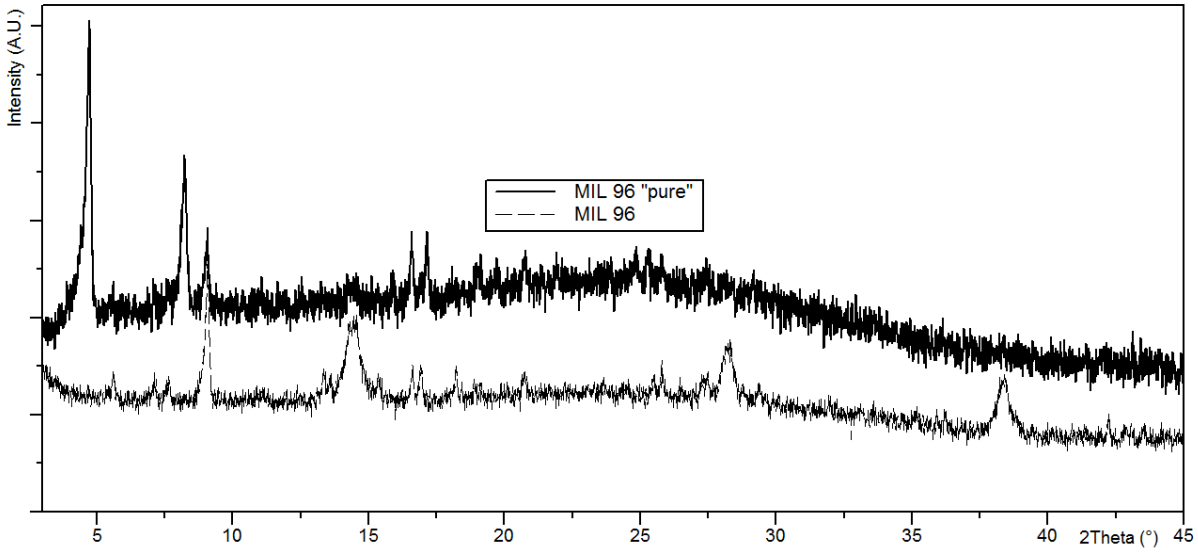

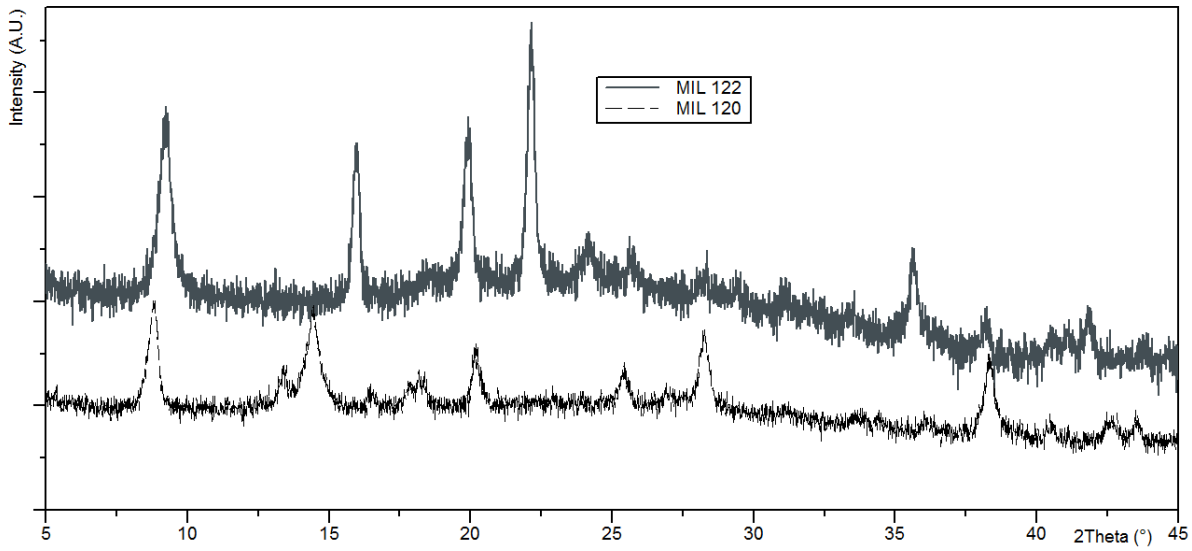

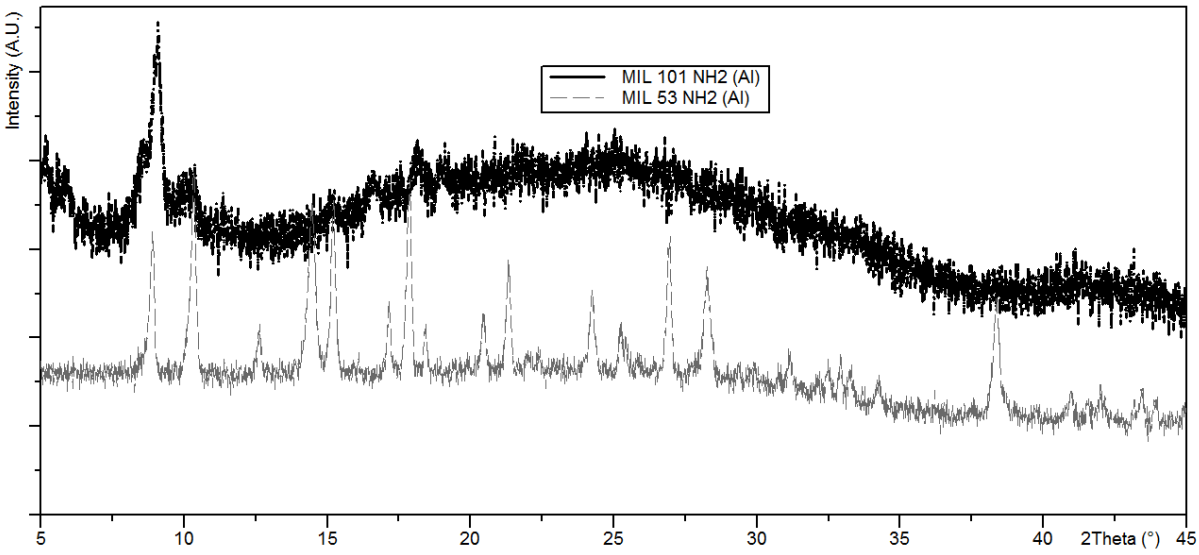
Intensity (A.U.)
MIL 101 NH2 (Al)
MIL 53 NH2 (Al)
5
10
15
20
25
30
35
40
2Theta (°)
45

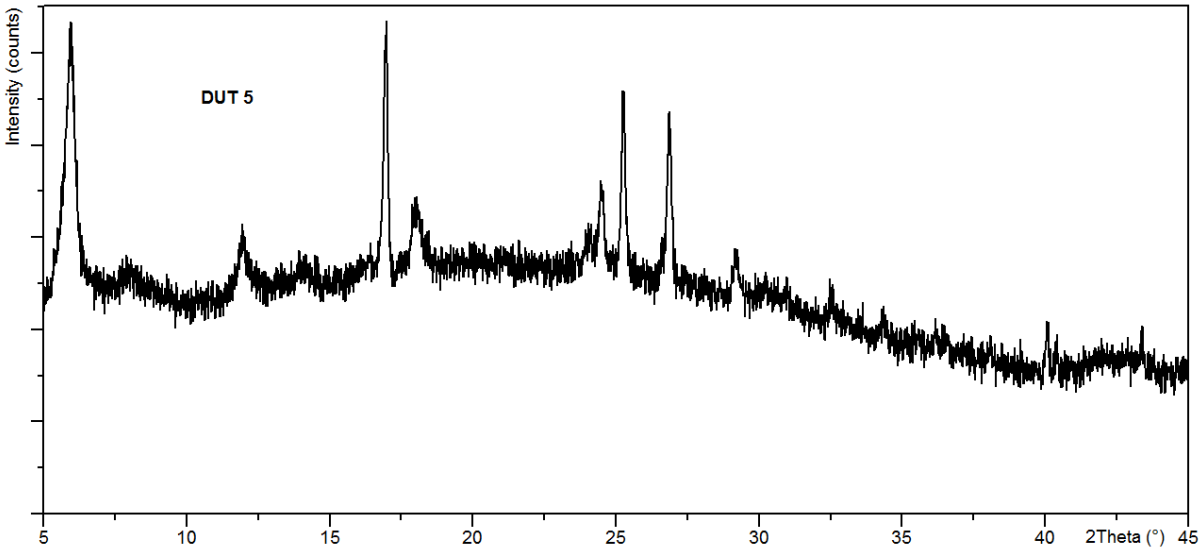
Intensity (counts)
DUT 5
5
10
15
20
25
30
35
40
2Theta (°)
45